Università degli Studi di Napoli Federico II

Dipartimento di Fisica Ettore Pancini

On the numerical evaluation of Feynman integrals through differential equations

Doctoral Thesis in Physics

Author:
Renato Maria Prisco

Supervisor:
Prof. Francesco Tramontano

38° Ciclo di Dottorato in Fisica

Years 2022–2025

Abstract

Particle colliders are able to probe the structure of matter at extremely short distances. The increasing precision of present and future experiments demands equally accurate theoretical predictions to test and advance our understanding of particle physics. These predictions are based on the computation of higher-order perturbative corrections to scattering cross sections and, ultimately, on the evaluation of Feynman integrals over virtual loop momenta. Analytical calculations rapidly grow in complexity as the number of loops, particles and energy scales increases, so that numerical approaches become essential and foster the development of automated tools. Within this context, the differential equation method has proved particularly effective. Feynman integrals can indeed be reduced, via integration-by-parts identities, to finite sets of master integrals that satisfy systems of first-order differential equations in the Lorentz-invariant kinematic variables. This thesis focuses on the development of algorithmic procedures for the numerical evaluation of Feynman integrals as series expansion solutions to this kind of differential equations.

Within the framework presented here, Feynman integrals are propagated in the phase space of the kinematic invariants by solving the differential equations on a line connecting a boundary point to any given target point. The radius of convergence for series solutions is finite due to the presence of singularities and, therefore, the propagation is split into several steps that iteratively move the solution closer to the target. Boundary conditions are obtained around singular kinematic configurations by imposing that the leading power behaviors of the solution agree with those extracted through techniques based on expansion by regions. To do so, the system is transformed to Fuchsian form and the equations are solved by using the considered singularity as the expansion point. This last approach also serves as a strategy for crossing singular points that lie on the propagation path. Since Feynman integrals exhibit branch point singularities, algorithms are provided to perform the analytic continuation of the solutions in agreement with the Feynman prescription.

The methods presented in this thesis have been implemented in a novel open-source computer program called LINE, which stands for Loop Integrals Numerical Evaluation. Aiming to make large-scale cluster computations more feasible, the code has been written in `C/C++` to enable good performance while avoiding the limitations imposed by proprietary software. LINE allows both the computation of boundary values and their propagation across the phase space within a unified framework. In particular, for integrals up to two

loops, the software includes an in-house implementation of the auxiliary mass flow method. The latter relies on the introduction of an auxiliary mass to obtain boundary conditions in the infinite-mass limit. Alternatively, around a singularity the program is able to receive and analyze expansion-by-regions information in order to minimize the number of leading coefficients to be provided as boundary values.

LINE leverages open-source libraries for arbitrary-precision arithmetic, and the numerical accuracy of the results can be assessed without relying on external tools for the evaluation of the integrals. The program has been tested on a variety of one- and two-loop examples, planar and non-planar, with and without masses.

Published work

Part of the work presented in this thesis has been published in the following paper:

R. M. Prisco, J. Ronca and F. Tramontano, *LINE: Loop Integrals Numerical Evaluation*, **JHEP** 07 (2025) 219, DOI: 10.1007/JHEP07(2025)219.

The research project has included the development of LINE, an open-source implementation of the methods presented here, available at the repository:

---

https://github.com/line-git/line.git

Contents

Chapter 1

Introduction

Particle physics aims to understand the fundamental constituents of matter and their interactions. Within the framework of quantum field theory, the Standard Model provides a description that successfully explains a wide range of experimental observations with remarkable precision. The discovery of the Higgs boson at the Large Hadron Collider (LHC) in 2012 [1, 2] represented a major milestone. It confirmed the Brout–Englert–Higgs mechanism [3, 4], which is responsible for the spontaneous breaking of the electroweak symmetry and allows particle masses without violating gauge invariance.

Today, precision measurements play a central role in testing the theory and probing possible signs of new physics. The development of collider physics has been crucial in this context. By reaching ever higher center-of-mass energies and luminosities, particle colliders make it possible to investigate the structure of matter at unprecedented short distances. The precision of the measurements has steadily improved over the past years. Statistical uncertainties are continuously reduced as larger data samples become available, and systematic effects are better controlled through refined detector calibrations and analysis techniques. The near-future collider experiments, like the High-Luminosity phase at the LHC and the Future Circular electron-positron Collider, aim at measuring physical observables at the per-mille precision level over wide phase space regions. To fully exploit such experimental precision, equally accurate theoretical predictions are required.

On the theory side, phenomenology calculations are based on the perturbative expansion of scattering cross sections through power series in the coupling constants. At energy scales relevant for the LHC, the largest contributions come from Quantum Chromodynamics (QCD), whose asymptotic freedom ensures the reliability of the perturbative approach. The truncation of the expansion at a given order introduces a theoretical uncertainty associated with the missing higher orders and so the terms of the series beyond the Leading Order (LO) are regarded as perturbative corrections. The main ingredients for their computation are Feynman amplitudes that, once expressed in terms of form factors, helicity structures or direct interferences, lead to Lorentz-scalar integrals over virtual loop momenta, known as Feynman Integrals (FIs). The integration over the loop momenta gives rise to infrared

divergences that, for infrared-safe observables, are canceled order by order by those arising from phase space integrals, in accordance with the Kinoshita-Lee-Nauenberg theorem [5, 6]. These phase space integrals, through the method of reverse unitarity, can in turn be mapped onto loop integrals, so that the same techniques developed for the latter can be employed. Therefore, the evaluation of FIs constitutes one of the main bottlenecks in the computation of higher-order corrections.

The expected precision of future collider experiments asks for computations that go beyond the Next-to-Leading Order (NLO) and include Next-to-Next-to-Leading Order (NNLO) and Next-to-Next-to-Next-to-Leading Order (N^3LO) contributions [7]. Typically, thousands of two-loop and three-loop integrals contribute to NNLO and N^3LO amplitudes. These rapidly become much harder to compute as the number of loops, external legs, and physical energy scales grows. Relevant advancements include the computation of two-loop, five-point NNLO QCD amplitudes [8–11], and six-point FIs [12, 13], along with some complete N^3LO results at three loops up to three-point contributions [14–17]. Significant progress has also been made in computing many three-loop, four- and five-point amplitudes [18–21]. For the inclusion of higher-loop contributions, results are available for two-point amplitudes [22–24] and vacuum integrals [25].

The computation of FIs is lightened by the fact that not all of them are independent, as they obey Integration-By-Parts (IBP) identities. These are linear relations satisfied by all the members of an integral family, namely the set of FIs that share the same graph topology but have different propagator powers. In particular, it is possible to find a finite set of independent Master Integrals (MIs) that form a basis: any integral of the family can be expressed as a linear combination of the MIs. The choice of the basis is not unique, since any set of independent linear combinations of MIs leads to an equally valid basis.

The task of computing the FIs of a given family is therefore reduced to the evaluation of MIs. Several analytical approaches have proved effective, such as direct integration through specific integral representations [26, 27] and the use of difference equations [28, 29]. Analytical calculations become much harder to employ when the number of legs, loops and masses increases. Therefore, numerical frameworks have been developed as well, including Monte Carlo-based techniques such as sector decomposition [30–34], Mellin-Barnes representations [35–39], and more recent tropical-integration methods [40].

One of the most successful approaches is the Differential Equation (DE) method [41–48], which relies on the fact that the derivatives of the MIs with respect to Lorentz kinematic invariants are themselves linear combinations of integrals of the same family. By means of IBP reduction, one is able to express the derivatives as linear combinations of the MIs, thus closing systems of first-order DEs whose unknown functions are the MIs themselves. Therefore, the computation of MIs can be carried out solving such systems of DEs. Public implementations of fully numerical methods have been developed, such as the Mathematica packages DiffExp [49] and SeaSyde [50]. They allow the numerical

solution of the DEs via series expansion, with the latter being suitable also for integrals with complex masses. The series expansion of a FI can be evaluated at several values of the kinematic invariants. However, Boundary Conditions (BCs) are necessary to fix the solution of the DEs in some kinematic configuration. These can be obtained using the DE method itself with the Mathematica package AMFlow [51–53], which computes FIs for fixed kinematic configurations. The method implemented in said package consists in solving the DEs with respect to an auxiliary mass that is introduced in the propagators of the integrals. Indeed, the leading behavior of FIs is known in the infinite-mass limit and can be used as BC for the propagation to the limit where the auxiliary mass vanishes, thus restoring the values of the original integrals. Although the introduction of the auxiliary mass generally increases the number of MIs, the boundary values obtained at fixed kinematics can then be propagated to many other points of the phase space by solving the DEs with respect to the kinematic invariants. These techniques have been successfully applied to a wide range of two- and three-loop computations, including NLO electroweak corrections to $gg \to HH$ [54], NLO QCD corrections to $pp \to Hj$ [55], and several other processes discussed, for instance, in [56–59].

Since it can be employed both for the computation of boundary values and for their propagation, the DE method proves to be a very powerful approach. Systems of DEs can be obtained also for integrals with Dirac δ-functions (phase space integrals) and propagators that depend linearly on the loop momenta (subtraction counterterms, integrals for effective field theories). Furthermore, it is possible to employ the DEs method in the computation of special functions for the reconstruction of FIs [60–67].

The present work focuses on the development of algorithmic methods for the numerical evaluation of FIs through the solution of DEs. The objective is to design systematic strategies that are well suited for implementation in computer code and are able to solve the DEs via series expansion to obtain BCs and propagate MIs across the phase space of the kinematic invariants. The presence of singularities causes the radius of convergence of the expansion to be finite and so the propagation is split into several steps, each moving the solution closer to the desired target point.

In the framework presented in this work, BCs are computed either with the Auxiliary Mass Flow (AMFlow) method or using Expansion By Regions (EBR). The latter is a technique that splits the integration domain into regions characterized by different scalings of the loop momenta, in order to determine the asymptotic expansion of FIs near singular kinematic configurations. The leading behaviors can be used as BCs for the DEs. For instance, the AMFlow method itself relies on the application of EBR when the auxiliary mass is pushed to infinity. To exploit EBR as just described, one must be able to solve the DEs around its singular points. In order for this to happen, the system of DEs must be turned to Fuchsian form by building an appropriate transformation matrix. Then, a suitable ansatz can be used for the series expansion of the solution around singular points.

The same method can be used to cross singular points that lie on the propagation path. However, as FIs have branch point singularities that develop branch cuts, particular care must be taken for the analytic continuation of the solution.

In this work, we present a set of procedures to address these issues in an algorithmic way. The techniques illustrated here have been implemented in an open-source software called LINE, which stands for Loop Integrals Numerical Evaluation. LINE is written in `C/C++` and implements from scratch the routines to perform the necessary algebraic manipulations, leveraging on the `GMP` family of public libraries for efficient arbitrary-precision arithmetic. The use of a low-level programming language provides higher efficiency compared to an equivalent implementation in higher-level languages, while avoiding any dependence on proprietary software. This choice makes massive cluster computations more feasible, as one can run as many instances of LINE as the available computational resources allow.

LINE presents an in-house implementation of the AMFlow method to generate BCs up to two loops. For some selected examples, BCs are automatically obtained using EBR around singular points, without the introduction of auxiliary parameters. Therefore, LINE combines the computation of boundary values and their propagation across the phase space within a single framework. Consequently, the numerical precision of the results can be estimated internally without relying on external tools for the computation of FIs, since any phase space point can be reached with propagations along different paths, possibly using distinct boundary points.

The theoretical framework on which LINE is based, as well as the techniques therein implemented, are presented here as follows. We begin by introducing the basic formalism of FIs in chapter 2. We define integral families of FIs, discuss the dependence of the integrals on the kinematic invariants and analyze the nature of their singularities. We show how to differentiate FIs and then we introduce IBP identities, thus providing all the notions necessary to build systems of DEs for MIs.

Chapter 3 is dedicated to a detailed analysis of the DEs. We describe an interpolation procedure to handle dimensional regularization and identify a block structure in the equations. This leads us to focus on the solution of univariate systems of non-homogeneous DEs. The problem is then studied in the neighborhood of singular points, where the system is transformed to Fuchsian form in agreement with its block structure. For the determination of BCs, we describe how the AMFlow method is implemented in LINE and show how to perform EBR on a few examples.

In chapter 4 we focus on the actual propagation of series expansion solutions. Given a line connecting a boundary and a target point, we outline a strategy to populate the path with intermediate expansion points. Recurrence relations are derived to iteratively compute the coefficients for the series expansion of the solution around these points, whether they are regular or singular. Furthermore, we show how to exploit EBR to systematically obtain linear constraints for the leading coefficients of the solution around poles of the DEs, thus

reducing the number of BCs needed as input when using a singularity as the starting point for a propagation.

The analytic continuation of the solutions is studied in section 5, where an algorithmic procedure is provided for determining the position and orientation of the branch cuts in the complex plane of the line parameter. This allows to cross branch points that are encountered on the propagation path.

In chapter 6 the methods described in the present work are applied, using LINE, to a selection of one- and two-loop examples, both planar and non-planar, with and without masses. Boundary values are obtained internally and propagated to several phase space points. The results are internally validated using different boundaries and paths.

Finally, conclusions are drawn in section 7, where the outlook of this work is discussed, while appendix A provides further implementation details.

Chapter 2

Feynman integrals

The perturbative expansion of scattering amplitudes in quantum field theory is built on Feynman integrals. In this chapter we introduce the formalism required to address their computation, aiming to derive systems of differential equations whose unknown functions are the FIs themselves.

The definition of a FI is closely related to the notion of graph, since its propagators can be identified with the edges of a graph through which momenta flow as in a circuit, with momentum conservation satisfied at each vertex. In this picture, the momenta of the particles involved in a scattering process are associated with external edges, while each loop of the graph introduces an integration over the independent momentum of a virtual off-shell particle. We start by exploring this correspondence and then proceed by introducing the concept of integral family, which naturally arises once arbitrary integer powers are allowed for the propagators. The further classification of integrals into sectors of the family is also investigated, as the hierarchy of the sectors is exploited in the subsequent chapters to determine a block structure in the DEs.

To identify a minimal set of independent variables that characterize the problem, we analyze the dependence of the FIs on the external momenta, which enter only through Lorentz invariants and are constrained by momentum conservation, on-shell conditions and Gram determinant relations. Next, we discuss how to differentiate FIs with respect to the external kinematic invariants and the propagator masses, a crucial step towards the construction of DEs. In particular, we show how the derivatives of a FI can be expressed as linear combinations of integrals that belong to the same family and, therefore, are related through integration-by-parts identities. These are linear relations that enable the reduction of all the members of a given integral family to a finite set of independent integrals, known as master integrals, which hence constitute a basis for the family. Finally we observe that, combining the differentiation rules with IBP identities, one can close a system of DEs for the MIs. The analysis of these equations and the methods to find their solutions are the main focus of the subsequent chapters of this thesis.

2.1 Integral families

Let us consider a connected graph $\mathcal{G}$ with N external edges, E internal edges, and V internal vertices. To each edge we can assign an orientation and a momentum flowing in the selected direction. We indicate with p_i the momenta associated with the N external edges, that we consider as incoming, and impose momentum conservation at each vertex, so that we have

$$\sum_{i=1}^{N} p_i = 0\,. \tag{2.1}$$

We can use this relation to express one of the external momenta, say p_N, in terms of the others, so that we keep $N-1$ external momenta while having $p_N = -(p_1 + \cdots + p_{N-1})$. In addition to eq. (2.1), there are other $V-1$ independent conditions that are obtained when imposing momentum conservation at each vertex. They allow us to determine all but L of the internal momenta, where

$$L = E - V + 1 \tag{2.2}$$

is the number of loops in the graph $\mathcal{G}$. We denote by k_l the independent momenta flowing through the internal edges and we refer to them as *loop momenta*.

So we start with $N+E$ momenta and, with the application of momentum conservation at V vertices, the total number of independent momenta is reduced to

$$N + E - V = L + N - 1\,, \tag{2.3}$$

namely, L loop momenta $k_1, \ldots, k_L$ and $N-1$ external momenta $p_1, \ldots, p_{N-1}$. Taken in this order, we collectively denote them by $v_1, \ldots, v_{L+N-1}$, so that

$$\begin{aligned} v_l &= k_l\,, \quad l = 1, \ldots, L\,, \\ v_{L+i} &= p_i\,, \quad i = 1, \ldots, N-1\,. \end{aligned}$$

To each internal edge of the graph $\mathcal{G}$ we can assign a mass m_α and an inverse propagator

$$D_\alpha \equiv q_\alpha^2 - m_\alpha^2 + i\varepsilon\,, \tag{2.4}$$

where q_α is the momentum flowing through the edge and $\varepsilon \to 0^+$ enforces the so-called *Feynman prescription*. With the graph $\mathcal{G}$ we then associate a FI defined as

$$F \equiv \int_{k_1,\ldots,k_L} \prod_{\alpha=1}^{E} \frac{1}{D_\alpha}\,, \tag{2.5}$$

where the integration is performed over the loop momenta with the measure

$$\int_{k_1,\dots,k_L} \equiv \int \prod_{l=1}^{L} \frac{d^d k_l}{i\pi^{\frac{d}{2}}}\,, \tag{2.6}$$

in a d-dimensional space-time. The integration measure typically used in quantum field theory is thus restored by means of a multiplicative factor, as in

$$\int \prod_{l=1}^{L} \frac{d^d k_l}{(2\pi)^d} = \frac{i}{(4\pi)^{d/2}} \int_{k_1,\dots,k_L}\,. \tag{2.7}$$

Furthermore, we assume that the integrals are carried out within the framework of dimensional regularization, where the space-time dimension d is regarded as a complex number that differs from a positive integer d_0 according to $d = d_0 - 2\epsilon$.

The internal momentum q_α of each propagator can be expressed, via momentum conservation, as a linear combination with coefficients ± 1 of the independent momenta v_j. By doing so, the quadratic momentum q_α^2 in eq. (2.4) turns into a linear combination of the scalar products

$$x_{ij} \equiv v_i \cdot v_j\,, \quad i,j = 1,\dots,L+N-1\,. \tag{2.8}$$

We can further distinguish those products that involve only the external momenta by introducing the notation

$$y_{ij} \equiv p_i \cdot p_j\,, \quad i,j = 1,\dots,N-1\,, \tag{2.9}$$

so that the inverse propagator becomes

$$D_\alpha = \sum_{i=1}^{L} \sum_{j=i}^{L+N-1} \mathbb{M}_{\alpha,ij}\, x_{ij} + \sum_{i=1}^{N-1} \sum_{j=i}^{N-1} \mathbb{N}_{\alpha,ij}\, y_{ij} - m_\alpha^2 + i\varepsilon\,, \tag{2.10}$$

where the coefficients $\mathbb{M}_{\alpha,ij}$ and $\mathbb{N}_{\alpha,ij}$ are integers and the sums are performed avoiding double counting. In particular, the first sum includes only scalar products that involve at least one loop momentum. There are $E_{\max}$ such products, with

$$E_{\max} = \frac{L(L+1)}{2} + L(N-1)\,. \tag{2.11}$$

If a given ordering is fixed for the scalar products x_{ij} of this kind, we can regard the pair ij in $\mathbb{M}_{\alpha,ij}$ as a unique index and $\mathbb{M}$ as a matrix of shape $E \times E_{\max}$. Although

in general $E \leq E_{\max}$, we can extend the set of propagators by introducing $E_{\max} - E$ auxiliary propagators in such a way that $\mathbb{M}$ becomes an invertible square matrix. In other words, the extended set of inverse propagators D_α, with $\alpha = 1, \ldots, E_{\max}$, is built on $E_{\max}$ independent linear combinations of the products x_{ij} that involve the loop momenta. This also means that the inverse propagators are linearly independent, in the sense that the only linear combination of the D_α's that does not depend on the loop momenta is the one where all coefficients are zero.

With an extended set of independent propagators, eq. (2.4) can be inverted as

$$x_{ij} = \sum_{\alpha=1}^{E_{\max}} \mathbb{M}^{-1}_{ij,\alpha} \left(D_\alpha - \sum_{h=1}^{N-1} \sum_{k=h}^{N-1} \mathbb{N}_{\alpha,hk}\, y_{hk} + m_\alpha^2 \right) = \sum_{\alpha=1}^{E_{\max}} \mathbb{M}^{-1}_{ij,\alpha} \left(D_\alpha + \widetilde{m}_\alpha^2 \right), \quad i \leq L\,,\, i \leq j\,, \tag{2.12}$$

where the modified squared mass $\widetilde{m}_\alpha^2$ is defined according to

$$\widetilde{m}_\alpha^2 \equiv m_\alpha^2 - \sum_{h=1}^{N-1} \sum_{k=h}^{N-1} \mathbb{N}_{\alpha,hk}\, y_{hk}\,, \tag{2.13}$$

so as to include any external kinematic factor y_{hk}. Note that the auxiliary propagators can always be chosen as massless, since the only thing that matters is their dependence on the momenta.

The valency of a vertex is the number of edges attached to it. If all the internal vertices of a graph $\mathcal{G}$ have the same valency v, we say that $\mathcal{G}$ is v-legged. We do not consider internal vertices of valency 2 since, as we discuss later on, these can be obtained by assigning integer powers to the propagators.[1] Vertices of valency $v > 3$ can instead be represented by shrinking some internal edges of a 3-legged graph, i.e., two vertices are merged into one vertex and the edge attached to them is removed. This operation is often also referred to as pinching a propagator, to which we assign a zero power. For instance, the vertex of valency 4 in the right panel of figure 2.1 is obtained by shrinking the middle edge of the 3-legged graph on the left. Therefore, without loss of generality, we only consider 3-legged graphs.

The number of auxiliary propagators can be predicted by counting the internal edges in a graph [68]. For 3-legged graphs we can distinguish between the case with $N = 0$ (vacuum integrals with no external edges) and $N \geq 3$. The simplest 3-legged vacuum integral is the sunrise-shaped graph with two vertices, $E = 3$ and $L = 2$. To introduce an additional loop, one has to place and connect two new internal vertices on the same edge or on two distinct edges, thus raising E by 3 (connecting two preexisting vertices would increase their valency). Therefore, the number of internal edges for a 3-legged vacuum

[1] This choice also implies that to each momentum q_α only one mass m_α is assigned.

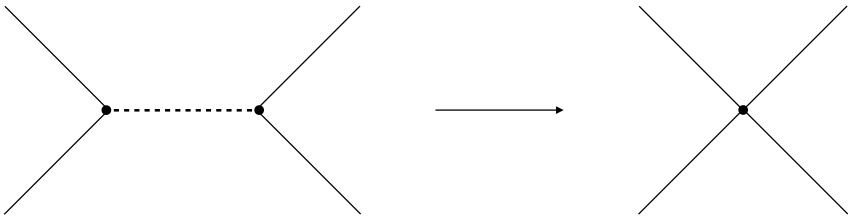

Figure 2.1: A 3-legged graph whose dashed edge is shrunk to produce a vertex of valency 4. The pinched propagator can be considered as having a zero power.

integral is given by

$$E = 3 + 3(L-2) = 3(L-1)\,, \tag{2.14}$$

and differs from $E_{\max} = L(L+1)/2$ by

$$E_{\max} - E = \frac{(L-2)(L-3)}{2}\,. \tag{2.15}$$

Auxiliary propagators are therefore needed for $L \geq 4$.

A 3-legged graph with $N \geq 3$ has $E = N - 3$ internal edges at tree level, as can be verified by starting from a graph with $N = 3$ and $E = 0$, and attaching one external edge at a time, thus increasing both N and E by one unit at each step. As for the vacuum integrals considered above, the introduction of an additional loop increases E by 3. Therefore, the number of internal edges for a non-vacuum 3-legged graph is given by

$$E = N - 3 + 3L\,, \tag{2.16}$$

which differs from $E_{\max}$ given in eq. (2.11) by

$$E_{\max} - E = \frac{(L-1)(L+2N-6)}{2}\,, \tag{2.17}$$

Therefore, auxiliary propagators are required when $L \geq \max\{2, 7-2N\}$.

Let us consider again the FI in eq. (2.5). We can extend its definition by allowing each inverse propagator D_α to appear with an integer power ν_α and introducing auxiliary propagators in the numerator (i.e., with non-positive powers) in such a way that the D_α's are linearly independent. The set of integrals

$$F^{\boldsymbol{\nu}} \equiv \int_{k_1,\ldots,k_L} \prod_{\alpha=1}^{E} \frac{1}{D_\alpha^{\nu_\alpha}} \prod_{\beta=E+1}^{E_{\max}} \frac{1}{D_\beta^{\nu_\beta}}\,, \tag{2.18}$$

obtained as $\boldsymbol{\nu}$ varies over all possible integer powers (with $\nu_\beta \leq 0$ for $\beta > E$) is referred to as an *integral family* of FIs. The auxiliary inverse propagators are called *irreducible*

numerators, since they only appear with non-positive powers. We refer to the FI of eq. (2.5) as the top-topology integral of the family defined in eq. (2.18). It can be obtained by setting $\nu_\alpha = 1$ for $\alpha \leq E$ and $\nu_\beta = 0$ for the irreducible numerators.

A propagator with a power $\nu_\alpha > 1$ is often represented in the associated graph $\mathcal{G}$ by placing $\nu_\alpha - 1$ dots that can be interpreted as vertices of valency 2. Propagators with negative powers are usually omitted from the graph, although one could draw the corresponding edges and attach to each of them an integer label equal to its power. After all, masses should also be considered as labels, even though they are often indicated by assigning to each mass a line of a specific color or shape. It is possible to find a set of edges to be associated also with irreducible numerators. These can be introduced in the graph by attaching additional external edges whose momenta are linear combinations of the external momenta [69]. Whenever a given power ν_α is zero, the corresponding edge can be shrunk.

The set of positive powers in the integral $F^{\boldsymbol{\nu}}$ identifies what is called a *sector* of the integral family. We denote by $\sigma(F^{\boldsymbol{\nu}})$ the sector to which $F^{\boldsymbol{\nu}}$ belongs. To each sector we can associate a binary vector $\boldsymbol{\theta}$ whose components are given by

$$\theta_\alpha(F^{\boldsymbol{\nu}}) \equiv \theta_H\left(\nu_\alpha - \frac{1}{2}\right) = \begin{cases} 1\,, & \nu_\alpha > 0\,, \\ 0\,, & \text{otherwise}\,, \end{cases} \tag{2.19}$$

so that all the integrals belonging to the same sector are mapped to the same $\boldsymbol{\theta}(F^{\boldsymbol{\nu}})$, that is,

$$\sigma(F^{\boldsymbol{\nu}}) = \left\{ F^{\boldsymbol{\nu}'} :\ \boldsymbol{\theta}(F^{\boldsymbol{\nu}'}) = \boldsymbol{\theta}(F^{\boldsymbol{\nu}}) \right\}\,. \tag{2.20}$$

This binary representation can be translated into its decimal equivalent with the introduction of the sector identification function

$$\rho(F^{\boldsymbol{\nu}}) \equiv \sum_{\alpha=1}^{E} \theta_\alpha(F^{\boldsymbol{\nu}})\, 2^{\alpha-1}\,. \tag{2.21}$$

If an integral $F^{\boldsymbol{\nu}_1}$ can be obtained from $F^{\boldsymbol{\nu}_2}$ by setting some positive powers to zero, the sector $\sigma(F^{\boldsymbol{\nu}_1})$ is said to be a *sub-sector* of $\sigma(F^{\boldsymbol{\nu}_2})$. The integral with $\nu_\alpha > 0$ for all $\alpha = 1, \ldots, E$ belongs to the so-called *top sector* of the integral family. By definition, any other sector is a sub-sector of the top sector. In section 3.2 it is discussed how the identification of sectors is closely related to the block structure of the DEs satisfied by FIs.

2.2 Kinematics

The Feynman integrals in eq. (2.5) are Lorentz scalars and so they depend on the external momenta only through the Lorentz invariants $y_{ij} = p_i \cdot p_j$. There are $N(N+1)/2$ such

invariants but, taking into account N conditions for momentum conservation

$$\sum_{j=1}^{N} y_{ij} = p_i \cdot \sum_{j=1}^{N} p_j = 0\,,$$

and N on-shell conditions, the number T of independent invariants is reduced to

$$T = \frac{N(N-3)}{2}\,. \tag{2.22}$$

However, in this counting we assumed that $N-1$ external momenta are independent, which would be impossible if $N-1 > d$, since there are at most d linearly independent vectors in a d-dimensional space. In this case, $N-1-d$ external momenta would necessarily be a linear combination of the other d momenta. To account for this effect, one should also consider the so-called Gram determinant conditions. We define the Gram matrix associated with a set of n momenta w_i as

$$\mathbb{G}(w_1,\ldots,w_n) \equiv \begin{pmatrix} w_1\cdot w_1 & \ldots & w_1\cdot w_n \\ \vdots & \ddots & \vdots \\ w_n\cdot w_1 & \ldots & w_n\cdot w_n \end{pmatrix}\,, \tag{2.23}$$

that is, $\mathbb{G}_{ij}(w_1,\ldots,w_n) = w_i\cdot w_j$. The vectors w_i are linearly independent if and only if

$$\Delta(w_1,\ldots,w_n) \equiv \det \mathbb{G}(w_1,\ldots,w_n) \neq 0\,. \tag{2.24}$$

This can be seen by looking for a linear combination $\sum_i c_i w_i = 0$ where the coefficients c_i are not all zero and projecting along all the vectors w_j. The matrix associated to the corresponding system of linear equations, $\sum_i c_i w_i\cdot w_j = 0$, is indeed the Gram matrix. This system has a non-zero solution if and only if eq. (2.24) is satisfied.

In our application, one can consider any subset of the N external momenta and form a Gram matrix whose elements are the invariants y_{ij}. It can be seen [70] that, for $N-1 > d$, there are additional constraints on the invariants y_{ij}, which correspond to

$$\bar{\Delta}_n \equiv (-1)^{n-1} \sum_{\{i_1,\ldots,i_n\}} \Delta(p_{i_1},\ldots,p_{i_n}) = 0\,, \quad \forall\, n = d+1,\ldots,N-1\,, \tag{2.25}$$

where the sum runs over all the possible subsets of n external momenta. Note that, for $n = N$, the condition $\bar{\Delta}_N = (-1)^{N-1}\Delta(p_1,\ldots,p_N) = 0$ is automatically satisfied, since the external momenta are linearly dependent because of momentum conservation.

The Gram determinant conditions in eq. (2.25) are non-linear relations that decrease the number of independent invariants in a non-trivial way. To predict the actual number,

we can perform an independent counting. We start from the dN degrees of freedom corresponding to the d components of the N external momenta. Then, we impose d momentum conservation relations and N on-shell conditions. Finally, to account for the Lorentz invariance, we also subtract the dimension of the Lorentz group, i.e., $d(d-1)/2$. We end up with

$$T = dN - N - d - \frac{d(d-1)}{2} \tag{2.26}$$

degrees of freedom. This formula actually corresponds to $N(N-3)/2$ as in eq. (2.22) for $N = d$ and $N = d+1$, while the latter must be replaced by it when $N > d+1$.

When the square of some of the external momenta is considered as a varying parameter, it must be added to the counting of the independent invariants. We consider this kind of external momentum as off-shell. Therefore, the total number of independent external invariants is given by

$$T = \text{number of off-shell momenta} + \begin{cases} \dfrac{N(N-3)}{2}\,, & N-1 \leq d\,, \\ dN - N - d - \dfrac{d(d-1)}{2}\,, & N-1 > d\,. \end{cases} \tag{2.27}$$

In the choice of T independent invariants, one is not restricted to scalar products such as $p_i \cdot p_j$, since any set of T independent linear combinations would do the job. For instance, the squares $(p_i+p_j)^2$, $(p_i+p_j+p_k)^2$, ... , are also valid candidates. Therefore, we generically denote by $t_1, \ldots, t_T$ the chosen set of independent kinematic invariants involving the external momenta. We collect these invariants in the T-dimensional vector $\mathbf{t}$. If the squared masses m_α^2 of some internal propagators are also varying parameters, we add them to the count in a separate vector $\mathbf{s}$ such that

$$\begin{aligned} s_i &= t_i\,, \qquad i = 1, \ldots, T\,, \\ s_{T+\alpha} &= m_\alpha^2\,, \quad \alpha = 1, \ldots, M\,, \end{aligned} \tag{2.28}$$

where M is the number of varying masses. To avoid double counting, M does not include squared masses that are equal to the square of off-shell external momenta. We denote the total number of independent kinematic invariants s_i by $S \equiv T + M$.

2.3 Singularities

Feynman integrals exhibit a rich analytic structure characterized by singularities in the phase space of the kinematic invariants. The understanding of the origin and nature of these singularities has a long history, dating back to the works of Bjorken [71], Landau [72] and Nakanishi [73], and plays a central role in modern techniques for the evaluation of FIs.

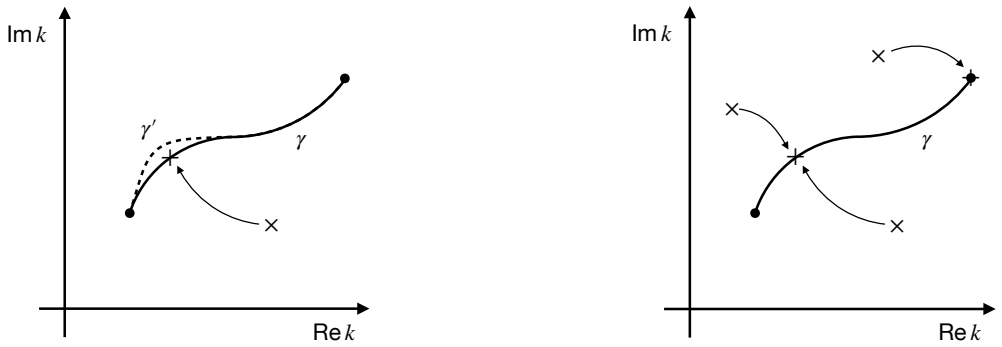

(a) **(b)**

Figure 2.2: **(a)** The integration contour γ in the complex plane of k is locally deformed to γ' to avoid the singularity, drawn as a cross, that is moving along the arrow. **(b)** The contour cannot be deformed because one singularity approaches an end point, while two others pinch the contour from opposite sides.

Given that FIs are defined by integration, their singularities are directly linked to those of their integrand. To see how this happens in a simple case, let us consider a function

$$f(s) = \int_\gamma dk\, g(k, s)\,, \tag{2.29}$$

where $s, k \in \mathbb{C}$, γ is an integration contour in the complex plane of k and $g(k, s)$ is an analytic function whose singularities are known as functions $\sigma_i(s)$, and so they move in the complex plane of k as s varies. The function $f(s)$ is certainly regular if no singular point $\sigma_i(s)$ is on the contour γ. We assume that this is the case at least in a neighborhood of some value of s, and consider the analytic continuation of $f(s)$ outside said neighborhood.

Suppose that for $s \to s_0$ a singularity $\sigma_i(s)$ tends to an internal point $\sigma_i(s_0) \in \gamma$. While this happens, the contour γ may be locally deformed to a second contour γ' so as to avoid $\sigma_i(s_0)$ keeping its end points fixed, as shown in figure 2.2a. If no other singularity falls within the area encircled by $\gamma \cup \gamma'$, Cauchy's theorem guarantees that, at any $s \neq s_0$,

$$f(s) = \int_{\gamma'} dk\, g(k, s)\,. \tag{2.30}$$

Since $\sigma_i(s) \notin \gamma'$, the latter integral is convergent. Therefore, $f(s)$ can be analytically continued to $s = s_0$ according to

$$f(s_0) \equiv \lim_{s \to s_0} f(s) = \lim_{s \to s_0} \int_{\gamma'} dk\, g(k, s) = \int_{\gamma'} dk\, g(k, s_0)\,. \tag{2.31}$$

However, $f(s)$ becomes singular when the contour γ cannot be deformed so as to avoid the singularity, which is the case if one of the following conditions occurs:

- A singularity moves to one of the end points of the integration contour, thus giving rise to an *end-point singularity*.
- Two or more singularities move to a common point trapping the contour from opposite sides, causing a *pinch singularity*.

An example for both kinds of singularity is represented in figure 2.2b.

The mechanism of contour deformation allows us to understand why such singularities may be branch points of the integral $f(s)$. Consider the motion of a point $s = s_p$ as it circles counter-clockwise around an end-point singularity $s = s_0$ at small distance r. In the complex plane of k, the corresponding singular point $\sigma_i(s_p)$ moves according to

$$\sigma_i(s_p) = \sigma_i(s_0 + re^{i\varphi}) = \sigma_i(s_0) + re^{i\varphi} \left.\frac{d}{ds}\sigma_i(s)\right|_{s=s_0} + \mathcal{O}(r^2)\,, \tag{2.32}$$

thus approximately circling around the end point $\sigma_i(s_0)$ of the integration contour γ. The integral $f(s)$ is analytically continued deforming γ. By Cauchy's theorem, after s_p completes a full rotation around s_0, $f(s)$ differs from its initial value by an integral over a contour closed around $\sigma_i(s)$:

$$\mathrm{Disc} f(s) = \int_{\gamma'} dk\, g(k,s) - \int_{\gamma} dk\, g(k,s) = \oint_{\sigma_i(s)} dk\, g(k,s) = 2\pi i\, \mathrm{Res}_{k=\sigma_i(s)}\, g(k,s)\,. \tag{2.33}$$

By contour deformation, $f(s)$ is therefore analytically continued to another Riemann sheet. This indicates that $f(s)$ is a multi-valued function and that $s = s_0$ is a branch point singularity. In order to make $f(s)$ a single-valued function, one has to arbitrarily place a branch cut developing from $s = s_0$ and define $f(s)$ as the analytic continuation performed on those curves in the complex plane of s that do not cross the cut. To assign a value to $f(s)$ at points lying on the branch cut, the latter must be oriented by prescribing the side from which it is to be approached. The same kind of reasoning can be applied also to the full rotation of s_p around a pinch singularity s_0, with two singular points $\sigma_i(s)$ and $\sigma_j(s)$ exchanging places.

In case there are multiple external variables $\mathbf{s}$, the function $f(\mathbf{s})$ becomes singular on hyper-surfaces that are defined by the same conditions as for the univariate case. If there are multiple integration variables $\mathbf{k}$ as well, $f(\mathbf{s})$ is defined by the integration

$$f(\mathbf{s}) = \int_{\Sigma} \prod_i dk_i\, g(\mathbf{k},\mathbf{s}) \tag{2.34}$$

over a hyper-contour Σ of the multi-dimensional complex space of $\mathbf{k}$, while the integrand $g(\mathbf{k},\mathbf{s})$ has singular hyper-surfaces Σ_i that we assume we are able to define by means of

equations in the form

$$\Sigma_i(\mathbf{s},\mathbf{k}) = 0\,. \tag{2.35}$$

While a rigorous treatment of this problem would require topological methods, the main ideas can be understood by following the discussion in [74]. For the contour Σ to be trapped between multiple singular surfaces Σ_i we must have that their normals are proportional, that is, there are some coefficients α_i such that

$$\sum_i \alpha_i \frac{\partial}{\partial k_j}\Sigma_i(\mathbf{s},\mathbf{k}) = 0\,, \quad \forall\, j\,. \tag{2.36}$$

If some surface Σ_i does not enter in this mechanism, the associated α_i can be set to zero. Therefore, we can consider the condition

$$\Sigma_i(\mathbf{s},\mathbf{k}) = 0 \quad \text{or} \quad \alpha_i = 0\,, \tag{2.37}$$

to be combined with eq. (2.36). Another possibility for $f(\mathbf{s})$ to develop a singularity is that different parts of the same singular surface Σ_i come to trap the contour Σ. We have

$$\frac{\partial}{\partial k_j}\Sigma_i(\mathbf{s},\mathbf{k}) = 0\,, \quad \forall\, j\,, \tag{2.38}$$

and Σ_i can be thought of as becoming locally cone-like. If the boundary of the contour Σ is also defined through equations in the form

$$\widetilde{\Sigma}_i(\mathbf{s},\mathbf{k}) = 0\,, \tag{2.39}$$

the normals to the surfaces $\widetilde{\Sigma}_i$ represent the directions along which the contour cannot be deformed. These boundary surfaces hence play a role analogous to that of the singular surfaces Σ_i. Therefore, we add to eq. (2.37) the conditions

$$\widetilde{\Sigma}_i(\mathbf{s},\mathbf{k}) = 0 \quad \text{or} \quad \widetilde{\alpha}_i = 0\,, \tag{2.40}$$

and extend eq. (2.36) according to

$$\sum_i \alpha_i \frac{\partial}{\partial k_j}\Sigma_i(\mathbf{s},\mathbf{k}) + \sum_k \widetilde{\alpha}_k \frac{\partial}{\partial k_j}\widetilde{\Sigma}_k(\mathbf{s},\mathbf{k}) = 0\,, \quad \forall\, j\,. \tag{2.41}$$

In order to apply the arguments illustrated above to FIs defined as in eq. (2.5), we can identify the singular surfaces Σ_i with the inverse propagators D_i, while the integration domain has no boundary. Then eq. (2.37) becomes

$$q_i^2 = m_i^2 \quad \text{or} \quad \alpha_i = 0\,, \tag{2.42}$$

while eq. (2.36) corresponds to

$$\sum_i \alpha_i \frac{\partial}{\partial k_j}(q_i^2 - m_i^2) = 0 \quad \forall\, j\,. \tag{2.43}$$

Here, the sum on the left-hand side takes contributions only from those propagators that depend on the loop momentum k_j, for which $\partial_{k_j} D_i = 2\, q_i$. Therefore, we can write the pinch condition as

$$\sum_{i \,\in \text{loop}\, j} \alpha_i q_i = 0\,, \tag{2.44}$$

with the sum running over the loop where k_j flows. The eqs. (2.42) and (2.44) are known as the *Landau equations*.

It is often useful to consider the Landau equations in the so-called Feynman parameter representation. This can be obtained by starting with the Feynman trick

$$\prod_{i=1}^{E} \frac{1}{A_i^{\nu_i}} = \frac{\Gamma(\nu)}{\prod_{i=1}^{E}\Gamma(\nu_i)} \left(\prod_{i=1}^{E}\int_0^1 d\alpha_i\right) \delta\left(1 - \sum_{i=1}^{E}\alpha_i\right) \frac{\prod_{i=1}^{E}\alpha_i^{\nu_i - 1}}{\left(\sum_{i=1}^{E}\alpha_i A_i\right)^{\nu}}\,, \tag{2.45}$$

where $\nu \equiv \sum_{j=1}^{E}\nu_j$ and the variables α_i are called *Feynman parameters*. This relation can be applied to FIs with the identification $A_i = D_i$, so that

$$F^{\boldsymbol{\nu}}(\epsilon, \mathbf{s}) = \frac{\Gamma(\nu)}{\prod_{i=1}^{E}\Gamma(\nu_i)} \int_{k_1,\ldots,k_L} \left(\prod_{i=1}^{E}\int_0^1 d\alpha_i\right) \delta\left(1 - \sum_{i=1}^{E}\alpha_i\right) \frac{\prod_{i=1}^{E}\alpha_i^{\nu_i - 1}}{\left[\sum_{i=1}^{E}\alpha_i D_i\right]^{\nu}}\,. \tag{2.46}$$

The denominator is a quadratic form in the loop momenta k_l,

$$\sum_{i=1}^{E}\alpha_i D_i = \sum_{i=1}^{E}\alpha_i(q_i^2 - m_i^2 + i\varepsilon) = \mathbf{k}^T \mathbb{A}\, \mathbf{k} + \mathbf{B}\cdot\mathbf{k} + C\,, \tag{2.47}$$

where $\mathbb{A}$ is symmetric and only depends on the Feynman parameters, the components of $\mathbf{B}$ are linear in the external momenta and $C = \sum_{i=1}^{E}\alpha_i(-m_i^2 + i\varepsilon)$. Completing the square by means of the linear change of variables

$$\mathbf{k} \to \mathbf{k}' = \mathbf{k} + \frac{1}{2}\,\mathbb{A}^{-1}\mathbf{B}\,, \tag{2.48}$$

the denominator becomes

$$\sum_{i=1}^{E} \alpha_i D_i = \mathbf{k'}^T \mathbb{A}\, \mathbf{k'} + \Delta\,, \tag{2.49}$$

where $\Delta \equiv C - (\mathbf{B}^T \mathbb{A}\, \mathbf{B})/4$. The loop integration can now be performed according to

$$\int_{k'_1,\dots,k'_L} \left(\mathbf{k'}^T \mathbb{A}\, \mathbf{k'} + \Delta\right)^{-\nu} = \frac{\Gamma(\nu - dL/2)}{\Gamma(\nu)} (\det \mathbb{A})^{-\frac{d}{2}} (\Delta)^{\nu - \frac{Ld}{2}}\,, \tag{2.50}$$

so that the FI turns into

$$F^{\boldsymbol{\nu}}(\epsilon, \mathbf{s}) = \frac{\Gamma(\nu)}{\prod_{i=1}^{E} \Gamma(\nu_i)} \left(\prod_{i=1}^{E} \int_0^1 d\alpha_i\right) \delta\left(1 - \sum_{i=1}^{E} \alpha_i\right) \left(\prod_{i=1}^{E} \alpha_i^{\nu_i - 1}\right) \frac{\mathcal{U}(\boldsymbol{\alpha})^{\nu - \frac{(L+1)d}{2}}}{\mathcal{F}(\boldsymbol{\alpha})^{\nu - \frac{Ld}{2}}}\,. \tag{2.51}$$

Here, $\mathcal{U}$ and $\mathcal{F}$ are known as the first and second *Symanzik polynomials*, respectively, and are defined by

$$\mathcal{U}(\boldsymbol{\alpha}) \equiv \det \mathbb{A}\,, \quad \mathcal{F}(\boldsymbol{\alpha}) \equiv (\det \mathbb{A}) \left(C - \frac{1}{4}\, \mathbf{B}^T \mathbb{A}\, \mathbf{B}\right)\,. \tag{2.52}$$

The polynomials $\mathcal{U}(\boldsymbol{\alpha})$ and $\mathcal{F}(\boldsymbol{\alpha})$ can be given a graph-related definition as follows [75]. Let $\mathcal{G}$ be the graph associated with the FI in question. For the first Symanzik polynomial, one has to consider all the possible spanning trees of $\mathcal{G}$, defined as connected graphs with no loops obtained by removing edges from $\mathcal{G}$ while keeping all of its vertices. Then $\mathcal{U}(\boldsymbol{\alpha})$ is given by

$$\mathcal{U}(\boldsymbol{\alpha}) = \sum_{\mathcal{T} \in \mathcal{T}_1} \prod_{i \notin \mathcal{T}} \alpha_i\,, \tag{2.53}$$

where $\mathcal{T}_1$ is the set of all the spanning trees of $\mathcal{G}$. Each term of the sum corresponds to a spanning tree $\mathcal{T}$ and is equal to the product of the Feynman parameters that are associated with the edges removed from $\mathcal{G}$ to obtain $\mathcal{T}$. The second Symanzik polynomial can instead be written as

$$\mathcal{F}(\boldsymbol{\alpha}) = \sum_{\mathcal{T} \in \mathcal{T}_2} \left(\prod_{i \notin \mathcal{T}} \alpha_i\right) t_{\mathcal{T}} - \mathcal{U}(\boldsymbol{\alpha}) \sum_{i=1}^{E} (m_i^2 - i\varepsilon)\,. \tag{2.54}$$

Here, $\mathcal{T}_2$ is the set of all the graphs $\mathcal{T}$ obtained by removing edges from $\mathcal{G}$ in such a way that $\mathcal{T}$ has two (separately) connected components and no loops, while containing all the vertices of $\mathcal{G}$. For each term in the first sum, only the parameters α_i associated with the removed edges are included in the product, while $t_{\mathcal{T}}$ is the square of the total momentum

flowing through said edges. By momentum conservation, $t_{\mathcal{T}}$ only depends on the external momenta.

Note that in eq. (2.54) the Feynman prescription is enforced through the assignment of a small, negative imaginary part to the squared masses m_i^2, that can be multiplied to the polynomial $\mathcal{U}(\boldsymbol{\alpha})$. The latter is positive-definite in the integration domain, as can be readily seen from eq. (2.53). Therefore, the Feynman prescription gives the polynomial $\mathcal{F}(\boldsymbol{\alpha})$ a small, positive imaginary part,

$$\operatorname{Im}\mathcal{F}(\boldsymbol{\alpha}) = \varepsilon\,, \quad \varepsilon \to 0^+\,. \tag{2.55}$$

In the Feynman parameter representation, there is only one singular surface for the integrand, which is simply given by

$$\mathcal{F}(\boldsymbol{\alpha}) = 0\,. \tag{2.56}$$

The integration domain is bounded by the surfaces $\alpha_i = 0$, since the Dirac δ-function accounts for the upper boundaries. The equivalent of eqs. (2.40) and (2.41) corresponds to

$$\alpha_i = 0 \quad \text{or} \quad \frac{\partial}{\partial\alpha_i}\mathcal{F}(\boldsymbol{\alpha}) = 0\,. \tag{2.57}$$

There are simple cases where the Landau equations in the Feynman parameter representation can be used to estimate the leading behavior of a FI around a singularity [72, 74, 76, 77]. To see this, let us use the δ-function to express $\alpha_E = 1 - \sum_{i=1}^{E-1}\alpha_i$ and consider a singularity with

$$\begin{aligned} \alpha_i &= 0\,, \quad i = 1,\ldots,A\,, \\ \frac{\partial}{\partial\alpha_i}\mathcal{F}(\boldsymbol{\alpha}) &= 0\,, \quad i = A+1,\ldots,E-1\,. \end{aligned} \tag{2.58}$$

If these equations can be solved obtaining relations in the form

$$\alpha_i = \bar{\alpha}_i(\mathbf{s})\,, \tag{2.59}$$

we can substitute these solutions into eq. (2.56) to arrive at

$$\mathcal{F}(\bar{\boldsymbol{\alpha}}(\mathbf{s})) = 0\,, \tag{2.60}$$

which is the equation of the singular surface in the kinematic space of the kinematic invariants $\mathbf{s}$. If we Taylor expand $\mathcal{F}(\boldsymbol{\alpha})$ around $\bar{\boldsymbol{\alpha}}(\mathbf{s})$ up to the second order, we have

$$\mathcal{F}(\boldsymbol{\alpha}) \simeq \mathcal{F}(\bar{\boldsymbol{\alpha}}(\mathbf{s})) + \sum_{i=1}^{A}(\alpha_i - \bar{\alpha}_i(\mathbf{s}))\left.\frac{\partial\mathcal{F}}{\partial\alpha_i}\right|_{\boldsymbol{\alpha}=\bar{\boldsymbol{\alpha}}(\mathbf{s})} + \sum_{i,j=1}^{E-1}(\alpha_i - \bar{\alpha}_i(\mathbf{s}))(\alpha_j - \bar{\alpha}_j(\mathbf{s}))\left.\frac{\partial^2\mathcal{F}}{\partial\alpha_i\partial\alpha_j}\right|_{\boldsymbol{\alpha}=\bar{\boldsymbol{\alpha}}(\mathbf{s})}\,, \tag{2.61}$$

whose integration domain can be extended to $\alpha_i \in [0, \infty[$ without altering the singularity that arises in the neighborhood of $\boldsymbol{\alpha} = \bar{\boldsymbol{\alpha}}$. The integration shows that [72, 76, 77]

$$F^{\boldsymbol{\nu}}(\epsilon, \mathbf{s}) \sim \mathcal{F}(\bar{\boldsymbol{\alpha}}(\mathbf{s}))^{\lambda}\,, \quad \lambda = \frac{Ld - E - 1 + A}{2}\,. \tag{2.62}$$

Moreover, if one identifies $z \equiv \mathcal{F}(\bar{\boldsymbol{\alpha}}(\mathbf{s}))$ as the kinematic parameter to specify the singular surface by $z \to 0$, the Feynman prescription becomes

$$z \to z + i\varepsilon\,, \quad \varepsilon \to 0^{+}\,. \tag{2.63}$$

Note that the reasoning that led us to (2.62) is based on simplistic assumptions that may fail in many applications, as pointed out, for instance, in [78]. A more rigorous approach for investigating the behaviors of FIs around their singularities is possible with the technique of expansion by regions, whose main points are briefly described in section 3.4.2.

2.4 Differentiation

Let us consider a family of Feynman integrals

$$F^{\boldsymbol{\nu}}(\epsilon, \mathbf{s}) = \int_{k_1,\ldots,k_L} \prod_{\alpha=1}^{E} \frac{1}{D_\alpha^{\nu_\alpha}}\,, \tag{2.64}$$

where we assume that $E = E_{\max}$ and the inverse propagators D_α are linearly independent (i.e., irreducible numerators have already been introduced if necessary). In this section we show that differentiation with respect to the kinematic invariants $\mathbf{s}$ yields expressions that can be rewritten as linear combinations of integrals belonging to the same family and, more specifically, to the sector $\sigma(F^{\boldsymbol{\nu}})$ and its sub-sectors.

This result is straightforward for derivatives with respect to the squared mass of one or more propagators, say m^2, which is different from the square of any of the external momenta. Inverting the order of differentiation and integration, we have

$$\frac{\partial}{\partial m^2} F^{\boldsymbol{\nu}}(\epsilon, \mathbf{s}) = \int_{k_1,\ldots,k_L} \frac{\partial}{\partial m^2} \prod_{\alpha=1}^{E} \frac{1}{D_\alpha^{\nu_\alpha}} = -\sum_{\substack{\beta=1 \\ m_\beta^2 = m^2}}^{E} \int_{k_1,\ldots,k_L} \frac{\nu_\beta}{D_\beta^{\nu_\beta+1}} \prod_{\substack{\alpha=1 \\ \alpha\neq\beta}}^{E} \frac{1}{D_\alpha^{\nu_\alpha}}\,, \tag{2.65}$$

which is a linear combination of FIs of the same family, each one having one of the propagators of mass m^2 with power raised by one. In particular, the integrals on the right-hand side belong to the sector of $F^{\boldsymbol{\nu}}(\epsilon, \mathbf{s})$, since raising a non-zero propagator power by one unit does not change the sector.

Now let us consider the derivative with respect to an external kinematic invariant. As pointed out in section 2.2, we can always choose a set of independent invariants of the form $y_{ij} = p_i \cdot p_j$ (including $i = j$ to take into account external masses for off-shell momenta). Therefore, it is sufficient to compute the derivatives $\partial_{y_{ij}}$ and then the derivative with respect to any other set of independent invariants can be obtained as for a linear change of coordinates.

Although FIs depend only on the kinematic invariants, this is only true at the integral level. Upon interchanging the order of differentiation and integration though, the derivative $\partial_{y_{ij}}$ is led to act on the integrand, which also depends on scalar products of external and loop momenta. It is therefore useful to express $\partial_{y_{ij}}$ in terms of the derivatives with respect to individual momenta p_i or p_j. Starting with the ansatz

$$\frac{\partial}{\partial(p_i \cdot p_j)} = \sum_{k=1}^{N-1} a_k^{(i,j)} p_k \cdot \frac{\partial}{\partial p_i} \equiv \mathcal{D}^{(i)}_{\mathbf{a}^{(i,j)}} , \tag{2.66}$$

we can make the right-hand side act on scalar products $p_m \cdot p_n$,

$$\mathcal{D}^{(i)}_{\mathbf{a}^{(i,j)}}(p_m \cdot p_n) = \sum_{k=1}^{N-1} a_k^{(i,j)} p_k \cdot \frac{\partial}{\partial p_i}(p_m \cdot p_n) = \sum_{k=1}^{N-1} a_k^{(i,j)} (\delta_{im} p_k \cdot p_n + \delta_{in} p_k \cdot p_m) , \tag{2.67}$$

and impose that the result, for $i \neq j$ (the case $i = j$ is considered later on), is equal to

$$\frac{\partial}{\partial(p_i \cdot p_j)}(p_m \cdot p_n) = \delta_{im}\delta_{jn} + \delta_{in}\delta_{jm} , \quad i \neq j . \tag{2.68}$$

We thus obtain linear constraints for the unknown coefficients $a_k^{(i,j)}$,

$$\sum_{k=1}^{N-1} a_k^{(i,j)} p_k \cdot p_n = \delta_{jn} , \quad i \neq j . \tag{2.69}$$

The reasoning behind this procedure is that, being a differential operator, $\mathcal{D}^{(i)}_{\mathbf{a}^{(i,j)}}$ acts on a function $f(\mathbf{y})$ as

$$\mathcal{D}^{(i)}_{\mathbf{a}^{(i,j)}} f(\mathbf{y}) = \sum_{mn} \left(\frac{\partial f(\mathbf{y})}{\partial y_{mn}} \right) \mathcal{D}^{(i)}_{\mathbf{a}^{(i,j)}} y_{mn} , \tag{2.70}$$

which corresponds to the result that $\partial_{p_i \cdot p_j}$ would produce, provided that $\mathcal{D}^{(i)}_{\mathbf{a}^{(i,j)}}$ acts on the scalar products y_{mn} in the same way as $\partial_{p_i \cdot p_j}$ does.

Note that, imposing eq. (2.68), we implicitly assume that $f(\mathbf{y})$ has already been expressed as a function of the independent invariants only. The number of linear constraints

obtained in this way may be less than the number of unknown coefficients $a_k^{(i,j)}$, meaning that more than one solution is up to the task. For instance, a solution to eq. (2.69) is given by $a_k^{(i,j)} = (\mathbb{G}^{-1})_{kj}$, where $\mathbb{G}$ is the Gram matrix of the first $N-1$ momenta. This solution leads to

$$\frac{\partial}{\partial(p_i \cdot p_j)} = \sum_{k=1}^{N-1} (\mathbb{G}^{-1})_{kj}\, p_k \cdot \frac{\partial}{\partial p_i} \,. \tag{2.71}$$

By $i \leftrightarrow j$ symmetry, if we had chosen the ansatz

$$\frac{\partial}{\partial(p_i \cdot p_j)} = \sum_{k=1}^{N-1} a_k^{(j,i)} p_k \cdot \frac{\partial}{\partial p_j} \equiv \mathcal{D}^{(j)}_{\mathbf{a}^{(j,i)}} \,, \tag{2.72}$$

we would have obtained

$$\frac{\partial}{\partial(p_i \cdot p_j)} = \sum_{k=1}^{N-1} (\mathbb{G}^{-1})_{ki}\, p_k \cdot \frac{\partial}{\partial p_j} \,. \tag{2.73}$$

Finally, when $i = j$, eq. (2.68) has to be replaced with

$$\frac{\partial}{\partial(p_i^2)}(p_m \cdot p_n) = \delta_{im}\delta_{in} \,, \tag{2.74}$$

so that the derivative is equal to

$$\frac{\partial}{\partial(p_i^2)} = \frac{1}{2} \sum_{k=1}^{N-1} (\mathbb{G}^{-1})_{ki}\, p_k \cdot \partial_{p_i} \,. \tag{2.75}$$

In order to see how this works in practice, let us consider a four-point function with massless external momenta p_i, $i = 1, \ldots, 4$. If we set on-shell conditions $p_i^2 = 0$ and impose momentum conservation as $p_4 = -p_1 - p_2 - p_3$, we are left with three Mandelstam invariants $s = 2p_1 \cdot p_2$, $t = 2p_2 \cdot p_3$, $u = 2p_1 \cdot p_3$, related by $s + u + t = 0$. Then a possible choice is to substitute $u = -s - t$, that is, for each function $f(s,t,u)$ of interest, we define

$$g(s,t) \equiv f(s,t,u)\Big|_{u=-s-t} \tag{2.76}$$

as the actual target of the differentiation with respect to s and t. An ansatz for ∂_s reads

$$\frac{\partial}{\partial s} = \frac{1}{2}\left(a_1^{(1,2)} p_1 + a_2^{(1,2)} p_2 + a_3^{(1,2)} p_3\right) \cdot \frac{\partial}{\partial p_1} \equiv \frac{1}{2}\,\mathcal{D}^{(1)}_{\mathbf{a}^{(1,2)}} \,. \tag{2.77}$$

Since by construction $\mathcal{D}^{(1)}_{\mathbf{a}^{(1,2)}} t = 0$, the only constraint to be satisfied is

$$1 = \frac{\partial}{\partial s}(2p_1 \cdot p_2) = \frac{1}{2}\mathcal{D}^{(1)}_{\mathbf{a}^{(1,2)}}(2p_1 \cdot p_2) = \frac{1}{2}\left[a_1^{(1,2)} s + a_3^{(1,2)} t\right] \,. \tag{2.78}$$

Therefore, there is a two-parameter family of solutions given by $a_1^{(1,2)} = (2 - a_3^{(1,2)})/s$ for any $a_2^{(1,2)}$, $a_3^{(1,2)}$. As discussed above, one of the solutions is given by

$$a_1^{(1,2)} = (\mathbb{G}^{-1})_{2,1} = \frac{1}{s}\,, \qquad a_2^{(1,2)} = (\mathbb{G}^{-1})_{2,2} = \frac{s+t}{st}\,, \qquad a_3^{(1,2)} = (\mathbb{G}^{-1})_{2,3} = \frac{1}{t}\,. \tag{2.79}$$

To highlight the importance of substituting $u = -s - t$ (corresponding to $p_1 \cdot p_3 = -p_1 \cdot p_2 - p_2 \cdot p_3$) *before* differentiating, note that any $p_1 \cdot p_3$ left in the integrand would lead to the wrong result, since

$$\frac{1}{2}\mathcal{D}^{(1)}_{(\mathbb{G}^{-1}_{2,1},\mathbb{G}^{-1}_{2,2},\mathbb{G}^{-1}_{2,3})}(p_1 \cdot p_3) = \frac{1}{2}\sum_{k=1}^{3}\mathbb{G}^{-1}_{2k}\,p_k \cdot p_3 = \frac{1}{2}\sum_{k=1}^{3}\mathbb{G}^{-1}_{2k}\mathbb{G}_{k3} = \frac{1}{2}\delta_{2,3} = 0\,, \tag{2.80}$$

while we should have

$$\frac{\partial}{\partial s}(p_1 \cdot p_3)\Big|_{u=-s-t} = \frac{\partial}{\partial s}\left(-\frac{s+t}{2}\right) = -\frac{1}{2}\,. \tag{2.81}$$

More generally, the solution corresponding to the Gram inverse matrix ends up satisfying eq. (2.68) for all the scalar products, even those that should be expressed in terms of the independent ones and might therefore have non-zero derivatives.

It is interesting to note that one could actually use eq. (2.81) as an additional constraint to obtain an alternative solution that, by construction, would work even when acting on $p_1 \cdot p_3$. In order to fix all the unknown coefficients and find such a solution, let us use a third condition as well, i.e., $\partial_s p_1^2 = 0$, a constraint incidentally satisfied by the Gram solution in eq. (2.79) as well. We obtain [47]

$$a_1^{(1,2)} = \frac{2s+t}{2s(s+t)}\,, \qquad a_2^{(1,2)} = \frac{1}{2s}\,, \qquad a_3^{(1,2)} = \frac{1}{2(s+t)}\,. \tag{2.82}$$

The difference between this and the Gram solution can be interpreted as follows: the action of the Gram solution on a function $f(s,t,u)$, where $u = -s - t$ is substituted only after the differentiation, corresponds to the first contribution on the right-hand side of

$$\frac{\partial}{\partial s}g(s,t) = \frac{\partial}{\partial s}f(s,t,-s-t) = \left[\frac{\partial}{\partial s}f(s,t,u) - \frac{\partial}{\partial u}f(s,t,u)\right]_{u=-s-t}\,, \tag{2.83}$$

while the second contribution, which is accounted for by the solution in eq. (2.82), acts as a correction

$$(\mathbb{G}^{-1})_{2k} \to (\mathbb{G}^{-1})_{2k} - (\mathbb{G}^{-1})_{3k} \tag{2.84}$$

to keep the derivative on $u = -s - t$. However, since $\partial_{p_2}(p_1 \cdot p_3) = 0$, a solution satisfying eq. (2.81) cannot be found using the $1 \leftrightarrow 2$ ansatz $D^{(2)}_{\mathbf{a}^{(2,1)}}$ proportional to ∂_{p_2}.

Once the derivative with respect to an external invariant has been expressed as in eq. (2.66) and proper values have been assigned to the coefficients $a_k^{(i,j)}$, one can operate on a FI exchanging the order of integration and differentiation,

$$\begin{aligned}\frac{\partial}{\partial(p_i\cdot p_j)}F^{\boldsymbol{\nu}}(\epsilon,\mathbf{s}) &= \sum_{k=1}^{N-1} a_k^{(i,j)} p_k \cdot \int_{k_1,\dots,k_L} \frac{\partial}{\partial p_i}\prod_{\alpha=1}^{E}\frac{1}{D_\alpha^{\nu_\alpha}} \\ &= -\sum_{k=1}^{N-1}\sum_{\beta=1}^{E} a_k^{(i,j)} p_k \cdot \int_{k_1,\dots,k_L}\left(\frac{\partial D_\beta}{\partial p_i}\right)\frac{\nu_\beta}{D_\beta^{\nu_\beta+1}}\prod_{\substack{\alpha=1\\\alpha\neq\beta}}^{E}\frac{1}{D_\alpha^{\nu_\alpha}}\,. \end{aligned} \tag{2.85}$$

Here, the terms $p_k\cdot\partial_{p_i}D_\beta$ are linear combinations of scalar products involving external and loop momenta, as it can be seen by acting with ∂_{p_i} on eq. (2.10). The products that do not depend on loop momenta are kinematic factors, while the others can be expressed, via eq. (2.12), as a linear combination of inverse propagators and kinematic factors. The result has the form

$$p_k\cdot\partial_{p_i}D_\beta = \sum_{j=1}^{S} b_{k,i,\beta,j}s_j + \sum_{\gamma=1}^{E} c_{k,i,\beta,\gamma}D_\gamma\,, \tag{2.86}$$

with $b_{k,i,\beta,j}$ and $c_{k,i,\beta,\gamma}$ being rational numbers, so that $\partial_{(p_i\cdot p_j)}F^{\boldsymbol{\nu}}$ can be manifestly written as a linear combination of integrals of the same family,

$$\begin{aligned}\frac{\partial}{\partial(p_i\cdot p_j)}F^{\boldsymbol{\nu}}(\epsilon,\mathbf{s}) = -\sum_{k=1}^{N-1}\sum_{\beta=1}^{E} a_k^{(i,j)}\nu_\beta\Bigg[&\left(\sum_{h=1}^{S} b_{k,i,\beta,h}s_h\right)\int_{k_1,\dots,k_L}\frac{1}{D_\beta^{\nu_\beta+1}}\prod_{\substack{\alpha=1\\\alpha\neq\beta}}^{E}\frac{1}{D_\alpha^{\nu_\alpha}} \\ &+\sum_{\gamma=1}^{E} c_{k,i,\beta,\gamma}\int_{k_1,\dots,k_L}\frac{D_\gamma}{D_\beta^{\nu_\beta+1}}\prod_{\substack{\alpha=1\\\alpha\neq\beta}}^{E}\frac{1}{D_\alpha^{\nu_\alpha}}\Bigg]\,. \end{aligned} \tag{2.87}$$

In particular, the terms on the right-hand side belong either to the sector $\sigma(F^{\boldsymbol{\nu}})$ or to its sub-sectors. Indeed, raising a non-zero propagator power by one unit, the sector does not change while, if we lower a power by one unit, we move to a sub-sector if that power was 1 or stay in the same sector otherwise.

2.5 Integration-by-parts identities

Feynman integrals of the same integral family obey linear relations whose coefficients are rational functions of the space-time dimension and the kinematic invariants. These relations are called *Integration-By-Parts* (IBP) identities and are derived from the absence

of boundary terms for dimensionally regulated integrals, i.e., from

$$\int_k \frac{\partial}{\partial k^\mu}\Big[v^\mu f(k)\Big] = 0\,, \tag{2.88}$$

where v can be either the loop momentum k or any other momentum that the function f depends on. For $v \neq k$, this is related to translation invariance in dimensional regularization,

$$\int_k f(k) = \int_k f(k+\lambda p)\,. \tag{2.89}$$

In fact, expanding the right-hand side for small λ,

$$\int_k f(k+\lambda p) = \int_k f(k) + \lambda \int_k p^\mu \frac{\partial}{\partial k^\mu} f(k) + \mathcal{O}(\lambda^2)\,, \tag{2.90}$$

and imposing the equality in eq. (2.89), we obtain eq. (2.88) for $v = p$. On the other hand, if v is the loop momentum k we can apply the same reasoning to the scaling property

$$\int_k f(k) = (1+\lambda)^d \int_k f(k+\lambda k)\,, \tag{2.91}$$

whose right-hand side expands to

$$\begin{aligned}(1+\lambda)^d \int_k f(k+\lambda k) &= \big[1+\lambda\, d + \mathcal{O}(\lambda^2)\big] \int_k \left[f(k) + \lambda\, k^\mu \frac{\partial}{\partial k^\mu} f(k) + \mathcal{O}(\lambda^2)\right] \\ &= \int_k f(k) + \lambda \int_k \frac{\partial}{\partial k^\mu}\Big[k^\mu f(k)\Big] + \mathcal{O}(\lambda^2)\,,\end{aligned} \tag{2.92}$$

and leads us to eq. (2.88) for $v = k$ once eq. (2.91) is imposed. In eq. (2.92) we used

$$\frac{\partial}{\partial k^\mu}\Big[k^\mu f(k)\Big] = k^\mu \frac{\partial}{\partial k^\mu} f(k) + f(k)\, d\,. \tag{2.93}$$

When applied to multi-loop FIs, IBP identities read

$$\int_{k_1,\ldots,k_L} \frac{\partial}{\partial k_i^\mu}\left[v_j^\mu \prod_{\alpha=1}^{E} \frac{1}{D_\alpha^{\nu_\alpha}}\right] = 0\,, \tag{2.94}$$

where v_j can be either a loop momentum k_j or an external momentum p_j. On a broader level, the operators $O_{ij} \equiv \partial_{k_i} v_j$ are associated with the infinitesimal transformations $k_i \to k_i + \lambda v_j$ and close the Lie algebra

$$[O_{ij}, O_{hk}] = \delta_{ik} O_{jh} - \delta_{jh} O_{ik}\,. \tag{2.95}$$

They are the generators of the group of linear changes of variables

$$k_i \to \mathbb{A}_{ij} k_j + \mathbb{B}_{ij} p_j, \qquad \det \mathbb{A} \neq 0\,. \tag{2.96}$$

In order to make explicit the action of the operator O_{ij} on the integrand of a FI, let us use eq. (2.93) to write $O_{ij} = \delta_{ij} d + v_j \partial_{k_i}$. Then we have

$$\begin{aligned} 0 &= \int_{k_1,\dots,k_L} \left(\delta_{ij} d + v_j \frac{\partial}{\partial k_i}\right) \prod_{\alpha=1}^{E} \frac{1}{D_\alpha^{\nu_\alpha}} \\ &= \delta_{ij} d \int_{k_1,\dots,k_L} \prod_{\alpha=1}^{E} \frac{1}{D_\alpha^{\nu_\alpha}} - \sum_{\beta=1}^{E} v_j \cdot \int_{k_1,\dots,k_L} \left(\frac{\partial D_\beta}{\partial k_i}\right) \frac{\nu_\beta}{D_\beta^{\nu_\beta+1}} \prod_{\substack{\alpha=1 \\ \alpha\neq\beta}}^{E} \frac{1}{D_\alpha^{\nu_\alpha}}\,. \end{aligned} \tag{2.97}$$

Here, every factor $v_j \cdot \partial_{k_i} D_\beta$ can be expressed as a linear combination of inverse propagators and kinematic factors. In particular

$$v_j \cdot \frac{\partial D_\beta}{\partial k_i} = v_j \cdot \sum_{k=1}^{L+N-1} \left(\frac{\partial D_\beta}{\partial x_{ik}}\right) \left(\frac{\partial x_{ik}}{\partial k_i}\right) = \sum_{k=1}^{L+N-1} (1+\delta_{ik})\, \mathbb{M}_{\beta,ik}\, x_{kj}\,, \tag{2.98}$$

where it is understood that x_{kj} is substituted with x_{jk} as soon as $k > j$. Then, if $j \leq L$ (i.e., v_j is a loop momentum) all the scalar products x_{kj} can be written in terms of the inverse propagators D_γ using eq. (2.12). Otherwise, when $j > L$ (i.e., v_j is an external momentum) the products x_{jk} with $k > L$ are just external kinematic factors y_{jk} and we can leave them as they are, using eq. (2.12) only for $k < L$. Ultimately we have

$$v_j \cdot \frac{\partial D_\beta}{\partial k_i} = \begin{cases} \displaystyle\sum_{k=1}^{L+N-1} \sum_{\gamma=1}^{E} (1+\delta_{ik})\, \mathbb{M}_{\beta,ik}\, \mathbb{M}^{-1}_{kj,\gamma} \left(D_\gamma + \widetilde{m}_\gamma^2\right)\,, & j \leq L\,, \\ \displaystyle\sum_{k=1}^{L} \sum_{\gamma=1}^{E} (1+\delta_{ik})\, \mathbb{M}_{\beta,ik}\, \mathbb{M}^{-1}_{kj,\gamma} \left(D_\gamma + \widetilde{m}_\gamma^2\right) + \sum_{k=1}^{N-1} \mathbb{M}_{\beta,ik}\, y_{k,j-L}\,, & j > L\,. \end{cases} \tag{2.99}$$

Substituting eq. (2.99) into the right-hand side of eq. (2.97) we obtain several terms, but it is clear that the resulting expression is a linear combination of FIs with different propagator powers where, as anticipated, the coefficients are rational functions of the space-time dimension and the kinematic factors. To be more specific, using $\boldsymbol{\nu}$ as *seed* as we just did, we end up with a linear relation involving the original FI with unchanged powers, FIs with a non-zero power that is raised by one unit and others that also have a power lowered by one unit. These are all integrals that belong to the sector of the original FI or to its sub-sectors, since propagators that were not there from the beginning cannot show up with a positive power.

By varying i, j and the seed $\boldsymbol{\nu}$, one is able to build a system of many IBP identities and it can be proved that the maximum number of independent FIs is finite [79]. This means that, for a given family, we can find a basis with a finite number of independent FIs and use IBP identities iteratively to express every member of the family as a linear combination of the element of the basis, which are called *Master Integrals* (MIs). If $\mathbf{I}(\epsilon, \mathbf{s})$ denotes such a basis, we have

$$F^{\boldsymbol{\nu}}(\epsilon, \mathbf{s}) = \mathbf{C}(\boldsymbol{\nu}; \epsilon, \mathbf{s}) \cdot \mathbf{I}(\epsilon, \mathbf{s}) = \sum_{k=1}^{I} C_k(\boldsymbol{\nu}; \epsilon, \mathbf{s})\, I_k(\epsilon, \mathbf{s})\,, \tag{2.100}$$

where I is the number of MIs and $\mathbf{C}(\boldsymbol{\nu}; \epsilon, \mathbf{s})$ is a vector of rational functions. The task of computing FIs is therefore reduced to that of evaluating MIs.

The procedure described above is often referred to as IBP reduction and can be cumbersome as the number of equations involved is usually very large. The Laporta algorithm [29] makes it possible to perform the reduction in a systematic way, collecting IBP identities that are then solved via Gauss elimination. Many computer implementations of this method are publicly available [80–86].

There are also other linear relations that FIs satisfy and are often used. For instance, as FIs are Lorentz scalars, they do not change if we apply a Lorentz transformation to the external momenta. Therefore, tensor identities can be obtained by acting on a FI with the generators of Lorentz transformations in the space of functions depending on the external momenta:

$$L_{\mu\nu} F^{\boldsymbol{\nu}}(\epsilon, \mathbf{s}) \equiv \sum_{k=1}^{N-1} \left[p_{k\mu} \frac{\partial}{\partial p_k^{\nu}} - p_{k\nu} \frac{\partial}{\partial p_k^{\mu}} \right] F^{\boldsymbol{\nu}}(\epsilon, \mathbf{s}) = 0\,. \tag{2.101}$$

This tensor equation is antisymmetric in the Lorentz indices (μ, ν) and, once contracted with all the possible antisymmetric tensors built with the external momenta, generates the scalar equations

$$(p_i^{\mu} p_j^{\nu} - p_i^{\nu} p_j^{\mu}) L_{\mu,\nu} F^{\boldsymbol{\nu}}(\epsilon, \mathbf{s}) = 0\,, \tag{2.102}$$

which contains differential operators in the form $p_i \cdot \partial_{p_j}$. As shown in section 2.4, the action of these operators on a FI generate linear combinations of FIs of the same family. The resulting relations are called *Lorentz invariance* identities, which end up being linear combinations of IBP identities [87].

FIs are homogeneous functions of the external momenta p_i and the independent propagator masses m_α of degree $L\,d - 2\sum_k \nu_k$, that is,

$$F^{\boldsymbol{\nu}}(\epsilon, \lambda p_1, \dots, \lambda m_1, \dots) = \lambda^{(dL - 2\sum_k \nu_k)} F^{\boldsymbol{\nu}}(\epsilon, p_1, \dots, m_1, \dots)\,, \tag{2.103}$$

which implies (through the Euler's theorem for homogeneous functions)

$$\left(\sum_i p_i \cdot \frac{\partial}{\partial p_i} + \sum_\alpha m_\alpha \frac{\partial}{\partial m_\alpha} - L\,d + \sum_k \nu_k\right) F^{\boldsymbol{\nu}}(\epsilon, p_1, \dots, m_1, \dots) = 0\,. \tag{2.104}$$

Here, we can substitute $m_\alpha \partial_{m_\alpha} = 2m_\alpha^2 \partial_{m_\alpha^2}$, while the action of the derivative with respect to a squared mass is shown in eq. (2.65). Once again, we can compute the derivatives on the left-hand side explicitly, obtaining linear relations denoted as *homogeneity identities*. These result to be linear combinations of IBP identities as well [68].

It is worth mentioning also the so-called *symmetry identities* that are useful when performing IBP reduction. These are originated when a change of variable belonging to the group in eq. (2.96) (but with $\det \mathbb{A} = 1$ to avoid the Jacobian factor and possibly with permutations of the external momenta that preserve the kinematic invariants) relates FIs of the same sector (*sector symmetries*) or of different sectors (*sector mappings*) [88]. Symmetries of this kind may be related, for instance, to the possible choices for the routing of the loop momenta in the graphs associated to the integrals.

2.6 Building systems of differential equations

As pointed out in section 2.5, the evaluation of a finite number of master integrals for a given integral family allows us to determine, via integration-by-parts reduction, the value of all the integrals of the family. We now show how the methods discussed in sections 2.4 and 2.5 can be combined to close a system of differential equations whose unknown functions are the MIs themselves.

Suppose $\mathbf{I}(\epsilon, \mathbf{s})$ is a basis of MIs for the integral family of eq. (2.64). As shown in section 2.4, differentiation with respect to the kinematic invariants can be carried out as in eq. (2.65), for derivatives with respect to squared masses, and eq. (2.87) for derivatives with respect to scalar products. In any case, the result is a linear combination of FIs of the same family,

$$\frac{\partial}{\partial s_i} I_j(\epsilon, \mathbf{s}) = \sum_k R_{ijk}(\epsilon, \mathbf{s}) F^{\boldsymbol{\nu}_{ijk}}(\epsilon, \mathbf{s})\,, \tag{2.105}$$

where the coefficients $R_{ijk}(\epsilon, \mathbf{s})$ are rational functions. On the other hand, IBP reduction allows us to expand the integrals $F^{\boldsymbol{\nu}_{ijk}}(\epsilon, \mathbf{s})$ in the basis $\mathbf{I}(\epsilon, \mathbf{s})$ as

$$F^{\boldsymbol{\nu}_{ijk}}(\epsilon, \mathbf{s}) = \sum_h C_h(\boldsymbol{\nu}_{ijk}; \epsilon, \mathbf{s})\, I_h(\epsilon, \mathbf{s})\,, \tag{2.106}$$

which, substituted back into eq. (2.105), leads to

$$\frac{\partial}{\partial s_i} I_j(\epsilon, \mathbf{s}) = \sum_{k,h} R_{ijk}(\epsilon, \mathbf{s})\, C_h(\boldsymbol{\nu}_{ijk}; \epsilon, \mathbf{s})\, I_h(\epsilon, \mathbf{s})\,. \tag{2.107}$$

If we define the matrices $\mathbb{A}_i(\epsilon, \mathbf{s})$ with elements given by the rational functions

$$(\mathbb{A}_i)_{jh}(\epsilon, \mathbf{s}) \equiv \sum_k R_{ijk}(\epsilon, \mathbf{s})\, C_h(\boldsymbol{\nu}_{ijk}; \epsilon, \mathbf{s})\,, \tag{2.108}$$

we can rewrite eq. (2.107) in matrix form as

$$\frac{\partial}{\partial s_i}\mathbf{I}(\epsilon, \mathbf{s}) = \mathbb{A}_i(\epsilon, \mathbf{s})\mathbf{I}(\epsilon, \mathbf{s})\,, \tag{2.109}$$

and in terms of the total differential $d = \sum_i ds_i\, \partial_{s_i}$ as

$$d\,\mathbf{I}(\epsilon, \mathbf{s}) = d\mathbb{A}(\epsilon, \mathbf{s})\mathbf{I}(\epsilon, \mathbf{s})\,. \tag{2.110}$$

Since the partial derivatives of the solution have to commute, we must have

$$\begin{aligned} 0 &= \left[\frac{\partial^2}{\partial s_i \partial s_j} - \frac{\partial^2}{\partial s_j \partial s_i}\right]\mathbf{I}(\epsilon, \mathbf{s}) = \frac{\partial}{\partial s_i}\left[\mathbb{A}_j(\epsilon, \mathbf{s})\mathbf{I}(\epsilon, \mathbf{s})\right] - \frac{\partial}{\partial s_j}\left[\mathbb{A}_i(\epsilon, \mathbf{s})\mathbf{I}(\epsilon, \mathbf{s})\right] \\ &= \left[\frac{\partial}{\partial s_i}\mathbb{A}_j(\epsilon, \mathbf{s}) + \mathbb{A}_j(\epsilon, \mathbf{s})\mathbb{A}_i(\epsilon, \mathbf{s}) - \frac{\partial}{\partial s_j}\mathbb{A}_i(\epsilon, \mathbf{s}) - \mathbb{A}_i(\epsilon, \mathbf{s})\mathbb{A}_j(\epsilon, \mathbf{s})\right]\mathbf{I}(\epsilon, \mathbf{s})\,, \end{aligned}$$

where eq. (2.109) was systematically applied whenever possible. On the right-hand side of the last equality we find a matrix that has to map all possible solutions to zero. This property immediately extends to every possible vector when considering any boundary condition in any point $(\epsilon, \mathbf{s})$, meaning that the matrix itself is identically zero. The resulting constraints for the DE matrices are the *integrability conditions*

$$\frac{\partial}{\partial s_i}\mathbb{A}_j(\epsilon, \mathbf{s}) - \frac{\partial}{\partial s_j}\mathbb{A}_i(\epsilon, \mathbf{s}) - [\mathbb{A}_i(\epsilon, \mathbf{s}), \mathbb{A}_j(\epsilon, \mathbf{s})] = 0\,. \tag{2.111}$$

A further condition for the matrices $\mathbb{A}_i(\epsilon, \mathbf{s})$ follows from the homogeneity of the solution $I_k(\epsilon, \mathbf{s})$ which, in terms of the kinematic invariants, is of degree $Ld/2 - \sum_\alpha \nu_\alpha(I_k)$, where $\nu_\alpha(I_k)$ is the power of the α-th inverse propagator of the master integral I_k. Note the factor $1/2$ here compared to eq. (2.103), where the degree of homogeneity with respect to momenta is taken into account. The analog of eq. (2.104) is then given by

$$\left[\sum_{i=1}^{S} s_i \frac{\partial}{\partial s_i} - \frac{Ld}{2} + \sum_{\alpha=1}^{E} \mathrm{diag}\Big(\nu_\alpha(I_1), \nu_\alpha(I_2), \dots\Big)\right]\mathbf{I}(\epsilon, \mathbf{s}) = 0\,. \tag{2.112}$$

Again, applying the DEs (2.109) and considering any possible boundary condition in any point $(\epsilon, \mathbf{s})$, we arrive at the matrix equation

$$\sum_{i=1}^{S} s_i \mathbb{A}_i(\epsilon, \mathbf{s}) - \frac{Ld}{2}\mathbb{1} + \sum_{\alpha=1}^{E} \mathrm{diag}\Big(\nu_\alpha(I_1), \nu_\alpha(I_2), \dots\Big) = 0\,. \tag{2.113}$$

The conditions in eqs. (2.111) and (2.113) only depend on the DE matrices and do not require to know the solution beforehand. For this reason and for their simplicity they are often used as a sanity check when building the system of DEs.

Given the partial DEs (2.109), one can consider the DE along any phase space curve $\mathbf{s}(\eta)$ with line parameter η. In fact, chain rule differentiation combined with eq. (2.109) leads to

$$\frac{\partial}{\partial\eta}\mathbf{I}(\epsilon,\mathbf{s}(\eta)) = \sum_{i=1}^{S}\frac{ds_i(\eta)}{d\eta}\left[\frac{\partial}{\partial s_i}\mathbf{I}(\epsilon,\mathbf{s})\right]_{\mathbf{s}=\mathbf{s}(\eta)} = \sum_{i=1}^{S}\frac{ds_i(\eta)}{d\eta}\mathbb{A}_i(\epsilon,\mathbf{s}(\eta))\mathbf{I}(\epsilon,\mathbf{s}(\eta))\,, \tag{2.114}$$

which, using the notation $\mathbf{I}(\epsilon,\eta)\equiv\mathbf{I}(\epsilon,\mathbf{s}(\eta))$, corresponds to the ordinary DE

$$\frac{\partial}{\partial\eta}\mathbf{I}(\epsilon,\eta) = \mathbb{A}(\epsilon,\eta)\mathbf{I}(\epsilon,\eta)\,, \quad \mathbb{A}(\epsilon,\eta)\equiv\sum_{i=1}^{S}\frac{ds_i(\eta)}{d\eta}\mathbb{A}_i(\epsilon,\mathbf{s}(\eta))\,. \tag{2.115}$$

The study of this kind of DE system is the main topic of this thesis. Indeed, if boundary conditions are available at some phase space point $\mathbf{s}_0$, we can consider a curve $\mathbf{s}(\eta)$ passing through $\mathbf{s}_0$ and solve eq. (2.115) to propagate the MIs to any other phase space point on the curve. For instance, given any target point $\mathbf{s}_1$, in LINE we build the DE along the straight line connecting the boundary and the target point, that is,

$$\mathbf{s}(\eta) = \mathbf{s}_0 + \eta\,(\mathbf{s}_1-\mathbf{s}_0)\,, \tag{2.116}$$

so that the DE matrix in eq. (2.115) is simply given by the linear combination

$$\mathbb{A}(\epsilon,\eta) = \sum_{i=1}^{S}(s_{1,i}-s_{0,i})\mathbb{A}_i(\epsilon,\,\mathbf{s}_0+\eta\,(\mathbf{s}_1-\mathbf{s}_0))\,. \tag{2.117}$$

Then, we solve the DE (2.115) via series expansion to propagate the solution from $\mathbf{s}_0$ to $\mathbf{s}_1$ along the phase space line. Since at any point the radius of convergence of the series solution is finite, we split the line as described in section 4.1 and solve in multiple propagation steps. At each iteration, we employ the techniques of sections 4.2 and 4.3 to solve around regular and singular points, respectively. In the presence of branch points, the method outlined in chapter 5 allows us to analytically continue the solution according to the Feynman prescription.

Chapter 3

Differential equations for Feynman integrals

Differential equations such as those obtained in chapter 2 can be solved along a curve in the phase space of the kinematic invariants. This provides a valid strategy for the numerical evaluation of Feynman integrals. In this chapter we analyze the structural and analytic aspects that are most relevant when finding the solution to this kind of DE system, paying attention to exposing the key concepts in a way that lends itself naturally to the algorithmic implementation in computer code.

First, in section 3.1 we address the dependence of the equations and their solutions on the regulator ϵ within the framework of dimensional regularization. The strategy adopted here consists in solving the equations for several numerical values of ϵ. The corresponding solutions can then be considered as interpolation samples for the coefficients of the Laurent expansion around $\epsilon = 0$. This procedure allows us to focus on the solution of univariate DEs whose coefficients are rational functions in the line parameter. Besides being well suited for computer implementations, this class of problems constitutes the foundation of several other numerical strategies.

The block structure of the DEs is then examined in section 3.2. A lower-triangular block disposition naturally emerges when the master integrals are ordered according to the sector hierarchy discussed in section 2.1. Each block on the diagonal corresponds to a sector of the integral family and couples only to its sub-sectors. This structure can be exploited to decompose the full system into a sequence of smaller problems of increasing complexity. To ensure that this strategy is also suitable for DEs that are not related to MIs, we discuss how it is possible to obtain the same block disposition by solely looking at the location of the non-zero elements of the DE matrix.

In section 3.3, the DEs are analyzed around their singularities. These must be regular singular points, in the neighborhood of which it is always possible to find a change of basis that transforms the system to Fuchsian form, meaning that the DE matrix in the new basis only presents simple poles around the singularity under consideration. An algorithmic

procedure is described to build such a transformation following the block structure of the DEs, thus preparing the system to be solved by means of the series expansion methods illustrated in chapter 4. Being able to solve the system around a singular point not only allows one to cross the singularity when propagating the MIs across the phase space, but it is also crucial for determining boundary conditions, which are necessary for the DE method to succeed.

Section 3.4 is indeed dedicated to the topic of BCs. Two related approaches are discussed: the AMFlow method and the technique of expansion by regions. The former is based on the introduction of an auxiliary mass in the propagators of the FIs. The mass is pushed to infinity, where the leading behaviors of the integrals are known and can be used as BCs when solving DEs with respect to the auxiliary parameter. The physical value of the original FIs is then recovered by propagating the solution to the limit where the auxiliary mass vanishes. The AMFlow method is among the most successful ways to obtain BCs, even though the introduction of an auxiliary parameter generally increases the number of MIs. However, once a boundary is obtained in a phase space point, the methods of section 4 allow its propagation to many other values of the kinematic invariants.

To analyze the infinite-mass limit, the AMFlow method relies on EBR. The latter is a technique for obtaining the asymptotic expansion of Feynman integrals near singular configurations by decomposing the integration domain into several regions, each characterized by a specific scaling of the loop momenta. In principle, the method of EBR does not require the introduction of auxiliary kinematic parameters. We discuss a few cases where EBR can be exploited to extract the leading power behaviors of the MIs and use them as BCs for the DEs. In particular we show that, for these examples, one only needs to know the powers appearing in the leading behaviors since, analyzing the DEs in the singular limit, it is possible to express the associated coefficients in terms of the MIs from the bottom sectors, which are simpler and thus are known analytically. This technique is illustrated in more detail in section 4.3.3 where, building on the tools developed throughout section 4.3, we show how to exploit the power behaviors predicted by the EBR to minimize the number of leading coefficients that must be provided as BCs in order to determine the solution.

3.1 Dependence on the dimensional regularization parameter

We consider Feynman integrals within the framework of dimensional regularization, where each integral is analytically continued to non-integer space-time dimensions $d = d_0 - 2\epsilon$, with $d_0 \in \mathbb{N}$ being the original number of dimensions and ϵ an infinitesimal regularization parameter. Infrared and ultraviolet divergences are thus regulated, so that they appear as

poles in the Laurent series of the integrals around $\epsilon = 0$. Therefore, when propagating a set of master integrals $\mathbf{I}(\epsilon, \eta)$ along a phase space line, the target quantities are the coefficients $\mathbf{I}_k(\eta)$ of the expansion

$$\mathbf{I}(\epsilon, \eta) = \epsilon^{-2L} \sum_{k=0}^{\texttt{ord}} \mathbf{I}_k(\eta)\epsilon^k + \mathcal{O}(\epsilon^{-2L+\texttt{ord}+1}) \,, \tag{3.1}$$

to be computed up to the desired order $-2L + \texttt{ord}$. To this end, one has to deal with the dependence on the regulator ϵ. Several methods are available in the literature. For instance, one can expand the matrix $\mathbb{A}(\epsilon, \eta)$ in ϵ and solve the differential equations order by order, looking directly for the coefficients $\mathbf{I}_k(\eta)$ of the Laurent expansion of the MIs. Assuming that poles in ϵ are removed both from $\mathbb{A}(\epsilon, \eta)$ and $\mathbf{I}(\epsilon, \eta)$ by normalizing the MIs with overall powers of ϵ, we have

$$\mathbf{I}(\epsilon, \eta) = \sum_{k=0}^{\infty} \mathbf{I}_k(\eta)\epsilon^k \,, \qquad \mathbb{A}(\epsilon, \eta) = \sum_{k=0}^{\infty} \mathbb{A}_k(\eta)\epsilon^k \,. \tag{3.2}$$

Substituting these expansions into the DE (2.115), we arrive at

$$\sum_{k=0}^{\infty} \frac{d}{d\eta}\mathbf{I}_k(\eta)\epsilon^k = \sum_{i=0}^{\infty}\sum_{j=0}^{\infty} \mathbb{A}_i(\eta)\mathbf{I}_j(\eta)\epsilon^{i+j} = \sum_{k=0}^{\infty}\sum_{j=0}^{k} \mathbb{A}_{k-j}(\eta)\mathbf{I}_j(\eta)\epsilon^k \,. \tag{3.3}$$

where, in the last equality, we changed indices to introduce $k = i + j$. Therefore, at any order ϵ^k, we have the non-homogeneous DE

$$\frac{d}{d\eta}\mathbf{I}_k(\eta) = \mathbb{A}_0(\eta)\mathbf{I}_k(\eta) + \sum_{j=0}^{k-1} \mathbb{A}_{k-j}(\eta)\mathbf{I}_j(\eta) \,, \tag{3.4}$$

where the last term in the sum is separated from the others to highlight the homogeneous part of the DE. One can begin by solving the homogeneous equation for the leading-order coefficient $\mathbf{I}_0(\eta)$ and then proceed to the subsequent orders, using the solutions of the previous steps to construct the non-homogeneous term. This is the approach used, for instance, in the packages DiffExp [49] and SeaSyde [50]. Note however that the parallel computation of different orders in ϵ is not possible within this framework, as each order enters the computation of the next one.

In [89] it was suggested to look for a change of basis[1] such that the DE matrix $\widetilde{\mathbb{A}}(\epsilon, \eta)$ for the transformed integrals $\widetilde{\mathbf{I}}(\epsilon, \eta)$ is simply proportional to ϵ, that is, $\widetilde{\mathbb{A}}(\epsilon, \eta) = \epsilon\widetilde{\mathbb{A}}(\eta)$. When this is done, we say that the matrix is in ϵ-form. In this case, the expansion of

[1] The formalism for a generic change of basis is discussed in section 3.3.

$\widetilde{\mathbb{A}}(\epsilon,\eta)$ in ϵ only contains the order ϵ, with $\widetilde{\mathbb{A}}_1(\eta) = \widetilde{\mathbb{A}}(\eta)$. Moreover, being $\widetilde{\mathbb{A}}_0(\eta) = 0$, we see from eq. (3.4) that the solution is given in terms of iterated integrals as in

$$\begin{aligned}\widetilde{\mathbf{I}}_k(\eta) &= \widetilde{\mathbf{I}}_k(0) + \int_0^\eta d\eta_1\, \widetilde{\mathbb{A}}(\eta_1)\widetilde{\mathbf{I}}_{k-1}(\eta_1) \\ &= \widetilde{\mathbf{I}}_k(0) + \int_0^\eta d\eta_1\, \widetilde{\mathbb{A}}(\eta_1)\widetilde{\mathbf{I}}_{k-1}(0) + \int_0^\eta d\eta_1\, \widetilde{\mathbb{A}}(\eta_1) \int_0^{\eta_1} d\eta_2\, \widetilde{\mathbb{A}}(\eta_2)\widetilde{\mathbf{I}}_{k-2}(\eta_2) = \dots \\ &= \widetilde{\mathbf{I}}_k(0) + \sum_{j=1}^{k} \int_0^\eta d\eta_1\, \widetilde{\mathbb{A}}(\eta_1) \int_0^{\eta_1} d\eta_2\, \widetilde{\mathbb{A}}(\eta_2) \cdots \int_0^{\eta_{j-1}} d\eta_j\, \widetilde{\mathbb{A}}(\eta_j)\widetilde{\mathbf{I}}_{k-j}(0)\,, \end{aligned} \tag{3.5}$$

where the leading-order coefficient is a constant, $\widetilde{\mathbf{I}}_0(\eta) = \widetilde{\mathbf{I}}_0(0)$. In terms of the kinematic invariants, the ϵ-form of the DEs can be written as

$$d\widetilde{\mathbf{I}}(\epsilon,\mathbf{s}) = \epsilon\, d\widetilde{\mathbb{A}}(\mathbf{s})\widetilde{\mathbf{I}}(\epsilon,\mathbf{s})\,, \tag{3.6}$$

and the solution formally corresponds to the path-ordered integral

$$\widetilde{\mathbf{I}}(\epsilon,\mathbf{s}(\eta)) = \mathcal{P}\exp\left[\epsilon \int_{\mathbf{s}(\eta)} d\widetilde{\mathbb{A}}\right] \widetilde{\mathbf{I}}(\epsilon,\mathbf{s}(0))\,. \tag{3.7}$$

One can try to transform the DEs in *canonical form*. In this representation, the total differential $d\widetilde{\mathbb{A}}(\mathbf{s})$ is given by

$$d\widetilde{\mathbb{A}}(\mathbf{s}) = \sum_k \widetilde{\mathbb{A}}_k\, \omega_k(\mathbf{s})\,, \tag{3.8}$$

where the $\omega_k(\mathbf{s})$'s are differential one-forms with at most simple poles. For instance, if the integrals correspond to polylogarithms, the one-forms are logarithmic, meaning that $\omega_k(\mathbf{s}) = d\log\alpha_k(\mathbf{s})$. The differentials $d\log\alpha_k(\mathbf{s})$ are called *letters*, while the set of independent letters is naturally referred to as the *alphabet*. In case the canonical form is obtainable with rational transformations, the functions $\alpha_k(\mathbf{s})$ are rational as well; otherwise, they are algebraic functions (which typically is the case for integrals with massive lines).

Finding a basis where the DEs are in canonical form is not always possible. It can happen that $\widetilde{\mathbb{A}}(\epsilon,\eta) = \widetilde{\mathbb{A}}_0(\eta) + \epsilon\widetilde{\mathbb{A}}_1(\eta)$ but the constant term $\widetilde{\mathbb{A}}_0(\eta)$ cannot be set to zero and gives rise to elliptic integrals [90–93].

To handle the dependence on the regulator ϵ, LINE follows the strategy proposed in [53] instead. The DE (2.115) is solved for different numerical values ϵ_1, ϵ_2, ... of the parameter ϵ and the coefficients of the Laurent expansion are interpolated at the desired precision from the results $\mathbf{I}(\epsilon_1)$, $\mathbf{I}(\epsilon_2)$, ... obtained for each sample value. The numerical setup implemented for this task is the one chosen for the AMFlow package presented in [53]. The interpolation of the ϵ-orders is described in detail in appendix A.2.

The main advantage of this procedure is that, for each value $\epsilon = \epsilon_i$, eq. (2.115) turns into a univariate problem and hence becomes much simpler to solve numerically. Furthermore, the computations at different values of ϵ are completely independent and can thus be carried out in parallel in a computer program implementation. Overall, we trade a two-variable problem for a set of multiple independent univariate problems with equal complexity. When higher orders are required for the Laurent expansion in eq. (3.1), it is sufficient to increase the working precision and perform the computation at more values of ϵ. Provided that enough computational resources are available, the conceptual complexity of the calculation remains the same.

It should be noted, however, that the price to pay for using this approach is that boundary conditions are required at arbitrary precision for the numerical values $\epsilon = \epsilon_i$, as opposed to only knowing their expansion up to the desired order. For instance, the AMFlow method described in section 3.4.1 allows one to generate boundary integrals working directly at $\epsilon = \epsilon_i$, since the behaviors of the integrals in the infinite-mass limit can be reconstructed through closed-form expressions in ϵ.

For ease of notation, in the rest of the work we often omit the dependence of any quantity on the regularization parameter ϵ, assuming that it has been fixed to a numerical value, and focus on the dependence on the line parameter η. We emphasize that the DE matrix elements are rational functions in η and so are particularly suited for computer implementations based on low-level programming languages. For instance, in LINE several routines are implemented to perform basic polynomial operations such as sums, products, simplifications or the computation of the polynomial least common multiple. Everything is done by solely looking at the coefficients of the polynomials in the numerators and at the roots of the denominators, which can be efficiently found numerically at arbitrary precision. More details on this point are given in appendix A.1.

Note that the formalism illustrated in this thesis can be employed in general to solve systems of ordinary DEs whose coefficients are rational functions and for which the non-homogeneous term has the same kind of series expansion as the solution. Therefore, it is well suited for DEs such as those in eq. (3.4) as well.

3.2 Block structure

As pointed out in section 2.4, the derivative of a Feynman integral is a linear combination of integrals that belong to the same sector as the original integral or to its sub-sectors. In the same way, when integration-by-parts reduction is performed on these integrals, the identities that are used also relate integrals of the same sector and its sub-sectors. By applying the same reasoning to $\partial_{s_i}\mathbf{I}(\epsilon, \mathbf{s})$ in eq. (2.109), we conclude that the only non-zero elements $(\mathbb{A}_i)_{jk}$ of the differential equation matrix are those such that I_k is in the same sector as I_j or in one of its sub-sectors.

A consequence of the property noted above is that the master integrals can be ordered in such a way that the associated DE matrices $\mathbb{A}_i(\epsilon, \mathbf{s})$ are composed of blocks whose disposition is lower triangular. To achieve this, it is sufficient to choose a partial ordering $\prec$ on the set of MIs such that $I_m \prec I_n$ when $\sigma(I_m)$ is a sub-sector of $\sigma(I_n)$, while I_m and I_n are incomparable otherwise. One can order the MIs accordingly and then handle incomparable pairs by grouping together MIs of the same sector. For instance, the sector identification function ρ defined in eq. (2.21) satisfies the condition

$$I_m \prec I_n \implies \rho(I_m) < \rho(I_n)\,, \tag{3.9}$$

while also providing a way to order incomparable integrals of different sectors if the partial ordering $\prec$ is extended by considering eq. (3.9) to hold in the opposite direction as well. When doing so, the only pair of integrals that remain incomparable are those composed of integrals within the same sector, which hence are placed next to each other in this ordering. While it is possible to also introduce a further internal ordering for MIs belonging to the same sector (e.g., by ordering with respect to the sum of the positive powers and the negative sum of the negative powers), different choices would lead to the same block structure for $\mathbb{A}_i(\epsilon, \mathbf{s})$.

Now let us consider any ordering of the MIs $\mathbf{I}(\epsilon, \mathbf{s})$ that is in agreement with the sector hierarchy specified above. Since MIs of the same sectors are arranged consecutively, we can identify the r-th sector with the index b_r of the first MI falling into the sector. The number of MIs in the sector is then given by $L_r = b_{r+1} - b_r$ (where we consider $b_{r+1} = I + 1$ for the last sector, I being the number of MIs). If B is the number of sectors, any DE matrix $\mathbb{A}_i$ can be split into a $B \times B$ grid of $L_r \times L_s$ blocks $\mathbb{A}_i^{(r,s)}$ as follows:

$$\mathbb{A}_i = \begin{pmatrix} \mathbb{A}_i^{(1,1)} & \dots & \mathbb{A}_i^{(1,B)} \\ \vdots & \ddots & \vdots \\ \mathbb{A}_i^{(B,1)} & \dots & \mathbb{A}_i^{(B,B)} \end{pmatrix}, \quad \mathbb{A}_i^{(r,s)} = \begin{pmatrix} (\mathbb{A}_i)_{b_r,\,b_s} & \dots & (\mathbb{A}_i)_{b_r,\,b_s+L_s-1} \\ \vdots & \ddots & \vdots \\ (\mathbb{A}_i)_{b_r+L_r-1,\,b_s} & \dots & (\mathbb{A}_i)_{b_r+L_r-1,\,b_s+L_s-1} \end{pmatrix}, \tag{3.10}$$

namely, $\mathbb{A}_i^{(r,s)}$ is the $L_r \times L_s$ block whose top-left element has matrix indices (b_r, b_s). The blocks $\mathbb{A}_i^{(r,r)}$ on the diagonal are square $L_r \times L_r$ matrices that represent the coupling between MIs of the same sector r, while each sub-diagonal block $\mathbb{A}_i^{(r,s)}$ with $r > s$ collects, from the derivatives of the MIs belonging to sector r, the components that lie within sector s. In light of the above discussion, $\mathbb{A}_i^{(r,s)}$ with $r \neq s$ can be non-zero only if sector s is a sub-sector of sector r. With the ordering of MIs under consideration, this can occur only when $r > s$, i.e., for blocks under the diagonal. Hence $\mathbb{A}_i^{(r,s)} = 0 \;\; \forall\, r < s$, meaning that the block grid in eq. (3.10) is lower triangular.

When solving the DE (2.115) along a curve with parameter η, the lower-triangular block structure of the matrix $\mathbb{A}(\eta)$ allows us to proceed sector by sector sequentially, thus

solving a smaller problem at each step. To see how, let us denote by $\mathbf{I}^{(r)}(\eta)$ the MIs of sector r and consider the L_1 homogeneous equations for the integrals of the first sector,

$$\frac{d}{d\eta}\mathbf{I}^{(1)}(\eta) = \mathbb{A}^{(1,1)}(\eta)\mathbf{I}^{(1)}(\eta)\,. \tag{3.11}$$

If these equations are solved, we can move to the L_2 equations for the second sector,

$$\frac{d}{d\eta}\mathbf{I}^{(2)}(\eta) = \mathbb{A}^{(2,1)}(\eta)\mathbf{I}^{(1)}(\eta) + \mathbb{A}^{(2,2)}(\eta)\mathbf{I}^{(2)}(\eta)\,, \tag{3.12}$$

which are non-homogeneous because of the term $\mathbb{A}^{(2,1)}(\eta)\mathbf{I}^{(1)}(\eta)$ generated by the solution of the previous sector. By iterating this procedure, we can solve for the first $r-1$ sectors and find, for the MIs of sector r, the system of L_r non-homogeneous differential equations

$$\frac{d}{d\eta}\mathbf{I}^{(r)}(\eta) = \mathbb{A}^{(r,r)}(\eta)\mathbf{I}^{(r)}(\eta) + \mathbf{J}^{(r)}(\eta)\,, \tag{3.13}$$

where the non-homogeneous term $\mathbf{J}^{(r)}(\eta)$ is built by contracting the r-th row of sub-diagonal blocks with the solution of the previous $r-1$ sectors, namely,

$$\mathbf{J}^{(r)}(\eta) \equiv \sum_{s=1}^{r-1} \mathbb{A}^{(r,s)}(\eta)\mathbf{I}^{(s)}(\eta)\,. \tag{3.14}$$

As the elements of $\mathbb{A}(\eta)$ are rational functions, $\mathbf{J}^{(r)}(\eta)$ inherits its series expansion from the solutions of the previous $r-1$ sectors. In particular, if $\mathbb{A}(\eta)$ is regular at the expansion point, then the solution has a Taylor series and so does the non-homogeneous term. When the expansion point is a regular singularity, the expansion for the solution is shared by $\mathbf{J}^{(r)}(\eta)$ with at most a negative integer shift in the power behaviors due to the possible presence of poles in the sub-diagonal blocks $\mathbb{A}^{(r,s)}(\eta)$.

The block strategy outlined above is very useful for a computer program implementation, as it allows us to focus only on the non-zero block components of the matrix $\mathbb{A}(\eta)$. Although we trade a homogeneous problem for a set of non-homogeneous ones, the computational cost of solving via series expansion eq. (3.13) is of the same order of magnitude as the one for its associated homogeneous equation. As shown in chapter 4, the recurrence relations for the two cases are indeed the same, the only difference being that also the series coefficients of the non-homogeneous term give their contribution.

Typically, as one moves to higher sectors, the computational complexity increases progressively, as the sectors grow in size, the number of vanishing off-diagonal blocks decreases and the rational functions in the DE matrix exhibit polynomials of higher degree with new roots appearing in the denominators. On the other hand, when solving DEs

sector by sector, the solution up to any given sector does not depend on the solution of the subsequent ones. Therefore, another benefit of this approach is that it allows one to address the simplest parts of the problem first and then move progressively toward the more difficult ones. Not only does this prove to be useful for debugging, but it also paves the way for alternative propagation strategies. For instance, MIs from sub-sectors may be propagated independently using larger step sizes, since their radius of convergence is wider owing to the presence of fewer poles in the upper rows of the DE matrix.

As the methods described in this work can be used to solve also DEs whose unknown functions are not FIs, it is useful to adopt an algorithmic approach for the ordering of $\mathbf{I}(\eta)$ that does not rely on the notion of sectors or any other concept related to FIs. Such a procedure is possible by solely looking at the disposition of the non-zero elements in the matrix $\mathbb{A}(\eta)$ [49]. Indeed, we can associate with $\mathbb{A}$ a directed graph $\mathcal{A}$ such that each pair (n, m) of vertices is connected by an edge $n \to m$ if and only if $\mathbb{A}_{mn} \neq 0$. Then each vertex represents one of the unknown functions and the edges indicate which pair of functions are directly coupled through the DE, with the direction specifying which one affects the other. The edge $n \to m$ points out that I_n affects I_m, since $\partial_\eta I_m$ depends on I_n. If the edge $m \to n$ is not present, the converse is not true.

A strongly connected component $\mathcal{A}_r$ of the graph $\mathcal{A}$ is a maximal subset of vertices such that each vertex can be reached by any other through a path of directed edges. The subset must be maximal in the sense that the inclusion of any further vertex would break the property stated above. In a strongly connected component $\mathcal{A}_r$, each vertex affects all the others, even if not directly. Each $\mathcal{A}_r$ can be represented by a single vertex in the so-called condensation $\mathcal{A}^{(c)}$ of the graph $\mathcal{A}$, where an edge $s \to r$ is placed if there is a directed path connecting a vertex of $\mathcal{A}_s$ to one of $\mathcal{A}_r$ (which implies that every vertex of $\mathcal{A}_r$ is reachable by any vertex of $\mathcal{A}_s$).

Therefore, to order the unknown functions one has to assign each I_m to its strongly connected component $\sigma(I_m)$, build the condensation graph $\mathcal{A}^{(c)}$, consider $I_m \prec I_n$ if the edge $\sigma(I_m) \to \sigma(I_n)$ is present in $\mathcal{A}^{(c)}$ (i.e., if there is a directed path from I_m to I_n), and place next to each other functions belonging to the same component. The parallel between the notation $\sigma(I_m)$ used here and the sector function σ is intended, since in the case of DEs for FIs the strongly connected components are precisely identified with the sectors of the integral family, while $\sigma(I_m) \to \sigma(I_n)$ means that $\sigma(I_m)$ is a sub-sector of $\sigma(I_n)$.

The strongly connected components of a directed graph can be efficiently identified using standard algorithms, such as those by Tarjan [94], Kosaraju [95] and Gabow [96], all operating in linear time with respect to the number of vertices and edges.

3.3 Regular singular points

The integral representation of Feynman integrals constrains their behavior near singular points to be bounded by powers of the kinematic invariants [47, 74], meaning that the poles of the differential equation matrices must be regular singular points. Solving the DEs around their singularities is a key ingredient for the framework developed in this work. In particular, we can analyze the solution around singular configurations where the FIs have a known behavior and obtain boundary conditions by imposing that the solution behaves accordingly. Furthermore, solving around a pole also provides a valid strategy to cross singularities that are encountered on the propagation path.

Not every singular point of the DE matrices corresponds to a singularity of the FIs. When the FIs are regular around a pole of the DEs, we refer to the latter as a spurious singularity. These are not physical in the sense that they are not predicted by unitarity cuts. When boundary values for the master integrals have been propagated up to the convergence disk of a spurious singularity and are matched with the solution to the DEs around the pole, the coefficients of the singular terms present in the general solution cancel out within the working precision, regardless of the prescription chosen for the analytic continuation. Conversely, one can generate BCs around spurious singularities by setting these coefficients to zero. However, to fully determine the solution, it is possible that the leading-order terms of the regular contributions have to be provided as well.

It may happen that a linear change of basis is performed in which the new MIs are expressed as linear combinations of the original MIs with singular coefficients. Even though the original MIs are regular, in the new basis both the DEs and their solutions may become singular. However, the singularities cancel out when transforming back to the original basis. When the coefficients of the transformation are rational functions, the new basis can only exhibit poles. If the coefficients are algebraic functions (a case not considered here), they may introduce algebraic branch points for which analytic continuation can be performed by choosing an arbitrary prescription.

Finally, singular points that are branch points for the MIs correspond to physical singularities predicted by unitary cuts. In this case, the physical solution does depend on the prescription chosen for the analytic continuation, which indeed must be performed in agreement with the Feynman prescription.

3.3.1 Fuchsian normal form

Let η be the line parameter of a phase space curve $\mathbf{s}(\eta)$ that goes through a pole for $\eta = 0$, that is, the corresponding differential equation matrix $\mathbb{A}(\eta)$ is singular at $\eta = 0$. We define the *Poincaré rank* of $\mathbb{A}(\eta)$ in $\eta = 0$ as the smallest integer p such that

$$\lim_{\eta \to 0} \eta^{p+1} \mathbb{A}(\eta) = \text{finite}\,. \tag{3.15}$$

Hence the Laurent expansion around $\eta = 0$ for a matrix $\mathbb{A}(\eta)$ with Poincaré rank p is

$$\mathbb{A}(\eta) = \frac{1}{\eta^{p+1}} \sum_{k=0}^{\infty} \mathbb{A}_{-p+k}\, \eta^k\,, \quad \mathbb{A}_{-p} \neq 0\,, \tag{3.16}$$

so that $p = 0$ means that $\mathbb{A}(\eta)$ has a simple pole around the singularity and in general $p \geq 0$ indicates a pole of order $p + 1$.

The regularity of the singular point $\eta = 0$ guarantees that the Poincaré rank of $\mathbb{A}(\eta)$ can be reduced to zero by means of a suitable transformation [97]. Given an invertible matrix $\mathbb{T}(\eta)$, we can indeed consider the change of basis $\widetilde{\mathbf{I}}(\eta) \equiv \mathbb{T}^{-1}(\eta)\mathbf{I}(\eta)$ and find the DE matrix for the transformed integrals. By differentiation, we have

$$\begin{aligned}\frac{d}{d\eta}\widetilde{\mathbf{I}}(\eta) &= \frac{d}{d\eta}\left[\,\mathbb{T}^{-1}(\eta)\mathbf{I}(\eta)\,\right] = \left[\frac{d}{d\eta}\mathbb{T}^{-1}(\eta)\right]\mathbf{I}(\eta) + \mathbb{T}^{-1}(\eta)\frac{d}{d\eta}\mathbf{I}(\eta) \\ &= \left[\frac{d}{d\eta}\mathbb{T}^{-1}(\eta) + \mathbb{T}^{-1}(\eta)\mathbb{A}(\eta)\right]\mathbf{I}(\eta) = \left[\frac{d}{d\eta}\mathbb{T}^{-1}(\eta) + \mathbb{T}^{-1}(\eta)\mathbb{A}(\eta)\right]\mathbb{T}(\eta)\widetilde{\mathbf{I}}(\eta)\,,\end{aligned} \tag{3.17}$$

where we used first $\partial_\eta \mathbf{I}(\eta) = \mathbb{A}(\eta)\mathbf{I}(\eta)$ and then $\mathbf{I}(\eta) = \mathbb{T}(\eta)\widetilde{\mathbf{I}}(\eta)$. As we observe, the transformed integrals satisfy the DE system

$$\frac{d}{d\eta}\widetilde{\mathbf{I}}(\eta) = \widetilde{\mathbb{A}}(\eta)\widetilde{\mathbf{I}}(\eta)\,, \tag{3.18}$$

where the matrix $\widetilde{\mathbb{A}}(\eta)$ is given by

$$\widetilde{\mathbb{A}}(\eta) \equiv \mathbb{T}^{-1}(\eta)\mathbb{A}(\eta)\mathbb{T}(\eta) - \mathbb{T}^{-1}(\eta)\frac{d}{d\eta}\mathbb{T}(\eta)\,. \tag{3.19}$$

Here, we used $(\partial_\eta \mathbb{T}^{-1}(\eta))\,\mathbb{T}(\eta) = -\mathbb{T}^{-1}(\eta)\partial_\eta \mathbb{T}(\eta)$ to rewrite the transformation law in the form that is commonly adopted in the literature.

It was proved by Horn [98] that the pole $\eta = 0$ is a regular singularity if and only if there exists a transformation matrix $\mathbb{T}(\eta)$ such that the transformed matrix $\widetilde{\mathbb{A}}(\eta)$ in eq. (3.19) is in *Fuchsian form*, that is, it has Poincaré rank zero. The matrix $\mathbb{T}(\eta)$ is analytic in some neighborhood of $\eta = 0$ with at most a pole at $\eta = 0$. Moser [97] defined the generalized Poincaré rank p' of $\mathbb{A}(\eta)$ as $p + r/I - 1$, where r is the rank of the leading coefficient $\mathbb{A}_{-p}$ and I is the size of the matrix. He then proved that p' can be reduced if and only if

$$\eta^r \det\left(\frac{\mathbb{A}_{-p}}{\eta} + \mathbb{A}_{-p+1} - \lambda\mathbb{1}\right)\Bigg|_{\eta=0} = 0 \quad \forall\,\lambda\,, \tag{3.20}$$

and provided a method to construct the corresponding matrix $\mathbb{T}(\eta)$. The algorithm was improved by Barkatou and Pflügel [99, 100], and later by Lee [101]. In the reduction

mechanism, the rank of $\mathbb{A}_{-p}$ is progressively lowered until $\mathbb{A}_{-p} = 0$, meaning that the Poincaré rank has been reduced by at least one unit. This procedure is iterated until $p = 0$. As shown in section 3.3.2, it is always possible to choose a transformation $\mathbb{T}(\eta)$ that shares the same block structure as $\mathbb{A}(\eta)$, so that the same partition is inherited by $\widetilde{\mathbb{A}}(\eta)$ as well.

In a Fuchsian basis the DE matrix $\widetilde{\mathbb{A}}(\eta)$ expands as

$$\widetilde{\mathbb{A}}(\eta) = \frac{1}{\eta} \sum_{k=0}^{\infty} \widetilde{\mathbb{A}}_k \eta^k \,, \quad \widetilde{\mathbb{A}}_0 \neq 0 \,. \tag{3.21}$$

While employing the series expansion method of section 4.3, we also require every block $\widetilde{\mathbb{A}}_0^{(r,r)}$ on the diagonal of the leading-order coefficient to be in Jordan normal form. Finally, by means of shearing transformations, in section 3.3.2 we shift each eigenvalue so that it lands on the interval $[0, 1[$. By doing so, $\widetilde{\mathbb{A}}_0$ becomes *free of resonances*, in the sense that no pair of its eigenvalues has an integer difference.

To summarize, around a regular singular point of the DE matrix $\mathbb{A}(\eta)$, it is always possible to find a transformation $\mathbb{T}(\eta)$ of rational functions such that, in the new basis, the transformed matrix $\widetilde{\mathbb{A}}(\eta)$ of eq. (3.19) has Poincaré rank zero and the blocks on the diagonal of its leading-order coefficient $\widetilde{\mathbb{A}}_0$ are in Jordan normal form and free of resonances. When all these conditions are met, we say that $\widetilde{\mathbb{A}}(\eta)$ is in *Fuchsian normal form* and the methods of section 4.3 can be applied to solve the system of DEs.

Let us now consider a DE system that has been transformed to Fuchsian normal form. It is known from text books such as [102] that a fundamental matrix solution to the DE (3.18) can be expressed in the form

$$\widetilde{\mathbb{H}}(\eta) = \mathbb{P}(\eta)\, \mathbb{Z}(\eta) \,, \tag{3.22}$$

where $\mathbb{P}(\eta)$ is analytic in a neighborhood of the origin and $\mathbb{P}(0) = \mathbb{1}$, while $\mathbb{Z}(\eta)$ is a fundamental matrix solution to the DE

$$\frac{d}{d\eta}\mathbb{Z}(\eta) = \frac{\widetilde{\mathbb{A}}_0}{\eta}\, \mathbb{Z}(\eta) \,. \tag{3.23}$$

The latter is obtained from the DE (3.18) by expanding the matrix $\widetilde{\mathbb{A}}(\eta)$ and keeping only its leading-order term. Therefore, $\mathbb{Z}(\eta)$ captures the leading-order behaviors of the matrix solution $\widetilde{\mathbb{H}}(\eta)$. Note that the matrix $\mathbb{Z}(\eta)$ is determined up to the multiplication on the right by any non-singular constant matrix. A possible choice is given by

$$\mathbb{Z}(\eta) = \eta^{\widetilde{\mathbb{A}}_0} = e^{\widetilde{\mathbb{A}}_0 \log(\eta)} = \sum_{\lambda \in \Lambda} \eta^\lambda \sum_{k=0}^{K_\lambda} \frac{\log^k(\eta)}{k!} \mathbb{Z}_{\lambda,k} \,, \tag{3.24}$$

where Λ is the set of eigenvalues of $\widetilde{\mathbb{A}}_0$. Therefore, in a Fuchsian basis, the solutions to the DE (3.18) have the series expansion

$$\widetilde{\mathbf{I}}(\eta) = \sum_{\lambda\in\Lambda} \eta^\lambda \sum_{k=0}^{K_\lambda} \frac{\log^k(\eta)}{k!} \sum_{n=0}^{\infty} \widetilde{\mathbf{I}}_{\lambda,k,n}\, \eta^n \,. \tag{3.25}$$

When transformed back to the original non-Fuchsian basis, the expansion becomes

$$\mathbf{I}(\eta) = \sum_{\lambda\in\Lambda} \eta^{\lambda-t_\lambda} \sum_{k=0}^{K_\lambda} \frac{\log^k(\eta)}{k!} \sum_{n=0}^{\infty} \mathbf{I}_{\lambda,k,n}\, \eta^n \,, \tag{3.26}$$

where t_λ is an integer shift. We refer to any expansion of this kind as a regular singular expansion. Note that powers η^λ with non-integer exponent λ and the logarithms $\log(\eta)$ have branch cuts developing from the singularity at $\eta = 0$.

In the case of DEs for FIs, the eigenvalues λ of the leading-order coefficient $\widetilde{\mathbb{A}}_0(\epsilon)$ play a crucial role in the determination of BCs. As shown in sections 3.4.2 and 4.3.3, with the method of EBR one can indeed predict the leading behaviors η^λ of FIs around singular kinematic configurations where some scales become negligible compared to others. The domain for the integration over loop momenta is split into different regions, each characterized by a specific scaling η^λ. EBR allows the determination of the leading-order coefficients for the expansion in eq. (3.25) and thus of the solution corresponding to the sought FIs. The eigenvalues λ are expected to be linear in the regulator ϵ, as it can be confirmed within the framework of EBR.

3.3.2 Sector-by-sector normalization

As discussed in section 3.2, the differential equation matrix $\mathbb{A}(\eta)$ is block lower triangular when the master integrals are ordered according to their sector hierarchy (with sub-sectors coming first). With this choice, the MIs up to any given sector r are not affected by those belonging to higher sectors and, therefore, it must be possible to normalize the first r sectors of $\mathbb{A}(\eta)$ independently of the subsequent ones. Since this is true for any r, the normalization of the matrix $\mathbb{A}(\eta)$ must follow its block structure, so that the final transformation matrix $\mathbb{T}(\eta)$ is lower block triangular as well.

In this section we describe a procedure to find a transformation matrix $\mathbb{T}(\eta)$ that is block lower triangular and such that the transformed matrix $\widetilde{\mathbb{A}}(\eta)$ of eq. (3.19) is in Fuchsian normal form. This task can be broken down into successive steps. Indeed, using the notation

$$\Phi_{\mathbb{T}}[\mathbb{A}](\eta) \equiv \widetilde{\mathbb{A}}(\eta) = \mathbb{T}^{-1}(\eta)\mathbb{A}(\eta)\mathbb{T}(\eta) - \mathbb{T}^{-1}(\eta)\frac{d}{d\eta}\mathbb{T}(\eta) \tag{3.27}$$

for the transformation law in eq. (3.19), we have that $\Phi_{\mathbb{T}}$ satisfies the composition property

$$\Phi_{\mathbb{T}_1\mathbb{T}_2}[\mathbb{A}] = \Phi_{\mathbb{T}_2}[\Phi_{\mathbb{T}_1}[\mathbb{A}]]\,. \tag{3.28}$$

Therefore, we can proceed by finding successive transformations $\mathbb{T}_1(\eta)$, $\mathbb{T}_2(\eta)$, ... and, for each $\mathbb{T}_k(\eta)$, updating $\widetilde{\mathbb{A}}(\eta)$ and $\mathbb{T}(\eta)$ according to

$$\begin{aligned}\widetilde{\mathbb{A}}(\eta) &\to \Phi_{\mathbb{T}_k}[\widetilde{\mathbb{A}}](\eta)\,,\\ \mathbb{T}(\eta) &\to \mathbb{T}(\eta)\mathbb{T}_k(\eta)\,.\end{aligned}$$

In LINE the DE matrix $\mathbb{A}(\eta)$ is transformed to Fuchsian normal form in two stages:

1. Each block $\mathbb{A}^{(r,r)}(\eta)$ on the diagonal of $\mathbb{A}(\eta)$ is transformed to Fuchsian form and the eigenvalues of their η^{-1}-order coefficients have their real part moved to the interval $[0,1[$ with integer shifts.[2] We refer to this step as *diagonal normalization*.

2. The off-diagonal blocks $\mathbb{A}^{(r,s)}(\eta)$ with $r > s$ are transformed to Fuchsian form without changing the blocks on the diagonal. We denote this step by *off-diagonal fuchsianization*.

In the following, we illustrate how both steps can be implemented.

1. Diagonal normalization. As mentioned in section 3.3.2, the algorithm presented by Lee in [101] allows the transformation to Fuchsian form of a square matrix that satisfies the reducibility condition in eq. (3.20). This can be applied to each block $\mathbb{A}^{(r,r)}(\eta)$ to obtain a transformation matrix $\mathbb{T}^{(r,r)}(\eta)$ of rational functions and the transformed block $\widetilde{\mathbb{A}}^{(r,r)}(\eta)$ in Fuchsian form, which has the series expansion

$$\widetilde{\mathbb{A}}^{(r,r)}(\eta) = \frac{1}{\eta}\sum_{k=0}^{\infty}\widetilde{\mathbb{A}}_k^{(r,r)}\eta^k\,, \quad \widetilde{\mathbb{A}}_0^{(r,r)} \neq 0\,. \tag{3.29}$$

Then, the leading-order coefficient $\widetilde{\mathbb{A}}_0^{(r,r)}$ is transformed to Jordan normal form by means of a constant transformation matrix $\mathbb{T}_J^{(r,r)}$, which is accumulated by updating the matrices $\mathbb{T}^{(r,r)}(\eta)$ and $\widetilde{\mathbb{A}}^{(r,r)}(\eta)$ according to

$$\begin{aligned}\mathbb{T}^{(r,r)}(\eta) &\to \mathbb{T}^{(r,r)}(\eta)\mathbb{T}_J^{(r,r)}\,,\\ \widetilde{\mathbb{A}}^{(r,r)}(\eta) &\to \mathbb{T}_J^{(r,r)-1}\widetilde{\mathbb{A}}^{(r,r)}(\eta)\mathbb{T}_J^{(r,r)}\,.\end{aligned}$$

[2] Although in cases of physical interest the eigenvalues are real, the mathematical procedure outlined in this section works out of the box for complex eigenvalues as well, provided that their real part is considered as a stopping criterion when performing the shift.

The leading term $\widetilde{\mathbb{A}}_0^{(r,r)}$ is further normalized by acting with *shearing transformations* that progressively shift the eigenvalue of each Jordan chain by one unit until its real part falls into the interval $[0,1[$. The transformation matrix to shift by $s=\pm 1$ is given by

$$\mathbb{T}_{\text{sh}}^{(r,r)}(\eta) \equiv \text{diag}(1,\dots,1,\underbrace{\eta^{-s},\dots,\eta^{-s}}_{\text{target chain}},1,\dots,1)\,, \tag{3.30}$$

where the term η^{-s} is placed at the indices corresponding to the Jordan chain of $\widetilde{\mathbb{A}}_0^{(r,r)}$ to be shifted. Indeed, when the block $\widetilde{\mathbb{A}}^{(r,r)}(\eta)$ is transformed according to

$$\widetilde{\mathbb{A}}^{(r,r)}(\eta) \to \mathbb{T}_{\text{sh}}^{(r,r)-1}(\eta)\widetilde{\mathbb{A}}^{(r,r)}(\eta)\mathbb{T}_{\text{sh}}^{(r,r)}(\eta) - \mathbb{T}_{\text{sh}}^{(r,r)-1}(\eta)\frac{d}{d\eta}\mathbb{T}_{\text{sh}}^{(r,r)}(\eta)\,, \tag{3.31}$$

the eigenvalue is shifted by the derivative contribution

$$-\mathbb{T}_{\text{sh}}^{(r,r)-1}(\eta)\frac{d}{d\eta}\mathbb{T}_{\text{sh}}^{(r,r)}(\eta) = \frac{s}{\eta}\,\text{diag}(0,\dots,0,1,\dots,1,0,\dots,0)\,, \tag{3.32}$$

which operates directly on the diagonal of the leading-order coefficient $\widetilde{\mathbb{A}}_0^{(r,r)}$. However, by acting with eq. (3.31), the effect of the contribution $\mathbb{T}_{\text{sh}}^{(r,r)-1}(\eta)\widetilde{\mathbb{A}}^{(r,r)}(\eta)\mathbb{T}_{\text{sh}}^{(r,r)}(\eta)$ is that the columns corresponding to the Jordan chain are multiplied by η^{-s} and the rows by η^{s}. Although the block of $\widetilde{\mathbb{A}}_0^{(r,r)}$ corresponding to the chain remains unchanged, some elements outside the block are multiplied by η^{-1} and so matrix elements from the next-to-leading coefficient $\widetilde{\mathbb{A}}_1^{(r,r)}$ may appear off-block in the leading order, spoiling its Jordan structure. So a new transformation $\mathbb{T}_J^{(r,r)}$ is found to transform $\widetilde{\mathbb{A}}_0^{(r,r)}$ to Jordan form again, with the overall result that the target Jordan chain is shifted as a whole and the others are preserved. The shearing and Jordan transformations are accumulated with the update

$$\mathbb{T}^{(r,r)}(\eta) \to \mathbb{T}^{(r,r)}(\eta)\mathbb{T}_{\text{sh}}^{(r,r)}(\eta)\mathbb{T}_J^{(r,r)}\,. \tag{3.33}$$

This procedure is iterated until all eigenvalues have their real part in the interval $[0,1[$, implying that $\widetilde{\mathbb{A}}_0^{(r,r)}$ is free of resonances.

Note that only shifts of one unit per step are allowed, since a shifting term η^{-s} with $|s|>1$ would act with $\eta^{-|s|}$ outside the Jordan blocks, thus spoiling the fuchsianization. However, multiple Jordan chains can be treated together with a single shearing transformation if the proper term $\eta^{\pm 1}$ is placed at the indices corresponding to each chain.

Once all the eigenvalues have been normalized, the block $\widetilde{\mathbb{A}}^{(r,r)}(\eta)$ is in Fuchsian normal form and the accumulated transformation matrix $\mathbb{T}^{(r,r)}(\eta)$ is such that $\widetilde{\mathbb{A}}^{(r,r)}(\eta)$ and $\mathbb{A}^{(r,r)}(\eta)$ are related by

$$\widetilde{\mathbb{A}}^{(r,r)}(\eta) = \mathbb{T}^{(r,r)-1}(\eta)\mathbb{A}^{(r,r)}(\eta)\mathbb{T}^{(r,r)}(\eta) - \mathbb{T}^{(r,r)-1}(\eta)\frac{d}{d\eta}\mathbb{T}^{(r,r)}(\eta)\,. \tag{3.34}$$

If the same is done for all the blocks on the diagonal, one can arrange each $\mathbb{T}^{(r,r)}(\eta)$ in a global block-diagonal transformation matrix

$$\mathbb{T}(\eta) \equiv \text{diag}(\mathbb{T}^{(1,1)}(\eta), \mathbb{T}^{(2,2)}(\eta), \dots, \mathbb{T}^{(B,B)}(\eta)) \tag{3.35}$$

that, acting on $\mathbb{A}(\eta)$ via eq. (3.27), transforms each block on the diagonal according to eq. (3.34). In the same global transformation, the off-diagonal blocks are changed as well, according to

$$\widetilde{\mathbb{A}}^{(r,s)}(\eta) = \mathbb{T}^{(r,r)-1}(\eta)\mathbb{A}^{(r,s)}(\eta)\mathbb{T}^{(s,s)}(\eta)\,, \quad s < r\,. \tag{3.36}$$

In general, these blocks are still non-Fuchsian and so must be transformed to Fuchsian form in the next stage.

2. Off-diagonal fuchsianization. We need to transform the off-diagonal blocks to Fuchsian form while preserving the blocks on the diagonal, which are in Fuchsian normal form after the first stage. With this in mind, we look for a transformation matrix $\mathbb{T}(\eta)$ that is block lower triangular with identity matrices on the diagonal, that is,

$$\mathbb{T}_{\text{off}}(\eta) = \begin{pmatrix} \mathbb{1} & 0 & 0 & \dots & 0 \\ \mathbb{T}^{(2,1)}_{\text{off}}(\eta) & \mathbb{1} & 0 & \dots & 0 \\ \mathbb{T}^{(3,1)}_{\text{off}}(\eta) & \mathbb{T}^{(3,2)}_{\text{off}}(\eta) & \mathbb{1} & \dots & 0 \\ \vdots & \vdots & \ddots & \ddots & \vdots \\ \mathbb{T}^{(B,1)}_{\text{off}}(\eta) & \mathbb{T}^{(B,2)}_{\text{off}}(\eta) & \dots & \mathbb{T}^{(B,B-1)}_{\text{off}}(\eta) & \mathbb{1} \end{pmatrix}, \tag{3.37}$$

since any such matrix leaves the blocks $\widetilde{\mathbb{A}}^{(r,r)}(\eta)$ on the diagonal unchanged when acting on $\widetilde{\mathbb{A}}(\eta)$. Furthermore, $\mathbb{T}_{\text{off}}(\eta)$ can be decomposed as

$$\begin{aligned} \mathbb{T}_{\text{off}}(\eta) &= \mathbb{T}^{\{2,1\}}_{\text{off}}(\eta)\,\mathbb{T}^{\{3,2\}}_{\text{off}}(\eta)\,\mathbb{T}^{\{3,1\}}_{\text{off}}(\eta)\dots \\ &\equiv \begin{pmatrix} \mathbb{1} & 0 & 0 & \dots & 0 \\ \mathbb{T}^{(2,1)}_{\text{off}}(\eta) & \mathbb{1} & 0 & \dots & 0 \\ 0 & 0 & \mathbb{1} & \dots & 0 \\ \vdots & \vdots & \ddots & \ddots & \vdots \\ 0 & 0 & \dots & 0 & \mathbb{1} \end{pmatrix} \begin{pmatrix} \mathbb{1} & 0 & 0 & \dots & 0 \\ 0 & \mathbb{1} & 0 & \dots & 0 \\ 0 & \mathbb{T}^{(3,2)}_{\text{off}}(\eta) & \mathbb{1} & \dots & 0 \\ \vdots & \vdots & \ddots & \ddots & \vdots \\ 0 & 0 & \dots & 0 & \mathbb{1} \end{pmatrix} \begin{pmatrix} \mathbb{1} & 0 & 0 & \dots & 0 \\ 0 & \mathbb{1} & 0 & \dots & 0 \\ \mathbb{T}^{(3,1)}_{\text{off}}(\eta) & 0 & \mathbb{1} & \dots & 0 \\ \vdots & \vdots & \ddots & \ddots & \vdots \\ 0 & 0 & \dots & 0 & \mathbb{1} \end{pmatrix} \dots, \end{aligned} \tag{3.38}$$

where we define $\mathbb{T}^{\{r,s\}}_{\text{off}}(\eta)$ as a global matrix with identity matrices on the diagonal, the off-diagonal block $\mathbb{T}^{(r,s)}_{\text{off}}(\eta)$ placed in position (r,s) and null blocks anywhere else. The

factorization in eq. (3.38) allows us to focus on each transformation $\mathbb{T}^{(r,s)}_{\text{off}}(\eta)$ separately, aiming to transform to Fuchsian form the off-diagonal blocks of $\widetilde{\mathbb{A}}(\eta)$ in the order

$$\widetilde{\mathbb{A}}^{(2,1)}(\eta)\,,\widetilde{\mathbb{A}}^{(3,2)}(\eta)\,,\widetilde{\mathbb{A}}^{(3,1)}(\eta)\,,\widetilde{\mathbb{A}}^{(4,3)}(\eta)\,,\widetilde{\mathbb{A}}^{(4,2)}(\eta)\,,\widetilde{\mathbb{A}}^{(4,1)}(\eta)\,,\dots\,. \tag{3.39}$$

When acting on $\widetilde{\mathbb{A}}(\eta)$ as in eq. (3.27), $\mathbb{T}^{(r,s)}_{\text{off}}(\eta)$ transforms each block according to

$$\widetilde{\mathbb{A}}^{(h,k)}(\eta) \to \begin{cases} \widetilde{\mathbb{A}}^{(r,s)}(\eta) - \mathbb{T}^{(r,s)}_{\text{off}}(\eta)\widetilde{\mathbb{A}}^{(s,s)}(\eta) + \widetilde{\mathbb{A}}^{(r,r)}(\eta)\mathbb{T}^{(r,s)}_{\text{off}}(\eta) - \dfrac{d}{d\eta}\mathbb{T}^{(r,s)}_{\text{off}}(\eta)\,, & h=r,\ k=s, \\ \widetilde{\mathbb{A}}^{(r,k)}(\eta) - \mathbb{T}^{(r,s)}_{\text{off}}(\eta)\widetilde{\mathbb{A}}^{(s,k)}(\eta)\,, & h=r,\ k<s, \\ \widetilde{\mathbb{A}}^{(h,s)}(\eta) + \widetilde{\mathbb{A}}^{(h,r)}(\eta)\mathbb{T}^{(r,s)}_{\text{off}}(\eta), & h>r,\ k=s, \\ \widetilde{\mathbb{A}}^{(h,k)}(\eta), & \text{otherwise}\,, \end{cases} \tag{3.40}$$

thus changing the block in position (r,s), as well as the r-th row of blocks from $(r,1)$ up to $(r,s-1)$ and the s-th column of blocks from $(r+1,s)$ down to (B,s). Aiming to exploit this transformation to lower the Poincaré rank p of $\widetilde{\mathbb{A}}^{(r,s)}(\eta)$, we choose the block $\mathbb{T}^{(r,s)}_{\text{off}}(\eta)$ in the form

$$\mathbb{T}^{(r,s)}_{\text{off}}(\eta) = \frac{\mathbb{G}^{(r,s)}}{\eta^p}\,, \qquad \mathbb{G}^{(r,s)} = \text{const}\,, \tag{3.41}$$

substitute its expression in eq. (3.40) for $h=r$, $k=s$, and impose the cancellation of the leading order $1/\eta^{p+1}$. We obtain

$$0 = \widetilde{\mathbb{A}}^{(r,s)}_{-p} - \mathbb{G}^{(r,s)}\widetilde{\mathbb{A}}^{(s,s)}_0 + \widetilde{\mathbb{A}}^{(r,r)}_0\mathbb{G}^{(r,s)} + p\,\mathbb{G}^{(r,s)}\,, \tag{3.42}$$

which constitutes a system of $L_r \times L_s$ linear equations that we solve for the unknown matrix elements of $\mathbb{G}^{(r,s)}$. The solution fixes the transformation $\mathbb{T}^{\{r,s\}}(\eta)$, that we use to transform $\widetilde{\mathbb{A}}(\eta)$ as in eq. (3.40). By construction, the Poincaré rank p of $\widetilde{\mathbb{A}}^{(r,s)}(\eta)$ is lowered, while the sub-row and the sub-column of (r,s) are changed as well. By iterating this procedure until $p=0$, the off-diagonal block $\widetilde{\mathbb{A}}^{(r,s)}(\eta)$ is transformed to Fuchsian form.

Note that, if we had already worked out the blocks on the sub-row and the sub-column of (r,s), their fuchsianization would be spoiled by the action of $\mathbb{T}^{\{r,s\}}(\eta)$. Instead, we transform the sub-diagonal blocks to Fuchsian form in the order specified in eq. (3.39), thus avoiding such a problem. This explains why, even though the factorization in eq. (3.38) holds for any ordering of the factors, we choose the one where the only non-zero off-diagonal block goes through each row r starting from the block $(r,r-1)$ and moving towards the block $(r,1)$, then proceeding with the next row and so on. This particular choice ensures that, after its Poincaré rank is reduced to zero with the method illustrated above, the block $\widetilde{\mathbb{A}}^{(r,s)}(\eta)$ remains unchanged in the subsequent iterations.

Following the ordering in eq. (3.39), we reduce to zero the Poincaré rank of all the off-diagonal blocks, the last one being $\widetilde{\mathbb{A}}^{(B,1)}(\eta)$ in the bottom-left corner. The global matrix $\widetilde{\mathbb{A}}(\eta)$ resulting from this procedure is in Fuchsian normal form, matching all the conditions that are necessary to solve the DE around the regular singular point $\eta = 0$ with the methods of section 4.3.

3.4 Boundary conditions

In order for the differential equation method to succeed, boundary conditions must be known to fully determine the solution in some kinematic configurations. The boundary values obtained for one point of the phase space can then be propagated to many other points. We now explore two approaches for the determination of boundary conditions, both of which are based on solving the differential equations around singular points.

3.4.1 The auxiliary mass flow method

In this section we describe the AMFlow method in its original formulation, which is the one implemented in LINE and relies on the introduction of the auxiliary mass η in all the propagators of the integral family in eq. (2.64). In particular, D_α is modified according to

$$D_\alpha = q_\alpha^2 - m_\alpha^2 + i\varepsilon \quad \longrightarrow \quad \mathcal{D}_\alpha \equiv q_\alpha^2 - m_\alpha^2 - \eta\,, \quad \mathrm{Im}\,\eta < 0\,, \tag{3.43}$$

where the auxiliary squared mass η is considered in the lower half of the complex plane so as to be consistent with the Feynman prescription. The physical value of the Feynman integrals then corresponds to the limit $\eta \to 0$ (with $\mathrm{Im}\,\eta \to 0^-$). Upon the introduction of the auxiliary mass, the number of MIs generally increases. Thus we move from a basis $\mathbf{I}(\epsilon, \mathbf{s})$ to an extended one $\boldsymbol{\mathcal{I}}(\epsilon, \mathbf{s}, \eta)$. Differentiating with respect to the auxiliary mass as in eq. (2.65) and applying the IBP identities of section 2.5, one can close a system of DEs for the extended basis in the form

$$\frac{\partial}{\partial\eta}\boldsymbol{\mathcal{I}}(\epsilon, \mathbf{s}, \eta) = \mathbb{M}(\epsilon, \mathbf{s}, \eta)\boldsymbol{\mathcal{I}}(\epsilon, \mathbf{s}, \eta)\,. \tag{3.44}$$

The key advantage of studying this system of DEs is that BCs can be obtained by pushing η to infinity in the lower half of the complex plane. In fact, when the auxiliary mass becomes much larger than the kinematic invariants $\mathbf{s}$, the MIs behave as

$$\mathcal{I}_i(\epsilon, \mathbf{s}, \eta) \overset{|\eta|\to+\infty}{\sim} \eta^{a_i}\left[\mathcal{I}_i(\epsilon, \mathbf{0}, 1) + \mathcal{O}(1/\eta)\right], \quad a_i = L\,\frac{d}{2} - \sum_j \nu_j(\mathcal{I}_i)\,, \tag{3.45}$$

where $\mathcal{I}_i(\epsilon, \mathbf{0}, 1)$ are unit-mass L-loop vacuum integrals that are known in the literature with their exact dependence on ϵ up to three-loop [26, 103, 104], and numerically up to

five-loop [25, 105, 106]. For instance, the one- and two-loop vacuum integrals can be computed using the analytical formulae

$$= (-1)^{\nu} \frac{\Gamma(\nu - 2 + \epsilon)}{\Gamma(\nu)} \,, \tag{3.46a}$$

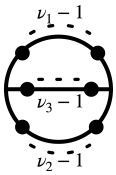

$$\begin{aligned} = (-1)^{\nu} \Bigg[& \frac{\Gamma(\nu_3 - 2 + \epsilon)\Gamma(\nu_1 + \nu_2 - 2 + \epsilon)}{\Gamma(\nu_3)\Gamma(\nu_1 + \nu_2)} \, {}_4F_3 \left(\begin{matrix} 2 - \epsilon, \nu_1, \nu_2, \nu_1 + \nu_2 - 2 + \epsilon \\ \frac{\nu_1+\nu_2}{2}, \frac{\nu_1+\nu_2}{2} + \frac{1}{2}, 3 - \nu_3 - \epsilon \end{matrix} ; \frac{1}{4} \right) \\ & + \frac{\Gamma(2 - \nu_3 - \epsilon)\Gamma(\nu_1 + \nu_3 - 2 + \epsilon)\Gamma(\nu_2 + \nu_3 - 2 + \epsilon)\Gamma(\nu + 2\epsilon - 4)}{\Gamma(\nu_1)\Gamma(\nu_2)\Gamma(2 - \epsilon)\Gamma(\nu + \nu_3 - 4 + 2\epsilon)} \\ & \times \, {}_4F_3 \left(\begin{matrix} \nu_3, \nu_1 + \nu_3 - 2 + \epsilon, \nu_2 + \nu_3 - 2 + \epsilon, \nu - 4 + 2\epsilon \\ \nu_3 - 1 + \epsilon, \frac{\nu+\nu_3-4}{2} + \epsilon, \frac{\nu+\nu_3-3}{2} + \epsilon \end{matrix} ; \frac{1}{4} \right) \Bigg] \,, \end{aligned} \tag{3.46b}$$

where the ν_i's are the powers for the loop currents k_1, k_2, k_1+k_2, and $\nu = \nu_1+\nu_2+\nu_3$. These formulae are implemented in LINE for the numerical evaluation at arbitrary precision for any value of ϵ.

The result in eq. (3.45) for the leading coefficient can be obtained in different ways. For instance, it is a direct consequence of the homogeneity properties given in eq. (2.103), as one can see by rescaling the auxiliary mass. Also, η tends to be the only important kinematic invariant as it grows much larger than the other invariants, so that eq. (3.45) follows from dimensionality arguments. Ultimately, EBR can be used to examine the limit $|\eta| \gg |\mathbf{s}|$, arriving once again at the same result. Notably, EBR goes beyond the determination of the leading behavior in eq. (3.45), as it also specifies that the only powers appearing in the full series for $\mathcal{I}_i(\epsilon, \mathbf{s}, \eta)$ are integer shifts of a_i.

The behaviors in eq. (3.45) can be used as BCs when solving the DE (3.44) in the limit $|\eta| \to +\infty$ at constant kinematics $\mathbf{s}$. To do this, one can change $\eta = 1/\xi$ so that the point at infinity becomes $\xi = 0$ in the new coordinate. Omitting the dependence on the fixed invariants $\mathbf{s}$, we define

$$\boldsymbol{\mathcal{I}}_\infty(\epsilon, \xi) \equiv \boldsymbol{\mathcal{I}}\left(\epsilon, 1/\xi\right) \,, \tag{3.47}$$

and differentiate with respect to ξ, obtaining

$$\frac{\partial}{\partial \xi} \boldsymbol{\mathcal{I}}_\infty(\epsilon, \xi) = -\frac{1}{\xi^2} \left[\frac{\partial}{\partial \eta} \boldsymbol{\mathcal{I}}(\epsilon, \eta) \right]_{\eta \to 1/\xi} = -\frac{1}{\xi^2} \mathbb{M}(\epsilon, 1/\xi) \boldsymbol{\mathcal{I}}_\infty(\epsilon, \xi) \,, \tag{3.48}$$

where eqs. (3.44) and (3.47) were used. Hence the integrals $\boldsymbol{\mathcal{I}}_\infty(\epsilon, \xi)$ satisfy the DE

$$\frac{\partial}{\partial \xi} \boldsymbol{\mathcal{I}}_\infty(\epsilon, \xi) = \mathbb{M}_\infty(\epsilon, \xi) \boldsymbol{\mathcal{I}}_\infty(\epsilon, \xi) \,, \quad \mathbb{M}_\infty(\epsilon, \xi) \equiv -\frac{\mathbb{M}\left(\epsilon, 1/\xi\right)}{\xi^2} \,. \tag{3.49}$$

In light of eq. (3.45), we further introduce the integrals $\underline{\boldsymbol{\mathcal{I}}}_\infty(\epsilon,\xi)$ according to

$$\boldsymbol{\mathcal{I}}_\infty(\epsilon,\xi) \equiv \mathrm{diag}(\xi^{-\mathbf{a}})\,\underline{\boldsymbol{\mathcal{I}}}_\infty(\epsilon,\xi)\,, \tag{3.50}$$

where $\xi^{-\mathbf{a}} \equiv (\xi^{-a_1}, \xi^{-a_2}, \dots)$ are indeed the leading power behaviors of $\boldsymbol{\mathcal{I}}_\infty(\epsilon,\xi)$. Then, from eq. (3.45) we know that the integrals $\underline{\boldsymbol{\mathcal{I}}}_\infty(\epsilon,\xi)$ must be Taylor series whose leading terms are the unit-mass vacuum integrals. Once again, the DE matrix for the newly introduced integrals can be found by differentiation, which is equivalent to use eq. (3.19) for a change of basis with transformation matrix $\mathbb{T}(\xi) = \mathrm{diag}(\xi^{-\mathbf{a}})$. In particular, using $\partial_\xi \mathbb{T}(\xi) = -\mathrm{diag}(\mathbf{a})\,\mathrm{diag}(\xi^{-\mathbf{a}})/\xi$, we have

$$\begin{aligned}
&\frac{\partial}{\partial\xi}\underline{\boldsymbol{\mathcal{I}}}_\infty(\epsilon,\xi) = \underline{\mathbb{M}}_\infty(\epsilon,\xi)\underline{\boldsymbol{\mathcal{I}}}_\infty(\epsilon,\xi)\,,\\
&\underline{\mathbb{M}}_\infty(\epsilon,\xi) \equiv \mathrm{diag}(\xi^{\mathbf{a}})\left(\mathbb{M}_\infty(\epsilon,\xi) + \frac{\mathrm{diag}(\mathbf{a})}{\xi}\right)\mathrm{diag}(\xi^{-\mathbf{a}})\,,
\end{aligned} \tag{3.51}$$

which is the actual DE we focus on. Even though the integrals $\underline{\boldsymbol{\mathcal{I}}}_\infty(\epsilon,\xi)$ are regular at $\xi = 0$, the origin is still a regular singularity for the matrix $\underline{\mathbb{M}}_\infty(\epsilon,\xi)$. In LINE eq. (3.51) is solved via series expansion using the recurrence relations that are obtained in section 4.3. Since $\underline{\boldsymbol{\mathcal{I}}}_\infty(\epsilon,\xi)$ expands as Taylor series, the BCs can be imposed by vetoing the presence of non-zero eigenvalues λ in the ansatz of eq. (3.25) and requiring that the leading-order coefficients for the null eigenvalue $\lambda = 0$ are the unit-mass vacuum integrals. More details on this procedure are given in section 4.3.3.

Once the Taylor coefficients for $\underline{\boldsymbol{\mathcal{I}}}_\infty(\epsilon,\xi)$ are known, the series can be summed at a point ξ_1 within its radius of convergence and multiplied by $\mathrm{diag}(\xi_1^{-\mathbf{a}})$ to evaluate the MIs $\boldsymbol{\mathcal{I}}(\epsilon,\eta)$ in a point $\eta_1 = 1/\xi_1$ in the lower half of the complex plane. After that, it is possible to solve via series expansion the DE (3.44) using $\boldsymbol{\mathcal{I}}(\epsilon,\eta_1)$ as boundary values, to propagate from η_1 to the limit $\eta \to 0$ (with $\mathrm{Im}\,\eta \to 0^-$ in agreement with the Feynman prescription) using the series expansion methods of section 4, thus recovering the physical values $\mathbf{I}(\epsilon,\mathbf{s})$ of the original MIs. In particular, following the procedure of section 4.1, one can draw a straight line connecting η_1 to the origin and propagate using series expansion around regular points η_1, η_2, ... with the recurrence relations given in section 4.2, until a point η_{last} is reached within the disk of convergence centered at $\eta = 0$, which may be a (regular) singularity. Then, the method outlined in section 4.3 can be employed to solve via series expansion around the singularity at $\eta = 0$, matching the boundary $\boldsymbol{\mathcal{I}}(\epsilon,\eta_{\mathrm{last}})$ and evaluating the limit $\eta \to 0$. The values $\mathbf{I}(\epsilon,\mathbf{s})$ obtained in this way can serve as BCs for propagation to many other points in the phase space of the kinematic invariants $\mathbf{s}$.

The AMFlow method is a robust strategy that has been extended to include integrals with Dirac δ-functions [107] (phase space integrals) and propagators that are linear in

the loop momenta [108] (subtraction counterterms, integrals for effective field theories). Furthermore, a reformulation of the method consists in introducing the auxiliary mass in fewer propagators, leading to a smaller increase in the number of MIs [52]. One can go as far as inserting η in just one propagator. Then, in the limit $|\eta| \to +\infty$ the MIs factorize into products of integrals with fewer loops, where the same procedure can be iterated by inserting another auxiliary mass η', analyzing the limit $|\eta'| \to +\infty$ and so on. After resolving all the sub-problems, one is finally able to obtain the values of the MIs at $|\eta| \to +\infty$ and use them as BCs for the propagation to $\eta \to 0$ as described above. The EBR notions that are necessary to analyze the factorization of the FIs in the large-mass limit are given in the next section.

Besides computational efficiency, the advantage of the iterative version of the AMFlow method is that no analytic expression for the boundary integrals at infinity is required, since they are computed with the introduction of additional auxiliary masses, thus enabling higher-loop computations.

3.4.2 Expansion by regions

The technique of expansion by regions [109, 110] is a systematic approach to obtain the asymptotic expansion of Feynman integrals near kinematic configurations where some physical scales become small compared to the others. In essence, the method is based on the identification of integration regions based on the scaling of the loop momenta with respect to a smallness parameter. In each region, the integrands are expanded in Taylor series and the integration is extended to the whole domain of the loop momenta. Scaleless integrals are set to zero and the remaining contributions are summed together, yielding the complete expansion of the original Feynman integral. However, many subtleties may arise while employing such a procedure. A detailed analysis of the conditions to be matched in order for the method to work properly can be found in [111], where the appearance of overlap contributions is taken into account.

Although originally formulated in the momentum space, the formalism of EBR can be extended to the Feynman parameter representation [112–115], where a geometric interpretation is possible. The MATHEMATICA code `asy.m` [113] was developed to find the relevant regions and its update `asy2.m` [116] (part of FIESTA [117]) is also able to detect the so-called potential and Glauber regions, that may be relevant in cases there the Symanzik polynomial $\mathcal{F}$ have terms with opposite signs. Other implementations of the EBR framework are publicly available as well, including PYSECDEC [33, 34, 118] and ASPIRE [114, 115].

In the following, we study some examples in which EBR can be exploited in order to obtain boundary conditions for the master integrals when solving differential equations

around singular points. We first consider the one-loop bubble integral with incoming momentum p and propagators of mass m,

$$B(\epsilon, p^2, m^2) = \int_k \frac{1}{D_1 D_2} = \int_k \frac{1}{[k^2 - m^2][(k+p)^2 - m^2]} \,. \tag{3.52}$$

The corresponding integral family has a basis of two MIs, namely the bubble itself and the tadpole of mass m, that we take as known through the analytical formula

$$A(\epsilon, m^2) = \int_k \frac{1}{D_1} = \int_k \frac{1}{(k^2 - m^2)} = -(m^2)^{1-\epsilon}\,\Gamma(\epsilon - 1) \,. \tag{3.53}$$

We vary the squared momentum by taking $p^2 = \eta$ while keeping m^2 fixed. The associated DE reads

$$\frac{\partial}{\partial \eta} B(\epsilon, \eta, m^2) = \frac{f_{B,B}(\epsilon, \eta, m^2)}{\eta} B(\epsilon, \eta, m^2) + \frac{f_{B,A}(\epsilon, \eta, m^2)}{\eta} A(\epsilon, m^2) \,, \tag{3.54}$$

where $f_{B,B}$ and $f_{B,A}$ are functions regular at $\eta = 0$ given by

$$f_{B,B}(\epsilon, \eta, m^2) = \frac{2m^2 - \epsilon\,\eta}{\eta - 4m^2} \,, \quad f_{B,A}(\epsilon, \eta, m^2) = \frac{2(1-\epsilon)}{\eta - 4m^2} \,. \tag{3.55}$$

As we can see, $\eta = 0$ is a regular singular point for the DE (3.54).

We now apply EBR in the limit of vanishing external kinematics $\eta \to 0$, which corresponds to $|p^2| \ll m^2$. The two contributions to be considered in the integration domain are the small-momentum region $k \sim \sqrt{|\eta|} \ll m$ and the large-momentum one $k \sim m \gg \sqrt{|\eta|}$. The bubble integral then splits into

$$B(\epsilon, \eta, m^2) = \int_{k \sim \sqrt{|\eta|}} \frac{1}{D_1 D_2} + \int_{k \gg \sqrt{|\eta|}} \frac{1}{D_1 D_2} \,. \tag{3.56}$$

Following the prescriptions of EBR, we expand in series both integrands and extend their integration to the whole loop momentum domain. In the zero-order term for the expansion in the first region, both k and p can be neglected with respect to the mass, so that

$$\int_{k \sim \sqrt{|\eta|}} \frac{1}{D_1 D_2} \to \int_k \frac{1}{(m^2)^2} + \mathcal{O}(\eta) = \text{ scaleless } + \mathcal{O}(\eta) = 0 + \mathcal{O}(\eta) \,, \tag{3.57}$$

where we set to zero the scaleless integral as EBR demands. Conversely, in the leading coefficient for the large-momentum region, p is negligible compared to the mass and the loop momentum. Hence we have

$$\int_{k \gg \sqrt{|\eta|}} \frac{1}{D_1 D_2} \to \int_k \frac{1}{(k^2 - m^2)^2} + \mathcal{O}(\eta) = m^{-2\epsilon}(\epsilon - 1)\Gamma(\epsilon - 1) + \mathcal{O}(\eta) \,, \tag{3.58}$$

where the leading term is just the bubble with $p = 0$ substituted into the integrand. Summing the two contributions we obtain

$$B(\epsilon, \eta, m^2) = m^{-2\epsilon}(\epsilon - 1)\Gamma(\epsilon - 1) + \mathcal{O}(\eta)\,, \tag{3.59}$$

which is the leading behavior of the bubble integral in the limit $\eta \to 0$.

We now use the behavior in eq. (3.59) as a BC informing us that, although $\eta = 0$ is a regular singularity for the DE (3.54), the bubble integral B expands around the singularity as a Taylor series starting at order zero. In particular, this implies that both B and its derivative $\partial_\eta B$ are regular at $\eta = 0$. Therefore, expanding the DE (3.54) around $\eta = 0$ and considering the coefficient of the leading behavior $1/\eta$, we have

$$0 = f_{B,B}(\epsilon, 0, m^2)B(\epsilon, 0, m^2) + f_{B,A}(\epsilon, 0, m^2)A(\epsilon, m^2)\,, \tag{3.60}$$

which allows us to express the leading order for the bubble in terms of the tadpole as

$$B(\epsilon, 0, m^2) = \frac{f_{B,A}(\epsilon, 0, m^2)}{f_{B,B}(\epsilon, 0, m^2)} A(\epsilon, m^2)\,. \tag{3.61}$$

Using eqs. (3.53) and (3.55) to substitute the values of A, $f_{B,B}$ and $f_{B,A}$, we obtain the same leading order $B(\epsilon, 0, m^2)$ as in eq. (3.59).

The analysis carried out above shows that, in the example under consideration, the only information necessary to fix the solution in the limit $\eta \to 0$ is what kind of power behavior the solution has. In other words, of eq. (3.59) we only need to know that $B(\epsilon, \eta, m^2)$ has a Taylor series around the singularity starting at order zero, meaning that all the other λ-contribution from the ansatz of eq. (3.25) must not figure in the solution. Having established this, the particular value of the leading coefficient $B(\epsilon, 0, m^2)$ can be extracted from the DE itself, as we observed in eqs. (3.60) and (3.61). In section 4.3.3, equipped with tools and techniques described throughout section 4.3, we come back to this example and show that the application of the boundary behavior is straightforward, as we do not even need to manually extract the relation in eq. (3.61) from the DE.

The same reasoning as for the bubble can be sequentially applied, for instance, to the massive triangle and box integrals, for which EBR also predicts a Taylor expansion in the limit of vanishing external kinematics. Indeed, we can consider the integral family

$$F^{\boldsymbol{\nu}}(\epsilon, s, t) = \int_k \frac{1}{D_1^{\nu_1} D_2^{\nu_2} D_3^{\nu_3} D_4^{\nu_4}}\,, \tag{3.62}$$

with massless external momenta $p_i^2 = 0$, $i = 1, \ldots, 4$, Mandelstam invariants $s = (p_1 + p_2)^2$, $t = (p_2 + p_3)^2$ and inverse propagators

$$\begin{aligned} D_1 &= k^2 - m^2\,, & D_2 &= (k + p_1)^2 - m^2\,, \\ D_3 &= (k + p_1 + p_2)^2 - m^2\,, & D_4 &= (k + p_1 + p_2 + p_3)^2 - m^2\,. \end{aligned} \tag{3.63}$$

A basis of 6 MIs consists of the tadpole $A(\epsilon, m^2)$ with propagator powers $\boldsymbol{\nu}_1 = (1,0,0,0)$, the s- and t-channel massive bubbles $B(\epsilon, s, m^2)$ and $B(\epsilon, t, m^2)$ with powers $\boldsymbol{\nu}_2 = (1,0,1,0)$ and $\boldsymbol{\nu}_3 = (0,1,0,1)$, the s- and t-channel triangle integrals $C(\epsilon, s, m^2)$ and $C(\epsilon, t, m^2)$ corresponding to $\boldsymbol{\nu}_4 = (1,1,1,0)$ and $\boldsymbol{\nu}_5 = (0,1,1,1)$, and the box $D(\epsilon, s, t, m^2)$ with $\boldsymbol{\nu}_6 = (1,1,1,1)$.

The method discussed above provides BCs for the two bubbles in the limit $s = t = \eta \to 0$ at fixed mass.[3] As seen for the bubble, the DE equation for the triangle also has a simple pole $1/\eta$. Indeed, it reads

$$\frac{\partial}{\partial\eta} C(\epsilon,\eta,m^2) = \frac{f_{C,C}(\epsilon,\eta,m^2)}{\eta} C(\epsilon,\eta,m^2) + \frac{f_{C,B}(\epsilon,\eta,m^2)}{\eta} B(\epsilon,\eta,m^2) + \frac{f_{C,A}(\epsilon,\eta,m^2)}{\eta} A(\epsilon,m^2)\,.$$

Imposing that C and $\partial_\eta C$ have no poles at $\eta = 0$ and using the result in eq. (3.61), one obtains for the triangle integral the leading coefficient

$$C(\epsilon,0,m^2) = \frac{\epsilon(\epsilon-1)}{2(m^2)^2} A(\epsilon,m^2)\,. \tag{3.64}$$

Proceeding similarly, the leading coefficient for the box integral is found to be

$$D(\epsilon,0,0,m^2) = -\frac{\epsilon(\epsilon^2-1)}{6(m^2)^3} A(\epsilon,m^2)\,. \tag{3.65}$$

Using eq. (3.53) to substitute the analytical formula of the tadpole in the expressions for $C(\epsilon,0,m^2)$ and $D(\epsilon,0,0,m^2)$, one arrives at the values of the vacuum integrals

$$C(\epsilon,0,m^2) = \int_k \frac{1}{(k^2-m^2)^3}\,, \quad D(\epsilon,0,0,m^2) = \int_k \frac{1}{(k^2-m^2)^4}\,, \tag{3.66}$$

in agreement with what is found using EBR. Although the leading coefficients in eq. (3.66) could be found by trivially evaluating the integrals with the external kinematics set exactly to zero, we stress that the key feature in this example is the absence of power behaviors in the form η^λ with non-integer λ. These contributions would be singular in the limit $\eta \to 0$ for $\lambda < 0$, while for $\lambda > 0$ they would make singular the derivatives of the solution. For instance, η^λ with $\lambda \in]0,1[$, has a singular first derivative. We now show an example where non-integer power behaviors come into play.

[3] When choosing a phase space line in the form $s(\eta) = s_0\eta$, $t(\eta) = t_0\eta$, one has to be careful not to stay on a singular surface of the DE. For instance, with $s_0 = -t_0$ one stays on the singular surface $s + t = 0$ for any value of η. Similar care is required in general for any integral family.

Let us consider the two-loop box with a massive loop that is described in detail in section 6.5 and that we denote here by $D^{(2)}(\epsilon, s, t, m^2)$ for simplicity. Its graph is shown on the left of figure 3.1. We analyze once again the limit $s, t \to 0$ of vanishing external kinematics. The integration regions are still identified by letting each loop momentum be either small, $k_i \sim \sqrt{|\eta|}$, or large, $k_i \gg \sqrt{|\eta|}$, but now, when both are large, they may either cancel or enhance each other.

In this example, both massless and massive propagators are present. To calculate the leading coefficient in each region, we note that the loop momentum current $k \in \{k_1, k_2, k_1 + k_2\}$ flowing into any given propagator is either small or large. If we denote by p the combination of external momenta for the propagator in question, we have[4]

$$(k+p)^2 \sim \begin{cases} (k+p)^2\,, & k \text{ small}\,, \\ k^2\,, & k \text{ large}\,, \end{cases} \qquad (k+p)^2 - m^2 \sim \begin{cases} -m^2\,, & k \text{ small}\,, \\ k^2 - m^2\,, & k \text{ large}\,. \end{cases} \tag{3.67}$$

Whenever a massive propagator reduces to $-m^2$, it can be pinched in the graph associated to the leading coefficient being computed. Furthermore, the loop current $k_1 + k_2$ becomes a single loop momentum when one of the two momenta is small. Because of these simplifications, the two-loop graph may factorize into the product of two one-loop graphs. Setting scaleless contributions to zero, only two regions contribute to the leading power behaviors:

k_1	k_2	$k_1 + k_2$	contribution		
S	S	S	scaleless		
S	L	L	$D^{(2)}_{S,L,L}$	$\longrightarrow$	$C(\epsilon, \eta, 0)\, D(\epsilon, 0, 0, m^2)$
L	S	L	scaleless		
L	L	S	scaleless		
L	L	L	$D^{(2)}_{L,L,L}$	$\longrightarrow$	$D^{(2)}(\epsilon, 0, 0, m^2)\,.$

(3.68)

Here, S and L stand for small and large, respectively, $C(\epsilon, \eta, 0)$ is the one-loop massless triangle and $D(\epsilon, 0, 0, m^2)$ is the one-loop massive box computed at vanishing external kinematics. As the former only depends on the scale η, its power behavior can be obtained by counting the energy dimension and using the homogeneity property in eq. (2.103), which leads to $\eta^{-1-\epsilon}$ in $4 - 2\epsilon$ dimensions. Therefore, the leading power behaviors for the double box are given by

$$D^{(2)}(\epsilon, \eta, \eta, m^2) \overset{\eta \to 0}{\sim} \eta^{-1-\epsilon} \left[C(\epsilon, 1, 0) D(\epsilon, 0, 0, m^2) + \mathcal{O}(\eta) \right] + D^{(2)}(\epsilon, 0, 0, m^2) + \mathcal{O}(\eta)$$

[4] Since the fixed mass is perceived as infinite from the vanishing kinematics, this exact same analysis is the one needed for the iterative version of the AMFlow method, where the auxiliary mass is inserted only in a limited number of propagators. Also, note that this example falls within the class of cases mentioned in [52], where it is possible to introduce the auxiliary mass only in those propagators that already present a given mass (m in this example), so that the number of MIs does not increase.

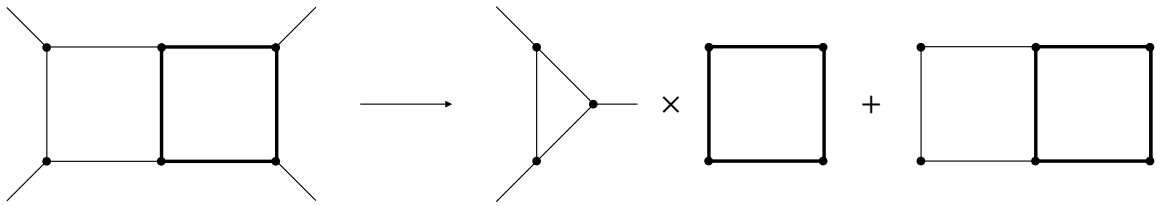

Figure 3.1: Leading coefficients for the expansion by regions of a planar double-box $D(\epsilon, s, t, m^2)$ in the limit of vanishing external kinematics. Massive edges are indicated with bold lines. The two contributions on the right corresponds to $C(\epsilon, 1, 0)D(\epsilon, 0, 0, m^2)$ and $D^{(2)}(\epsilon, 0, 0, m^2)$, respectively.

$$= \eta^{-1-\epsilon} \left[\text{const.} + \mathcal{O}(\eta) \right] + \text{const.} + \mathcal{O}(\eta) \,, \tag{3.69}$$

which corresponds to figure 3.1. As we can see, setting the external kinematics to zero does not suffice in this case to identify all the leading coefficients, as it would leave out the power behavior $\eta^{-1-\epsilon}$. In section 4.3.3 we discuss how eq. (3.69) can be used as a BC when solving the DEs for the associated integral family. Once again, it turns out that the specific values of the leading coefficients are not important, as long as we know what power behaviors they multiply. This means that, knowing the power behaviors of the solution, the corresponding leading coefficients can be extracted from the analysis of the DEs.

Chapter 4

Series expansion methods for differential equations

Given the differential equations for a set of master integrals and boundary conditions at a phase space point, the series expansion method can be used to solve the differential equations along lines connecting the boundary point to multiple target points. This allows for the numerical propagation of the integrals across the phase space. In this chapter we describe all the steps necessary for such propagation, providing algorithmic procedures that are implemented in LINE.

Since Feynman integrals have singularities, the radius of convergence of the series solution at any point is finite. Therefore, in section 4.1 we show how to identify a sequence of intermediate points on the phase space path, around which the system of DEs must be solved locally to progressively move closer to the target point. The solution evaluated at any path point can be stored to be later used as boundary value for the propagation towards different targets, possibly following a scheme that populates the phase space according to a grid for Monte Carlo integration. The intermediate points on the path can be either regular or regular singular. In both cases we adopt the block strategy outlined in section 3.2, where the equations are solved sector by sector. Therefore, the techniques illustrated in this chapter deal with systems of non-homogeneous DEs.

Section 4.2 is devoted to the expansion around regular points, where the solution has a Taylor series. Substituting its expression into the DEs, we derive recurrence relations that express the higher-order coefficients of the series in terms of the lower-order ones, thus allowing the numerical evaluation of the solution up to the desired order. A similar procedure is carried out in section 4.3 to find the solution around singular points, except that here the series expansion of the MIs also includes non-integer powers of the line parameter and integer powers of its logarithm, as discussed in section 3.3. First, in section 4.3.1 we build the general solution to the associated homogeneous equation as a linear combination of independent solutions with unknown coefficients. Then, we add a particular solution to the non-homogeneous equation found in section 4.3.2. Finally,

in section 4.3.3 we show how to fix the unknown coefficients by matching BCs. This is straightforward when the MIs are known in a regular point within the radius of convergence, so that the main focus is on the case where the BCs are given in terms of the leading behaviors of the MIs around the singularity. In particular, expanding on the discussion in section 3.4.2, we describe a systematic method to automatically obtain linear constraints on the unknown coefficients by imposing that the powers in the leading behaviors of the solution are the ones predicted through expansion by regions. In this way, the number of leading coefficients to be actually provided as BCs is reduced as much as possible. We show this procedure at work on a few examples.

4.1 Navigating the phase space

Let $\mathbf{s}(\eta)$ be a phase space curve passing through a boundary point $\mathbf{s}_0$ at $\eta = \eta_0$ and let $\mathbb{A}(\eta)$ be the associated differential equation matrix as in eq. (2.115). The DEs can be solved via series expansion around the boundary point η_0. However, as the matrix $\mathbb{A}(\eta)$ has in general several singularities, the series solution only has a finite radius of convergence $\mathcal{R}(\eta_0)$, equal to the distance between η_0 and its closest pole, while the target point $\mathbf{s}_1 = \mathbf{s}(\eta_1)$ may lie outside said range. Nonetheless, even when this happens, we can still move a step closer to the target by evaluating the solution in a point within the disk of convergence $|\eta - \eta_0| < \mathcal{R}(\eta_0)$, and use it as a new boundary point to solve again via series expansion. By iterating this procedure, we can advance step by step along the curve $\mathbf{s}(\eta)$ to get closer and closer to the target, until eventually η_1 lies within the radius of convergence of the last boundary point.

Complications arise whenever a pole of $\mathbb{A}(\eta)$ is encountered along the curve, say at $\eta = \eta_s$. This happens for instance when the kinematic invariants $\mathbf{s}(\eta)$ cross the singular surface corresponding to a threshold for the production of intermediate on-shell states, as discussed in section 5.2. If we were to apply the strategy outlined above without modifications even after η_s becomes the closest pole, the radius of convergence would decrease at each step so that we would endlessly get closer to the singularity and never cross it. Two different approaches are possible to overcome this problem. In the first one we use the singularity as expansion point, solve via series expansion using the ansatz of eq. (3.25), match the boundary values computed at the previous propagation step and evaluate the solution beyond η_s. We refer to this procedure by saying that we cross the singular point. Alternatively, we could take a detour around the singularity performing steps of regular propagations in the complex plane of η, coming back to the real axis beyond the pole η_s. Both the crossing and the detour require prior knowledge of the branch cut configuration of the master integrals if η_s is a branch point. A detailed prescription to handle the analytic continuation is provided in section 5.3. In the following, we assume that all singular points encountered along the path are crossed, since solving by expansion

around a singularity remains necessary to determine boundary conditions (see section 3.4) and to evaluate limits corresponding to degenerate kinematic configurations.

We now discuss how the choice of the expansion and the evaluation points can be made algorithmic. First of all, we need to choose the size $\mathcal{S}(\eta)$ of each step along the path. As we know, any value smaller than $\mathcal{R}(\eta)$ is a suitable choice when expanding around a given point η. However, the closer $\mathcal{S}(\eta)$ is to the radius of convergence, the more terms we need to include in the series solution in order to evaluate its sum at a given working precision, as the convergence becomes slower. On the other hand, smaller values for $\mathcal{S}(\eta)$ demand a larger number of propagation steps to reach the target point. We choose $\mathcal{S}(\eta) = \mathcal{R}(\eta)/2$ as a reasonable compromise between these competing two effects, where the factor $1/2$ also finds an independent justification, as an upper limit, in the prescription for the analytic continuation discussed in section 5.3.2.

To populate the path with the expansion points, we start by identifying the singular points $\eta = \sigma_i$ that are located on the path and hence split the interval $[0, 1]$ into several segments. We label these points in increasing order, $\sigma_i < \sigma_{i+1}$. For each σ_i, we compute the radius of convergence as

$$\mathcal{R}(\sigma_i) = \min \{ \, |\pi - \sigma_i| : \, \pi \in \Pi \, , \, \pi \neq \sigma_i \, \} \, , \tag{4.1}$$

where Π is the set of all the DE poles, including those outside the path. We then place two matching points $\mu_{i,L}, \mu_{i,R}$ on the left and on the right of σ_i, respectively:

$$\mu_{i,L} = \sigma_i - \mathcal{S}(\sigma_i) \, , \qquad \mu_{i,R} = \sigma_i + \mathcal{S}(\sigma_i) \, . \tag{4.2}$$

While solving around σ_i, the matching point on the left is used as boundary point and the one on the right as target. For the propagation along the segment between a matching point $\mu_{i,R}$ on the right of σ_i and the point $\mu_{i+1,L}$ on the left of the next singularity σ_{i+1}, we place a set of regular points $\rho_{i,j}$ according to

$$\rho_{i,1} = \mu_{i,R} + \mathcal{S}(\mu_{i,R}) \, , \qquad \rho_{i,k+1} = \rho_{i,k} + \mathcal{S}(\rho_{i,k}) \, , \quad k \geq 1 \, , \tag{4.3}$$

until eventually the condition $\rho_{i,K} + \mathcal{R}(\rho_{i,K})/2 > \mu_{i+1,L}$ is satisfied for some K, meaning that $\rho_{i,k+1}$ lies within the disk of convergence centered at the singular point σ_{i+1} and so it can be discarded in favor of $\mu_{i+1,L}$. The path segment is thus split as

$$\mathcal{P}_i \equiv (\, \sigma_i \, , \, \mu_{i,R} \, , \, \rho_{i,1} \, , \, \rho_{i,2} \, , \, \ldots \, , \, \rho_{i,K} \, , \, \mu_{i+1,L} \, , \, \sigma_{i+1} \,) \, . \tag{4.4}$$

Merging all the segments we obtain the complete list $\mathcal{P} \equiv \bigcup_i \mathcal{P}_i$ of path points.

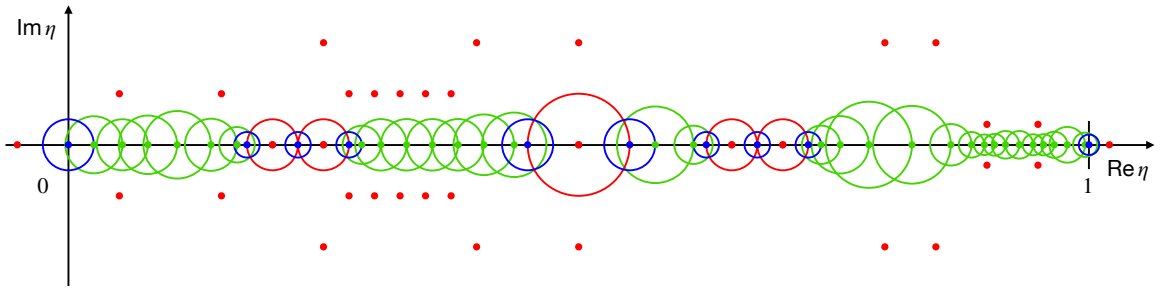

Figure 4.1: Poles and path points in the complex plane of the line parameter η. The propagation path corresponds to the interval $[0, 1]$. Red dots are singularities of the DE matrix, blue dots are matching points and green dots are regular points. In this example, $\eta = 0$ and $\eta = 1$ are regular and therefore considered as matching points. Each point η on the path is at the center of a circle of radius $\mathcal{S}(\eta)$ equal to half the distance from its closest pole. The closer singularities lie to the path, the smaller the step size $\mathcal{S}(\eta)$ becomes, and vice versa.

If $\eta = 0$ is not a pole of the DE, we consider it as a matching point when populating the first segment of the path with regular points. Otherwise, we can label $\sigma_0 = 0$ and treat it as any other singular point. The same reasoning applies to the last segment in the cases where $\eta = 1$ is regular or singular. Figure 4.1 represents a schematic configuration of poles and path points in the complex plane of η.

In the following sections, we focus on how to solve the differential equation

$$\frac{d}{d\eta}\mathbf{I}(\eta) = \mathbb{A}(\eta)\mathbf{I}(\eta) \tag{4.5}$$

employing the series expansion method around any regular or singular point of the path. We omit the dependence on the dimensional regularization parameter ϵ, assuming that it has been fixed to a numerical value as prescribed in section 3.1. By means of a shift, we can always center the problem around the path point at hand so that, without loss of generality, $\eta = 0$ becomes the expansion point. As discussed in section 3.2, we order the MIs so as to make the matrix $\mathbb{A}(\eta)$ lower block triangular and we solve sector by sector, trading the homogeneous problem in eq. (4.5) for a set of smaller non-homogeneous sector equations to be solved sequentially. Omitting the sector index (r) for an easier notation, the DE for a generic sector is in the form

$$\frac{d}{d\eta}\mathbf{I}(\eta) = \mathbb{A}(\eta)\mathbf{I}(\eta) + \mathbf{J}(\eta)\,, \tag{4.6}$$

where $\mathbb{A}(\eta)$ now indicates the block matrix $\mathbb{A}^{(r,r)}(\eta)$ of eq. (3.13) and the non-homogeneous term $\mathbf{J}(\eta)$ is generated combining the sub-diagonal blocks and the solution of the previous $r-1$ sectors as for $\mathbf{J}^{(r)}(\eta)$ in eq. (3.14).

By dropping the sector index, we stress that the results obtained in the following sections are valid for any non-homogeneous DE as the one in eq. (4.6), provided that the non-homogeneous term has a regular or regular singular series expansion. Despite this, we always refer to any quantity as to a block or sector object, in order to keep track of the original block-structured problem.

Finally, note that the series expansions considered in the next sections formally include an infinite number of terms. However, any numerical implementation of the methods provided in this chapter would only involve the (finite) number of orders necessary to observe convergence on all the digits of working precision, as discussed in appendix A.3.

4.2 Solving around regular points

In this section we focus on the Cauchy problem consisting of the differential equation (4.6) together with the boundary condition $\mathbf{I}(0) = \mathbf{I}_{\text{bc}}$. As explained in section 4.1, in our framework of iterated propagation steps, $\mathbf{I}_{\text{bc}}$ is the solution of the previous step evaluated at the (regular) expansion point that we use as origin $\eta = 0$ at the current step. Since by assumption the DE matrix $\mathbb{A}(\eta)$ is regular at $\eta = 0$, the solution has the Taylor expansion

$$\mathbf{I}(\eta) = \sum_{j=0}^{\infty} \mathbf{I}_j \eta^j \,. \tag{4.7}$$

Using this series as ansatz, the BC can be imposed right away by choosing $\mathbf{I}_0 = \mathbf{I}_{\text{bc}}$, since the series is equal to its zero-order coefficient when evaluated at the origin.

It is useful to multiply both sides of eq. (4.6) by the least common denominator $g(\eta)$ of the block matrix $\mathbb{A}(\eta)$, arriving at

$$g(\eta)\frac{d}{d\eta}\mathbf{I} = \mathbb{B}(\eta)\mathbf{I}(\eta) + \mathbf{Y}(\eta) \,, \tag{4.8}$$

where we define the functions

$$\mathbb{B}(\eta) \equiv g(\eta)\mathbb{A}(\eta) \,, \quad \mathbf{Y}(\eta) \equiv g(\eta)\mathbf{J}(\eta) \,. \tag{4.9}$$

We then consider the series expansion of all the quantities appearing in eq. (4.8), namely, eq. (4.7) for the solution and

$$g(\eta) = \sum_{k=0}^{\infty} g_k \eta^k \,, \quad \mathbb{B}(\eta) = \sum_{k=0}^{\infty} \mathbb{B}_k \eta^k \,, \quad \mathbf{Y}(\eta) = \sum_{k=0}^{\infty} \mathbf{Y}_k \eta^k \,. \tag{4.10}$$

Here, the series of $g(\eta)$ and $\mathbb{B}(\eta)$ only contain a finite number of terms. In fact, $g_k = 0$ for $k > D(g)$, where $D(g)$ is the polynomial degree of $g(\eta)$; at the same time $\mathbb{B}(\eta)$ is a

matrix of polynomials since, by construction, all the denominators of $\mathbb{A}(\eta)$ were canceled out upon multiplication by $g(\eta)$, and so $\mathbb{B}_k = 0$ for k greater than the maximum among the polynomial degrees of the elements in $\mathbb{B}(\eta)$, that we indicate with $D(\mathbb{B})$. On the other hand, the non-homogeneous term $\mathbf{J}(\eta)$ has an infinite number of coefficients coming from the solutions of the previous sectors and the expansion of the denominators in the sub-diagonal blocks $\mathbb{A}^{(r,s)}(\eta)$, $r > s$, that are in general not canceled out by the action of $g(\eta)$. These coefficients can be computed using efficient algorithms for the expansion of the inverse of a polynomial [119].

We now derive recurrence relations for the coefficients $\mathbf{I}_k$ of the ansatz by inserting into eq. (4.8) the Taylor series of eqs. (4.7) and (4.10). At first we obtain

$$\sum_{m,k=0}^{\infty} k g_m \mathbf{I}_k \eta^{m+k-1} = \sum_{n,k=0}^{\infty} \mathbb{B}_n \mathbf{I}_k \eta^{n+k} + \sum_{j=0}^{\infty} \mathbf{Y}_j \eta^j \,. \tag{4.11}$$

Then, we aim to change indices in such a way that all the sums have the same power η^j factored out, since this would allow us to obtain a relation for any order j. We have

$$\begin{aligned} m \to j+1-k \quad &\Longrightarrow \quad \sum_{m,k=0}^{\infty} k g_m \mathbf{I}_k \eta^{m+k-1} = \sum_{j=0}^{\infty} \sum_{k=0}^{j+1} k g_{j+1-k} \mathbf{I}_k \eta^j \,, \\ n \to j-k \quad &\Longrightarrow \quad \sum_{n,k=0}^{\infty} \mathbb{B}_n \mathbf{I}_k \eta^{n+k} = \sum_{j=0}^{\infty} \sum_{k=0}^{j} \mathbb{B}_{j-k} \mathbf{I}_k \eta^j \,, \end{aligned} \tag{4.12}$$

where the upper limits of the sums over k can be easily deduced by vetoing the presence of coefficients g_m and $\mathbb{B}_n$ with negative index. In terms of the new indices, eq. (4.11) reads, for any order j,

$$\sum_{k=0}^{j+1} k g_{j+1-k} \mathbf{I}_k = \sum_{k=0}^{j} \mathbb{B}_{j-k} \mathbf{I}_k + \mathbf{Y}_j \,. \tag{4.13}$$

The key feature here is that, due to the polynomial nature of $g(\eta)$ and $\mathbb{B}(\eta)$, the sums only involve a finite number of terms and so we can isolate the highest-order coefficient $\mathbf{I}_{j+1}$ figuring in the sum on the left-hand side to express it as a combination of lower-order coefficients:

$$\mathbf{I}_{j+1} = \frac{1}{(j+1) g_0} \left[\mathbf{Y}_j - \sum_{k=a_1(j)}^{j} k g_{j+1-k} \mathbf{I}_k + \sum_{k=a_2(j)}^{j} \mathbb{B}_{j-k} \mathbf{I}_k \right] , \tag{4.14}$$

where the lower limits $a_1(j) = \max\{0,\, j{+}1{-}D(g)\}$ and $a_2(j) = \max\{0,\, j{-}D(\mathbb{B})\}$ explicitly show how many non-zero orders are included in each sum. Note that $g_0 \neq 0$ in the

denominator of eq. (4.14), since by assumption $\eta = 0$ is a regular point and so it is not a root of $g(\eta)$. Eq. (4.14) is the recurrence relation we were looking for, since its repeated application allows us to start from the lowest-order coefficient $\mathbf{I}_0 = \mathbf{I}_{\text{bc}}$ and build the rest of the series solution up to the desired order.

4.3 Solving around regular singular points

Suppose now that boundary conditions for eq. (4.6) are assigned at some regular point $\eta = \eta_{\text{bc}} < 0$ that lies within the disk of convergence of a regular singular point $\eta = 0$. Then, solving the differential equations around the singularity would allow us to evaluate the series solution at any other point within said disk, or evaluate the limit $\eta \to 0$ when this exists. In the following, we assume that the system has been transformed to Fuchsian normal form following the methods discussed in section 3.3.2.

The approach for solving eq. (4.6) around a regular singular point is in principle very similar to the regular case, with two modifications. First of all, motivated by the discussion in section 3.3.1, we use the ansatz

$$\mathbf{I}(\eta) = \sum_{\lambda \in \Lambda} \eta^\lambda \sum_{k=0}^{K_\lambda} \frac{\log^k(\eta)}{k!} \sum_{n=0}^{\infty} \mathbf{I}_{\lambda,k,n} \eta^n \,, \tag{4.15}$$

where Λ is the set of eigenvalues of the leading-order coefficient $\mathbb{A}_0$, and K_λ is the highest logarithmic power associated with the eigenvalue λ. Second, we define $g(\eta)$ to be the least common denominator of $\eta\,\mathbb{A}(\eta)$ instead of $\mathbb{A}(\eta)$. In fact, in a Fuchsian basis the multiplication by η removes the root $\eta = 0$ from the denominators, ensuring that $g_0 \neq 0$. With this choice, the actual least common denominator of $\mathbb{A}(\eta)$ is $\eta\, g(\eta)$, which we multiply on both sides of eq. (4.6) to get

$$\eta\, g(\eta) \frac{d}{d\eta} \mathbf{I}(\eta) = \mathbb{B}(\eta) \mathbf{I}(\eta) + \mathbf{Y}(\eta) \,, \tag{4.16}$$

where this time we define $\mathbb{B}(\eta)$ and $\mathbf{Y}(\eta)$ as

$$\mathbb{B}(\eta) \equiv \eta\, g(\eta) \mathbb{A}(\eta) \,, \quad \mathbf{Y}(\eta) \equiv \eta\, g(\eta) \mathbf{J}(\eta) \,. \tag{4.17}$$

Combining the Taylor series of $g(\eta)$ and $\mathbb{B}(\eta)$ with the ansatz in eq. (4.15), we can expand in series each term of eq. (4.16) as

$$\eta\, g(\eta) \frac{d}{d\eta} \mathbf{I}(\eta) = \sum_{i,\lambda,k,n} g_i \left[\mathbf{I}_{\lambda,k+1,n-i} + (\lambda + n - i) \mathbf{I}_{\lambda,k,n-i} \right] \frac{\log^k(\eta)}{k!} \eta^{\lambda+n} \,,$$

$$\mathbb{B}(\eta)\mathbf{I}(\eta) = \sum_{j,\lambda,k,n} \mathbb{B}_j \mathbf{I}_{\lambda,k,n-j} \frac{\log^k(\eta)}{k!} \eta^{\lambda+n}\,, \tag{4.18}$$

while the series expansion of $\mathbf{Y}(\eta)$ picks up powers of $\log(\eta)$ and non-integer powers of η from the solutions of the previous sectors:

$$\mathbf{Y}(\eta) = \sum_{\lambda\in\Lambda} \eta^\lambda \sum_{k=0}^{K_\lambda} \frac{\log^k(\eta)}{k!} \sum_{m=0}^{\infty} \mathbf{Y}_{\lambda,k,m} \eta^m\,. \tag{4.19}$$

Substituting each piece into eq. (4.16) we obtain, for any λ, n, k,

$$\sum_{i=0}^{\min\{D(g),n\}} g_i \mathbf{I}_{\lambda,k+1,n-i} + \sum_{i=0}^{\min\{D(g),n\}} (\lambda+n-i)\, g_i \mathbf{I}_{\lambda,k,n-i} = \sum_{i=0}^{\min\{D(\mathbb{B}),n\}} \mathbb{B}_i \mathbf{I}_{\lambda,k,n-i} + \mathbf{Y}_{\lambda,k,n}\,. \tag{4.20}$$

This equation involves a finite number of orders of the ansatz solution. Depending on whether we want to isolate the coefficients of the highest power of η or $\log(\eta)$, we can extract two recurrence relations:

$$\mathbf{I}_{\lambda,k+1,n} = \frac{1}{g_0}\left[\sum_{i=0}^{\min\{D(\mathbb{B}),n\}} \mathbb{B}_i \mathbf{I}_{\lambda,k,n-i} - \sum_{i=0}^{\min\{D(g),n\}} (\lambda+n-i) g_i \mathbf{I}_{\lambda,k,n-i} - \sum_{i=1}^{\min\{D(g),n\}} g_i \mathbf{I}_{\lambda,k+1,n-i} + \mathbf{Y}_{\lambda,k,n}\right], \tag{4.21a}$$

$$\mathbf{I}_{\lambda,k,n} = [\mathbb{B}_0 - (\lambda+n) g_0 \mathbb{1}]^{-1} \times \left[\sum_{i=0}^{\min\{D(g),n\}} g_i \mathbf{I}_{\lambda,k+1,n-i} - \sum_{i=1}^{\min\{D(\mathbb{B}),n\}} \mathbb{B}_i \mathbf{I}_{\lambda,k,n-i} - \sum_{i=1}^{\min\{D(g),n\}} (\lambda+n-i) g_i \mathbf{I}_{\lambda,k,n-i} - \mathbf{Y}_{\lambda,k,n}\right]. \tag{4.21b}$$

Note that the matrix on the right-hand side of the second relation,

$$\mathbb{B}_0 - (\lambda+n) g_0 \mathbb{1} = g_0 \left[\mathbb{A}_0 - (\lambda+n)\mathbb{1}\right]\,, \tag{4.22}$$

is invertible if and only if $\lambda+n$ is not an eigenvalue of the Jordan matrix $\mathbb{A}_0$. Given the absence of resonances, this is guaranteed only for $n > 0$.

The recurrence relation in eq. (4.21a) connects the logarithmic order $k+1$ with lower ones, but also with the same order $k+1$ at lower powers of η. At the same time eq. (4.21b) connects higher orders in η with lower ones but also with higher logarithmic orders. Therefore, to properly compute all the coefficients of the series solutions, the two relations have to be applied according to a precise scheme.

In the next sections, we illustrate how to employ eq. (4.21) to build a particular solution to eq. (4.6), to be added to the general solution of the associated homogeneous DE, the latter being a linear combination of independent solutions with unconstrained coefficients. We then fix these coefficients in order to match the BCs of the Cauchy problem.

4.3.1 General solution to the homogeneous equation

In this section we solve the homogeneous equation associated with eq. (4.6). That is, we consider the non-homogeneous term $\mathbf{Y}(\eta)$ to be zero so that, in the recurrence relations in eq. (4.21), we can set $\mathbf{Y}_{\lambda,k,n} = 0$.

To begin with, we set some notation for the Jordan structure of the matrix $\mathbb{A}_0$. Let L be the dimension of the block and λ_j, $j = 1, \dots, L$, the eigenvalue on the j-th column of the Jordan matrix $\mathbb{A}_0$. We indicate with $a(j)$ the Jordan chain of eigenvalue λ_j and length $L(j)$ that includes the generalized eigenvector associated with column j. Therefore, for a chain that starts on column k, we have $\lambda_{k+i} = \lambda_k$, $a(k+i) = a(k)$ and $L(k+i) = L(k)$ for any $i = 0, \dots, L(k) - 1$.

The general solution to the homogeneous equation can be represented stacking together L independent solutions as columns of an $L \times L$ matrix $\mathbb{H}(\eta)$ in the form

$$\mathbb{H}[i,j](\eta) = \sum_{\lambda\in\Lambda} \eta^\lambda \sum_{k=0}^{K_\lambda} \frac{\log^k(\eta)}{k!} \sum_{n=0}^{\infty} \mathbb{H}_{\lambda,k,n}[i,j]\eta^n \,, \tag{4.23}$$

where $\mathbb{H}_{\lambda,k,n}$ is a matrix of coefficients and the square brackets $[i,j]$ indicate the row and column indices. We use the notation $[j]$ with a single index in square brackets to select the j-th column of a matrix. Thus for instance $\mathbb{H}[j](\eta)$ is the independent solution stored as j-th column of the matrix $\mathbb{H}(\eta)$.

Our objective is to apply the recurrence relations in eq. (4.21) to compute all the coefficient matrices $\mathbb{H}_{\lambda,k,n}$ appearing in the ansatz of eq. (4.23). We do so following three main steps that are described below.

1. Initialization. We start by initializing the lowest $\log(\eta)$- and η- orders to diagonal matrices according to

$$\mathbb{H}_{\lambda,0,0}[i,j] = \begin{cases} \delta_{ij}\,, & \lambda = \lambda_j\,, \\ 0\,, & \text{otherwise}\,. \end{cases} \tag{4.24}$$

We see right away how this implies, through eqs. (4.21a) and (4.21b), that $\mathbb{H}_{\lambda,k,n}[j] = 0$ $\forall\, k, n$ if $\lambda \neq \lambda_j$, that is, $\mathbb{H}_{\lambda,k,n}$ only has components along the columns associated with the eigenvalue λ_j and, at the same time, the column solution $\mathbb{H}[j](\eta)$ only exhibits the eigenvalue λ_j. As discussed in section 3.3.1, this initialization ensures that the columns $\mathbb{H}[j](\eta)$ are indeed independent solutions of the homogeneous equation.

2. Leading orders for each logarithmic power. Setting $n = 0$ in the recurrence relation (4.21a) with $\mathbf{Y}_{\lambda,k,n} = 0$, the coefficients with logarithmic order $k+1$ on the right-hand side disappear, so that we have

$$\mathbb{H}_{\lambda_j,k+1,0}[j] = \frac{1}{g_0}\left(\mathbb{B}_0 - \lambda_j g_0 \mathbb{1}\right)\mathbb{H}_{\lambda_j,k,0}[j] = (\mathbb{A}_0 - \lambda_j \mathbb{1})\mathbb{H}_{\lambda_j,k,0}[j]\,, \tag{4.25}$$

a relation that we can use to sequentially compute the zero-order coefficients of the Taylor series that multiplies any logarithmic power, starting by using $k = 0$ and going up.

To analyze the resulting structure, we start by iteratively applying eq. (4.25) to relate a given logarithmic order directly to the lowest one:

$$\begin{aligned}\mathbb{H}_{\lambda_j,k,0}[j] &= (\mathbb{A}_0 - \lambda_j \mathbb{1})\,\mathbb{H}_{\lambda_j,k-1,0}[j] \\ &= (\mathbb{A}_0 - \lambda_j \mathbb{1})^2\,\mathbb{H}_{\lambda_j,k-2,0}[j] \\ &= \dots \\ &= (\mathbb{A}_0 - \lambda_j \mathbb{1})^k\,\mathbb{H}_{\lambda_j,0,0}[j]\,.\end{aligned} \tag{4.26}$$

Since $\mathbb{A}_0$ is in Jordan form, $\mathbb{A}_0 - \lambda_j\mathbb{1}$ is a Jordan matrix too (each eigenvalue being just shifted by $-\lambda_j$) and thus each Jordan subspace is invariant under its action. Taking into account that $\mathbb{H}_{\lambda_j,k,0}$ is initialized with non-zero components only along the subspace spanned by the vectors of the chain $a(j)$, we conclude that eq. (4.26) can generate non-zero components at higher logarithmic orders only within said subspace.

In light of the above discussion, we can focus only on the Jordan block of the chain $a(j)$ in the matrix $\mathbb{A}_0 - \lambda_j\mathbb{1}$, which is given by

$$[\mathbb{A}_0 - \lambda_j \mathbb{1}]_{a(j)} = \begin{pmatrix} 0 & 1 & 0 & \dots & 0 \\ 0 & 0 & 1 & \dots & 0 \\ \vdots & \vdots & \vdots & \ddots & \vdots \\ 0 & 0 & 0 & \dots & 1 \\ 0 & 0 & 0 & \dots & 0 \end{pmatrix}, \tag{4.27}$$

This is a nilpotent matrix with degree equal to the length $L(j)$ of the chain, i.e., $L(j)$ is the smallest integer such that

$$\underbrace{[\mathbb{A}_0 - \lambda_j \mathbb{1}]_{a(j)} \times [\mathbb{A}_0 - \lambda_j \mathbb{1}]_{a(j)} \times \dots}_{L(j)\text{ times}} = 0\,. \tag{4.28}$$

Together with eq. (4.26) this implies that, at order zero in η, the maximum logarithmic power for the eigenvalue λ_j is $L(j) - 1$. In particular, the m-th vector of the chain is

initialized at logarithmic order zero with 1 as the m-th component on the associated Jordan subspace and 0 elsewhere; then, the non-zero component is shifted up by one position after every application of $[\mathbb{A}_0 - \lambda_j \mathbb{1}]_{a(j)}$, reaching the boundary of the subspace after $m-1$ iterations and disappearing at the m-th one:

$$\begin{array}{l} i=1 \\ \vdots \\ i=m-1 \\ i=m \\ i=m+1 \\ \vdots \end{array} \begin{array}{c} \\ \begin{pmatrix} 0 \\ \vdots \\ 0 \\ 1 \\ 0 \\ \vdots \end{pmatrix} \\ k=0 \end{array} \rightarrow \begin{array}{c} \\ \begin{pmatrix} 0 \\ \vdots \\ 1 \\ 0 \\ 0 \\ \vdots \end{pmatrix} \\ k=1 \end{array} \rightarrow \ \ldots \ \rightarrow \begin{array}{c} \\ \begin{pmatrix} 1 \\ \vdots \\ 0 \\ 0 \\ 0 \\ \vdots \end{pmatrix} \\ k=m-1 \end{array} \rightarrow \begin{array}{c} \\ \begin{pmatrix} 0 \\ \vdots \\ 0 \\ 0 \\ 0 \\ \vdots \end{pmatrix} \\ k=m \end{array} . \tag{4.29}$$

Therefore, at order zero in η, the m-th vector of a Jordan chain acquires $m-1$ logarithmic powers, whose components are given in eq. (4.29). We indicate with K_j the maximum logarithmic power for the zero η-order of the solution $\mathbb{H}[j](\eta)$.

If we denote by K_λ the maximum logarithmic power at order zero in η among all the solutions with eigenvalue λ, we have

$$K_\lambda = \max\{L(j) : \lambda_j = \lambda\}_j - 1 \,. \tag{4.30}$$

As shown in the next step, K_λ stays the maximum logarithmic power also when considering higher orders in η.

3. Higher orders for each logarithmic power. Having computed every coefficient $\mathbb{H}_{\lambda,k,0}$ of the solution, we are left with the task of computing the non-zero orders in η for each Taylor series. The main complication of eq. (4.21b) is that the logarithmic order k takes contributions also from the logarithmic order $k+1$. Moreover, at higher η-orders the components of different Jordan subspaces mix together. Thus for example, even if $\mathbb{H}_{\lambda_j,k,0}[j] = 0$ in a given subspace, $\mathbb{H}_{\lambda_j,k,1}[j]$ may pick up non-zero contributions from other subspaces due to the term $\mathbb{B}_1 \mathbb{H}_{\lambda_j,k,0}[j]$ on the right-hand side of eq. (4.21b).

An important simplification arises from the following observation. We know that K_j is the maximum logarithmic power of the solution $\mathbb{H}[j](\eta)$ at order zero in η. If we set $\mathbb{H}_{\lambda_j,K_j+1,n}[j] = 0$ for $n \geq 1$ too, then eq. (4.21b) implies $\mathbb{H}_{\lambda_j,k,n}[j] = 0 \ \forall\, k \geq K_j + 2, n \geq 1$ as well. Therefore, we can generalize the results of the previous step at higher η-orders:

- The maximum logarithmic power for the solution associated with the m-th vector of a Jordan chain is $m-1$ at any order in η.
- The maximum logarithmic power for the solution associated with the eigenvalue λ is K_λ given in eq. (4.30).

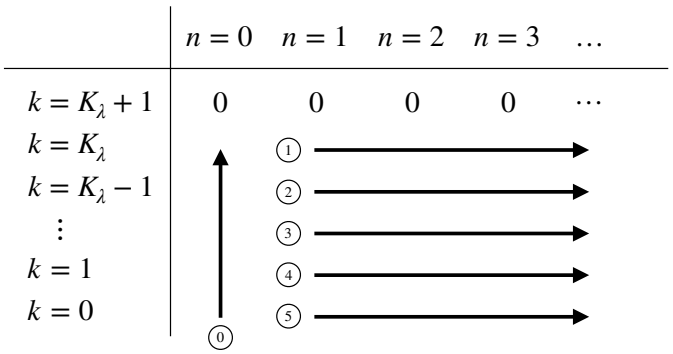

Figure 4.2: Schematic representation of the order followed in computing the coefficients of the solution to the homogeneous DE. Each arrow represents the computation of a sequence of coefficients, to be carried out following the order indicated by the orientation of the arrow. The circled numbers indicate the order in which the arrows themselves are to be followed.

Note that, although we are dealing with the homogeneous equation for the r-th sector, the full-size DE is also homogeneous and so the same results still apply. Therefore, we have proved that, around a regular singular point of a homogeneous DE with matrix $\mathbb{A}(\eta)$, the maximum logarithmic power in the series expansion of the solution is equal to the length, reduced by one unit, of the longest Jordan chain of the leading order $[\eta\mathbb{A}(\eta)]_{\eta=0}$ in a Fuchsian basis.

Returning to the computation of the solution $\mathbb{H}[j](\eta)$, we can now use the recurrence relation in eq. (4.21b) to sequentially fill the η-orders $n = 1$, $n = 2$, ... of the maximum logarithmic power $k = K_j$ (note that for $n \geq 1$ the matrix $\mathbb{B}_0 - (\lambda + n)g_0\mathbb{1}$ is invertible). Then, the same procedure can be repeated for the logarithmic powers $k = K_j - 1$, $k = K_j - 2$, ..., $k = 0$ following this prescribed order, as schematically represented in figure 4.2, thus completing all the coefficients of the solution.

4.3.2 Particular solution to the non-homogeneous equation

We now look for a particular solution $\mathbf{P}(\eta)$ to the recurrence relations of eq. (4.21) without turning off the non-homogeneous term $\mathbf{Y}(\eta)$. Note that, by construction, the eigenvalues λ in the series expansion of the latter come from the solution of the previous sectors. As these eigenvalues contribute to eq. (4.21), they must appear in the general solution for the current sector. On the other hand, the block eigenvalues that are not present in $\mathbf{Y}(\eta)$ are already accounted for in the solution to the homogeneous equation. Therefore, we only need to include the eigenvalues of the non-homogeneous term in our search for a particular solution $\mathbf{P}(\eta)$.

Based on the above observations, we can prove by induction that the set of eigenvalues that contribute to the solution of the first r sectors is precisely the union of the eigenvalues appearing up to sector r. In fact, the DE for the first block is homogeneous and thus its solution only includes the eigenvalues of that block, providing us with a valid base case.

For the induction step, we take the result to be true for the first $r-1$ sectors. This implies that $\mathbf{Y}(\eta)$ has the eigenvalues of the previous $r-1$ sectors. Since the solution for the r-th sector inherits the eigenvalues of $\mathbf{Y}(\eta)$ and also introduces the eigenvalues of sector r, the proof by induction is complete.

While building the particular solution, we distinguish between the eigenvalues present only in $\mathbf{Y}(\eta)$ and those shared by $\mathbf{Y}(\eta)$ and the block $\mathbb{A}_0$. We denote by $K_\lambda[\mathbf{Y}]$ the maximum logarithmic power for the λ-contribution to the non-homogeneous term. To avoid confusion, for block eigenvalues we update the notation of eq. (4.30) and indicate with $K_\lambda[\mathbb{A}]$ (instead of just K_λ) the length, reduced by one unit, of the longest Jordan chain with eigenvalue λ in the block matrix $\mathbb{A}_0$.

Eigenvalues only present in the non-homogeneous term. When λ is not an eigenvalue of $\mathbb{A}_0$, the matrix $\mathbb{B}_0 - \lambda\mathbb{1}$ is invertible and so eq. (4.21b) can be used even with $n = 0$. Because of this, we are able to build a solution relying on eq. (4.21b) alone. In particular, we look for a solution with maximum logarithmic power equal to $K_\lambda[\mathbf{Y}]$. Hence we set $P_{\lambda,K_\lambda[\mathbf{Y}]+1,n} = 0 \;\forall\, n$, so that eq. (4.21b) gives us

$$\mathbf{P}_{\lambda,K_\lambda[\mathbf{Y}],0} = -g_0^{-1}\left(\mathbb{A}_0 - \lambda\mathbb{1}\right)^{-1}\mathbf{Y}_{\lambda,K_\lambda[\mathbf{Y}],0}\,. \tag{4.31}$$

This is consistent with eq. (4.21a), since the insertion of the expression we obtained for $\mathbf{P}_{\lambda,K_\lambda[\mathbf{Y}],0}$ into said recurrence relation leads to

$$\begin{aligned}\mathbf{P}_{\lambda,K_\lambda[\mathbf{Y}]+1,0} &= \left(\mathbb{A}_0 - \lambda\mathbb{1}\right)\mathbf{P}_{\lambda,K_\lambda[\mathbf{Y}],0} + g_0^{-1}\mathbf{Y}_{\lambda,K_\lambda[\mathbf{Y}],0}\\ &= -g_0^{-1}\left(\mathbb{A}_0 - \lambda\mathbb{1}\right)\left(\mathbb{A}_0 - \lambda\mathbb{1}\right)^{-1}\mathbf{Y}_{\lambda,K_\lambda[\mathbf{Y}],0} + g_0^{-1}\mathbf{Y}_{\lambda,K_\lambda[\mathbf{Y}],0}\\ &= -g_0^{-1}\mathbf{Y}_{\lambda,K_\lambda[\mathbf{Y}],0} + g_0^{-1}\mathbf{Y}_{\lambda,K_\lambda[\mathbf{Y}],0} = 0\,.\end{aligned} \tag{4.32}$$

This was to be expected since the two relations in eq. (4.21) are fully equivalent when the matrix $\mathbb{A}_0 - \lambda\mathbb{1}$ is invertible. So $K_\lambda[\mathbf{Y}]$ is indeed the maximum logarithmic power of the solution we are building. Also, note that this choice is possible only because $\mathbf{Y}_{\lambda,k,n}$ does not contribute to eq. (4.21) for logarithmic orders higher than the maximum $K_\lambda[\mathbf{Y}]$.

The remaining coefficients for $k = K_\lambda[\mathbf{Y}]$ can be computed using eq. (4.21b) with $n = 1$, $n = 2$, ... and the same procedure can be repeated for the logarithmic orders $k = K_\lambda[\mathbf{Y}] - 1$, $k = K_\lambda[\mathbf{Y}] - 2$, ..., $k = 0$.

It is interesting to note that the λ-contribution computed in this section,

$$\mathbf{P}_\lambda(\eta) \equiv \eta^\lambda \sum_{k=0}^{K_\lambda[\mathbf{Y}]} \frac{\log^k(\eta)}{k!} \sum_{n=0}^{\infty} \mathbf{P}_{\lambda,k,n}\eta^n\,, \tag{4.33}$$

is unique, in the sense that any other solution differs from $\mathbf{P}_\lambda(\eta)$ by a solution to the homogeneous equation, which does not involve the eigenvalue λ since the latter is not a sector eigenvalue. Therefore, we can conclude that

- The contributions to the solution that are associated with eigenvalues that do not appear on the block $\mathbb{A}_0$ are unique.
- The method outlined above, consisting in using eq. (4.21b) to fill the logarithmic orders starting from $k = K_\lambda[\mathbf{Y}]$ and going down to $k = 0$, automatically selects these contributions.

An important consequence is that any boundary condition on the coefficients of $\mathbf{P}_\lambda(\eta)$ is automatically satisfied for the eigenvalues that are not present on the block. Hence these conditions do not give any valuable information to determine the final solution.

Eigenvalues shared by the non-homogeneous term and the block. As we did for the homogeneous equation, for these eigenvalues λ we start by computing the zero η-orders for each logarithmic power with eq. (4.21a). This time though, we initialize $\mathbf{P}_{\lambda,0,0} = 0$ since the non-homogeneous term is able to give non-zero contributions on its own. The leading coefficients up to the logarithmic order $K_\lambda[\mathbf{Y}] + 1$ are given by

$$\mathbf{P}_{\lambda,k+1,0} = (\mathbb{A}_0 - \lambda\mathbb{1})\,\mathbf{P}_{\lambda,k,0} + g_0^{-1}\mathbf{Y}_{\lambda,k,0}\,, \quad k \leq K_\lambda[\mathbf{Y}]\,. \tag{4.34}$$

Then, at logarithmic powers higher than $K_\lambda[\mathbf{Y}] + 1$ the non-homogeneous term does not contribute anymore, so that

$$\begin{aligned}\mathbf{P}_{\lambda,K_\lambda[\mathbf{Y}]+1+k',0} &= (\mathbb{A}_0 - \lambda\mathbb{1})\,\mathbf{P}_{\lambda,K_\lambda[\mathbf{Y}]+k',0} \\ &= (\mathbb{A}_0 - \lambda\mathbb{1})^2\,\mathbf{P}_{\lambda,K_\lambda[\mathbf{Y}]+k'-1,0} \\ &= \dots \\ &= (\mathbb{A}_0 - \lambda\mathbb{1})^{k'}\mathbf{P}_{\lambda,K_\lambda[\mathbf{Y}]+1,0}\,, \qquad k' \geq 1\,.\end{aligned} \tag{4.35}$$

As it was the case for the homogeneous equation, within the Jordan subspaces of eigenvalue λ there are no logarithmic powers greater than $K_\lambda[\mathbf{P}] \equiv K_\lambda[\mathbf{Y}] + K_\lambda[\mathbb{A}] + 1$, since the corresponding blocks in the matrix $\mathbb{A}_0 - \lambda\mathbb{1}$ are nilpotent with degree less than or equal to $K_\lambda[\mathbb{A}] + 1$. However, the same is not true for all the other blocks and so eq. (4.35) can produce non-zero components outside the subspaces of eigenvalue λ with no upper bound on the logarithmic order.[1] Furthermore, there is no chance that these coefficients are canceled out by a solution of the homogeneous equation, since the latter can only admit a finite number of logarithmic orders.

To find a solution with some maximum logarithmic power, we look for an auxiliary function $\mathbf{P}'(\eta)$ that satisfies eq. (4.21a) with $\mathbf{Y}(\eta) = 0$, since the sum $\mathbf{P}(\eta) + \mathbf{P}'(\eta)$ would

[1] The reason why this issue did not arise for the homogeneous equation is that the solution for a given λ was initialized to zero outside the λ-subspace. In this case though, the non-homogeneous terms may provide, through eq. (4.34), a non-zero input to eq. (4.35).

be a solution to the same equation with $\mathbf{Y}(\eta) \neq 0$. The idea is to make $\mathbf{P}'(\eta)$ cancel out the logarithm powers exceeding a given threshold. Given that these powers are spread across multiple vector components, we look for a linear combination of multiple auxiliary terms in the form

$$\mathbf{P}'(\eta) = \sum_{\lambda \in \Lambda[\mathbb{A}]} \sum_{j=1}^{L} c'_{\lambda,j}\, \mathbb{P}'_{\lambda}[j](\eta)\,, \tag{4.36}$$

where $\Lambda[\mathbb{A}]$ is the set of block eigenvalues, $c'_{\lambda,j}$ are the unknown coefficients to be found and $\mathbb{P}'_{\lambda}[j](\eta)$ is the j-th column of a matrix that correspond to the contribution of a single λ and has the usual kind of series expansion. The initialization of its coefficients is given by

$$\mathbb{P}'_{\lambda,0,0}[i,j] = \begin{cases} \delta_{i,j}\,, & \lambda \neq \lambda_j\,, \\ 0\,, & \lambda = \lambda_j\,. \end{cases} \tag{4.37}$$

As we can see, contrary to what we had for the homogeneous equation, for each column j all eigenvalues λ but the column eigenvalue λ_j contribute and they do so with non-zero components outside their λ-subspaces.

The analysis of eqs. (4.34) and (4.35) showed that the maximum logarithmic power of the final solution cannot be less than $K_\lambda[\mathbf{P}] = K_\lambda[\mathbb{A}] + K_\lambda[\mathbf{Y}] + 1$. Therefore, aiming to cancel out the power located one unit above, we use eq. (4.21a) with $n = 0$ and $\mathbf{Y}_{\lambda,k,n} = 0$ to compute the leading coefficients $\mathbb{P}_{\lambda,k,0}$ up to the logarithmic order $k = K_\lambda[\mathbf{P}] + 1$. Then, we combine $\mathbf{P}(\eta)$ and $\mathbf{P}'(\eta)$ in such a way that the logarithmic power $k = K_\lambda[\mathbf{P}] + 1$ cancels out in the sum. That is, for each λ we impose

$$0 = \mathbf{P}_{\lambda,K_\lambda[\mathbf{P}]+1,0} + \mathbf{P}'_{\lambda,K_\lambda[\mathbf{P}]+1,0} = \mathbf{P}_{\lambda,K_\lambda[\mathbf{P}]+1,0} + \sum_{j=1}^{L} c'_{\lambda,j} \mathbb{P}'_{\lambda,K_\lambda[\mathbf{P}]+1,0}[j]\,. \tag{4.38}$$

The vector components outside the Jordan subspaces associated with λ form a system of linear equations for the unknown coefficients $c'_{\lambda,j}$. Solving the system allows us to fix $\mathbf{P}'_{\lambda,k,0}$ and redefine the leading coefficients for each logarithmic power according to

$$\mathbf{P}_{\lambda,k,0} \to \mathbf{P}_{\lambda,k,0} + \mathbf{P}'_{\lambda,k,0}\,. \tag{4.39}$$

The new solution has $\mathbf{P}_{\lambda,K_\lambda[\mathbf{P}]+1,0} = 0$ by construction, while eq. (4.21a) with $n = 0$ confirms that any power greater than $K_\lambda[\mathbf{P}] + 1$ vanishes as well:

$$\mathbf{P}_{\lambda,K_\lambda[\mathbf{P}]+1+k',0} = (\mathbb{A}_0 - \lambda \mathbb{1})^{k'} \mathbf{P}_{\lambda,K_\lambda[\mathbf{P}]+1,0} = 0\,, \quad k' \geq 1\,. \tag{4.40}$$

For these logarithmic powers we can set to zero also the higher orders in η,

$$\mathbf{P}_{\lambda,k,n} = 0 \quad \forall\, k > K_\lambda[\mathbf{P}]\,, n > 0\,, \tag{4.41}$$

and stay consistent with eq. (4.21b).

As usual, the remaining coefficients can be computed using eq. (4.21b) with $n = 0$, $n = 1, \dots$ to determine the Taylor series for the logarithmic orders $k = K_\lambda[\mathbf{P}]$, $k = K_\lambda[\mathbf{P}] - 1, \dots, k = 0$, respectively.

Note that, for each block eigenvalue, the addition of any solution to the homogeneous equation leaves unchanged the coefficients of the logarithmic orders higher than $K_\lambda[\mathbb{A}]$. In this sense, the contribution

$$\mathbf{P}_{\lambda,k>K_\lambda[\mathbb{A}]}(\eta) \equiv \eta^\lambda \sum_{k=K_\lambda[\mathbb{A}]+1}^{K_\lambda[\mathbf{P}]} \frac{\log^k(\eta)}{k!} \sum_{n=0}^{\infty} \mathbf{P}_{\lambda,k,n} \eta^n \tag{4.42}$$

is unique, hence any boundary condition on its coefficients does not provide any useful information to fix the solution.

4.3.3 Matching boundary conditions

Having computed a particular solution to eq. (4.6) and L independent solutions to its associated homogeneous equation, we are ready to write down the general solution. Recalling that we assumed to operate in a Fuchsian basis, we restore the tilde notation to indicate any quantity evaluated in such basis. Also, we introduce back the sector index (r), so that the general solution in a Fuchsian basis is given by

$$\widetilde{\mathbf{I}}^{(r)}(\eta) = \widetilde{\mathbf{P}}^{(r)}(\eta) + \sum_{j=1}^{L_r} c_j \widetilde{\mathbb{H}}^{(r)}[j](\eta)\,, \tag{4.43}$$

where the unknown coefficients c_j are to be determined imposing boundary conditions. These may be provided as the value of the solution at a given point $\eta = \eta_{\text{bc}}$ within the radius of convergence, or rather as constraints on the leading coefficients of the series expansion around $\eta = 0$.

In the first case, the conditions $\mathbf{I}(\eta_{\text{bc}}) = \mathbf{I}_{\text{bc}}$ can be imposed directly in the Fuchsian basis by transforming the boundary values according to

$$\widetilde{\mathbf{I}}^{(r)}_{\text{bc}} = \sum_{s=1}^{r} \mathbb{T}^{(r,s)-1}(\eta)\, \mathbf{I}^{(s)}_{\text{bc}}\,, \tag{4.44}$$

where $\mathbb{T}(\eta)$ is the transformation matrix. The coefficients c_j are to be found as solution of

$$\widetilde{\mathbf{I}}^{(r)}_{\text{bc}} = \widetilde{\mathbf{I}}^{(r)}(\eta_{\text{bc}}) = \widetilde{\mathbf{P}}^{(r)}(\eta_{\text{bc}}) + \sum_{j=1}^{L_r} c_j\, \widetilde{\mathbb{H}}^{(r)}[j](\eta_{\text{bc}})\,, \tag{4.45}$$

which is a system of L_r linear equations with matrix $\widetilde{\mathbb{H}}^{(r)}(\eta_{\rm bc})$ and constant term equal to $\widetilde{\mathbf{I}}^{(r)}_{\rm bc} - \widetilde{\mathbf{P}}^{(r)}(\eta_{\rm bc})$. As discussed in section 5, to evaluate both the matrix and the constant term at $\eta = \eta_{\rm bc}$, we need to perform the analytic continuation of the complex logarithm $\log(\eta)$ and the powers η^λ to ensure that the branch cut structure is the expected one. Once this is done and the coefficients c_j are known, the solution is completely determined, ready to be evaluated at any target point $\eta = \eta_{\rm t}$ within the radius of convergence and transformed back to the original non-Fuchsian basis:

$$\mathbf{I}^{(r)}(\eta_{\rm t}) = \sum_{s=1}^{r} \mathbb{T}^{(r,s)}(\eta_{\rm t})\, \widetilde{\mathbf{I}}^{(s)}(\eta_{\rm t})\,. \tag{4.46}$$

The situation is more involved when BCs are assigned in terms of the leading coefficients of the series expansion around $\eta = 0$. As these conditions are given in the non-Fuchsian basis, we transform back the entire series solution:

$$\begin{aligned}
\mathbf{I}^{(r)}(\eta) &= \sum_{s=1}^{r} \mathbb{T}^{(r,s)}(\eta)\, \widetilde{\mathbf{I}}^{(s)}(\eta) \\
&= \sum_{s=1}^{r-1} \mathbb{T}^{(r,s)}(\eta) \widetilde{\mathbf{I}}^{(s)}(\eta) + \mathbb{T}^{(r,r)}(\eta) \widetilde{\mathbf{P}}^{(r)}(\eta) + \sum_{j=1}^{L_r} c_j \mathbb{T}^{(r,r)}(\eta) \widetilde{\mathbb{H}}^{(r)}[j](\eta) \\
&\equiv \mathbf{I}^{(r)}_{\rm pb}(\eta) + \mathbf{P}^{(r)}(\eta) + \sum_{j=1}^{L_r} c_j \mathbb{H}^{(r)}[j](\eta)
\end{aligned} \tag{4.47}$$

As the transformation matrix consists of rational functions, the series expansion of its blocks is in the form

$$\mathbb{T}^{(r,s)}(\eta) = \frac{1}{\eta^{t^{(r,s)}}} \sum_{m=0}^{\infty} \mathbb{T}^{(r,s)}_m \eta^m\,, \tag{4.48}$$

where $t^{(r,s)}$ is an integer, and so each term of eq. (4.47) expands in series as

$$\begin{aligned}
\mathbf{I}^{(r)}_{\rm pb}(\eta) &\equiv \sum_{s=1}^{r-1} \mathbb{T}^{(r,s)}(\eta)\, \widetilde{\mathbf{I}}^{(s)}(\eta) = \sum_{\lambda \in \Lambda^{(<r)}} \sum_{s=1}^{r-1} \eta^{\lambda - t^{(r,s)}} \sum_{k=0}^{K_\lambda^{(<r)}} \frac{\log^k(\eta)}{k!} \sum_{n,m=0}^{\infty} \eta^{n+m}\, \mathbb{T}^{(r,s)}_m \widetilde{\mathbf{I}}^{(s)}_{\lambda,k,n}\,, \\
\mathbf{P}^{(r)}(\eta) &\equiv \mathbb{T}^{(r,r)}(\eta) \widetilde{\mathbf{P}}^{(r)}(\eta) = \sum_{\lambda \in \Lambda^{(<r)}} \eta^{\lambda - t^{(r,r)}} \sum_{k=0}^{K_\lambda^{(r)[\mathbf{P}]}} \frac{\log^k(\eta)}{k!} \sum_{n,m=0}^{\infty} \eta^{n+m}\, \mathbb{T}^{(r,r)}_m \widetilde{\mathbf{P}}^{(r)}_{\lambda,k,n}\,, \\
\mathbb{H}^{(r)}(\eta) &\equiv \mathbb{T}^{(r,r)}(\eta) \widetilde{\mathbb{H}}^{(r)}(\eta) = \sum_{\lambda \in \Lambda^{(r)}} \eta^{\lambda - t^{(r,r)}} \sum_{k=0}^{K_\lambda^{(r)[\mathbb{A}]}} \frac{\log^k(\eta)}{k!} \sum_{n,m=0}^{\infty} \eta^{n+m}\, \mathbb{T}^{(r,r)}_m \widetilde{\mathbb{H}}^{(r)}_{\lambda,k,n}\,.
\end{aligned} \tag{4.49}$$

Here, we introduced the notation $\Lambda^{(r)}$ to indicate the set of eigenvalues of $\widetilde{\mathbb{A}}^{(r,r)}_0$, while $\Lambda^{(<r)} \equiv \bigcup_{s<r} \Lambda^{(s)}$ are the eigenvalues of the previous sectors. At the same time, $K_\lambda^{(<r)}$ is

the maximum logarithmic power for the λ-contribution to the solution for the first $r-1$ sectors, while $K_\lambda^{(r)}[\mathbf{P}] \equiv K_\lambda[\widetilde{\mathbf{P}}^{(r)}]$ and $K_\lambda^{(r)}[\mathbb{A}] \equiv K_\lambda[\widetilde{\mathbb{A}}^{(r,r)}]$. From eqs. (4.47) and (4.49) one can easily read off the coefficients $\mathbf{I}^{(r)}_{\lambda,k,n}$ for the series expansion of the solution in the non-Fuchsian basis,

$$\mathbf{I}^{(r)}(\eta) = \sum_{\lambda\in\Lambda^{(<r)}\cup\Lambda^{(r)}} \eta^{\lambda-t^{(r)}} \sum_{k=0}^{K_\lambda^{(r)}} \frac{\log^k(\eta)}{k!} \sum_{n=0}^{\infty} \eta^n \, \mathbf{I}^{(r)}_{\lambda,k,n} \,, \tag{4.50}$$

with $t^{(r)}$ being an integer. As expected, the expansion is of the same kind as in eq. (3.26), with non-integer powers of η and integer powers of η and $\log(\eta)$, the only difference with the Fuchsian basis being that now the leading behaviors $\eta^{\lambda-t^{(r)}}$ may have exponents that do not belong to the interval $[0,1[$.

To determine the value of the coefficients c_j, $j=1,\ldots,L_r$, we need L_r independent BCs. As pointed out in the previous sections, varying the coefficients c_j one is only able to affect those contributions $\mathbf{I}^{(r)}_{\lambda,k,n}$ that are associated with block eigenvalues $\lambda\in\Lambda^{(r)}$ and logarithmic orders $k\leq K_\lambda^{(r)}[\mathbb{A}]$. BCs involving other leading coefficients are automatically satisfied and hence are not useful to fix the solution.

BCs can be decoupled depending on which block eigenvalue λ they are associated with. If a given $\lambda\in\Lambda^{(r)}$ appears on a number $\mathrm{am}^{(r)}(\lambda)$ of columns of $\widetilde{\mathbb{A}}_0^{(r)}$, i.e., it is an eigenvalue of algebraic multiplicity $\mathrm{am}^{(r)}(\lambda)$, BCs concerning the components of $\mathbf{I}^{(r)}_{\lambda,k,0}$ only involve the coefficients c_j associated with those columns. Therefore, out of the L_r independent BCs that are necessary, one can use at most $\mathrm{am}^{(r)}(\lambda)$ independent conditions on the components of $\mathbf{I}^{(r)}_{\lambda,k,0}$, since these would be sufficient to fix the corresponding $\mathrm{am}^{(r)}(\lambda)$ coefficients c_j, making any other condition redundant. This means that the L_r boundary conditions have to be distributed according to the algebraic multiplicities of the block eigenvalues.

A specific kind of BCs consists in assigning the list of the leading power behaviors for the solution,

$$I_i^{(r)}(\eta) \overset{\eta\to 0}{\sim} u^{(r)}_{i,1}\eta^{\lambda^{(r)}_{i,1}-t^{(r)}_{i,1}} + u^{(r)}_{i,2}\eta^{\lambda^{(r)}_{i,2}-t^{(r)}_{i,2}} + \ldots\,, \qquad u^{(r)}_{i,k}\neq 0\,,\ \lambda^{(r)}_{i,k}\in[0,1[\,,\ t^{(r)}_{i,k}\in\mathbb{Z}\,, \tag{4.51}$$

where the leading coefficients $u^{(r)}_{i,k}$ are not specified. As discussed in section 3.4.2, these behaviors can be obtained, for instance, performing an EBR analysis around the singularity. One can easily match each $\lambda^{(r)}_{i,k}$ appearing in eq. (4.51) to a specific block eigenvalue $\lambda\in\Lambda^{(r)}$. In particular, the comparison of eq. (4.51) and the series expansion of $\mathbb{H}^{(r)}$ in eq. (4.49) may lead to three different conclusions for each eigenvalue λ:

- λ does not figure at all in the boundary behavior, so the corresponding $\mathrm{am}^{(r)}(\lambda)$ coefficients c_j must be zero. In light of this, one can be efficient and skip from the very beginning the computation of the associated column solutions to the homogeneous equation.

- λ does show up as one of the exponents $\lambda_{i,k}^{(r)}$ in the boundary behavior, but the overall leading behavior $\eta^{\lambda-t_i^{(r)}}$ emerging in the series solution for the integral $I_i(\eta)$ has an integer shift greater than the expected one, that is, $\lambda - t_i^{(r)} < \lambda - t_{i,k}^{(r)}$. Therefore, we can obtain $t_i^{(r)} - t_{i,k}^{(r)}$ conditions $I_{\lambda,0,n,i} = 0$ for $n = 0, \ldots, t_i^{(r)} - t_{i,k}^{(r)} - 1$, translating into linear relations among the coefficients c_j associated with λ. The number of independent conditions, which in any case cannot exceed $\mathrm{am}^{(r)}(\lambda)$, can be used to further constraint the unknown coefficients of the sought solution.

- λ does corresponds to a certain $\lambda_{i,k}^{(r)}$ in the boundary behavior but either the associated integer shifts $t_i^{(r)}$ are the expected ones, or the number of independent constraints obtained at the previous point, say m, are not enough to determine all the $\mathrm{am}^{(r)}(\lambda)$ coefficients. In this case, it is necessary to know the actual value of $\mathrm{am}^{(r)}(\lambda) - m$ different leading coefficients $u_{i,k}^{(r)}$, so that linear constraints can be obtained from the conditions $I_{\lambda,0,n,i} = u_{i,k}^{(r)}$ for $\mathrm{am}^{(r)}(\lambda) - m$ different vector components i.

The above analysis shows that, knowing the leading power behaviors for the solution as in eq. (4.51), we may be able to reduce the number of leading coefficients $u_{i,k}^{(r)}$ needed in input. In particular, while one normally needs L_r coefficients distributed according to the algebraic multiplicities of the block eigenvalue, some constraints may be provided from the structure of the DE itself. Furthermore, we showed how these constraints can be obtained in an algorithmic way, by setting up systems of linear equations for the unknown coefficients c_j.

When applying the method outlined above, it may happen that, for a given sector r, no input at all is needed to determine the solution. This means that the structure of the DE allows us to automatically obtain BCs for the MIs of the sector r in terms of the solution for the previous $r-1$ sectors. If the same happens iteratively, it may be possible to find the proper solution for the entire system of DEs by using as input only the leading coefficients for the first few MIs, which are the simplest to compute and may be known analytically. Even if this is not possible, this strategy still allows us to reduce as much as possible the complexity of the computation for the boundary coefficients.

The technique illustrated in this section can be applied to the examples discussed in section 3.4.2. As it was shown therein, the integral family in eq. (3.62) for the one-loop massive box has 6 MIs that expand as Taylor series around $s, t \to 0$ whose leading-order coefficient can be extracted from the DEs. We now analyze how this works in the framework described in this section.

The DE matrix $\mathbb{A}(\eta)$ for $s = t = \eta$ has Poincaré rank zero and its leading-order coefficient $\mathbb{A}_0$ is given by

$$\mathbb{A}_0 = \mathrm{diag}(\lambda_1, \ldots, \lambda_6) = \mathrm{diag}\left(0, -\frac{1}{2}, -\frac{1}{2}, -1, -1, -\frac{3}{2}\right) , \tag{4.52}$$

which corresponds to a trivial Jordan matrix with one-dimensional chains. In the 1×1 block of the s-channel bubble integral $I_2(\eta) \equiv B(\epsilon, \eta, m^2)$, the general solution to the associated homogeneous equation has power behavior $\eta^{-1/2}$, while the particular solution to the non-homogeneous equation only inherits a null eigenvalue from the constant tadpole $I_1(\eta) \equiv A(\epsilon, m^2)$ and so it has a Taylor series. Therefore, the general solution for this sector is

$$I_2(\eta) = c\,\eta^{-\frac{1}{2}} h(\eta) + p(\eta)\,, \tag{4.53}$$

where $h(\eta)$ and $p(\eta)$ have Taylor series. Since we know from EBR that $I_2(\eta)$ also expands as a Taylor series, we must have $c = 0$ and so the solution is completely determined as $I_2(\eta) = p(\eta)$. This implies that, building the particular solution $p(\eta)$ as prescribed in section 4.3, one can completely skip the computation of the solution to the homogeneous equation. In fact, the Taylor contribution given by $p(\eta)$ is unique, so that $p(\eta)$ is automatically built as the only regular solution to the non-homogeneous equation for $I_2(\eta)$.

The third block is identical to the first one, so we can focus directly on the triangle integral $I_4(\eta) = C(\epsilon, \eta, m^2)$, which is the same as $I_5(\eta) = C(\epsilon, \eta, m^2)$. When following the normalization procedure of section 3.3.2, the block eigenvalue $\lambda = -1$ is shifted to $\lambda = 0$ by means of a shearing transformation. However, the 1×1 transformation matrix $\mathbb{T}^{(4)}(\eta)$ is simply composed by the element η^{-1}, which is thus also the power behavior of the solution to the homogeneous equation. The particular solution instead inherits its regular behavior from the tadpole and the bubble. The general solution is thus given by

$$I_4(\eta) = c\,\eta^{-1} h_4(\eta) + p_4(\eta)\,, \tag{4.54}$$

where $h_4(\eta)$ and $p_4(\eta)$ have Taylor series. Once again, $c = 0$ is the only choice that makes $I_4(\eta)$ expandable as a Taylor series, so that $I_4(\eta) = p_4(\eta)$. Similarly, for the box integral $I_6(\eta) \equiv B(\epsilon, \eta, \eta, m^2)$ the eigenvalue $\lambda = -3/2$ is normalized to $\lambda = 1/2$, but $\mathbb{T}^{(6)}(\eta)$ consists of the shifting term η^{-2} which gives to the solution of the homogeneous equation the power behavior $\eta^{-3/2}$. The regularity of the box then implies that $I_6(\eta)$ is simply given by the particular solution, which is indeed the only regular solution.

In general, whenever it is known that the MIs are regular together with their derivatives (i.e., they expand as Taylor series), their leading coefficients may be automatically obtained. This happens if, for each block eigenvalue λ_j, either $\lambda_j \neq 0$ or λ_j is shifted back to a negative integer by the transformation matrix $\mathbb{T}(\eta)$, so that the associated coefficient c_j can be determined by imposing the cancellation of any power behavior. The situation where the MIs must expand as Taylor series arises, for instance, in the AMFlow method, when the DEs with respect to the auxiliary squared mass are solved at infinity. As shown in section 3.4.1, one can indeed factor out beforehand the leading power behavior of each MIs and solve the DEs (3.51), whose unknown functions have Taylor series. In LINE

these DEs are solved with the approach of section (4.3), avoiding to insert λ-contributions to the solution if $\lambda \neq 0$. However, for this application the DEs are in general not enough to determine all the leading-order coefficients, which are equal-mass vacuum integrals that must be computed for at least some of the MIs.

To conclude this section, let us analyze the case of the double box with a massive loop discussed in section 3.4.2. The integral family admits a basis of 32 MIs. The first one is a squared tadpole and has a Taylor series; the second master, which is the product of a tadpole and a massless bubble, has power behavior $\eta^{-\epsilon}$. Their leading-order coefficients, which must be provided as input, can be computed at arbitrary precision using the analytical formula in eq. (3.53) for the tadpole and

$$B(\epsilon, p^2, 0) = \int_k \frac{1}{k^2(k+p)^2} = \frac{\Gamma(1-\epsilon)^2\Gamma(\epsilon)}{\Gamma(2(1-\epsilon))}\, s^{-\epsilon} \tag{4.55}$$

for the bubble. For the subsequent sectors, EBR can be employed to predict the leading power behaviors which, in $4-2\epsilon$ dimensions, are always in the form $\eta^{\lambda-t}$ with integer t and either $\lambda = 0$ or $\lambda = 1-\epsilon$.

With the list of the power behaviors, one is able to determine all the coefficients for the solutions to the homogeneous equations by vetoing any undesired behavior. For instance, in the top sector we have four MIs $\mathbf{I}^{(B)}(\eta)$, namely the double box itself (in last position) and integrals that share the same denominator but with irreducible numerators (see eq. (6.16) for the exact list of propagator powers). In section 3.4.2 it was shown that the double box $I_4^{(B)}(\eta)$ collects a Taylor series from the LLL region, while a massless triangle factors out in the SLL region, causing the emergence of the power behavior $\eta^{-1-\epsilon}$. The same is true for the other MIs, except that $(k_1+p_3)^2$ is in the numerator of the triangle for $I_3^{(B)}(\eta)$, which hence behaves as $\eta^{-\epsilon}$. So the analysis of the power behaviors provides the BCs

$$\mathbf{I}^{(B)}(\eta) \sim \left(\eta^{-1-\epsilon}, \eta^{-1-\epsilon}, \eta^{-\epsilon}, \eta^{-1-\epsilon}\right) + \text{regular terms}\,. \tag{4.56}$$

On the other hand, the leading-order coefficient $\widetilde{\mathbb{A}}_0^{(B)}$ has the trivial Jordan structure

$$\mathbb{A}_0 = \text{diag}(\lambda_1, \lambda_2, \lambda_3, \lambda_4) = \text{diag}\left(\frac{1}{2}-\epsilon, \frac{1}{2}-\epsilon, 1-\epsilon, 1-\epsilon\right)\,. \tag{4.57}$$

As the eigenvalues $\lambda_1 = \lambda_2 = 1/2-\epsilon$ have been vetoed in all the solutions from the previous sectors, they only appear in the solution to the associated homogeneous equation. Thus we immediately conclude that $c_1 = c_2 = 0$, since they cannot be present in the final solution. We are then left with the task of determining the coefficients c_3 and c_4.

When transformed back to the non-Fuchsian basis, the last two columns of the matrix solution $\widetilde{\mathbb{H}}^{(B)}(\eta)$ both have the same behavior, namely

$$\mathbb{H}^{(B)}[j](\eta) = \mathbb{T}^{(B,B)}(\eta)\widetilde{\mathbb{H}}^{(B)}[j](\eta) \sim \left(\eta^{-2-\epsilon}, \eta^{-2-\epsilon}, \eta^{-1-\epsilon}, \eta^{-2-\epsilon}\right)\,, \quad j = 3, 4\,, \tag{4.58}$$

which is also shared by the particular solution and the solution from the previous sectors:

$$\mathbf{I}^{(B)}_{\text{pb}}(\eta) + \mathbf{P}^{(B)}(\eta) = \sum_{s=1}^{B-1} \mathbb{T}^{(B,s)}(\eta)\, \widetilde{\mathbf{I}}^{(s)}(\eta) + \mathbb{T}^{(B,B)}(\eta) \widetilde{\mathbf{P}}^{(B)}(\eta) \sim \left(\eta^{-2-\epsilon}, \eta^{-2-\epsilon}, \eta^{-1-\epsilon}, \eta^{-2-\epsilon}\right) . \tag{4.59}$$

By comparison with the boundary behavior in eq. (4.56), we have that the leading-order coefficient of each component must cancel out. This generates a system of four linear equations for the unknown coefficients c_3 and c_4, that is,

$$0 = \mathbf{I}^{(B)}_{1-\epsilon,0,0} = c_3\, \mathbb{H}^{(B)}_{1-\epsilon,0,0}[3] + c_4\, \mathbb{H}^{(B)}_{1-\epsilon,0,0}[4] + \mathbf{I}^{(B)}_{\text{pb},1-\epsilon,0,0} + \mathbf{P}^{(B)}_{1-\epsilon,0,0}\,. \tag{4.60}$$

The first two conditions turn out to be independent and so they can be used to find the values of c_3 and c_4, hence fixing the solution of the top sector. Overall, the 32 MIs are completely determined by the knowledge of their leading power behaviors and the analytical formulae for the massive tadpole and the one-loop massless bubble.

Chapter 5

Analytic continuation of Feynman integrals

Feynman integrals are multi-valued functions of the kinematic invariants and are made single-valued by identifying branch cuts emerging from branch point singularities, where the orientation of the cuts is dictated by the Feynman prescription. Taking into account the branch cut configuration of the master integrals is crucial when these are propagated across the phase space as solutions to differential equations. This chapter is devoted to the development of an algorithmic strategy, implemented in LINE, for the analytic continuation of the series expansion solutions obtained in chapter 4.

In section 5.1, we begin by discussing how a Cauchy problem is affected by the presence of discontinuities in the solutions to the differential equations. We show that boundary conditions alone are not sufficient to uniquely determine a discontinuous solution. Consequently, one must know in advance the branch cut structure for the sought solution in order to select, among the infinitely many solutions that satisfy the boundary conditions, the one whose discontinuity is placed accordingly.

Since the target functions are Feynman integrals, their discontinuities are analyzed in section 5.2. For any given integral, the branch cuts on the physical sheet are identified with the Cutkosky cuts of the associated graph, which in turn are associated with threshold singularities. Building on this, in section 5.3 we provide a method to place the branch cuts in the complex plane of the line parameter. The main idea is that the cuts must be mapped to the threshold-singularity surfaces in the space of the kinematic invariants. The orientation is chosen so as to be consistent with the Feynman prescription. The resulting rules are simple and well suited for implementation in computer code.

The procedure outlined in this chapter allows one to properly assign the position of the branch cut in the complex plane of the line parameter when a branch point is encountered on the path. While this method can be employed when solving the differential equations using the corresponding singular ansatz, the knowledge of the branch cut configuration also provides an alternative strategy for crossing the branch point, as pointed out in

section 5.3.3. There, we show how to deform the path to circle around the singularity through a sequence of regular propagation steps in the complex plane of the line parameter.

Throughout this section, we measure any angle φ in the complex plane counter-clockwise, identifying the positive real axis with an angle $\varphi = 0$, while $\varphi > 0$ ($\varphi < 0$) indicates the upper (lower) half of the complex plane. The negative real axis is selected with $\varphi = -\pi$. Of course, to specify a range of angles in the form of an interval $[\varphi_1, \varphi_2]$, we must have $\varphi_1 \leq \varphi_2$ and so occasionally we opt for one of them to fall outside the interval $]-\pi, \pi[$, which provides an easier notation than expressing $[\varphi_1, \varphi_2]$ as the union of two intervals. For the argument function, we consider $\arg(z) \in [-\pi, \pi[$ while, for any angle φ, we define the function $\arg^{(\varphi)}$ to pick up angles counter-clockwise with a jump of 2π at the angle φ. In particular we choose

$$\arg^{(\varphi)}(z) \in \begin{cases} [\varphi, \varphi + 2\pi[\,, & \varphi \in [-\pi, 0]\,, \\ [\varphi - 2\pi, \varphi[\,, & \varphi \in]0, \pi]\,. \end{cases} \tag{5.1}$$

We denote by $\log(z)$ the real-valued logarithm function and by $\mathrm{Log}(z)$ its complex-valued continuation. We use the notation $\mathrm{Log}^{(\varphi)}(z)$ to specify that the logarithm has a branch cut at angle φ. We choose its Riemann sheet in such a way that its imaginary part lies in $[\varphi, \varphi + 2\pi[$ for a branch cut in the lower half-plane at angle $\varphi \in [-\pi, 0]$, while $\mathrm{Im}\,\mathrm{Log}^{(\varphi)}(z) \in [\varphi - 2\pi, \varphi[$ when the branch cut is in the upper half-plane at angle $\varphi \in]0, \pi[$. Therefore, in this notation we have

$$\mathrm{Log}^{(\varphi)}(z) \equiv \log(|z|) + i\, \arg^{(\varphi)}(z)\,. \tag{5.2}$$

With this convention, the logarithm is evaluated on its branch cut by approaching the cut with a clockwise rotation, that is,

$$\mathrm{Log}^{(\varphi)}(re^{i\varphi}) \equiv \lim_{\theta \to 0^+} \mathrm{Log}^{(\varphi)}(re^{i(\varphi+\theta)})\,, \quad r > 0\,. \tag{5.3}$$

The choice of shifting down by 2π the range of angles for the imaginary part of the logarithm when the branch cut is in the upper half-plane ensures that the logarithm of a positive real number is always real. For instance for a branch cut at $\varphi = \pi/2$, we have that $\mathrm{Im}\,\mathrm{Log}^{(\varphi)}(z)$ belongs to $[-3\pi/2, \pi/2[$ instead of $[\pi/2, 5\pi/2[$, so that for positive real numbers the imaginary part of the logarithm is zero instead of 2π. On the other hand, for $z < 0$ we have $\mathrm{Im}\,\mathrm{Log}^{(\varphi)}(z) = \pi$ when $\varphi \in]-\pi, 0]$ and $\mathrm{Im}\,\mathrm{Log}^{(\varphi)}(z) = -\pi$ if $\varphi \in]0, \pi]$.

Finally, note that we are not forced to use a straight line to define the boundary between two consecutive branches for the logarithm function. For instance, consider any curved line $\gamma : [0, +\infty[\to \mathbb{C}$ that leaves the origin and stretches out to infinity. For simplicity we

also assume that the curve does not coil, that is, for any $r > 0$ there is only one point of γ at distance r from the origin, so that we can find a line parameter $r \geq 0$ such that $|\gamma(r)| = r$. Then we could define the logarithm $\mathrm{Log}^{(\gamma)}(z)$ with curved branch cut γ as the function that, circling counter-clockwise around the origin at distance r, continuously picks up values from a given branch of the multi-valued logarithm function, until the cut is encountered at $z = \gamma(r)$, where the imaginary part undergoes a discontinuity jumping down by 2π. For the purposes of this work, we are interested in what happens to the logarithm only on a given circle around the origin. Therefore, in the choice of the Riemann sheet, we define $\mathrm{Log}^{(\gamma)}(z)$ as

$$\mathrm{Log}^{(\gamma)}(z) \equiv \mathrm{Log}^{(\arg(\gamma(|z|)))}(z) = \log(|z|) + i \arg^{(\arg(\gamma(|z|)))}(z)\,, \tag{5.4}$$

that is, as the function that, at any distance $|z|$ from the origin, evaluates to the logarithm with a linear branch cut at angle $\arg(\gamma(|z|))$.

5.1 Discontinuous solutions to differential equations

Let us consider the differential equation

$$\frac{df(z)}{dz} = \frac{1}{z}\,, \tag{5.5}$$

where $f : D \subseteq \mathbb{C} \setminus \{0\} \to \mathbb{C}$ is a function defined over a complex domain D that does not include the origin. Any function in the form

$$f(z) = \mathrm{Log}(z) + \text{const.} \tag{5.6}$$

would be a solution to eq. (5.5), provided that we place a branch cut and select a Riemann sheet for the complex logarithm, which would otherwise be multi-valued. The solution then becomes

$$f^{(\varphi)}(z) = \mathrm{Log}^{(\varphi)}(z) + \text{const.} \tag{5.7}$$

for every choice of the constant and the angle φ. However, note that $f^{(\varphi)}(z)$ solves eq. (5.5) everywhere except along a ray from the origin at angle φ, where the logarithm has its branch cut and the function is therefore not differentiable.

Now suppose we are looking for a solution along with a boundary condition, i.e., we want to solve the Cauchy problem

$$\frac{d}{dz} f(z) = \frac{1}{z}\,, \qquad f(z_0) = B\,, \tag{5.8}$$

for some $B \in \mathbb{C}$. The boundary condition $f^{(\varphi)}(z_0) = B$ allows us to fix the constant in the definition of $f^{(\varphi)}(z)$ and find the class of solutions

$$f^{(\varphi)}(z) = \mathrm{Log}^{(\varphi)}(z) - \mathrm{Log}^{(\varphi)}(z_0) + B\,. \tag{5.9}$$

Now, two different angles φ_1, φ_2 give two different solutions $f^{(\varphi_1)}(z)$, $f^{(\varphi_2)}(z)$ that satisfy the same DE and have the same boundary value B at $z = z_0$. Therefore, it might seem that the uniqueness of the solution to the Cauchy problem in eq. (5.8) is violated. The catch is that $f^{(\varphi_1)}(z)$, $f^{(\varphi_2)}(z)$ are discontinuous functions that do not solve the exact same problem, since they are defined in different domains of the complex plane. In fact, at the infinitesimal level the uniqueness of the solution is roughly speaking due to the continuity of the function that allows us to start from z_0 with the boundary value B and use the DE for its propagation through infinitesimal steps, approximating the solutions at first order around any regular point z as

$$f(z + dz) \simeq f(z) + dz\,\frac{d}{dz} f(z) = f(z) + \frac{dz}{z}\,. \tag{5.10}$$

However, when crossing a branch cut, this procedure would smoothly vary the value of the solution, leading us to the neighboring Riemann sheet instead of staying on the same one by catching the discontinuity of the logarithm. It is worth noting that the very same circumstance arises when using the DE method to propagate Feynman integrals via Taylor series expansions on a path of regular points that crosses a branch cut.

A two-dimensional example with the same features is given by the homogeneous system of DEs for the Cauchy problem

$$\frac{d}{dz}\mathbf{f}(z) = \mathbb{A}(z)\mathbf{f}(z)\,, \qquad \mathbb{A}(z) = \begin{pmatrix} 0 & \frac{1}{z^2} \\ 0 & \frac{1}{z} \end{pmatrix}, \qquad \mathbf{f}(z_0) = \begin{pmatrix} B \\ z_0 \end{pmatrix}, \tag{5.11}$$

whose solution with branch cut at angle φ is

$$\mathbf{f}^{(\varphi)}(z) = \Big(\mathrm{Log}^{(\varphi)}(z) - \mathrm{Log}^{(\varphi)}(z_0) + B\,,\, z\Big)^T\,. \tag{5.12}$$

This example is closer to the type of DEs encountered in the computation of FIs. In fact, following the procedure outlined in section 3.3, one would use a transformation matrix such as

$$\mathbb{T}(z) = \begin{pmatrix} \frac{1}{z} & 0 \\ 0 & 1 \end{pmatrix} \tag{5.13}$$

to transform the DE system to Fuchsian form according to

$$\mathbb{A}(z) \longrightarrow \widetilde{\mathbb{A}}(z) = \mathbb{T}(z)^{-1}\mathbb{A}(z)\mathbb{T}(z) - \mathbb{T}(z)^{-1}\frac{d}{dz}\mathbb{T}(z) = \frac{1}{z}\begin{pmatrix} 1 & 1 \\ 0 & 1 \end{pmatrix} . \tag{5.14}$$

In this basis, the coefficient of the simple pole z^{-1} is a Jordan matrix with a chain of eigenvalue $\lambda = 1$ and length 2. As shown in section 3.3.1, this leads to the appearance of a logarithm in the solution, which is indeed the case of eq. (5.12).

A key aspect of the examples described above is that the solution is uniquely determined once the geometric configuration of its branch cut is indicated. This happens because any point of the domain of regularity D, which is now fixed, can be reached from the boundary point z_0 following a path entirely enclosed in D. A different situation arises when z_0 lies exactly on the branch cut: in this case, one has to prescribe beforehand from which side the branch cut must be approached when evaluating the solution on it, since any path connecting z_0 to a target point $z \in D$ must leave the cut on that side. Naturally the same prescription is also needed when the target point itself is on the cut.

Based on the arguments discussed so far, we are led to the following conclusions:

- When solving a Cauchy problem in the presence of a singular point, the specification of BCs may not be sufficient to uniquely fix a solution.

- It is necessary to know beforehand the analytic properties of the sought solution, i.e., the configuration of the branch cuts and possibly the prescribed side from which they must be approached, so that we can choose the proper Riemann sheet when solving the DEs.

Our problem of interest is solving DEs for Feynman integrals, a case in which the configuration of the branch cuts is known in advance and the Feynman prescription specifies how to approach them. As a step towards our goal, consider a DE around a regular singular point at $z = 0$, whose series expansion solution is in the form

$$f(z) = \sum_{k=0}^{K}\sum_{n=0}^{\infty} f_{k,n}\left[\mathrm{Log}^{(0)}(z)\right]^k z^n , \tag{5.15}$$

where $f_{k,n}$ are unknown coefficients. Observing the logarithms we know that the solution has a branch point at $z = 0$ and develops a branch cut on the positive real axis $z > 0$. Suppose that we want to solve the DE along a line segment with parameter $\eta \in [0, 1]$ that goes from a boundary point $z = z_0$ to a target $z = z_1$ passing through $z = 0$. We have

$$z(\eta) = z_0 + \eta(z_1 - z_0) ,$$

$$\begin{aligned} z(0) &= z_0 \quad \text{boundary point}\,, \\ z(1) &= z_1 \quad \text{target point}\,. \end{aligned} \tag{5.16}$$

Even though it belongs to a real segment, the line parameter η has to be regarded as a complex variable when solving the DE with respect to η via series expansion, so that eq. (5.16) becomes a linear change of variables between two complex variables η and z. Let $g(\eta)$ be the sought solution in the η variable. The simple but crucial point is that we want $g(\eta)$ to be just $f(z)$ expressed in terms of η, that is, $g(\eta) = f(z(\eta))$. Therefore, the branch cut of $g(\eta)$ in the complex plane of η is precisely inherited from the branch cut of $f(z)$ in the complex plane of z. In particular, we have the conditions

$$z(\eta) = 0 \qquad \text{branch point}\,, \tag{5.17a}$$

$$z(\eta) > 0 \qquad \text{branch cut}\,. \tag{5.17b}$$

Let us indicate with $\eta = \eta_b$ the branch point in the η-plane. We then parameterize the branch cut as a half line starting at $\eta = \eta_b$ at an angle φ_b with respect to the positive real axis, i.e. $\{\eta = \eta_b + re^{i\varphi_b}, r > 0\}$. In principle, we could invert the map in eq. (5.16) as $\eta = (z - z_0)/(z_1 - z_0)$ and let $z = a > 0$ be the parameter that describes the branch cut in η. Instead, we solve the conditions in eq. (5.17) directly, a method that better adapts to the more general case of non-linear maps $z(\eta)$ that are not easily invertible. From $z(\eta_b) = 0$ we get

$$\eta_b = -\frac{z_0}{z_1 - z_0}\,. \tag{5.18}$$

To find the branch cut, we evaluate the left-hand side of (5.17b), obtaining

$$\begin{aligned} z(\eta_b + re^{i\varphi_b}) &= z_0 + \left(\eta_b + re^{i\varphi_b}\right)(z_1 - z_0) \\ &= z_0 + \eta_b\,(z_1 - z_0) + re^{i\varphi_b}\,(z_1 - z_0) \\ &= re^{i\varphi_b}\,(z_1 - z_0)\,, \end{aligned} \tag{5.19}$$

where we used the condition $z_0 + \eta_b\,(z_1 - z_0) = 0$ that defines η_b. The right-hand side of eq. (5.19) must be real and positive, meaning that

$$\varphi_b = -\arg\,(z_1 - z_0)\,. \tag{5.20}$$

Therefore, the sought solution $g(\eta) = f(z_0 + \eta(z_1 - z_0))$ has a branch point at $\eta = \eta_b$ specified by eq. (5.18) that develops a branch cut at angle $\varphi = \varphi_b$ given by eq. (5.20), as illustrated in figure 5.1

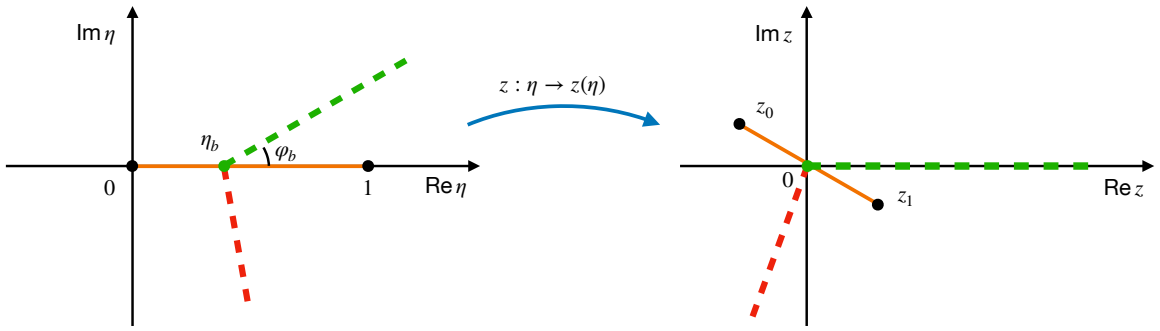

Figure 5.1: Branch cuts in the complex planes of the line parameter η (left) and of the invariant z (right) are shown as dashed lines. The DEs are solved along the orange line connecting z_0 and z_1, which corresponds to the segment $[0, 1]$ in the η-plane. The branch cut drawn in green represents the correct choice, as it is mapped onto the positive real axis of the z-plane, whereas the red one is not.

Moving to the operational point of view, in our framework we solve the DE in η via series expansion around $\eta = \eta_b$ using the ansatz

$$g(\eta) = \sum_{k=0}^{K} \sum_{n=0}^{\infty} g_{k,n} \left[\mathrm{Log}^{(\varphi)}(\eta - \eta_b)\right]^k (\eta - \eta_b)^n \tag{5.21}$$

and solving for the unknown coefficients $g_{k,n}$. Here, $\eta_b \in]0, 1[$ by construction, since we are interested in branch points lying on the path. To determine all the coefficients $g_{l,k}$, we must also impose BCs at $\eta = 0$, thus evaluating the logarithm for a negative real value $\eta - \eta_b < 0$ of its argument. Although any choice of φ would successfully solve the Cauchy problem, among all the solutions that match the boundary we seek the only one that has its branch cut mapped onto the positive real axis $z > 0$, that is, we select the branch cut at angle $\varphi = \varphi_b$ of eq. (5.20). The choice of the branch enables the evaluation of the logarithm, and thus of the solution, at the target point $\eta = 1$ as well, where $\eta - \eta_b > 0$. This completely solves the task under consideration.

Equipped with the methodology implemented in this section, we are now ready to address the specific case of DEs for Feynman integrals.

5.2 Discontinuities of Feynman integrals

As mentioned in section 3.3, Feynman integrals develop branch cuts when analytically continued to complex values of the kinematic invariants. In this section we discuss how to identify such cuts and extract the information that we need for the analytic continuation of the solutions to the differential equations.

The discontinuities of FIs on the physical sheet are described by the cutting rules first given by Cutkosky [120]. To see how they work, let $F(\mathbf{s})$ be a FI depending on the

kinematic invariants $\mathbf{s}$ and $\mathcal{G}$ its corresponding graph. We define a *Cutkosky cut* $\mathcal{C}$ of the integral $F(\mathbf{s})$ as any deletion of a set of edges that cuts the graph $\mathcal{G}$ into two disjoint sub-graphs, each containing at least one external leg. The cutting rules state that the discontinuity $\mathrm{Disc}F(\mathbf{s})$ of the integral is given by

$$\mathrm{Disc}F(\mathbf{s}) = \sum_{\mathcal{C}} \int_{k_1,\dots,k_L} \prod_{e\in\mathcal{C}} (-2\pi i)\,\delta(q_e^2 - m_e^2)\,\theta_H^*(q_e^0) \prod_{e'\in\mathcal{G}\setminus\mathcal{C}} \frac{1}{q_{e'}^2 - m_{e'}^2 + i0^+}\,, \tag{5.22}$$

where the products run over edges of a given set and the sum is over all the possible Cutkosky cuts of the graph $\mathcal{G}$. To each cut $\mathcal{C}$, which is also interpreted as the set of deleted edges, is assigned a fixed (arbitrary) orientation, and the function $\theta_H^*(q_e^0)$ determines the sign of the energy by evaluating to the Heaviside step function $\theta_H(q_e^0)$ for momenta flowing through the cut in the forward direction and to $\theta_H(-q_e^0)$ for those flowing in the opposite direction. Then eq. (5.22) expresses the discontinuity of a FI as a sum of cut contributions where the momentum q_e of each cut propagator is set on-shell substituting the propagator with a factor $(-2\pi i)\,\delta(q_e^2 - m_e^2)\,\theta_H^*(q_e^0)$.

A significant amount of useful information is contained in the cutting rules of eq. (5.22). To see this, let us focus on the contribution coming from a single oriented cut $\mathcal{C}$ and let $P_{\mathcal{C}} = \sum_{e\in\mathcal{C}} q'_e$ be the total momentum flowing through the cut, where q'_e is defined as oriented in the forward direction. By momentum conservation, $P_{\mathcal{C}}$ is equal to the sum of a certain number of external momenta, so that its square $t_{\mathcal{C}} \equiv P_{\mathcal{C}}^2 = (p_{i_1} + p_{i_2} + \dots)^2$ is an external kinematic invariant. In order for the cut $\mathcal{C}$ to give a non-zero contribution to the discontinuity in eq. (5.22), none of the on-shell factors can vanish. From a kinematic point of view, this means that $t_{\mathcal{C}}$ must be large enough to produce a set of on-shell particles of momenta q'_e with positive energy. The corresponding threshold value for $t_{\mathcal{C}}$ is equal to the square of the sum of the cut masses and leads to the condition

$$z_{\mathcal{C}} \equiv t_{\mathcal{C}} - \left(\sum_{e\in\mathcal{C}} m_e\right)^2 \geq 0\,, \tag{5.23}$$

where we refer to $z_{\mathcal{C}}$ as the *Cutkosky invariant* associated with the cut $\mathcal{C}$. Eq. (5.23) locates a branch cut in the phase space of the kinematic invariants for the analytic continuation of the integral $F(\mathbf{s})$ to complex-valued kinematics.

Since the kinematic configurations selected by $z_{\mathcal{C}} \geq 0$ are able to set on-shell the cut propagators, they are solutions to the on-shell Landau equation (2.42) with $\alpha_{e'} = 0$ for each uncut propagator. In addition, the threshold value $z_{\mathcal{C}} = 0$ is also a solution to the Landau loop equation (2.44) and corresponds to a branch point singularity for the integral. To make this manifest, let us consider the loops that are cut open by $\mathcal{C}$. It is always possible to choose the routing of the loop momenta in such a way that any loop momentum k_i flowing through the cut appears in exactly two cut propagators. If we indicate with q'_{i1}

and q'_{i2} their momenta (defined as flowing in the forward direction of the cut), one of them, say q'_{i1}, must be oriented as k_i and the other in the opposite direction. At the threshold $z_{\mathcal{C}} = 0$, any cut momentum is produced at rest in the center of mass frame of $P_{\mathcal{C}}$, so that $q'_{i1} = (m_{i1}, \mathbf{0})$ and $q'_{i2} = (m_{i2}, \mathbf{0})$ in such a frame. As $\alpha_{e'} = 0$ for uncut propagators, the Landau loop equation (2.44) reads

$$\alpha_{i1} q'_{i1} - \alpha_{i2} q'_{i2} = 0 \iff \alpha_{i1} m_{i1} - \alpha_{i2} m_{i2} = 0 \,, \tag{5.24}$$

whose solutions are non-negative. All the loop equations can be satisfied simultaneously, which leads to a solution of the Landau equation (2.44) with $\alpha_e \geq 0$ for each cut propagator.

Note that for $z_{\mathcal{C}} > 0$ the on-shell momenta are produced with non-zero spatial components $\mathbf{q}_e$ that add up to zero in the center of mass frame of $P_{\mathcal{C}}$. This is incompatible with the Landau loop equation that instead asks for spatial vectors that are proportional and oriented in the same direction. Therefore, $z_{\mathcal{C}} > 0$ selects kinematic configurations where the FI, although discontinuous, is not singular.

The side from which the branch cut in eq. (5.23) must be approached is dictated by the Feynman prescription. This translates to a specific choice for the sign of the imaginary part of $z_{\mathcal{C}}$. To see how, recall that, as pointed out in section 2.3, the second Symanzik polynomial $\mathcal{F}$ inherits a small, positive imaginary part, $\mathrm{Im}\mathcal{F} = \varepsilon \to 0^+$. This is equivalent to assign $i\varepsilon$ to the external kinematic invariants appearing in $\mathcal{F}$, i.e., those corresponding to the squared sum of external momenta. As $t_{\mathcal{C}}$ is one of these invariants, we have

$$z_{\mathcal{C}} \to z_{\mathcal{C}} + i\varepsilon \,, \quad \varepsilon \to 0^+ \,, \tag{5.25}$$

that is, the Cutkosky invariant $z_{\mathcal{C}}$ acquires an infinitesimal, positive imaginary part according to the Feynman prescription. The same result was also found in eq. (2.63), where one has to identify $z_{\mathcal{C}}$ with $\mathcal{F}(\bar{\boldsymbol{\alpha}}(\mathbf{s}))$.

We can summarize the observations made in this section as follows. Each branch point on the physical sheet of a FI is related to a Cutkosky cut $\mathcal{C}$, which is in turn associated with a Cutkosky invariant $z_{\mathcal{C}}$, defined in eq. (5.23). The latter allows us to identify the branch cut in terms of the kinematic invariants. In the complex plane of $z_{\mathcal{C}}$, the branch point is at the origin $z_{\mathcal{C}} = 0$ and develops a branch cut on the positive real axis $z_{\mathcal{C}} > 0$ that, according to the Feynman prescription, must be approached from above. These properties of $z_{\mathcal{C}}$ resemble those of the complex variable z in the example at the end of section 5.1. In fact, the approach we are about to describe follows very closely the one adopted in that example. In particular, the knowledge of the branch cut configuration in the complex plane of $z_{\mathcal{C}}$ is what guides us in the selection of the proper solution to the Cauchy problem in the line parameter η.

5.3 Phase space propagation in the presence of branch cuts

As discussed in section 5.1, when differential equations admit discontinuous solutions, the boundary conditions are not enough to uniquely determine the proper solution and so we need to know a priori the location of its branch cuts. In the case of DEs for Feynman integrals, the analysis of section 5.2 showed how to get this information beforehand, thanks to the introduction of the Cutkosky invariant $z_{\mathcal{C}}$. In the following, we combine the observations of both sections to outline an algorithmic procedure for the propagation of FIs via series expansion in the presence of branch cuts. The strategy prescribed here is the one implemented in LINE. Although we are only interested in physically relevant cases, we shall consider generic complex values for all the kinematic invariants in order to make the mathematical arguments more natural. Nevertheless, we shall separately highlight the algorithmic prescriptions for the physical cases, where the branch cuts lie on the real axis.

Recall that, in our framework, we solve DEs along a phase space line with parameter η. The propagation is split into several steps, each one consisting in computing series expansion solutions within a finite radius of convergence. Whenever a regular singular point of the DEs is encountered on the path, the singularity is crossed by expanding the solution around it. The singular point may or may not be a branch point for the master integrals. If it is not, then the position of the branch cut in the complex plane of η is irrelevant, since the final result does not depend on the choice of the branch. On the other hand, a singularity that is also a branch point for the MIs requires us to apply the methodology seen in the previous sections. In fact, the branch cut in the η-complex plane is mapped onto the phase space of the kinematic invariants through the line parameterization in eq. (2.116), and we need to ensure that the mapping is consistent with the actual position of the branch cut in said space.

Suppose that, after a certain number of propagation steps, a branch point is met on the path at $\eta = \eta_b$. We save for later the cases $\eta_b \in \{0, 1\}$ of a singularity at one of the end points, so that for now we can assume $\eta_b \in]0, 1[$. The BCs are given by the sum of the series solution from the previous step evaluated at a point $\eta < \eta_b$. Let $\mathcal{C}$ be the Cutkosky cut associated with the branch point under consideration and $t_{\mathcal{C}}$ the square of the total momentum flowing through the cut. If we express the invariant $t_{\mathcal{C}}$ as a linear combination of T independent external invariants t_i with coefficients α_i, we can write the Cutkosky invariant $z_{\mathcal{C}}$ of eq. (5.23) as

$$z_{\mathcal{C}} = \sum_{i=1}^{T} \alpha_i t_i - \left(\sum_{e \in \mathcal{C}} m_e \right)^2 . \tag{5.26}$$

If we plug into this equation the parameterization in eq. (2.116), we obtain a map $z_{\mathcal{C}}(\eta)$

from the complex plane of η onto the one of $z_{\mathcal{C}}$. We then proceed as in the example at the end of section 5.1, choosing the branch cut in η in such a way that $z_{\mathcal{C}}(\eta)$ maps it onto the positive real axis of the $z_{\mathcal{C}}$-complex plane.

First, we focus on the case where the cut masses are kept fixed in the propagation, where the example of section 5.1 mentioned above can be followed closely. Then, we consider the general case of varying masses, where some extensions ought to be made. In both scenarios, we provide rules for the computation of the logarithm $\mathrm{Log}(\eta - \eta_b)$, since the analytic continuation of non-integer powers $(\eta - \eta_b)^\lambda$ can be performed according to $(\eta - \eta_b)^\lambda = e^{\lambda \,\mathrm{Log}(\eta - \eta_b)}$. These rules specify how to assign the imaginary part to $\mathrm{Log}(\eta - \eta_b)$ for $\eta < \eta_b$ and $\eta > \eta_b$. We emphasize that the choice of the Riemann sheet for the logarithm does not matter as long as the location of its branch cut and its orientation are correct. In other words, we are allowed to shift both the imaginary parts at $\eta < \eta_b$ and $\eta > \eta_b$ by the same integer multiple of 2π, since the coefficients for matching the BCs at the previous path point would compensate the change in the value of $\mathrm{Im}\,\mathrm{Log}(\eta - \eta_b)$.

5.3.1 Cut with fixed masses

Suppose that the cut masses do not change in value during the phase space propagation so that, in the expression for the Cutkosky invariant $z_{\mathcal{C}}$, only the external invariants t_i evolve. The insertion of the line parameterization

$$t_i(\eta) = t_{0,i} + \left(\frac{\eta - \eta_0}{\eta_1 - \eta_0}\right)(t_{1,i} - t_{0,i}) \tag{5.27}$$

into eq. (5.26) gives the linear map

$$z_{\mathcal{C}}(\eta) = \sum_{k=1}^{T} \alpha_k t_{0,k} - \left(\sum_{e\in\mathcal{C}} m_e\right)^2 + \eta \sum_{k=1}^{T} \alpha_k \left(t_{1,k} - t_{0,k}\right) . \tag{5.28}$$

With $\eta = \eta_0$ indicating the boundary point and $\eta = \eta_1$ the target one, we have

$$z_{\mathcal{C}}(\eta) = z_{\mathcal{C},0} + \left(\frac{\eta - \eta_0}{\eta_1 - \eta_0}\right)\left(z_{\mathcal{C},1} - z_{\mathcal{C},0}\right), \tag{5.29}$$

where $z_{\mathcal{C},0} \equiv z_{\mathcal{C}}(\eta_0)$ and $z_{\mathcal{C},1} \equiv z_{\mathcal{C}}(\eta_1)$. Note that the difference $z_{\mathcal{C},1} - z_{\mathcal{C},0}$ does not depend on the masses:

$$z_{\mathcal{C},1} - z_{\mathcal{C},0} = (\eta_1 - \eta_0) \sum_{k=1}^{T} \alpha_k \left(t_{1,k} - t_{0,k}\right) . \tag{5.30}$$

We thus find precisely the same situation of the example at the end of section 5.1. Therefore, following the same reasoning, the branch cut in the complex plane of η must be placed at

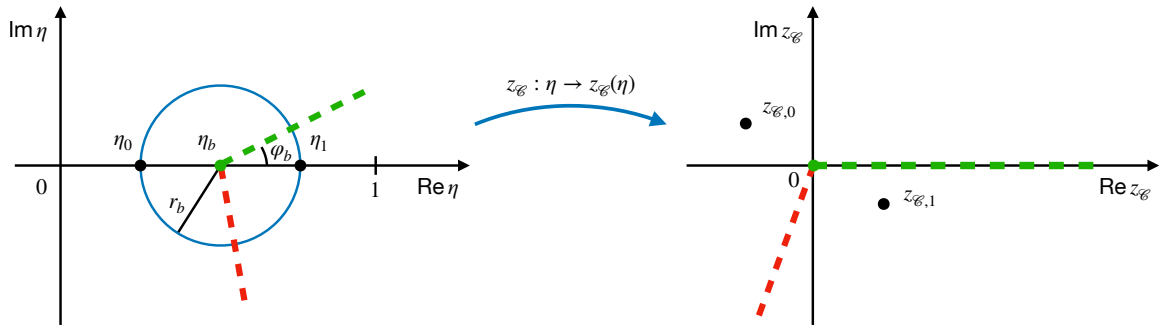

Figure 5.2: Branch cuts in the complex plane of the line parameter η (on the left) and the Cutkosky invariant $z_{\mathcal{C}}$ (on the right), indicated with dashed lines. The DEs are solved within the circle of radius r_b (in blue), centered at the branch point η_b. The boundary point η_0 and the target point η_1 are mapped to $z_{\mathcal{C},0}$ and $z_{\mathcal{C},1}$, respectively. As in figure 5.1, the correct branch cut is the green one, since it is mapped to $z_{\mathcal{C}} > 0$.

an angle φ_b given by

$$\varphi_b = -\arg\left(z_{\mathcal{C},1} - z_{\mathcal{C},0}\right) , \tag{5.31}$$

as shown in figure 5.2.

Having located the branch cut, we are ready for the evaluation of the logarithm $\mathrm{Log}(\eta - \eta_b)$ at $\eta < \eta_b$ to match the boundary and at $\eta > \eta_b$ to sum the series solution. If the branch cut is not on the real axis, we have:

- $\arg\left(z_{\mathcal{C},1} - z_{\mathcal{C},0}\right) \in]0, \pi[\implies$ branch cut in the lower half-plane:

$$\mathrm{Log}(\eta - \eta_b) = \begin{cases} \log(\eta - \eta_b) , & \eta > \eta_b , \\ \log(\eta_b - \eta) + i\pi , & \eta < \eta_b , \end{cases} \tag{5.32}$$

- $\arg\left(z_{\mathcal{C},1} - z_{\mathcal{C},0}\right) \in]-\pi, 0[\implies$ branch cut in the upper half-plane:

$$\mathrm{Log}(\eta - \eta_b) = \begin{cases} \log(\eta - \eta_b) , & \eta > \eta_b , \\ \log(\eta_b - \eta) - i\pi , & \eta < \eta_b . \end{cases} \tag{5.33}$$

If $z_{\mathcal{C},1} - z_{\mathcal{C},0}$ is real, as it is always the case for real-valued kinematics, the branch cut lies on the real axis and so we need to follow the Feynman prescription to evaluate the logarithm upon its cut. As discussed in section 5.2, this means that the branch cut must be approached in such a way that $z_{\mathcal{C}}(\eta)$ lands on the positive real axis from above. For the sake of completeness, we also give results for the opposite prescription, i.e., with $z_{\mathcal{C}}(\eta)$ reaching the axis from below. We parameterize the motion of $z_{\mathcal{C}}(\eta)$ as a rotation in the complex plane. In particular, $z_{\mathcal{C}} = ae^{i\phi}$ for some $a > 0$ approaches the positive real axis

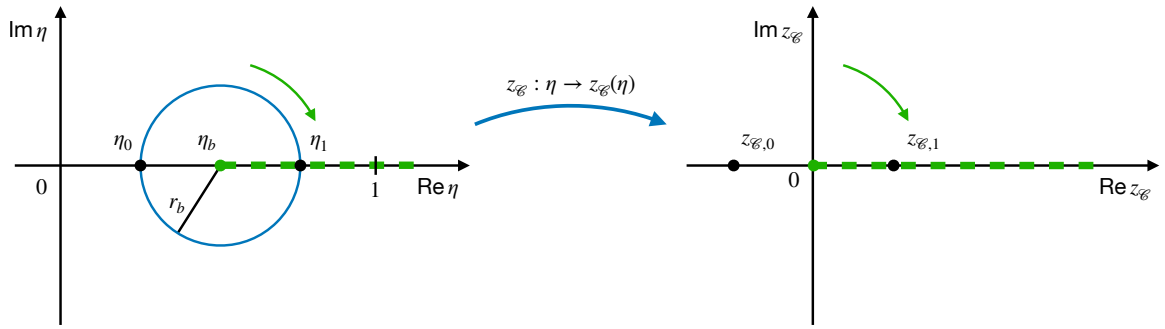

(a) Branch cut at $\eta > \eta_b$.

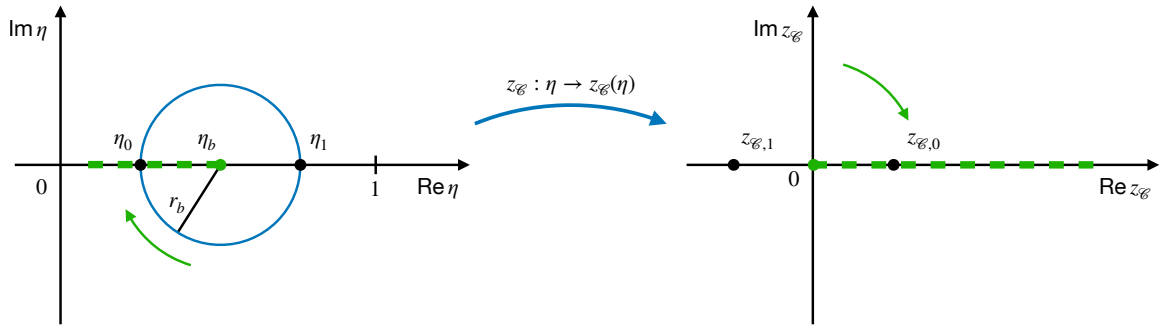

(b) Branch cut at $\eta < \eta_b$.

Figure 5.3: Branch cuts (dashed green lines) on the real axis of the complex planes of η (left) and $z_{\mathcal{C}}$ (right), as it is the case for real-valued kinematics. The branch cut at $z_{\mathcal{C}} > 0$ must always be approached from above. In the η-plane, this corresponds to a clockwise rotation on the blue circle of radius r_b, centered at the branch point η_b. **(a)** η_0 rotates clockwise towards η_1, reaching the cut from above. **(b)** η_1 rotates clockwise towards η_0, reaching the cut from below.

from above (below) in the limit $\phi \to 0^+$ ($\phi \to 0^-$). This rotation is the image through $z_{\mathcal{C}}(\eta)$ of a corresponding infinitesimal rotation of angle δ around the branch point in the complex plane of η. We then look for the sign of δ, which tells us if the branch cut in η must be approached with a clockwise or counter-clockwise rotation. We have

$$ae^{i\phi} = z_{\mathcal{C},0} + (\eta_b + re^{i(\varphi_b+\delta)})(z_{\mathcal{C},1} - z_{\mathcal{C},0}) = re^{i(\varphi_b+\delta)}(z_{\mathcal{C},1} - z_{\mathcal{C},0})\,, \tag{5.34}$$

where we used eq. (5.31). This means that

$$\phi = \varphi_b + \delta + \arg(z_{\mathcal{C},1} - z_{\mathcal{C},0}) = \delta\,. \tag{5.35}$$

The conclusion is that, in order for the positive real axis of $z_{\mathcal{C}}$ to be approached from above (below), the branch cut in η must be reached with a clockwise (counter-clockwise) rotation, as illustrated in figure 5.3. This translates to:

- $z_{\mathcal{C},1} > z_{\mathcal{C},0} \implies$ branch cut at $\eta > \eta_b$ approached from above (below):

$$\mathrm{Log}(\eta - \eta_b) = \begin{cases} \log(\eta - \eta_b) + i2\pi\theta_H(-\phi)\,, & \eta > \eta_b\,, \\ \log(\eta_b - \eta) + i\pi\,, & \eta < \eta_b\,, \end{cases} \tag{5.36}$$

- $z_{\mathcal{C},1} < z_{\mathcal{C},0} \implies$ branch cut at $\eta < \eta_b$ approached from below (above):

$$\mathrm{Log}(\eta - \eta_b) = \begin{cases} \log(\eta - \eta_b)\,, & \eta > \eta_b\,, \\ \log(\eta_b - \eta) - i\pi + i2\pi\theta_H(-\phi)\,, & \eta < \eta_b\,. \end{cases} \tag{5.37}$$

The Feynman prescription is selected by $\phi > 0$, in which case the Heaviside step function $\theta_H(-\phi)$ does not contribute to the formulae above.

5.3.2 Cut with varying masses

A more involved situation arises in the general case where the cut masses change in value during the phase space propagation. In fact, if we were to linearly vary the squared masses of the cut propagators according to

$$m_e^2(\eta) = m_{0,e}^2 + \eta(m_{1,e}^2 - m_{0,e}^2)\,, \tag{5.38}$$

as we do for any other invariant, we would end up with a map

$$z_{\mathcal{C}}(\eta) = \sum_{k=1}^{T} \alpha_k t_{0,k} + \eta \sum_{k=1}^{T} \alpha_k \left(t_{1,k} - t_{0,k}\right) - \left(\sum_{e\in\mathcal{C}} \sqrt{m_{0,e}^2 + \eta(m_{1,e}^2 - m_{0,e}^2)}\right)^2\,, \tag{5.39}$$

featuring square roots that may lead to a complicated structure for the branch cut in the complex plane of η. To overcome this problem, let us vary the *linear* masses instead of the squared ones,

$$m_e(\eta) = m_{0,e} + \eta(m_{1,e} - m_{0,e})\,, \tag{5.40}$$

assuming that the propagation is confined to non-negative values $\mathrm{Re}\, m_e(\eta) \geq 0$. The Cutkosky invariant is then given by

$$z_{\mathcal{C}}(\eta) = \sum_{k=1}^{T} \alpha_k t_{0,k} + \eta \sum_{k=1}^{T} \alpha_k \left(t_{1,k} - t_{0,k}\right) - \left[\sum_{e\in\mathcal{C}} m_{0,e} + \eta \sum_{e\in\mathcal{C}} (m_{1,e} - m_{0,e})\right]^2\,, \tag{5.41}$$

which is just a quadratic polynomial in η. As we are about to see, this kind of map implies a non-trivial but nonetheless manageable branch cut structure.

To begin with, note that $z_{\mathcal{C}}(\eta)$ has two roots now, meaning that the branch point of the MIs is split into two different branch points in the η-complex plane, each generating a distinct branch cut. By construction, one of the roots is the branch point $\eta_b \in]0,1[$ that we are using as expansion point for the series solution; the other one, say $\eta = \eta'_b$, is still a pole of the DEs and so, by the definition of radius of convergence $\mathcal{R}(\eta_b)$ as the distance between η_b and its closest pole, η'_b lies at a distance $|\eta'_b - \eta_b| \geq \mathcal{R}(\eta_b)$. On the other hand, we are expanding within $|\eta - \eta_b| < \mathcal{R}(\eta_b)/2$, as prescribed in section 4.1. As we prove later on, the branch cut originating from η'_b also stays outside this domain and, in fact, this feature plays a key role in the choice of the factor 1/2 multiplying $\mathcal{R}(\eta_b)$. Note however that here we are implicitly assuming that the initial and target phase space points are such that $\eta_b \neq \eta'_b$, i.e., the two branch points do not overlap in the complex plane of η.

Another consequence of the quadratic nature of the map $z_{\mathcal{C}}(\eta)$ is that generally the branch cuts in the η-complex plane are *curved*. This aspect is not problematic since the logarithms in the series solution can be analytically continued using a generic branch curve, as shown in eq. (5.4). On top of that, we only need to evaluate the logarithms at two real points $\eta_0 = \eta_b - r_b$ and $\eta_1 = \eta_b + r_b$, where $r_b \equiv \mathcal{S}(\eta_b) = \mathcal{R}(\eta_b)/2$, to impose BCs and reconstruct the series at the next path point, respectively. Therefore, if we parameterize the branch cut of η_b as $\{\eta = \eta_b + \gamma(r), r \geq 0\}$, with $\gamma : \mathbb{R}^+ \to \mathbb{C}$ being the branch curve, we are only interested in the position of $\gamma(r_b)$, i.e., the intersection point of the curve γ with the radius of the expansion. What is more, the only thing that matters is whether $\gamma(r_b)$ lies in the upper or lower half of the η-complex plane.

To unveil the answer, we make a point η_p rotate on the circle of radius r_b centered at η_b, while observing the motion of its image $z_{\mathcal{C}}(\eta_p)$. As proved below, $z_{\mathcal{C}}(\eta_p)$ also rotates in the same direction as η_p, with no inversions and completing no more than one full turn. Suppose that η_p starts from the boundary point η_0 and proceeds, say, counter-clockwise, thus moving into the lower half of the complex plane, as shown in figure 5.4. If the branch cut is somewhere in the lower half, it will be crossed by η_p before the latter can reach the target point η_1. This corresponds to $z_{\mathcal{C}}(\eta_p)$ intersecting the positive real axis in the complex plane of $z_{\mathcal{C}}$ and, to know if this event occurs or not, we can compare the angles of the initial point, $z_{\mathcal{C},0} = z_{\mathcal{C}}(\eta_0)$, and the final one, $z_{\mathcal{C},1} = z_{\mathcal{C}}(\eta_1)$. In particular, we have:

- $0 < \arg^{(0)}(z_{\mathcal{C},1}) < \arg^{(0)}(z_{\mathcal{C},0}) \implies$ branch cut in the lower half-plane:

$$\operatorname{Log}(\eta - \eta_b) = \begin{cases} \log(r_b)\,, & \eta = \eta_b + r_b\,, \\ \log(r_b) + i\pi\,, & \eta = \eta_b - r_b\,, \end{cases} \tag{5.42}$$

- $0 < \arg^{(0)}(z_{\mathcal{C},0}) < \arg^{(0)}(z_{\mathcal{C},1}) \implies$ branch cut in the upper half-plane:

$$\operatorname{Log}(\eta - \eta_b) = \begin{cases} \log(r_b)\,, & \eta = \eta_b + r_b\,, \\ \log(r_b) - i\pi\,, & \eta = \eta_b - r_b\,. \end{cases} \tag{5.43}$$

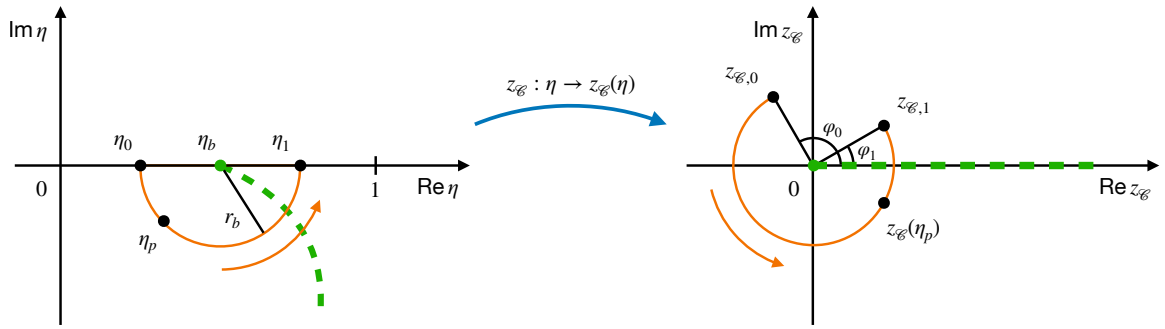

(a) Branch cut in the lower half of the η-complex plane.

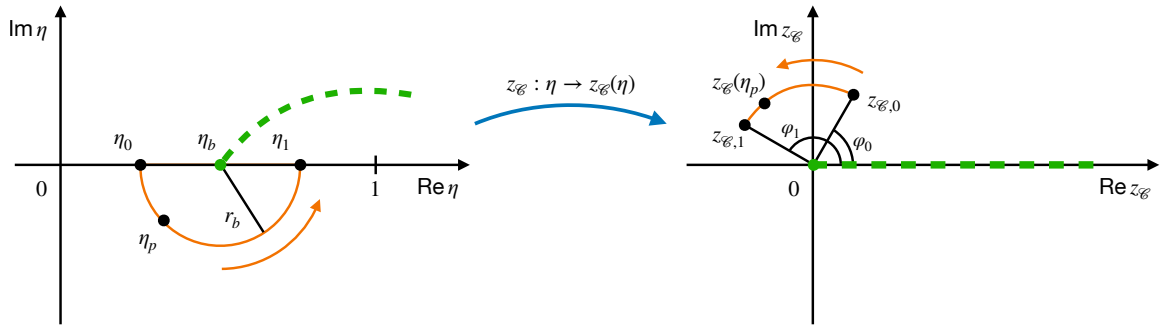

(b) Branch cut in the upper half of the η-complex plane.

Figure 5.4: Branch cuts (dashed green lines) in the complex planes of η (left) and $z_{\mathcal{C}}$ (right) for the case where the cut masses are varied during the propagation. The point η_p rotates counter-clockwise on the half-circle (drawn in orange) of radius r_b, centered at the branch point η_b. At the same time, its image $z_{\mathcal{C}}(\eta_p)$ rotates counter-clockwise in the z-plane, from $z_{\mathcal{C},0}$ to $z_{\mathcal{C},1}$. **(a)** $\arg^{(0)} z_{\mathcal{C},1} < \arg^{(0)} z_{\mathcal{C},0}$ and so $z_{\mathcal{C}}(\eta_p)$ crosses the real axis. Therefore, η_p finds the branch cut. **(b)** The opposite is true.

The edge cases of $\gamma(r_b)$ being on the positive or negative real axis in the η-plane take place when $z_{\mathcal{C},1}$ or $z_{\mathcal{C},0}$ are on the positive real axis of the $z_{\mathcal{C}}$-plane, respectively, as shown in figure 5.3. This happens for real-valued kinematics and leads to:

- $z_{\mathcal{C},1} > 0 \implies$ branch cut at $\eta > \eta_b$:

$$\mathrm{Log}(\eta - \eta_b) = \begin{cases} \log(r_b) + i2\pi\theta_H(-\phi)\,, & \eta > \eta_b\,, \\ \log(r_b) + i\pi\,, & \eta < \eta_b\,, \end{cases} \tag{5.44}$$

- $z_{\mathcal{C},0} > 0 \implies$ branch cut at $\eta < \eta_b$:

$$\mathrm{Log}(\eta - \eta_b) = \begin{cases} \log(r_b)\,, & \eta > \eta_b\,, \\ \log(r_b) - i\pi + i2\pi\theta_H(-\phi)\,, & \eta < \eta_b\,. \end{cases} \tag{5.45}$$

Once again, $\phi > 0$ selects the Feynman prescription while $\phi < 0$ enforces the opposite one.

For the reasoning developed in this section to be complete, two properties remain to be proved:

1. As a point η_p performs a complete counter-clockwise rotation at distance $r_b = \mathcal{R}(\eta_b)/2$ around the branch point $\eta = \eta_b$, its image $z_{\mathcal{C}}(\eta_p)$ also moves counter-clockwise around the origin, maintaining its orientation and completing exactly one rotation.

2. The branch cut originating from the spare branch point, $\eta = \eta_b'$, does not enter the circle of radius r_b centered at $\eta = \eta_b$.

Note that the first property implies the second one. For if $z_{\mathcal{C}}(\eta)$ crosses the real axis only once, then the point η_p encounters a single branch cut in its full rotation around the branch point $\eta = \eta_b$, and that cut must be the one originating from η_b itself. Given this observation, we now proceed to prove the first property.

First of all, let us write the quadratic polynomial $z_{\mathcal{C}}(\eta)$ in the factorized form

$$z_{\mathcal{C}}(\eta) = z_2(\eta - \eta_b)(\eta - \eta_b')\,, \tag{5.46}$$

where the value of the coefficient $z_2 \neq 0$ multiplying the highest power η^2 can be easily read off from eq. (5.41), but plays no role in the proof. We introduce the transformation $\eta = \eta_b + x(\eta_b' - \eta_b)$ so that, in the complex plane of the variable x, the two roots $\eta = \eta_b, \eta_b'$ are mapped to $x = 0, 1$, respectively. In terms of x, the Cutkosky invariant becomes

$$z_{\mathcal{C}} = z_2(\eta_b' - \eta_b)^2 x(x-1)\,, \tag{5.47}$$

while the full rotation of a point η_p on the circle $|\eta_p - \eta_b| = r_b$ corresponds to $x = re^{i\varphi}$ with $\varphi \in [-\pi, \pi]$ and $r = r_b/|\eta_b' - \eta_b|$. Since we expand around η_b within half the radius of convergence $\mathcal{R}(\eta_b)$, we are sure that $r \leq 1/2$ (with the equal sign occurring when η_b' is the pole closest to η_b). The rotation of $z_{\mathcal{C}}$ can thus be parameterized by

$$z_{\mathcal{C}} = z_2(\eta_b' - \eta_b)^2 re^{i\varphi}(re^{i\varphi} - 1)\,. \tag{5.48}$$

To make sure that $z_{\mathcal{C}}$ always proceeds counter-clockwise, we consider how its argument evolves in φ. We have

$$\arg z_{\mathcal{C}} = \arg\left(z_2(\eta_b' - \eta_b)^2\right) + \arg\left(re^{i\varphi}(re^{i\varphi} - 1)\right) \equiv \text{const.} + \arg\xi(\varphi)\,, \tag{5.49}$$

where the first contribution is constant, while the second one is the argument of

$$\xi(\varphi) \equiv e^{i\varphi}(re^{i\varphi} - 1) = r\cos(2\varphi) - \cos(\varphi) + i\left(r\sin(2\varphi) - \sin(\varphi)\right)\,. \tag{5.50}$$

For the arctan function taking values in $[-\pi/2, \pi/2]$, we have

$$\arg \xi(\varphi) = \arctan\left(\frac{r\sin(2\varphi) - \sin(\varphi)}{r\cos(2\varphi) - \cos(\varphi)}\right) + \{0, \pm\pi\}\,, \tag{5.51}$$

where the notation $+\{0, \pm\pi\}$ means that either π or $-\pi$ must be added when $\xi(\varphi)$ is in the second or third quadrant of the complex plane, respectively, while no addition is needed for $\xi(\varphi)$ in the first or fourth quadrant. Differentiating with respect to φ we obtain

$$\frac{d}{d\varphi}\arg z(\varphi) = \frac{d}{d\varphi}\arg \xi(\varphi) = \frac{1 + 2r^2 - 3r\cos(\varphi)}{1 + r^2 - 2r\cos(\varphi)}\,. \tag{5.52}$$

This derivative has a positive denominator for any $r \neq 0$, since

$$1 + r^2 - 2r\cos(\varphi) \geq 1 + r^2 - 2r = (r-1)^2\,, \tag{5.53}$$

so that its sign is determined by the numerator only. The latter is non-negative for $\cos(\varphi) \leq (1 + 2r^2)/3r$. This is always the case if $(1 + 2r^2)/3r \geq 1$, which holds true for $r \leq 1/2$ and $r \geq 1$. Since in our framework $r \leq 1/2$, we can conclude that $z_{\mathcal{C}}(\eta)$ moves counter-clockwise and never turns back in its rotation around the origin. Note that, if we were to take $r \in]1/2, 1[$, we would have $(1 + 2r^2)/3r < 1$ and the derivative would become negative for some values of φ. Therefore, expanding within half the distance from the other pole η_b' is necessary to guarantee the success of the method outlined in this section.

Finally, we need to exclude the possibility that $z_{\mathcal{C}}(\eta_p)$ completes more than one rotation around the origin as η_p performs a single one. This can be easily done by noting that the imaginary part of $\xi(\varphi)$,

$$\operatorname{Im}\xi(\varphi) = r\sin(\varphi)\,(2r\cos(\varphi) - 1)\,, \tag{5.54}$$

only vanishes twice, i.e., when $\sin(\varphi) = 0$, since $2r\cos(\varphi) - 1 < 0$ for $r < 1/2$. Even in the edge case $r = 1/2$, we have $2r\cos(\varphi) - 1 = 0$ for $\cos(\varphi) = 1$, which happens together with $\sin(\varphi) = 0$ and so it does not introduce an additional zero. Therefore, $\xi(\varphi)$ crosses the real axis only twice, meaning that $z_{\mathcal{C}}(\eta_p)$, which is a constant times $\xi(\varphi)$, completes only a single rotation. Note that $\operatorname{Im}\xi(\varphi) = 0$ at four angles for $r \geq 1/2$, reflecting the fact that $\xi(\varphi)$ inverts the direction of its rotation twice in that case.

5.3.3 Circling around a branch point

In the previous sections we provided rules for the analytic continuation of the logarithms appearing in the solutions around any given branch point $\eta_b \in [0, 1[$. The reasoning applied

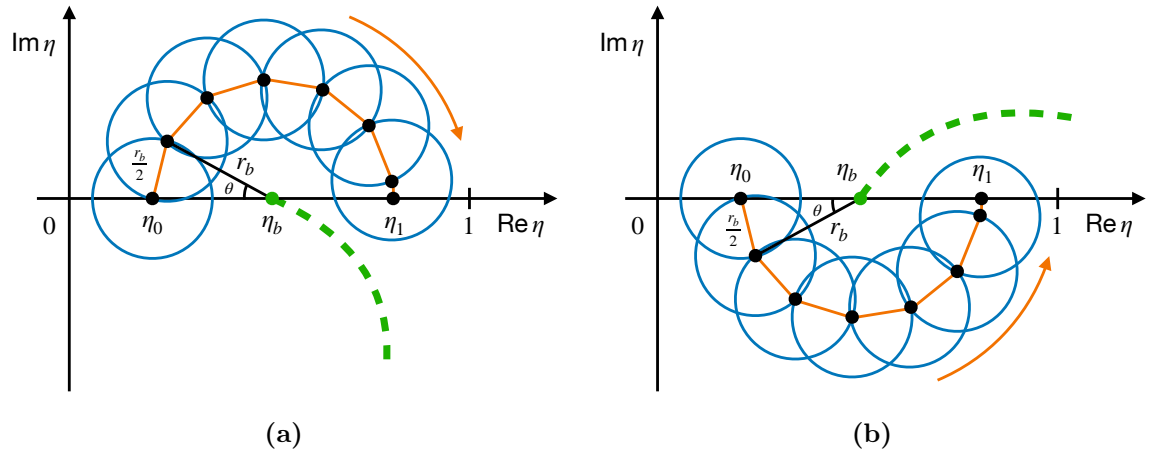

Figure 5.5: Regular propagation steps to circle around a branch point η_b in the complex plane of the line parameter η. The path (drawn in orange) consists of straight lines connecting points at distance r_b from the branch point η_b. The first six steps have length $r_b/2$ and correspond to an angle $\theta = \arccos(7/8) \simeq \pi/6.22$. The half-rotation is completed in seven steps, with the last one being shorter than the others. (a) The branch cut is in the lower half-plane and so the rotation takes place in the upper half. (b) The opposite is true.

to accomplish this task was based on identifying in which half of the η-complex plane the branch cut is located. In the case where the cut masses vary during the propagation, we explicitly followed the hypothetical rotation of a point η_p around the branch point on a circle of radius $r_b = \mathcal{R}(\eta_b)/2$, in order to detect whether this rotation intersects the branch cut. This methodology actually provides an alternative strategy for crossing the branch cut without using η_b as expansion point for the solution of the differential equations.

Suppose that the propagation has been carried out until the master integrals are evaluated at the previous path point $\eta_0 = \eta_b - r_b$. Following the prescriptions given in the previous sections, the arguments of $z_{\mathcal{C},0} = z_{\mathcal{C}}(\eta_b - r_b)$ and $z_{\mathcal{C},1} = z_{\mathcal{C}}(\eta_b + r_b)$ can be compared to determine whether, at fixed distance r_b from the branch point, the branch cut is in the upper or lower half of the η-complex plane. Having established that the cut is, say, in the upper half, we can perform a set of regular propagation steps in the lower half-plane to circle around the branch point counter-clockwise and evaluate the solution at $\eta_1 = \eta_b + r_b$. In particular, introducing the new path points at distance $r_b = \mathcal{R}(\eta_b)/2$ from the branch point, it is ensured that closest pole remains η_b at all the stages, so that the step size at any point is $r_b/2 = \mathcal{R}(\eta_b)/4$. Each step corresponds to a rotation of angle $\theta = \arccos(7/8) \simeq \pi/6.22$ and so the half-rotation can be completed in seven propagation steps (six steps with angle $\theta = \arccos(7/8)$ with the addition of a shorter final step or, equivalently, seven equal steps of angle $\pi/7$), as in figure 5.5. Naturally, if the branch cut is in the lower half of the complex plane, the propagation steps must be performed following a clockwise rotation in the upper half-plane.

For real-valued kinematics, the branch cut is on the real axis. Nonetheless, the methods

described in the previous sections allow one to identify the proper half of the complex plane, so that the branch cut is left (or approached) according to the Feynman prescription.

Following this approach, one can modify the strategy given in section 4.1 for the identification of the path points. In particular, after populating the phase space line with the procedure therein described, any singular point σ_i could be removed in favor of six additional regular points on the circle of radius $\mathcal{R}(\sigma_i)/2$, as prescribed in this section.

Chapter 6

Applications

This chapter presents a series of numerical applications of the methods discussed throughout this work. In particular, we employ LINE to evaluate, in $4-2\epsilon$ dimensions, the coefficients of the Laurent expansion in ϵ for the master integrals of representative one– and two–loop topologies at various phase–space points, reaching orders up to ϵ^4 and ϵ^2, respectively. Note that although, for any given topology, the dependence on one of the kinematic invariants could always be factored out by means of the homogeneity property in eq. (2.103), we always maintain the dependence on all the invariants to assess more deeply the implementation of LINE. The numerical results are provided with 16 digits of precision and arranged in tables, while section 6.7 shows how LINE performs on some of the examples provided.

For each application presented in this chapter, boundary conditions are generated with the LINE implementation of the AMFlow method, discussed in section 3.4.1, which we denote by AMF^0. To perform integration-by-parts reduction with the auxiliary mass, an interface to Kira has been programmed in LINE, along with coding structure to handle topology information. In this way, LINE is able to call Kira and use its results to build the DEs with respect to the auxiliary mass. For some examples, boundary conditions are generated also by exploiting the expansion by regions around a singular point of the DEs, as illustrated in sections 3.4.2 and 4.3.3. The results of the propagation to other kinematic points are validated by running AMF^0 on those points as well, with perfect agreement observed at all orders in ϵ.

While developing LINE, numerous cross-checks have been carried out against the Mathematica package AMFlow. However, we emphasize that LINE is designed in such a way that the precision of the results at any phase space point can be internally estimated without relying on external tools for the evaluation of Feynman integrals, since the same point can be approached along different paths and possibly from several boundary points, solving DEs with respect to the physical kinematic invariants and/or the auxiliary mass.

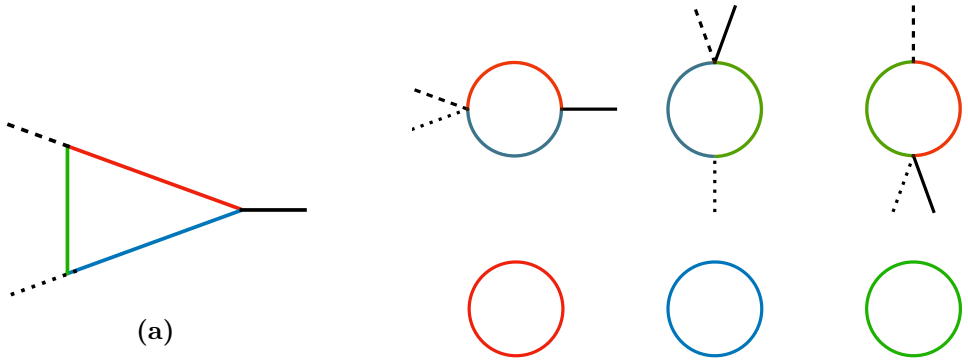

Figure 6.1: **(a)** One-loop triangle with six scales corresponding to three distinct propagator masses and three distinct squared momenta. Each mass is associated with a color-specific solid line, while external momenta are represented with black lines of different styles. **(b)** Graphs for the MIs obtained from the triangle by pinching some propagators. In the top row, bubble integrals resulting from pinching one propagator; in the bottom row, tadpole integrals resulting from pinching two propagators.

6.1 One-loop triangle with six scales

As a first example, let us consider the full-scale one-loop triangle of figure 6.1a. There are three off-shell external momenta p_1, p_2 and p_3 that can be described with three independent Lorentz invariants once momentum conservation is taken into account. For instance, a possible choice of the invariants is given by $s = (p_1 + p_2)^2$, p_1^2, p_2^2. In addition, the internal propagators have different masses so that the total number of parameters grows up to six when m_1^2, m_2^2 and m_3^2 are included too. This makes the triangle discussed here the most general scalar one-loop three-point function obeying Lorentz invariance and momentum conservation.

The family of Feynman integrals that we have to consider is given by

$$F^{\boldsymbol{\nu}}(\epsilon, s, p_1^2, p_2^2, m_1^2, m_2^2, m_3^2) = \int_k \frac{1}{D_1^{\nu_1} D_2^{\nu_2} D_3^{\nu_3}} \,. \tag{6.1}$$

with inverse propagators

$$\begin{aligned} D_1 &= k^2 - m_1^2 \,, \\ D_2 &= (k + p_1)^2 - m_2^2 \,, \\ D_3 &= (k + p_1 + p_2)^2 - m_3^2 \,. \end{aligned} \tag{6.2}$$

A basis of MIs for this family can be found by collecting three tadpoles with masses m_1, m_2 and m_3, the three bubbles with squared external momenta p_1^2, s and p_2^2, resulting

from the pinch of one propagator in the triangle integral, and the full-scale triangle itself. Bubbles and tadpoles are shown in figure 6.1b. The corresponding 7 integrals are $I_i = F^{\boldsymbol{\nu}_i}$ with powers

$$\begin{aligned} \boldsymbol{\nu}_1 &= (1,0,0)\,, & \boldsymbol{\nu}_2 &= (0,1,0)\,, \\ \boldsymbol{\nu}_3 &= (0,0,1)\,, & \boldsymbol{\nu}_4 &= (1,1,0)\,, \\ \boldsymbol{\nu}_5 &= (1,0,1)\,, & \boldsymbol{\nu}_6 &= (0,1,1)\,, \\ \boldsymbol{\nu}_7 &= (1,1,1)\,. \end{aligned} \tag{6.3}$$

Boundary conditions for the full-scale kinematics can be generated within LINE using EBR or the AMFlow method. Then, subsequent propagations allow us to explore the entire phase space. The possible target points also include degenerate cases where some invariants are zero or share the same value. In particular, the following runs are performed, whose numerical results are presented in table 6.1:

- First of all, a boundary is generated at the phase space point P_1 with kinematic invariants $s = 50$, $p_1^2 = 2$, $p_2^2 = -1/3$, $m_1^2 = 5$, $m_2^2 = 7$, $m_3^2 = 10$. This is achieved through two independent approaches which yield identical results up to all the required digits of working precision: AMF^0 and EBR. In the latter case, the regularity of the solution is imposed while solving the DEs around the regular singular point with vanishing external kinematics s, p_1^2, $p_2^2 \to 0$ and fixed masses. This allows us to express the leading coefficients for the bubbles and the triangle in terms of the tadpoles, whose values are obtained thanks to the analytical formula in eq. (3.53), available in LINE for evaluation at arbitrary precision. With BCs at our disposal, we are now ready for propagation to other phase space points.

- We move along a line connecting P_1 to point P_2 with invariants $s = 1$, $p_1^2 = 2$, $p_2^2 = -1/3$, $m_1^2 = 10$, $m_2^2 = 10$, $m_3^2 = 10$. By doing so, we encounter and cross the branch point whose Cutkosky invariant is $z = s - (m_1 + m_2)^2$. Perfect agreement is found when AMF^0 is applied directly to the triangle integral in P_2, thereby proving the numerical consistency of the result.

- We also propagate from P_1 to point P_3 with complex masses $m_1^2 = 1-i$, $m_2^2 = 8/3-2i$, $m_3^2 = 17 - i/4$ and kinematics $s = 1$, $p_1^2 = 2$, $p_2^2 = -1/3$. The transition to the complex plane is continuous since the masses acquire a negative imaginary part according to the Feynman prescription. This means that we stay on the same Riemann sheet and encounter no discontinuity.

- Finally, from P_3 we land on point P_4 with $s = -1$ and all the other invariants set to zero. As P_4 is a regular singular point, the solution has to be computed as a limit and the result is in agreement both with the analytical formula

$$F^{\boldsymbol{\nu}_7}(\epsilon, s, 0, 0, 0, 0, 0) = \frac{1}{\epsilon^2} \frac{\Gamma(1+\epsilon)\Gamma^2(1-\epsilon)}{\Gamma(1-2\epsilon)} \frac{(-s)^{-\epsilon}}{s}\,, \tag{6.4}$$

target	P_1	P_2	P_3	P_4
from	AMF^0, EBR	AMF^0, P_1	P_1	AMF^0, P_3
ϵ^{-2}	0	0	0	-1.000000000000000e0
ϵ^{-1}	0	0	0	+5.772156649015329e-1
ϵ^0	-7.599624851460716e-2 -1.024202715501841e-1*i	-5.114624184386078e-2	-9.105983456552547e-2 -3.405963008295366e-2*i	+6.558780715202539e-1
ϵ^1	+2.851448508579519e-1 +1.498241156232269e-1*i	+1.461267744725764e-1	+2.054866656214297e-1 +2.780936409230585e-2*i	+2.362111171285093e0
ϵ^2	-4.359339557414683e-1 -7.119426049903811e-2*i	-2.508159227043435e-1	-3.033284294289876e-1 -2.327298560596528e-2*i	+1.692738940537638e0
ϵ^3	+4.673966245020759e-1 +5.243128182287680e-3*i	+3.394894906445344e-1	+3.792260921703711e-1 +1.589606675868420e-2*i	+2.728361494345973e0
ϵ^4	-4.703087868710451e-1 +4.807793030293406e-3*i	-4.033919909274164e-1	-4.294046913943785e-1 -9.903139892953955e-3*i	+1.673348221588670e0

Table 6.1: Coefficients of the Laurent expansion in ϵ for the full-scale one-loop triangle at different phase space points. The heading row indicates the target points whose kinematics is listed in the text. The second row specifies, for each propagation, the starting point or the method used to get boundaries. Each entry in subsequent rows corresponds to the coefficients associated with the power of ϵ listed in the first column. When multiple starting points are indicated, all the propagations yield the same numerical results.

and with running AMF^0 directly on the one-scale massless triangle.

6.2 One-loop massless box

The one-loop box of figure 6.2a has massless propagators as well as massless external momenta p_1, p_2, p_3 and p_4. Momentum conservation $p_4 = -p_1 - p_2 - p_3$ and on-shell conditions $p_1^2 = p_2^2 = p_3^2 = p_4^2 = 0$ leave us with two independent Lorentz invariants, that can be chosen to be the Mandelstam variables $s = (p_1 + p_2)^2 = 2\,p_1 \cdot p_2$ and $t = (p_2 + p_3)^2 = 2\,p_2 \cdot p_3$, while $u = (p_1 + p_3)^2 = 2p_1 \cdot p_3$ is expressed as $u = -s - t$.

The integral family associated with the box described above is

$$F^{\boldsymbol{\nu}}(\epsilon, s, t) = \int_k \frac{1}{D_1^{\nu_1} D_2^{\nu_2} D_3^{\nu_3} D_4^{\nu_4}}\,, \tag{6.5}$$

with inverse propagators

$$\begin{aligned} D_1 &= k^2\,, & D_2 &= (k + p_1)^2\,, \\ D_3 &= (k + p_1 + p_2)^2\,, & D_4 &= (k + p_1 + p_2 + p_3)^2\,. \end{aligned} \tag{6.6}$$

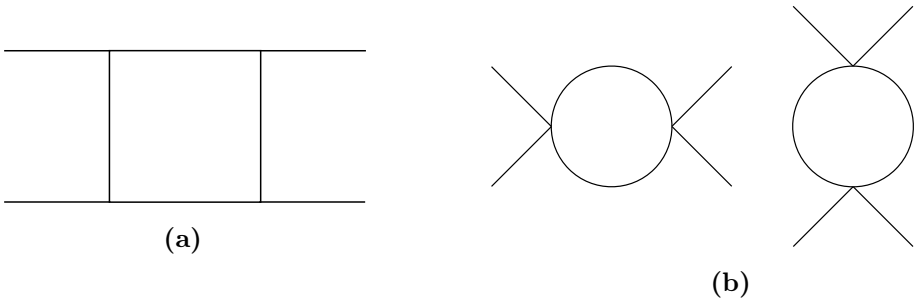

(a) **(b)**

Figure 6.2: **(a)** One-loop box with massless propagators and external momenta. **(b)** Graphs for the bubble integrals obtained from the box by pinching two propagators on opposite sides.

A basis of 3 MIs consists of the s- and t-channel massless bubbles shown in figure 6.2b, together with the box itself. So we have $I_i = F^{\boldsymbol{\nu}_i}$ with powers

$$\begin{aligned} \boldsymbol{\nu}_1 &= (1,0,1,0)\,, \\ \boldsymbol{\nu}_2 &= (0,1,0,1)\,, \\ \boldsymbol{\nu}_3 &= (1,1,1,1)\,. \end{aligned} \tag{6.7}$$

As for the full-scale triangle, we generate BCs using both AMF^0 and EBR with perfect agreement. The boundary point is P_1 with Mandelstam invariants $s = 1$ and $t = -3$. For the EBR we exploit the limit $u = -s - t \to 0$, solving the DEs around the singular point $s = 1$, $t = -1$ and imposing once again the regularity of the solution in said limit. In this way, the leading coefficient for the box is expressed in terms of the massless bubbles, which are evaluated at arbitrary precision using the analytical formula in eq. (4.55).

The boundary obtained in P_1 is then propagated to point P_2 with invariants $s = -11$, $t = 5$. Along the path, both the branch points with Cutkosky invariants $z_1 = s$ and $z_2 = t$ are crossed, in agreement with the output of AMF^0 applied to the box at point P_2.

The numerical results are arranged in table 6.2.

6.3 Full-scale sunrise

Let us focus on the sunrise graph in figure 6.3 with three different masses m_1, m_2, m_3 and incoming momentum p. Leaving the masses aside, the only kinematic invariant that the FI depends on is the square of the incoming momentum, $s = p^2$.

The integral family under consideration is

$$F^{\boldsymbol{\nu}}(\epsilon, s, m_1^2, m_2^2, m_3^2) = \int_{k_1,k_2} \frac{D_4^{-\nu_4} D_5^{-\nu_5}}{D_1^{\nu_1} D_2^{\nu_2} D_3^{\nu_3}}\,, \tag{6.8}$$

target	P_1	P_2
from	AMF^0, EBR	AMF^0, P_1
ϵ^{-2}	-1.333333333333333e0	-7.272727272727273e-2
ϵ^{-1}	+1.502029078980784e0 -2.094395102393195e0*i	+1.877005278194741e-1 -1.142397328578107e-1*i
ϵ^{0}	+3.741614747275086e0 +3.509845858409871e0*i	+2.698156090946971e-3 +3.398758787451875e-1*i
ϵ^{1}	-2.706665331892672e0 +5.235878433110419e0*i	-2.846794253590710e-1 -1.143352529230017e-1*i
ϵ^{2}	-5.048478376080319e0 -1.796965802540394e0*i	+9.893611975701797e-2 -1.978243414027738e-1*i
ϵ^{3}	+6.051530711191679e-1 -7.108042701350626e0*i	+1.402991837463381e-1 -3.176949541572250e-2*i
ϵ^{4}	+6.960674788336404e0 -6.425634195584692e0*i	+1.001382259037354e-1 +7.729488085430293e-3*i

Table 6.2: Coefficients of the Laurent expansion in ϵ for the one-loop massless box at different phase space points. The meaning of each entry is the same as for table 6.1.

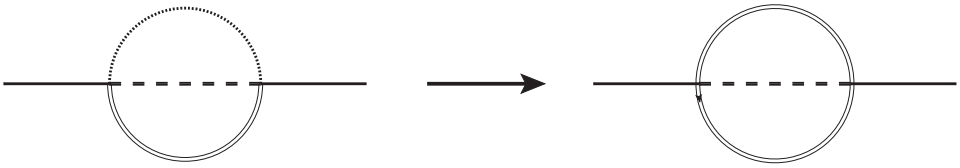

Figure 6.3: (Left) Sunrise graph with four different scales (as in the phase space point P_1 described in the text). (Right) The masses are varied in such a way that two internal masses coincide and the third one is equal to the external invariant with opposite sign (as in point P_3).

with inverse propagators

$$\begin{aligned} D_1 &= k_1^2 - m_1^2\,, & D_2 &= (k_2 - p)^2 - m_2^2\,, \\ D_3 &= (k_1 + k_2)^2 - m_3^2\,, & D_4 &= k_2^2\,, \\ D_5 &= (k_1 + p)^2\,. \end{aligned} \tag{6.9}$$

Note that we introduced D_4 and D_5 in order to complete a set of independent linear combinations of scalar products. They are massless and appear with negative powers (i.e., in the numerator) in the chosen basis of MIs, namely $I_i = F^{\boldsymbol{\nu}_i}$ with

$$\begin{aligned} \boldsymbol{\nu}_1 &= (1,1,0,0,0)\,, & \boldsymbol{\nu}_2 &= (1,0,1,0,0)\,, \\ \boldsymbol{\nu}_3 &= (0,1,1,0,0)\,, & \boldsymbol{\nu}_4 &= (1,1,1,-2,0)\,, \\ \boldsymbol{\nu}_5 &= (1,1,1,-1,0)\,, & \boldsymbol{\nu}_6 &= (1,1,1,0,-1)\,, \\ \boldsymbol{\nu}_7 &= (1,1,1,0,0)\,. \end{aligned} \tag{6.10}$$

target	P_1	P_2	P_3	P_4
from	AMF^0, EBR	AMF^0, P_1	P_1	AMF^0, P_3
ϵ^{-4}	0	0	0	0
ϵ^{-3}	0	0	0	0
ϵ^{-2}	+5.000000000000000e0	+5.000000000000000e0	+5.500000000000000e0	0
ϵ^{-1}	-3.251477438310050e0	-1.850147743831005e1	-5.693751438257865e0	+2.500000000000000e-1
ϵ^{0}	+1.188378767646979e1	+6.552872234370230e1 -1.758371010882413e1*i	+1.867337540448070e1	+1.336392167549234e0
ϵ^{1}	+1.952137703514755e1	-1.091156083475895e2 +2.967183417356042e1*i	+4.626131138234519e0	+5.066904534261821e0
ϵ^{2}	-2.160341605441262e1	+3.251877471184126e2 -1.125285386030628e1*i	+7.465797730320954e0	+1.434873581897869e1

Table 6.3: Coefficients of the Laurent expansion in ϵ for the top-topology sunrise integral at different phase space points. The meaning of each entry is the same as for table 6.1.

We generate BCs for this topology by looking for a regular solution to the DEs in the limit $s \to 0$ with fixed masses $m_1^2 = 10$, $m_2^2 = 10$, $m_3^2 = 10$. The solution is then propagated to point P_1 with $s = -1$ and masses $m_1^2 = 2$, $m_2^2 = 3$, $m_3^2 = 5$, finding agreement with a run of AMF^0. The values of the MIs at P_1 serve as BCs to propagate toward two different target points: the first one is point P_2, which we reach keeping the masses fixed and varying s up to $s = 60$, crossing the branch point with Cutkosky invariant $z = s-(m_1+m_2+m_3)^2$; the second point is P_3 with $m_1^2 = -s = 1$ and $m_2^2 = m_3^2 = 5$. Finally, from P_3 we compute the limit of vanishing masses $m_1^2, m_2^2, m_3^2 \to 0$ at fixed $s = -1$, defining point P_4. To validate the accuracy of the results, we also perform AMF^0 propagations in P_2 and P_4, finding perfect agreement in both cases.

The numerical output of the steps described above is shown in table 6.3.

6.4 Two-loop non-planar triangle with mass

The two-loop non-planar triangle in figure 6.4 has incoming momenta p_1, p_2 and p_3, with $p_1^2 = p_2^2 = m^2$ while p_3 is off-shell. The same mass m is also shared by four propagators arranged on two massive lines that, starting from the external momenta p_1 and p_2, meet at the vertex corresponding to p_3. Although only one invariant is needed to describe the external off-shell kinematics, e.g., $s = p_3^2 = (p_1 + p_2)^2$, as usual we also consider DEs with respect to the squared mass m^2.

Let $F^{\boldsymbol{\nu}}(\epsilon, s, m^2)$ be the integral family associated with the triangle described above.

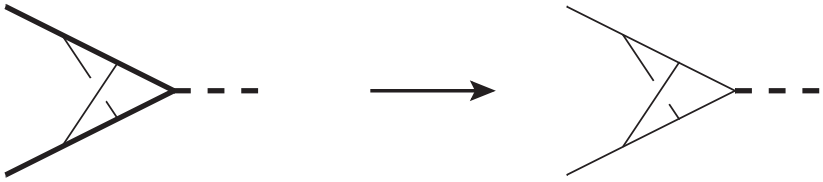

Figure 6.4: (Left) Non-planar triangle with a common mass, highlighted with a bold line, shared by two external momenta and four propagators (as in the phase space point P_1 described in the text). (Right) The same diagram in the massless limit (as in point P_3).

We have

$$F^{\boldsymbol{\nu}}(\epsilon, s, m^2) = \int_{k_1,k_2} \frac{D_7^{-\nu_7}}{D_1^{\nu_1} D_2^{\nu_2} D_3^{\nu_3} D_4^{\nu_4} D_5^{\nu_5} D_6^{\nu_6}} \tag{6.11}$$

with inverse propagators

$$\begin{aligned}
D_1 &= k_1^2\,, & D_2 &= k_2^2\,,\\
D_3 &= (k_1 - p_1)^2 - m^2\,, & D_4 &= (k_2 + p_2)^2 - m^2\,,\\
D_5 &= (k_1 + k_2 - p_1)^2 - m^2\,, & D_6 &= (k_1 + k_2 + p_2)^2 - m^2\,,\\
D_7 &= (k_1 + k_2)^2\,.
\end{aligned} \tag{6.12}$$

The auxiliary inverse propagator D_7 only appears in the numerator of one of the 16 MIs that form the selected basis $I_i = F^{\boldsymbol{\nu}_i}$ with powers

$$\begin{aligned}
\boldsymbol{\nu}_1 &= (0,0,1,1,0,0,0)\,, & \boldsymbol{\nu}_2 &= (1,1,0,0,1,0,0)\,,\\
\boldsymbol{\nu}_3 &= (1,-1,0,1,1,0,0)\,, & \boldsymbol{\nu}_4 &= (1,0,0,1,1,0,0)\,,\\
\boldsymbol{\nu}_5 &= (0,0,1,1,1,0,0)\,, & \boldsymbol{\nu}_6 &= (0,0,1,0,1,1,0)\,,\\
\boldsymbol{\nu}_7 &= (1,1,0,1,1,0,0)\,, & \boldsymbol{\nu}_8 &= (1,-1,1,1,1,0,0)\,,\\
\boldsymbol{\nu}_9 &= (1,0,1,1,1,0,0)\,, & \boldsymbol{\nu}_{10} &= (1,1,0,0,1,1,0)\,,\\
\boldsymbol{\nu}_{11} &= (-1,0,1,1,1,1,0)\,, & \boldsymbol{\nu}_{12} &= (0,0,1,1,1,1,0)\,,\\
\boldsymbol{\nu}_{13} &= (1,1,1,-1,1,1,0)\,, & \boldsymbol{\nu}_{14} &= (1,1,1,0,1,1,0)\,,\\
\boldsymbol{\nu}_{15} &= (1,1,1,1,1,1,-1)\,, & \boldsymbol{\nu}_{16} &= (1,1,1,1,1,1,0)\,.
\end{aligned} \tag{6.13}$$

We generate boundary values at point P_1 with $s = 10$, $m^2 = 1$ running AMF^0. The introduction of the auxiliary mass increases the number of MIs to 52. We then cross the branch point with Cutkosky invariant $z = s - 4m^2$ to propagate the boundary to point P_2 with $s = 1$, $m^2 = 3$. From P_2, we move to P_3 computing the massless limit $m^2 \to 0$ at fixed $s = 1$. Finally, we approach the same point by acting with AMF^0 directly on the one-scale topology with massless propagators and on-shell momenta $p_1^2 = p_2^2 = 0$, finding agreement on all the required digits.

The numerical results are listed in table 6.4.

target	P_1	P_2	P_3
from	AMF^0	P_1	AMF^0, P_2
ϵ^{-4}	0	0	+1.000000000000000e0
ϵ^{-3}	0	0	-1.154431329803066e0 +6.283185307179586e0*i
ϵ^{-2}	0	0	-2.894245735565264e1 -7.253505969566414e0*i
ϵ^{-1}	+2.532501153536048e-1 +1.376560680870821e-1*i	-3.058450755305179e-2	+6.680132569623135e-1 -9.916741832990889e1*i
ϵ^{0}	-1.137868788629137e0 +1.315450793632957e0*i	+6.882432933483959e-2	+2.306015883275194e2 -9.125506150626736e1*i
ϵ^{1}	-5.535444498587951e0 -1.578608277056101e0*i	+5.232509250247894e-2	+4.317677285401460e2 +3.615355918032282e2*i
ϵ^{2}	-1.199497745643981e1 -8.780073080609521e0*i	+8.195254040212031e-1	+1.850496772277360e1 +1.260787755350661e3*i

Table 6.4: Coefficients of the Laurent expansion in ϵ for the top-topology two-loop non-planar triangle integral at different phase space points. The meaning of each entry is the same as for table 6.1.

6.5 Two-loop planar box with a massive loop

Let us consider the double box in figure 6.5. The external kinematics, which is the same as for the one-loop box of the integral family in eq. (6.5), can be described by the Mandelstam invariants $s = (p_1 + p_2)^2$ and $t = (p_2 + p_3)^2$. In addition, we also consider the squared mass m^2 shared by four propagators closing a loop.

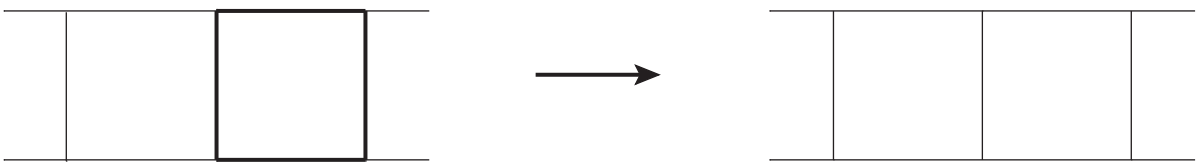

Figure 6.5: (Left) Double box diagram with a massive loop highlighted with a bold line (phase space point P_1 in the text). (Right) The same diagram in the massless limit (phase space point P_3 in the text).

The associated integral family is given by

$$F^{\boldsymbol{\nu}}(\epsilon, s, t, m^2) = \int_{k_1,k_2} \frac{D_8^{-\nu_8} D_9^{-\nu_9}}{D_1^{\nu_1} D_2^{\nu_2} D_3^{\nu_3} D_4^{\nu_4} D_5^{\nu_5} D_6^{\nu_6} D_7^{\nu_7}} \tag{6.14}$$

with inverse propagators

$$\begin{aligned}
&D_1 = k_1^2\,, && D_2 = (k_1 - p_1)^2\,,\\
&D_3 = (k_1 + p_2)^2\,, && D_4 = (k_2 - p_2)^2 - m^2\,,\\
&D_5 = (k_2 + p_1)^2 - m^2\,, && D_6 = (k_1 + k_2)^2 - m^2\,,\\
&D_7 = (k_2 - p_2 - p_3)^2 - m^2\,, && D_8 = k_2^2\,,\\
&D_9 = (k_1 + p_3)^2\,,
\end{aligned} \tag{6.15}$$

where D_8 and D_9 are auxiliary numerators used to complete a basis in the space of the scalar products. The chosen basis $I_i = F^{\boldsymbol{\nu}_i}$ consists of 32 MIs with the following powers:

$$\begin{aligned}
&\boldsymbol{\nu}_1 = (0,0,0,1,0,1,0,0,0)\,, && \boldsymbol{\nu}_2 = (0,1,1,1,0,0,0,0,0)\,, && \boldsymbol{\nu}_3 = (-1,1,0,1,0,1,0,0,0)\,,\\
&\boldsymbol{\nu}_4 = (0,1,0,1,0,1,0,0,0)\,, && \boldsymbol{\nu}_5 = (0,0,0,1,1,1,0,0,0)\,, && \boldsymbol{\nu}_6 = (1,-1,0,0,0,1,1,0,0)\,,\\
&\boldsymbol{\nu}_7 = (1,0,0,0,0,1,1,0,0)\,, && \boldsymbol{\nu}_8 = (0,1,1,1,1,0,0,0,0)\,, && \boldsymbol{\nu}_9 = (1,-1,0,1,1,1,0,0,0)\,,\\
&\boldsymbol{\nu}_{10} = (1,0,0,1,1,1,-1,0,0)\,, && \boldsymbol{\nu}_{11} = (1,0,0,1,1,1,0,0,0)\,, && \boldsymbol{\nu}_{12} = (-1,1,1,0,0,1,1,0,0),\\
&\boldsymbol{\nu}_{13} = (0,1,1,0,0,1,1,0,0)\,, && \boldsymbol{\nu}_{14} = (1,0,0,1,0,1,1,0,0)\,, && \boldsymbol{\nu}_{15} = (0,1,0,1,0,1,1,0,0)\,,\\
&\boldsymbol{\nu}_{16} = (0,0,0,1,1,1,1,0,0)\,, && \boldsymbol{\nu}_{17} = (0,1,1,1,1,1,0,0,0)\,, && \boldsymbol{\nu}_{18} = (0,1,1,1,1,0,1,0,0)\,,\\
&\boldsymbol{\nu}_{19} = (1,1,1,-1,0,1,1,0,0)\,, && \boldsymbol{\nu}_{20} = (1,1,1,0,0,1,1,0,0)\,, && \boldsymbol{\nu}_{21} = (1,1,-1,1,0,1,1,0,0)\,,\\
&\boldsymbol{\nu}_{22} = (1,1,0,1,0,1,1,0,0)\,, && \boldsymbol{\nu}_{23} = (0,1,1,1,0,1,1,0,0)\,, && \boldsymbol{\nu}_{24} = (1,-1,0,1,1,1,1,0,0)\,,\\
&\boldsymbol{\nu}_{25} = (1,0,0,1,1,1,1,-1,0)\,, && \boldsymbol{\nu}_{26} = (1,0,0,1,1,1,1,0,0)\,, && \boldsymbol{\nu}_{27} = (1,1,1,1,0,1,1,0,0)\,,\\
&\boldsymbol{\nu}_{28} = (0,1,1,1,1,1,1,0,0)\,, && \boldsymbol{\nu}_{29} = (1,1,1,1,1,1,1,-2,0)\,, && \boldsymbol{\nu}_{30} = (1,1,1,1,1,1,1,-1,0)\,,\\
&\boldsymbol{\nu}_{31} = (1,1,1,1,1,1,1,0,-1)\,, && \boldsymbol{\nu}_{32} = (1,1,1,1,1,1,1,0,0)\,.
\end{aligned} \tag{6.16}$$

We generate a boundary at point P_1 with $s = -1$, $t = 2$, $m^2 = 10$ by using EBR in the limit $s, t \to 0$ of vanishing external kinematics at fixed mass, as described in the discussion of this example in sections 3.4.2 and 4.3.3. The first two MIs behave as a squared tadpole and a tadpole times a massless s-channel bubble, respectively. Vetoing any undesired power behaviors, we can relate the leading coefficients of the remaining MIs to those of the first two. The resulting solution can be evaluated at any $s, t \neq 0$ within the radius of convergence of the series expansion, including $s = -1$, $t = 2$ as in P_1. The outcome is in complete agreement with an AMF^0 run performed at P_1, that increases the number of MIs to 68 upon the introduction of the auxiliary mass in every propagator. Note that an implementation of the recursive AMFlow method would leave the number of MIs unchanged if no auxiliary mass is introduced and m^2 is pushed to infinity in the lower half of the complex plane.

Once the boundary is ready, we propagate from P_1 to point P_2 with $s = 70$, $t = 50$, $m^2 = 10$, crossing three different branch points with Cutkosky invariants $z_1 = s$, $z_2 = s - 4m^2$ and $z_3 = t - 4m^2$. After that, we fix the external kinematics and move to point P_3 with zero mass. The values obtained fully agree with a run of AMF^0 performed directly at P_3 on the massless topology.

target	P_1	P_2	P_3
from	AMF^0, EBR	P_1	AMF^0, P_2
ϵ^{-4}	0	0	+1.632653061224490e-5
ϵ^{-3}	0	0	-1.507074533571472e-4 +1.025826172600749e-4*i
ϵ^{-2}	-1.684311982263061e-3	+7.121750612221514e-5 +1.223851404355579e-4*i	+2.720746512604996e-4 -9.469228566160803e-4*i
ϵ^{-1}	+4.026956116103587e-3	-7.645333935948279e-4 -3.758110807119310e-4*i	+1.572347464421193e-3 +3.059428585636381e-3*i
ϵ^{0}	-3.997722931454625e-3	+1.621191987913520e-3 -1.376157443003446e-4*i	-8.340803170789194e-3 -2.581654837967916e-3*i
ϵ^{1}	+6.237012138664067e-3	-2.779941041112323e-3 -3.108819053117712e-5*i	+1.483674698459523e-2 -8.593463886823766e-3*i
ϵ^{2}	-4.987777863769356e-3	+5.841649978319638e-3 -1.900890782973601e-3*i	-4.995133665555594e-3 +2.645276326148751e-2*i

Table 6.5: Coefficients of the Laurent expansion in ϵ for the top-topology two-loop planar box at different phase space points. The meaning of each entry is the same as for table 6.1.

Table 6.5 presents the values at every phase space point of the top-topology integral $F^{\boldsymbol{\nu}_{32}}$.

6.6 Two-loop non-planar boxes with mass

We now focus on the two non-planar boxes in figure 6.6, that share the same external kinematics with four momenta p_1, p_2, p_3, p_4, where $p_1^2 = p_2^2 = 0$ and $p_3^2 = p_4^2 = m^2$. As for the other boxes, the on-shell kinematics is described by the Mandelstam invariants $s = (p_1 + p_2)^2$ and $t = (p_2 + p_3)^2$. The squared mass m^2, which is also regarded as a varying parameter, appears in different propagators forming one massive line of the first box and two massive lines of the second one.

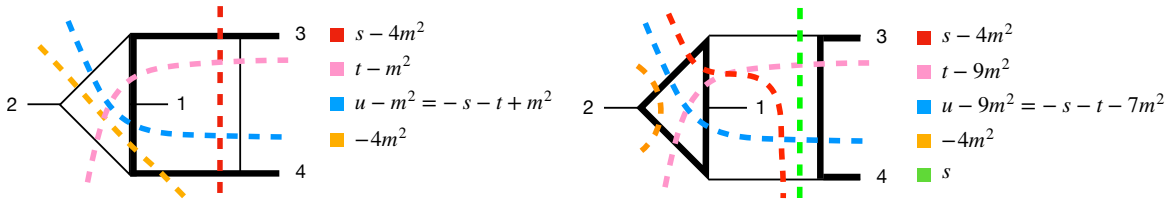

Figure 6.6: Non-planar boxes with a common mass, highlighted with a bold line, shared by two external momenta and some propagators. Cutkosky cuts are displayed with dashed lines and the corresponding Cutkosky invariants are listed next to each graph.

For both box diagrams the integral family has the form

$$F^{\boldsymbol{\nu}}(\epsilon, s, t, m^2) = \int_{k_1,k_2} \frac{D_8^{-\nu_8} D_9^{-\nu_9}}{D_1^{\nu_1} D_2^{\nu_2} D_3^{\nu_3} D_4^{\nu_4} D_5^{\nu_5} D_6^{\nu_6} D_7^{\nu_7}} \tag{6.17}$$

where the inverse propagators are separately specified below for the two cases and D_8, D_9 are irreducible numerators that complete the set of independent linear combinations of scalar products.

1st box. Let us focus on the box in the left panel of figure 6.6, with inverse propagators

$$\begin{aligned}
&D_1 = k_2^2\,, && D_2 = (k_2 - p_2)^2\,,\\
&D_3 = (k_2 - k_1 - p_2 - p_3)^2\,, && D_4 = k_1^2 - m^2\,,\\
&D_5 = (k_1 - p_1)^2 - m^2\,, && D_6 = (k_2 - k_1 - p_2)^2 - m^2\,,\\
&D_7 = (k_2 - k_1 + p_1)^2 - m^2\,, && D_8 = (k_1 + p_3)^2\,,\\
&D_9 = (k_1 + p_2)^2\,.
\end{aligned} \tag{6.18}$$

A basis of 55 MIs is formed by $I_i = F^{\boldsymbol{\nu}_i}$ with powers

$$\begin{aligned}
&\boldsymbol{\nu}_1 = (0,0,0,1,0,1,0,0,0)\,, && \boldsymbol{\nu}_2 = (1,-1,1,1,0,0,0,0,0)\,, && \boldsymbol{\nu}_3 = (1,0,1,1,0,0,0,0,0)\,,\\
&\boldsymbol{\nu}_4 = (0,1,1,1,0,0,0,0,0)\,, && \boldsymbol{\nu}_5 = (-1,1,1,0,1,0,0,0,0)\,, && \boldsymbol{\nu}_6 = (0,1,1,0,1,0,0,0,0)\,,\\
&\boldsymbol{\nu}_7 = (1,-1,0,0,1,1,0,0,0)\,, && \boldsymbol{\nu}_8 = (1,0,0,0,1,1,0,0,0)\,, && \boldsymbol{\nu}_9 = (0,0,0,1,0,1,1,0,0)\,,\\
&\boldsymbol{\nu}_{10} = (1,-1,1,1,0,1,0,0,0)\,, && \boldsymbol{\nu}_{11} = (1,0,1,1,0,1,0,0,0)\,, && \boldsymbol{\nu}_{12} = (1,0,1,0,1,1,0,0,0)\,,\\
&\boldsymbol{\nu}_{13} = (-1,1,1,0,1,1,0,0,0)\,, && \boldsymbol{\nu}_{14} = (0,1,1,0,1,1,0,0,0)\,, && \boldsymbol{\nu}_{15} = (1,0,0,1,1,1,0,0,0)\,,\\
&\boldsymbol{\nu}_{16} = (1,-1,0,1,0,1,1,0,0)\,, && \boldsymbol{\nu}_{17} = (1,0,-1,1,0,1,1,0,0)\,, && \boldsymbol{\nu}_{18} = (1,0,0,1,0,1,1,0,0)\,,\\
&\boldsymbol{\nu}_{19} = (1,1,1,1,1,-1,0,0,0)\,, && \boldsymbol{\nu}_{20} = (1,1,1,1,1,0,0,0,0)\,, && \boldsymbol{\nu}_{21} = (1,1,1,-1,1,1,0,0,0)\,,\\
&\boldsymbol{\nu}_{22} = (1,1,1,0,1,1,-1,0,0)\,, && \boldsymbol{\nu}_{23} = (1,1,1,0,1,1,0,0,0)\,, && \boldsymbol{\nu}_{24} = (1,-1,1,1,1,1,0,0,0)\,,\\
&\boldsymbol{\nu}_{25} = (1,0,1,1,1,1,-1,0,0)\,, && \boldsymbol{\nu}_{26} = (1,0,1,1,1,1,0,-1,0)\,, && \boldsymbol{\nu}_{27} = (1,0,1,1,1,1,0,0,0)\,,\\
&\boldsymbol{\nu}_{28} = (0,1,1,1,1,1,0,0,0)\,, && \boldsymbol{\nu}_{29} = (1,1,1,1,-1,0,1,0,0)\,, && \boldsymbol{\nu}_{30} = (1,1,1,1,0,-1,1,0,0)\,,\\
&\boldsymbol{\nu}_{31} = (1,1,1,1,0,0,1,0,0)\,, && \boldsymbol{\nu}_{32} = (1,0,1,1,1,0,1,0,0)\,, && \boldsymbol{\nu}_{33} = (-1,1,1,1,1,0,1,0,0)\,,\\
&\boldsymbol{\nu}_{34} = (0,1,1,1,1,-1,1,0,0)\,, && \boldsymbol{\nu}_{35} = (0,1,1,1,1,0,1,-1,0)\,, && \boldsymbol{\nu}_{36} = (0,1,1,1,1,0,1,0,0)\,,\\
&\boldsymbol{\nu}_{37} = (1,-1,1,1,0,1,1,0,0)\,, && \boldsymbol{\nu}_{38} = (1,0,1,1,0,1,1,0,0)\,, && \boldsymbol{\nu}_{39} = (-1,1,1,0,1,1,1,0,0)\,,\\
&\boldsymbol{\nu}_{40} = (0,1,1,0,1,1,1,0,0)\,, && \boldsymbol{\nu}_{41} = (1,-1,0,1,1,1,1,0,0)\,, && \boldsymbol{\nu}_{42} = (1,0,0,1,1,1,1,0,0)\,,\\
&\boldsymbol{\nu}_{43} = (1,1,1,1,1,1,-1,0,0)\,, && \boldsymbol{\nu}_{44} = (1,1,1,1,1,1,0,-1,0)\,, && \boldsymbol{\nu}_{45} = (1,1,1,1,1,1,0,0,0)\,,\\
&\boldsymbol{\nu}_{46} = (1,1,1,1,1,-1,1,0,0)\,, && \boldsymbol{\nu}_{47} = (1,1,1,1,1,0,1,-1,0)\,, && \boldsymbol{\nu}_{48} = (1,1,1,1,1,0,1,0,0)\,,\\
&\boldsymbol{\nu}_{49} = (1,1,0,1,1,1,1,0,0)\,, && \boldsymbol{\nu}_{50} = (1,0,1,1,1,1,1,0,0)\,, && \boldsymbol{\nu}_{51} = (0,1,1,1,1,1,1,0,0)\,,\\
&\boldsymbol{\nu}_{52} = (1,1,1,1,1,1,1,-2,0)\,, && \boldsymbol{\nu}_{53} = (1,1,1,1,1,1,1,-1,0)\,, && \boldsymbol{\nu}_{54} = (1,1,1,1,1,1,1,0,-1)\,,\\
&\boldsymbol{\nu}_{55} = (1,1,1,1,1,1,1,0,0)\,.
\end{aligned} \tag{6.19}$$

target	Q_1	Q_2	P_1	P_2
from	AMF^0	AMF^0, Q_1	AMF^0	AMF^0, P_1
ϵ^{-4}	0	0	0	0
ϵ^{-3}	-2.634309928357791e-7	+7.825617108436437e-8 -2.554478084014810e-7*i	0	0
ϵ^{-2}	+2.177434402618331e-6 -1.655185743641498e-6*i	+5.136099594647812e-9 +3.245051324395477e-6*i	0	0
ϵ^{-1}	+2.177434402618331e-6 +1.533076938553119e-5*i	+5.136099594647812e-9 -3.407024087192466e-5*i	0	0
ϵ^{0}	-2.810879169233962e-5 -3.761642841819541e-5*i	+2.470711494037188e-4 -6.343358651146831e-5*i	+2.576938753803745e-1 -2.465521721983634e-1*i	+2.518740723653660e-1 -1.169079848124980e-1*i
ϵ^{1}	+6.424181660342731e-5 +3.595559671704640e-5*i	+3.561272520516187e-5 +6.872261543040661e-4*i	+9.839059948409147e-1 -1.447010196851563e-1*i	+8.377932210850515e-1 +2.609108724913395e-1*i
ϵ^{2}	-1.721862393547420e-4 -1.231788432398794e-5*i	-7.247299398344942e-4 +6.092012063072394e-5*i	+1.881565035678200e0 -4.606206236766448e-3*i	+1.544162064068738e0 +1.125263466661532e0*i

Table 6.6: Coefficients of the Laurent expansion in ϵ for the two-loop non-planar box on the left (phase space points Q_1 and Q_2 described in the text) and on the right (points P_1 and P_2) of figure 6.6. The meaning of each entry is the same as for table 6.1. More points (P_3, P_4, P_5 and P_6) for the second box are shown in table 6.7.

We use AMF^0, extending the basis to 144 MIs, to obtain a boundary at point Q_1 with $s = 1$, $t = 2$, $m^2 = 100$. Then, from Q_1 we move to point Q_2 with $s = 500$, $t = 150$, $m^2 = 100$. By doing so, we cross the three branch points corresponding to $z_1 = s - 4m^2$, $z_2 = t - m^2$, $z_3 = -s - t + m^2$. The result agrees with an AMF^0 run performed at Q_2.

Table 6.6 lists the numerical values for the top-topology integral $F^{\boldsymbol{\nu}_{55}}$.

2nd box. The inverse propagators for the box in the right panel of figure 6.6 are

$$\begin{aligned} D_1 &= (k_2 - k_1 - p_2)^2\,, & D_2 &= (k_2 - k_1 + p_1)^2\,, \\ D_3 &= k_1^2 - m^2\,, & D_4 &= k_2^2 - m^2\,, \\ D_5 &= (k_1 - p_1)^2 - m^2\,, & D_6 &= (k_2 - p_2)^2 - m^2\,, \\ D_7 &= (k_2 - k_1 - p_2 - p_3)^2 - m^2\,, & D_8 &= (k_1 + p_3)^2\,, \\ D_9 &= (k_1 + p_2)^2\,. \end{aligned} \tag{6.20}$$

The chosen basis $I_i = F^{\boldsymbol{\nu}_i}$ consists of 54 MIs with powers

$$\begin{aligned} &\boldsymbol{\nu}_1 = (0,0,1,1,0,0,0,0,0)\,, && \boldsymbol{\nu}_2 = (1,1,1,0,0,0,0,0,0)\,, && \boldsymbol{\nu}_3 = (1,-1,0,1,1,0,0,0,0)\,, \\ &\boldsymbol{\nu}_4 = (1,0,0,1,1,0,0,0,0)\,, && \boldsymbol{\nu}_5 = (-2,0,1,1,0,0,1,0,0)\,, && \boldsymbol{\nu}_6 = (0,0,1,1,0,0,1,0,0)\,, \\ &\boldsymbol{\nu}_7 = (0,0,0,1,1,0,1,0,0)\,, && \boldsymbol{\nu}_8 = (-2,0,0,0,1,1,1,0,0)\,, && \boldsymbol{\nu}_9 = (0,0,0,0,1,1,1,0,0)\,, \end{aligned}$$

target	P_3	P_4	P_5	P_6
from	AMF^0	AMF^0, P_3	AMF^0	AMF^0, P_5
ϵ^0	+2.751593454707949e-1 -3.815281539209958e-1*i	+2.506591535092400e-1 -4.235680397875819e-1*i	-2.405260844173886e-1 -5.984661196233730e-3*i	-4.831181490833649e-1
ϵ^1	+1.257054227433279e0 +4.342974425182124e-1*i	+1.187415013371159e0 -5.997939132016630e-1*i	-5.588054474320729e-1 -3.250774673987693e-2*i	-1.396083737425863e0
ϵ^2	+2.478546160626464e0 -2.47049854421279e-1*i	+2.372121269639779e0 -5.961585949177441e-1*i	-1.124284189077083e0 -8.467242364778369e-2*i	-3.146872480560270e0

Table 6.7: Coefficients of the Laurent expansion in ϵ for the two-loop non-planar box on the right of figure 6.6 at different phase space points. The meaning of each entry is the same as for table 6.1.

$$
\begin{aligned}
&\boldsymbol{\nu}_{10} = (1,1,1,1,-1,0,0,0,0)\,, && \boldsymbol{\nu}_{11} = (1,1,1,1,0,0,0,0,0)\,, && \boldsymbol{\nu}_{12} = (1,0,1,1,1,0,0,0,0)\,,\\
&\boldsymbol{\nu}_{13} = (1,1,1,0,0,0,1,0,0)\,, && \boldsymbol{\nu}_{14} = (1,0,1,1,0,0,1,0,0)\,, && \boldsymbol{\nu}_{15} = (1,-1,0,1,1,0,1,0,0)\,,\\
&\boldsymbol{\nu}_{16} = (1,0,0,1,1,0,1,0,0)\,, && \boldsymbol{\nu}_{17} = (0,0,1,1,1,0,1,0,0)\,, && \boldsymbol{\nu}_{18} = (1,0,0,0,1,1,1,0,0)\,,\\
&\boldsymbol{\nu}_{19} = (0,0,1,0,1,1,1,0,0)\,, && \boldsymbol{\nu}_{20} = (1,1,1,1,1,0,0,0,0)\,, && \boldsymbol{\nu}_{21} = (1,0,1,1,1,1,0,0,0)\,,\\
&\boldsymbol{\nu}_{22} = (1,1,1,1,-2,0,1,0,0)\,, && \boldsymbol{\nu}_{23} = (1,1,1,1,-1,0,1,0,0)\,, && \boldsymbol{\nu}_{24} = (1,1,1,1,0,0,1,0,0)\,,\\
&\boldsymbol{\nu}_{25} = (1,-1,1,1,1,0,1,0,0)\,, && \boldsymbol{\nu}_{26} = (1,0,1,1,1,-1,1,0,0)\,, && \boldsymbol{\nu}_{27} = (1,0,1,1,1,0,1,-1,0)\,,\\
&\boldsymbol{\nu}_{28} = (1,0,1,1,1,0,1,0,0)\,, && \boldsymbol{\nu}_{29} = (1,1,-2,0,1,1,1,0,0)\,, && \boldsymbol{\nu}_{30} = (1,1,-1,0,1,1,1,0,0)\,,\\
&\boldsymbol{\nu}_{31} = (1,1,0,0,1,1,1,0,0)\,, && \boldsymbol{\nu}_{32} = (-1,1,1,0,1,1,1,0,0)\,, && \boldsymbol{\nu}_{33} = (0,1,1,-1,1,1,1,0,0)\,,\\
&\boldsymbol{\nu}_{34} = (0,1,1,0,1,1,1,-1,0)\,, && \boldsymbol{\nu}_{35} = (0,1,1,0,1,1,1,0,0)\,, && \boldsymbol{\nu}_{36} = (-2,0,1,1,1,1,1,0,0)\,,\\
&\boldsymbol{\nu}_{37} = (-1,-1,1,1,1,1,1,0,0)\,, && \boldsymbol{\nu}_{38} = (-1,0,1,1,1,1,1,0,0)\,, && \boldsymbol{\nu}_{39} = (0,0,1,1,1,1,1,0,0)\,,\\
&\boldsymbol{\nu}_{40} = (1,1,1,1,1,1,-2,0,0)\,, && \boldsymbol{\nu}_{41} = (1,1,1,1,1,1,0,0,0)\,, && \boldsymbol{\nu}_{42} = (1,1,1,1,1,-1,1,0,0)\,,\\
&\boldsymbol{\nu}_{43} = (1,1,1,1,1,0,1,0,0)\,, && \boldsymbol{\nu}_{44} = (1,1,1,-1,1,1,1,0,0)\,, && \boldsymbol{\nu}_{45} = (1,1,1,0,1,1,1,0,0)\,,\\
&\boldsymbol{\nu}_{46} = (1,-2,1,1,1,1,1,0,0)\,, && \boldsymbol{\nu}_{47} = (1,-1,1,1,1,1,1,0,0)\,, && \boldsymbol{\nu}_{48} = (1,0,1,1,1,1,1,-1,0)\,,\\
&\boldsymbol{\nu}_{49} = (1,0,1,1,1,1,1,0,0)\,, && \boldsymbol{\nu}_{50} = (1,1,1,1,1,1,1,-3,0)\,, && \boldsymbol{\nu}_{51} = (1,1,1,1,1,1,1,-2,0)\,,\\
&\boldsymbol{\nu}_{52} = (1,1,1,1,1,1,1,-1,-1)\,, && \boldsymbol{\nu}_{53} = (1,1,1,1,1,1,1,-1,0)\,, && \boldsymbol{\nu}_{54} = (1,1,1,1,1,1,1,0,0)\,.
\end{aligned}
\tag{6.21}
$$

We cross the branch points with Cutkosky invariants $z_1 = s - 4m^2$, $z_2 = t - 9m^2$, $z_3 = -s - t - 7m^2$ performing three separate propagations: for each one of them, we produce boundary conditions with AMF^0 on one side of the branch surface, cross to the other side and validate the result with another run of AMF^0. In particular:

- We cross z_1 generating boundary values at point P_1 with $s = 3$, $t = 2$, $m^2 = 1$ ($z_1 < 0$) and moving to P_2 with $s = 5$ at fixed t and m^2 ($z_1 > 0$).
- We cross z_2 generating boundary values at point P_3 with $s = 2$, $t = 8$, $m^2 = 1$ ($z_2 < 0$) and moving to P_4 with $t = 10$ at fixed s and m^2 ($z_2 > 0$).

- We cross z_3 generating boundary values at point P_5 with $s = -3$, $t = -5$, $m^2 = 1$ ($z_3 > 0$) and moving to P_6 with $s = -1$, $t = -3$ at fixed m^2 ($z_3 < 0$).

Tables 6.6 and 6.7 list the numerical values for the top-topology integral $F^{\boldsymbol{\nu}_{54}}$.

6.7 Performance

A fair comparison between LINE and other tools for the numerical solution of differential equations is somewhat difficult to establish. First of all, LINE allows both the computation of boundary conditions and their propagation, two tasks that are implemented separately in other codes. Compared to standard phase space propagation, the generation of boundary conditions with the AMFlow method involves integration-by-parts reduction for the topology with the auxiliary mass and more master integrals. Therefore, the computation of boundary values with this technique is an intrinsically harder task than solving the DEs with respect to the kinematic invariants. Furthermore, the algorithms adopted may vary from tool to tool, depending on which stage of the computation is being considered. For instance, DiffExp solves DEs order per order in the regulator ϵ, while AMFlow uses numerical values of ϵ but solves DEs with respect to the auxiliary mass. Even if we focus on the latter problem, AMFlow implements iterative strategies to insert the mass in fewer propagators. Moreover, LINE has the unfair advantage of being written in `C/C++`, which is a lower-level language compared to the one adopted by Mathematica packages. Finally, we stress that, although LINE has been developed with attention to optimization, no explicit attempt has yet been made to improve its speed.

Nevertheless, in table 6.8 we report the execution time of LINE for the generation of boundary conditions with AMF^0 for three illustrative examples among the ones treated in this chapter, namely:

- point P_1 for the integral family of the non-planar triangle in eq. (6.12) (2 singular and 12 regular propagations);
- point P_1 for the integral family of the planar box with an internal mass in eq. (6.15) (2 singular and 16 regular propagations);
- point Q_1 for the integral family of the non-planar box with an internal and external mass in eq. (6.18) (2 singular and 31 regular propagations).

In particular, to isolate the performance of the DE solver we consider pure propagation times, taking into account only the time spent after the IBP reduction with the auxiliary mass η is over. Therefore, the execution times include the processing of IBP results for the construction of the DEs with respect to η, the computation of the leading behaviors at $\eta \to \infty$ and the propagation up to $\eta \to 0$.

precision digits				
results	decimal	8	16	32
internal	binary	313	506	893
topology	**# η-MIs**	**running time (sec)**		
non-planar triangle	52	102	210	531
planar box	68	158	286	762
non-planar box	144	3066	6600	14350

Table 6.8: Pure propagation time for the computation of boundary conditions using LINE in the AMF^0 mode. Results are obtained by varying the target precision for three different two-loop topologies.

The tests are performed on a machine equipped with an AMD Opteron Processor 4386 and 64GB of RAM. We show the running times by varying the target precision of the results, choosing 8, 16 and 32 digits for the coefficients of the Laurent expansions. Indicating with N the corresponding number of working precision digits, we observe that the propagation times scale roughly as $N^{1.5}$. This is consistent with the average scaling of standard arithmetic operations, showing that the execution time of LINE is dominated by numerical rather than high-level operations.

The choice of analyzing the generation of boundary conditions with AMF^0 makes it possible to compare the execution times with the AMFlow package set on the *all propagator mode*, which forces the introduction of the auxiliary mass in all the propagators. In this way, the exact same DEs are solved both by LINE and AMFlow, using the same numerical values of ϵ. It turns out that LINE runs roughly six times faster for the first two examples and about three times faster for the last one.

Chapter 7

Conclusions and outlook

The work presented in this thesis has focused on the numerical evaluation of Feynman integrals within the framework of the differential equation method. The motivations behind this research stem from the increasing precision required in modern collider phenomenology, where theoretical predictions must match the experimental accuracy achieved by current and future facilities. In this context, the differential equation approach has proved to be very effective for the computation of Feynman integrals that enter higher-order perturbative corrections to scattering amplitudes. The method is particularly well suited for numerical implementations, which become essential as the number of loops, external legs and energy scales increases. This work has addressed the key ingredients required for the complete application of the differential equation method, providing algorithmic procedures suitable for computer implementation and combining them into a unified framework based on series expansion techniques. Within this approach, Feynman integrals are propagated on a phase space line connecting a boundary point to any given target point. The singular nature of Feynman integrals makes the radius of convergence for series expansion solutions finite, therefore the propagation path is split into several segments and the method is iterated to move the solution progressively closer to the target.

A central aspect of the method concerns the determination of boundary conditions, for which two complementary strategies have been explored. The first one relies on the auxiliary mass flow method, which introduces an auxiliary mass in the propagators of the integrals and exploits their known leading behaviors in the infinite-mass limit. These constitute BCs for the propagation from infinity to the limit of vanishing mass. The second approach is based on expansion by regions, which identifies regions of the integration domain characterized by specific momentum scalings, in order to obtain the asymptotic expansion of the integrals in singular limits. The leading coefficients emerging in this ways can be used to impose BCs when solving the DEs around the considered singularity. In general, it might not be necessary to compute all of these coefficients, as long as their associated power behaviors are known. Indeed, the strategy presented here makes it possible to systematically obtain linear constraints on the leading coefficients by

simply vetoing the appearance in the solution of any undesired power behavior. Following this procedure, the number of boundary coefficients to be actually provided as input is minimized.

Solving DEs around singular points is therefore a key aspect for the generation of BCs. The techniques illustrated in this work allow one to transform the DEs to Fuchsian form and solve them by series expansion using the singularity as expansion point. The same procedure can be applied also to cross branch points that are encountered on the propagation path. FIs indeed develop branch cuts from these points, and thus the framework built in this thesis has been completed with an algorithmic prescription for the analytic continuation of the solutions. The latter also offers an alternative strategy for crossing branch points by circling them with a detour of regular propagation steps in the complex plane of the line parameter.

The methods presented here have been implemented in an open-source software called LINE, which stands for Loop Integrals Numerical Evaluation. The code is written in `C/C++` and only depends on open-source libraries, making the program suitable for large-scale computations on computing clusters. LINE includes an in-house implementation of the AMFlow method for the generation of BCs up to two loops. It also accepts as input EBR information to automatically minimize the number of necessary BCs around singular points. Therefore, the software allows the computation of boundary values and their propagation across the phase space within a single framework. The numerical precision of the results is internally verified by comparing different propagation paths or using distinct boundaries, without relying on external tools for the evaluations of FIs. To test the techniques discussed in this thesis, LINE has been applied on a selection of one- and two-loop examples, with and without masses, for both planar and non-planar configurations.

Note that, as a DE solver, LINE can be employed to solve problems that go beyond the computation of loop integrals. In fact, the DE method is also suitable for the propagation of integrals with Dirac δ-functions and propagators with linear dependence on the loop momenta. This enables, for instance, the computation of phase space integrals, subtraction counterterms and integrals for effective field theories. Furthermore, FIs can be expressed as combinations of special functions (such as pentagon functions) that also satisfy DEs of the same kind as the ones considered in this work. Ultimately, LINE is suitable for solving any problem involving systems of non-homogeneous first-order ordinary DEs whose coefficients are rational functions, both around regular and regular singular points, provided that the non-homogeneous term has the same kind of expansion as the solution.

The framework illustrated in this work suggests several directions for further development. For instance, it is straightforward to extend LINE to handle differential equations whose coefficients involve algebraic functions, such as square roots, to further enlarge the generality of the software. Furthermore, the generation of BCs in LINE could be enhanced

in two ways. The first one involves the implementation of the iterative formulation of the AMFlow method, which would provide infinite-mass leading behaviors at any number of loops without relying on their analytic expressions. The other approach would be to further investigate EBR strategies to iteratively compute the leading coefficients that remain unconstrained after vetoing the presence of undesired power behaviors in the solution.

Another natural development would be the implementation of algorithms to efficiently populate interpolation grids for Monte Carlo integration. The objective would be to minimize the computational time required to evaluate each target point, for instance by carefully selecting the boundary points and the propagation sequence. The current structure of LINE makes it possible to interface it with high-level wrappers that could handle the logic of the population strategy and call the program for each propagation step, thus minimizing the need for structural modifications of the core code.

In general, LINE could benefit from the introduction of object-oriented structures to handle those components that are not directly involved in the propagation itself and therefore would not impact the overall efficiency, as they correspond to infrequent or computationally inexpensive operations. Such an extension would allow a more structured management of the graph topologies associated with the integrals and would facilitate the implementation of iterative strategies for the computation of BCs. At the same time, efforts can be directed towards improving the efficiency of the core numerical routines that perform the actual calculations.

In conclusion, this thesis has presented methods for the computation of Feynman integrals through the numerical solution of differential equations, from the generation of boundary conditions to the computation of series expansion solutions and their analytic continuation. The techniques discussed here, implemented in an open-source code, aim to contribute to the ongoing effort towards the automation of precision calculations in particle physics.

Appendix A

Implementation details

A.1 Parsing, representing and manipulating rational functions

The ultimate goal of the methods described in this work is solving differential equations for Feynman integrals in the form

$$\frac{\partial}{\partial s_i}\mathbf{I}(\epsilon,\mathbf{s}) = \mathbb{A}_i(\epsilon,\mathbf{s})\mathbf{I}(\epsilon,\mathbf{s})\,, \tag{A.1}$$

on a phase space line $\mathbf{s}(\eta)$. The main elements to be provided as input for a computer implementation of such techniques are the DE matrices $\mathbb{A}_i(\epsilon,\mathbf{s})$, which are expected to be composed of rational functions depending on the space-time dimension and the kinematic invariants. The corresponding mathematical expressions can be stored as text strings in input files, which may reach considerable sizes. For instance, in some of the examples considered in chapter 6, one can find individual matrix elements represented by strings whose size is of the order of megabytes. In the early stages of the program, it is necessary to parse these input strings and turn them into an internal representation that allows the code to perform the mathematical operations that are needed to obtain the univariate system of DEs

$$\frac{d}{d\eta}\mathbf{I}(\eta) = \mathbb{A}(\eta)\mathbf{I}(\eta)\,. \tag{A.2}$$

In LINE, mathematical expressions are first converted to *symbolic trees*, where each node may represent an operation, a number or a symbolic variable. Operation nodes are themselves at the top of a sub-tree, since they have child nodes to represent the input of the operation. Conversely, symbolic and numeric nodes are terminal and have no children. For instance, figure A.1a shows the symbolic tree associated with the fragment `"m2*s^7*t^4*(8-6*d+d^2)"` of a mathematical expression, where `"d"` is the symbol for

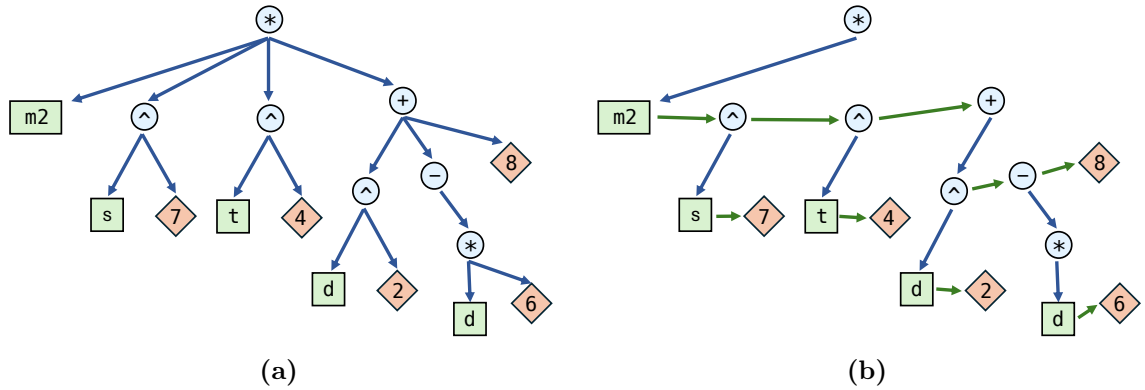

Figure A.1: **(a)** Symbolic tree associated with the expression `"m2*s^7*t^4*(8-6*d+d^2)"`. Green rectangles represent symbols, orange rhombus indicate numbers and blue circles correspond to operation nodes. The connection between a parent and its child nodes are represented by blue arrows. **(b)** The same tree, but with parent nodes pointing only to their first child and sibling nodes represented by linked lists whose connections are shown with green arrows.

the space-time dimension, `"s"`, `"t"` and `"m2"` are symbols for the kinematic invariants, `"*"` represents a product and `"^"` a power. LINE features a lightweight implementation of such a structure, tailored to perform basic algebraic operations such as substitutions, expansions of products or extractions of polynomial coefficients, which are essential in our framework. For their realization, it is often required to insert or delete a node in a tree. To simplify memory management when these situations arise, LINE makes use of *linked lists* to represent the children of each operation node. In particular, only the link between a parent node and its first child is maintained, while each child points to one sibling, as shown in figure A.1b. Naturally, the choice of the first child is arbitrary for commutative operations.

As symbolic trees are recursively defined, most operations on them are also performed recursively: a typical algorithm would descend through successive sub-trees until specific stopping conditions are met, execute the desired operation, and then climb back up to repeat this descent-and-ascent mechanism iteratively over the remaining child nodes. For instance, such a procedure can be followed to substitute the parameterization of the phase space line $\mathbf{s}(\eta) = \mathbf{s}_0 + \eta(\mathbf{s}_1 - \mathbf{s}_0)$ and a numeric value for the regulator ϵ, turning all the matrix elements into rational function of the line parameter η.

Rational functions are the building blocks for most of the algorithms described in this work. More elaborate procedures, such as the transformation of a system to Fuchsian normal form, can be reduced to a few core operations on rational functions, including sums, products, shifts and expansions around poles. A computer implementation would therefore benefit from an efficient representation of rational functions, tailored to the execution of

these operations. Consider a rational function

$$R(\eta) = \frac{N(\eta)}{D(\eta)} = \frac{\sum_{j=0}^{d(N)} a_j \eta^j}{\sum_{k=0}^{d(D)} b_k \eta^k}\,, \tag{A.3}$$

where $d(N)$ and $d(D)$ are the polynomial degrees of numerator and denominator, respectively, and a_j, b_k are rational coefficients. In LINE the numerator is represented as a list of $d(N)+1$ coefficients a_j, while the coefficients of the denominator are used to find the roots r_k for its factorized form

$$D(\eta) = \prod_k (\eta - r_k)^{m_k}\,, \tag{A.4}$$

where m_k is the multiplicity of r_k and thus $\sum_k m_k = d(D)$. Note that we implicitly chose to make the denominator *monic* by setting $b_{d(D)} = 1$, which is always possible by redefining the other coefficients to be normalized as $a_j \to a_j/b_{d(D)}$, $b_k \to b_k/b_{d(D)}$. Both numerator coefficients and denominator roots are stored at the required working precision.

Compared to the representation by coefficients, the factorization in eq. (A.4) allows a faster execution of operations such as the simplification of common polynomial factors or the computation of the polynomial least common multiple of two denominators. Furthermore, to make the implementation more efficient and tailored to DEs for Feynman integrals, we observe that typically each root appears many times across denominators of different matrix elements. LINE exploits this property by storing each root only once. In particular, the denominators of the DE matrix $\mathbb{A}(\eta)$ are scanned to find their roots numerically and, meanwhile, a list of unique roots is updated. Each time a root is found for the first time, a unique integer label is assigned to it and the root is stored into the global list. The denominator of each matrix element is represented only by the list of integer labels corresponding to its roots and the associated integer multiplicities. In this way, many operations that involve denominators reduce to fast computations performed on integers.

For each matrix element, the conversion of the associated symbolic tree to its representation in terms of coefficients and roots is performed by a decoding routine that navigates the tree recursively, analyzing numerators and denominators as soon as they are encountered. Algorithms to find polynomial roots numerically can be found, for instance, in [119]. LINE makes use of the Laguerre's method therein described, where a root r_k is iteratively updated until the polynomial $D(r_k)$ is zero within the roundoff error. Note however that, in the proximity of a root r_k, we have

$$D(\eta) \sim \text{const.} \times (\eta - r_k)^{m_k} + \mathcal{O}((\eta - r_k)^{m_k+1}) \tag{A.5}$$

so that, for multiple roots (i.e. roots r_k with $m_k > 1$), $D(\eta)$ goes to zero faster than for single roots. Therefore, multiple roots would be found with a number of precision digits

roughly divided by a factor m_k. To overcome this problem, LINE detects the presence of multiple roots and dynamically increases the working precision of the same factor m_k when needed, so that the root r_k is recomputed at the desired working precision. This is possible because the coefficients of the denominator are rationals and so they can be represented with arbitrary precision.

The approach discussed above works better when the denominators in the input matrices $\mathbb{A}_i(\epsilon, \mathbf{s})$ are presented as products of low-degree polynomials. When this is not the case, algorithms for the efficient factorization of high-degree polynomials into lower-degree ones (with exact rational coefficients) would be advantageous. For instance, when Kira is called to perform IBP reduction in the application of the AMFlow method, the output polynomials $P_i(\eta)$ are not factorized. They have rational coefficients and a degree that increases progressively when master integrals of more coupled sectors are considered. In LINE these polynomials are therefore factorized identifying a list of unique polynomial factors $F_j(\eta)$ with rational coefficients as follows:

- The first polynomial $P_1(\eta)$ is considered as a factor $F_1(\eta)$ that, as any other factor, is represented by roots with integer labels and multiplicities, as described above.

- After $i-1$ polynomials have been analyzed, the i-th one, $P_i(\eta)$, is evaluated at the roots of the factors previously found, so that one can detect what are those factors $F_k(\eta)$ that divide $P_i(\eta)$ exactly (i.e. the polynomial division $P_i(\eta)/F_k(\eta)$ yields a polynomial with rational coefficients and its remainder is an exact zero).

- $P_i(\eta)$ is divided by these factors and the result is identified as a new factor $F_{\text{new}}(\eta) = P_i(\eta)/F_k(\eta)$, whose roots are found to update the global list of unique roots.

- Comparing the labels of the roots in $F_{\text{new}}(\eta)$ with those of the roots in the previous factors, one can detect if $F_{\text{new}}(\eta)$ divides exactly some $F_k(\eta)$, so that the latter can be split as $F_k(\eta) \to \{F_k(\eta)/F_{\text{new}}(\eta), F_{\text{new}}(\eta)\}$, where $F_k(\eta)/F_{\text{new}}(\eta)$ is a new factor with rational coefficients.

- The newly introduced factor $F_k(\eta)/F_{\text{new}}(\eta)$ may in turn divide exactly other factors $F_j(\eta)$; this occurrence is detected and additional splits are iteratively performed whenever possible.

Each $P_i(\eta)$ is therefore represented by a list of integer labels associated with its factors, which in turn are represented by a list of labels associated with their roots. When a factor $F_k(\eta)$ previously found is split, the labels assigned to the polynomials $P_i(\eta)$ are updated accordingly. Each individual factor $F_k(\eta)$ is of lower degree compared to the original polynomials $P_i(\eta)$, and so the numerical determination of their roots is more stable.

A.2 Dimensional regularization via interpolation

A dimensionally regulated master integral has the Laurent expansion

$$I(\epsilon) = \sum_{k=0}^{\infty} I_k \, \epsilon^k \,, \tag{A.6}$$

where the prefactor ϵ^{-2L} is omitted for simplicity (for instance we can imagine to absorb it into the definition of the master integrals, so that they all start at order zero). Suppose our task is to use N_ϵ samples $I(\epsilon_1)$, …, $I(\epsilon_{N_\epsilon})$ to estimate the truncated series

$$I^{(\texttt{ord})}(\epsilon) \equiv \sum_{k=0}^{\texttt{ord}} I_k \, \epsilon^k \,, \tag{A.7}$$

which only includes the first $\texttt{ord} + 1$ orders. We denote by $\hat{I}_k$ our estimate of the coefficients I_k, that we want to compute within a given relative precision $E_{\texttt{prec}}$, so that

$$E_k \equiv \frac{|\hat{I}_k - I_k|}{|I_k|} \lesssim E_{\texttt{prec}} \,. \tag{A.8}$$

We compute the coefficients $\hat{I}_k$ by imposing that the polynomial

$$\hat{I}^{(\texttt{ord})} \equiv \sum_{k=0}^{\texttt{ord}} \hat{I}_k \, \epsilon^k \tag{A.9}$$

is equal to the samples $I(\epsilon_1)$, …, $I(\epsilon_{N_\epsilon})$ when evaluated at the corresponding points ϵ_1, …, ϵ_{N_ϵ}. Therefore the $\hat{I}_k$'s are the solution to the system of linear equations

$$\sum_{k=0}^{\texttt{ord}} \hat{I}_k \, \epsilon_i^k = I^{(\texttt{ord})}(\epsilon_i) \,, \qquad i = 1, \ldots, N_\epsilon \,. \tag{A.10}$$

To make the number of unknown coefficients $\hat{I}_k$ equal to the number of equations, let us truncate the Laurent series at order $N_\epsilon - 1 \geq \texttt{ord}$ (aiming to consider only the first $\texttt{ord}+1$ coefficients of the result). Then, we can write the system in compact form as

$$\mathbb{V}(\boldsymbol{\epsilon}) \, \hat{\mathbf{I}}^{(N_\epsilon - 1)} = \mathbf{I}(\boldsymbol{\epsilon}) \,, \tag{A.11}$$

where $\hat{\mathbf{I}}^{(N_\epsilon-1)} \equiv (\hat{I}_0, \ldots, \hat{I}_{N_\epsilon-1})$, $\boldsymbol{\epsilon} \equiv (\epsilon_1, \ldots, \epsilon_{N_\epsilon})$, $\mathbf{I}(\boldsymbol{\epsilon}) \equiv (I(\epsilon_1), \ldots, I(\epsilon_{N_\epsilon}))$ and $\mathbb{V}(\boldsymbol{\epsilon})$ corresponds to the Vandermonde matrix

$$\mathbb{V}(\boldsymbol{\epsilon}) \equiv \begin{pmatrix} 1 & \epsilon_1 & \epsilon_1^2 & \ldots & \epsilon_1^{N_\epsilon - 1} \\ \vdots & \vdots & \vdots & \ddots & \vdots \\ 1 & \epsilon_{N_\epsilon} & \epsilon_{N_\epsilon}^2 & \ldots & \epsilon_{N_\epsilon}^{N_\epsilon - 1} \end{pmatrix} . \tag{A.12}$$

We have $\det \mathbb{V}(\boldsymbol{\epsilon}) = \prod_{i<j}(\epsilon_j - \epsilon_i)$, and so the Vandermonde matrix is invertible as long as all the sample points are distinct. The coefficients $\hat{I}_k$ are thus given by

$$\hat{\mathbf{I}}^{(N_\epsilon-1)} = \mathbb{V}^{-1}(\boldsymbol{\epsilon})\,\mathbf{I}(\boldsymbol{\epsilon})\,. \tag{A.13}$$

To estimate the relative error of this computation we observe that

$$I(\epsilon) = \sum_{k=0}^{N_\epsilon-1} I_k\,\epsilon^k + \sum_{k=N_\epsilon}^{\infty} I_k\,\epsilon^k \equiv \sum_{k=0}^{N_\epsilon-1} I_k\,\epsilon^k + R^{(N_\epsilon)}(\epsilon)\,, \tag{A.14}$$

where $R^{(N_\epsilon)}(\epsilon)$ is the remainder of the series. When evaluated at the sample points, this relation can be written in vectorial form as

$$\mathbf{I}(\boldsymbol{\epsilon}) = \mathbb{V}(\boldsymbol{\epsilon})\mathbf{I}^{(N_\epsilon-1)} + \mathbf{R}^{(N_\epsilon)}(\boldsymbol{\epsilon})\,, \tag{A.15}$$

where $\mathbf{I}^{(N_\epsilon-1)} \equiv (I_0, \dots, I_{N_\epsilon-1})$ and $\mathbf{R}^{(N_\epsilon)}(\boldsymbol{\epsilon}) \equiv \big(R^{(N_\epsilon)}(\epsilon_1), \dots, R^{(N_\epsilon)}(\epsilon_{N_\epsilon})\big)$. Substituting this expression into eq. (A.13), we arrive at

$$\hat{\mathbf{I}}^{(N_\epsilon-1)} = \mathbf{I}^{(N_\epsilon-1)} + \mathbb{V}^{-1}(\boldsymbol{\epsilon})\mathbf{R}^{(N_\epsilon)}(\boldsymbol{\epsilon})\,, \tag{A.16}$$

which can be used to estimate the absolute error as

$$|\hat{I}_k - I_k| = \left|\sum_{i=1}^{N_\epsilon} \mathbb{V}^{-1}_{k+1,i}(\boldsymbol{\epsilon}) R^{(N_\epsilon)}(\epsilon_i)\right| \leq \sum_{i=1}^{N_\epsilon} \left|\mathbb{V}^{-1}_{k+1,i}(\boldsymbol{\epsilon})\right| \left|R^{(N_\epsilon)}(\epsilon_i)\right|. \tag{A.17}$$

Denoting by $\mathcal{R}$ the radius of convergence for the Laurent expansion and assuming that $|\epsilon_i| \sim r \ll \mathcal{R}$, one has that the remainder $R^{(N_\epsilon)}(\epsilon_i)$ is bounded as in

$$\left|R^{(N_\epsilon)}(\epsilon_i)\right| = \left|\sum_{k=N_\epsilon}^{\infty} I_k \epsilon_i^k\right| \leq \sum_{k=N_\epsilon}^{\infty} |I_k||\epsilon_i|^k \lesssim \sum_{k=N_\epsilon}^{\infty} \left(\frac{r}{\mathcal{R}}\right)^k = \frac{(r/\mathcal{R})^{N_\epsilon}}{1 - r/\mathcal{R}} \simeq \left(\frac{r}{\mathcal{R}}\right)^{N_\epsilon}, \tag{A.18}$$

while $\mathbb{V}^{-1}_{k+1,i}(\boldsymbol{\epsilon}) \sim 1/r^k$. Substituting these behaviors in eq. (A.17), we obtain

$$|\hat{I}_k - I_k| \lesssim \sum_{i=1}^{N_\epsilon} \frac{1}{r^k}\left(\frac{r}{\mathcal{R}}\right)^{N_\epsilon} = N_\epsilon \frac{1}{r^k}\left(\frac{r}{\mathcal{R}}\right)^{N_\epsilon}, \tag{A.19}$$

which, divided by $|I_k| \sim 1/\mathcal{R}^k$, leads to the relative error

$$E_k = \frac{|\hat{I}_k - I_k|}{|I_k|} \sim \left(\frac{r}{\mathcal{R}}\right)^{N_\epsilon - k}, \tag{A.20}$$

where we omitted the factor N_ϵ. As we can see, the relative error is larger the higher is the order in ϵ. Therefore, to ensure that all the coefficients are determined within the target precision $E_{\texttt{prec}}$ as in eq. (A.8), it is sufficient to choose N_ϵ and r in such a way that

$$E_{\texttt{ord}} \lesssim \left(\frac{r}{\mathcal{R}}\right)^{N_\epsilon - \texttt{ord}} \sim E_{\texttt{prec}}\,, \tag{A.21}$$

so that the precision is enough for the highest-order coefficient to be determined. This implies that

$$N_\epsilon \sim \texttt{ord} - \frac{\texttt{prec}}{\log_{10}(r/\mathcal{R})}\,, \tag{A.22}$$

where $\texttt{prec} = -\log_{10}(E_{\texttt{prec}})$ is the required number of decimal digits of precision.

Note that so far we assumed the samples $I(\epsilon_i)$ to be known without error. In reality, they are computed at working precision and their error affects the determination of the coefficients $\hat{I}_k$. Therefore, the chosen number of working precision digits $\texttt{wp}$ must at least match the precision of the lowest-order coefficient $\hat{I}_0$, that is,

$$\texttt{wp} = -\log_{10}(E_0) \sim -N_\epsilon \log_{10}\left(\frac{r}{\mathcal{R}}\right) = \texttt{prec} - \texttt{ord}\,\log_{10}\left(\frac{r}{\mathcal{R}}\right) \tag{A.23}$$

where eq. (A.22) was used. As pointed out in [53], the choice of r can be made by minimizing the quantity $N_\epsilon T(\texttt{wp})$, where $T(\texttt{wp})$ is the average time necessary to compute one sample with precision $\texttt{wp}$. Typically $T(\texttt{wp}) \sim \texttt{wp}^\alpha$ for some $\alpha > 0$ (see for instance the considerations in section 6.7, where we roughly estimate $\alpha \simeq 1.5$ on some of the proposed examples). Using eqs. (A.22) and (A.23), one has

$$N_\epsilon T(\texttt{wp}) \sim \left(\texttt{ord} - \frac{\texttt{prec}}{\log_{10}(r/\mathcal{R})}\right)\left[\texttt{prec} - \texttt{ord}\,\log_{10}\left(\frac{r}{\mathcal{R}}\right)\right]^\alpha\,. \tag{A.24}$$

Differentiating with respect to $\log_{10}(r/\mathcal{R})$ and looking for solutions with $\log_{10}(r/\mathcal{R}) < 0$, the minimum is found to be

$$\log_{10}(r/\mathcal{R}) \sim -\frac{\texttt{prec}}{(\alpha\,\texttt{ord})}\,, \tag{A.25}$$

which, inserted back into eqs. (A.22) and (A.23), leads to

$$N_\epsilon = (1+\alpha)\,\texttt{ord}\,, \quad \texttt{wp} = \left(\frac{1+\alpha}{\alpha}\right)\texttt{prec}\,. \tag{A.26}$$

As the authors of [53] point out, these are only rough estimates that may need some adjustments in practical computations. For instance, the numerical setup actually chosen in

the package AMFlow presented in [53] has proved effective for all the examples analyzed with LINE so far. In this setup, the number N_ϵ of sample points and the values for ϵ are given by

$$\begin{aligned} N_\epsilon &= \text{ceil}\left(5\frac{\texttt{ord}}{2} + 2L\right), \\ \epsilon_k &= (101+k) \times 10^{(-\texttt{prec}/(\texttt{ord}+1)-L/2-2)}. \end{aligned} \tag{A.27}$$

Note that it is possible to detect the first non-zero order in ϵ comparing the lowest-order coefficient $\hat{I}_0$ computed using N_ϵ and $N_\epsilon - 1$ samples: coefficients that are zero vary on almost all digits of working precision. If the leading-order turns out to be zero, one can repeat the interpolation starting directly at order ϵ and including the order $\epsilon^{\texttt{ord}+1}$. The same procedure can be iterated until the leading order is stable under this mechanism.

A.3 Numerical precision control

The techniques presented in this work are meant to be applied within numerical frameworks at arbitrary precision. To this end, LINE links the `GMP` family of libraries, which are efficient, open-source and well maintained. The calculations are performed at a working precision `wp` which, as discussed in appendix A.2, depends on the precision desired for the output coefficients of the Laurent expansions in the dimensional regulator ϵ.

Being able to evaluate the numerical precision of the final result is crucial to ensure the reliability of the computation. The framework of phase space propagation through differential equations is particularly well suited for this purpose, as one can reach the same kinematic points along different paths and compare on how many digits the results agree. These paths may share a common boundary point or even use boundary conditions generated in distinct points, solving differential equations in the auxiliary mass and/or in the kinematic invariants.

In addition to the procedure described above, it is also possible to employ local tests to assess *on the fly* the validity of the computation at the working precision. For instance, around a given point on the path, one could match the same series solution with different BCs prepared at the previous propagation step, producing distinct predictions for the evaluation at the next point on the path. In the presence of a branch point, a tighter test consists in propagating the solution to the other side of the singularity both solving the DEs around the pole and using the procedure of section 5.3.3 to circle around it in the complex plane of the line parameter.

The techniques discussed so far rely on the comparison of solutions constructed with different (local or global) paths. Another aspect to be taken into account is that, when using the methods of chapter 4 to calculate the coefficients of the series solutions, the

number of terms to be included in the series expansions depends on `wp`. In fact, the order at which the series are truncated must be large enough to observe convergence on all the digits of working precision. In LINE, the convergence of the solution is checked at each point of the path so that, if necessary, the number of orders is dynamically increased until convergence is obtained on all digits of working precision.

As an additional check, once a solution around a point is built in LINE, the residual of the DE is evaluated at the next point of the path to detect potential losses of precision, which may require an increase of `wp`. The same technique is also useful to expose bugs or errors in the computation of the solution.

We conclude by noting that the interpolation procedure described in section A.2 also provides a method to estimate the precision of the final result. In fact, once the first non-zero order is detected, one can observe how many digits vary when the leading order is interpolated with one fewer sample, in order to check that the number of stable digits is in agreement with the expected precision. This test could be performed virtually at no cost at any path point (provided that the output from all the samples is available), since the computational time spent for the interpolation is negligible compared to the time needed to solve the DEs for each sample.

List of figures

List of tables

Bibliography

[1] ATLAS collaboration, *Observation of a new particle in the search for the Standard Model Higgs boson with the ATLAS detector at the LHC*, *Phys. Lett. B* **716** (2012) 1 [1207.7214].

[2] CMS collaboration, *Observation of a New Boson with Mass Near 125 GeV in pp Collisions at $\sqrt{s}$ = 7 and 8 TeV*, *JHEP* **06** (2013) 081 [1303.4571].

[3] F. Englert and R. Brout, *Broken Symmetry and the Mass of Gauge Vector Mesons*, *Phys. Rev. Lett.* **13** (1964) 321.

[4] P.W. Higgs, *Spontaneous Symmetry Breakdown without Massless Bosons*, *Phys. Rev.* **145** (1966) 1156.

[5] T. Kinoshita, *Mass singularities of Feynman amplitudes*, *J. Math. Phys.* **3** (1962) 650.

[6] T.D. Lee and M. Nauenberg, *Degenerate Systems and Mass Singularities*, *Phys. Rev.* **133** (1964) B1549.

[7] F. Caola, W. Chen, C. Duhr, X. Liu, B. Mistlberger, F. Petriello et al., *The Path forward to N^3LO*, in *Snowmass 2021*, 3, 2022 [2203.06730].

[8] S. Badger, H.B. Hartanto, Z. Wu, Y. Zhang and S. Zoia, *Two-loop amplitudes for $\mathcal{O}(\alpha_s^2)$ corrections to $W\gamma\gamma$ production at the LHC*, 2409.08146.

[9] B. Agarwal, F. Buccioni, F. Devoto, G. Gambuti, A. von Manteuffel and L. Tancredi, *Five-parton scattering in QCD at two loops*, *Phys. Rev. D* **109** (2024) 094025 [2311.09870].

[10] G. De Laurentis, H. Ita, M. Klinkert and V. Sotnikov, *Double-virtual NNLO QCD corrections for five-parton scattering. I. The gluon channel*, *Phys. Rev. D* **109** (2024) 094023 [2311.10086].

[11] G. De Laurentis, H. Ita and V. Sotnikov, *Double-virtual NNLO QCD corrections for five-parton scattering. II. The quark channels*, *Phys. Rev. D* **109** (2024) 094024 [2311.18752].

[12] S. Abreu, P.F. Monni, B. Page and J. Usovitsch, *Planar Six-Point Feynman Integrals for Four-Dimensional Gauge Theories*, 2412.19884.

[13] J. Henn, A. Matijašić, J. Miczajka, T. Peraro, Y. Xu and Y. Zhang, *Complete function space for planar two-loop six-particle scattering amplitudes*, 2501.01847.

[14] M. Bonetti, K. Melnikov and L. Tancredi, *Three-loop mixed QCD-electroweak corrections to Higgs boson gluon fusion*, *Phys. Rev. D* **97** (2018) 034004 [1711.11113].

[15] M. Fael, F. Lange, K. Schönwald and M. Steinhauser, *Massive Vector Form Factors to Three Loops*, *Phys. Rev. Lett.* **128** (2022) 172003 [2202.05276].

[16] F. Forner, C. Nega and L. Tancredi, *On the photon self-energy to three loops in QED*, 2411.19042.

[17] C. Duhr, F. Gasparotto, C. Nega, L. Tancredi and S. Weinzierl, *On the electron self-energy to three loops in QED*, *JHEP* **11** (2024) 020 [2408.05154].

[18] J.M. Henn, J. Lim and W.J. Torres Bobadilla, *First look at the evaluation of three-loop non-planar Feynman diagrams for Higgs plus jet production*, *JHEP* **05** (2023) 026 [2302.12776].

[19] T. Gehrmann, J. Henn, P. Jakubčík, J. Lim, C.C. Mella, N. Syrrakos et al., *Graded transcendental functions: an application to four-point amplitudes with one off-shell leg*, 2410.19088.

[20] M.-M. Long, *Three-loop ladder diagrams with two off-shell legs*, 2410.15431.

[21] D. Canko and M. Pozzoli, *A first computation of three-loop master integrals for the production of two off-shell vector bosons with different masses*, 2412.06972.

[22] S. Laporta, *High-precision calculation of the 4-loop contribution to the electron g-2 in QED*, *Phys. Lett. B* **772** (2017) 232 [1704.06996].

[23] T. Aoyama, T. Kinoshita and M. Nio, *Revised and Improved Value of the QED Tenth-Order Electron Anomalous Magnetic Moment*, *Phys. Rev. D* **97** (2018) 036001 [1712.06060].

[24] S. Volkov, *Calculating the five-loop QED contribution to the electron anomalous magnetic moment: Graphs without lepton loops*, *Phys. Rev. D* **100** (2019) 096004 [1909.08015].

[25] T. Luthe, *Fully massive vacuum integrals at 5 loops*, Ph.D. thesis, Bielefeld U., 2015.

[26] A.I. Davydychev and J.B. Tausk, *Two loop selfenergy diagrams with different masses and the momentum expansion*, *Nucl. Phys. B* **397** (1993) 123.

[27] N.I. Usyukina and A.I. Davydychev, *An Approach to the evaluation of three and four point ladder diagrams*, *Phys. Lett. B* **298** (1993) 363.

[28] O.V. Tarasov, *Connection between Feynman integrals having different values of the space-time dimension*, *Phys. Rev. D* **54** (1996) 6479 [hep-th/9606018].

[29] S. Laporta, *High-precision calculation of multiloop Feynman integrals by difference equations*, *Int. J. Mod. Phys. A* **15** (2000) 5087 [hep-ph/0102033].

[30] T. Binoth and G. Heinrich, *An automatized algorithm to compute infrared divergent multiloop integrals*, *Nucl. Phys. B* **585** (2000) 741 [hep-ph/0004013].

[31] G. Heinrich, *Sector Decomposition*, *Int. J. Mod. Phys. A* **23** (2008) 1457 [0803.4177].

[32] S. Borowka, G. Heinrich, S.P. Jones, M. Kerner, J. Schlenk and T. Zirke, *SecDec-3.0: numerical evaluation of multi-scale integrals beyond one loop*, *Comput. Phys. Commun.* **196** (2015) 470 [1502.06595].

[33] S. Borowka, G. Heinrich, S. Jahn, S.P. Jones, M. Kerner, J. Schlenk et al., *pySecDec: a toolbox for the numerical evaluation of multi-scale integrals*, *Comput. Phys. Commun.* **222** (2018) 313 [1703.09692].

[34] G. Heinrich, S.P. Jones, M. Kerner, V. Magerya, A. Olsson and J. Schlenk, *Numerical scattering amplitudes with pySecDec*, *Comput. Phys. Commun.* **295** (2024) 108956 [2305.19768].

[35] E.E. Boos and A.I. Davydychev, *A Method of evaluating massive Feynman integrals*, *Theor. Math. Phys.* **89** (1991) 1052.

[36] V.A. Smirnov, *Analytical result for dimensionally regularized massless on shell double box*, *Phys. Lett. B* **460** (1999) 397 [hep-ph/9905323].

[37] J.B. Tausk, *Nonplanar massless two loop Feynman diagrams with four on-shell legs*, *Phys. Lett. B* **469** (1999) 225 [hep-ph/9909506].

[38] M. Czakon, *Automatized analytic continuation of Mellin-Barnes integrals*, *Comput. Phys. Commun.* **175** (2006) 559 [hep-ph/0511200].

[39] J. Gluza, K. Kajda and T. Riemann, *AMBRE: A Mathematica package for the construction of Mellin-Barnes representations for Feynman integrals*, *Comput. Phys. Commun.* **177** (2007) 879 [0704.2423].

[40] M. Borinsky, H.J. Munch and F. Tellander, *Tropical Feynman integration in the Minkowski regime*, *Comput. Phys. Commun.* **292** (2023) 108874 [2302.08955].

[41] G. Barucchi and G. Ponzano, *Differential equations for one-loop generalized feynman integrals*, *J. Math. Phys.* **14** (1973) 396.

[42] A.V. Kotikov, *Differential equations method: New technique for massive Feynman diagrams calculation*, *Phys. Lett. B* **254** (1991) 158.

[43] A.V. Kotikov, *Differential equation method: The Calculation of N point Feynman diagrams*, *Phys. Lett. B* **267** (1991) 123.

[44] Z. Bern, L.J. Dixon and D.A. Kosower, *Dimensionally regulated one loop integrals*, *Phys. Lett. B* **302** (1993) 299 [hep-ph/9212308].

[45] E. Remiddi, *Differential equations for Feynman graph amplitudes*, *Nuovo Cim. A* **110** (1997) 1435 [hep-th/9711188].

[46] T. Gehrmann and E. Remiddi, *Differential equations for two loop four point functions*, *Nucl. Phys. B* **580** (2000) 485 [hep-ph/9912329].

[47] J.M. Henn, *Lectures on differential equations for Feynman integrals*, *J. Phys. A* **48** (2015) 153001 [1412.2296].

[48] M. Argeri, S. Di Vita, P. Mastrolia, E. Mirabella, J. Schlenk, U. Schubert et al., *Magnus and Dyson Series for Master Integrals*, *JHEP* **03** (2014) 082 [1401.2979].

[49] M. Hidding, *DiffExp, a Mathematica package for computing Feynman integrals in terms of one-dimensional series expansions*, *Comput. Phys. Commun.* **269** (2021) 108125 [2006.05510].

[50] T. Armadillo, R. Bonciani, S. Devoto, N. Rana and A. Vicini, *Evaluation of Feynman integrals with arbitrary complex masses via series expansions*, *Comput. Phys. Commun.* **282** (2023) 108545 [2205.03345].

[51] X. Liu, Y.-Q. Ma and C.-Y. Wang, *A Systematic and Efficient Method to Compute Multi-loop Master Integrals*, *Phys. Lett. B* **779** (2018) 353 [1711.09572].

[52] X. Liu and Y.-Q. Ma, *Multiloop corrections for collider processes using auxiliary mass flow*, *Phys. Rev. D* **105** (2022) L051503 [2107.01864].

[53] X. Liu and Y.-Q. Ma, *AMFlow: A Mathematica package for Feynman integrals computation via auxiliary mass flow*, *Comput. Phys. Commun.* **283** (2023) 108565 [2201.11669].

[54] H.-Y. Bi, L.-H. Huang, R.-J. Huang, Y.-Q. Ma and H.-M. Yu, *Electroweak Corrections to Double Higgs Production at the LHC*, *Phys. Rev. Lett.* **132** (2024) 231802 [2311.16963].

[55] R. Bonciani, V. Del Duca, H. Frellesvig, M. Hidding, V. Hirschi, F. Moriello et al., *Next-to-leading-order QCD corrections to Higgs production in association with a jet*, *Phys. Lett. B* **843** (2023) 137995 [2206.10490].

[56] X. Chen, X. Guan, C.-Q. He, X. Liu and Y.-Q. Ma, *Heavy-Quark Pair Production at Lepton Colliders at NNNLO in QCD*, *Phys. Rev. Lett.* **132** (2024) 101901 [2209.14259].

[57] P. Bargiela, F. Caola, H. Chawdhry and X. Liu, *Two-loop mixed QCD-electroweak amplitudes for Z+jet production at the LHC: bosonic corrections*, *JHEP* **06** (2024) 150 [2312.14145].

[58] T. Armadillo, R. Bonciani, S. Devoto, N. Rana and A. Vicini, *Two-loop mixed QCD-EW corrections to charged current Drell-Yan*, *JHEP* **07** (2024) 265 [2405.00612].

[59] Y. Liu, A. Matijašić, J. Miczajka, Y. Xu, Y. Xu and Y. Zhang, *An Analytic Computation of Three-Loop Five-Point Feynman Integrals*, 2411.18697.

[60] D. Chicherin, J. Henn and V. Mitev, *Bootstrapping pentagon functions*, *JHEP* **05** (2018) 164 [1712.09610].

[61] T. Gehrmann, J.M. Henn and N.A. Lo Presti, *Pentagon functions for massless planar scattering amplitudes*, *JHEP* **10** (2018) 103 [1807.09812].

[62] D. Chicherin and V. Sotnikov, *Pentagon Functions for Scattering of Five Massless Particles*, *JHEP* **20** (2020) 167 [2009.07803].

[63] D. Chicherin, V. Sotnikov and S. Zoia, *Pentagon functions for one-mass planar scattering amplitudes*, *JHEP* **01** (2022) 096 [2110.10111].

[64] S. Abreu, D. Chicherin, H. Ita, B. Page, V. Sotnikov, W. Tschernow et al., *All Two-Loop Feynman Integrals for Five-Point One-Mass Scattering*, *Phys. Rev. Lett.* **132** (2024) 141601 [2306.15431].

[65] S. Badger, M. Becchetti, E. Chaubey, R. Marzucca and F. Sarandrea, *One-loop QCD helicity amplitudes for $pp \to t\bar{t}j$ to $O(\varepsilon^2)$*, *JHEP* **06** (2022) 066 [2201.12188].

[66] S. Badger, M. Becchetti, E. Chaubey and R. Marzucca, *Two-loop master integrals for a planar topology contributing to $pp \to t\bar{t}j$*, *JHEP* **01** (2023) 156 [2210.17477].

[67] S. Badger, M. Becchetti, N. Giraudo and S. Zoia, *Two-loop integrals for $t\bar{t}$+jet production at hadron colliders in the leading colour approximation*, *JHEP* **07** (2024) 073 [2404.12325].

[68] A.G. Grozin, *Integration by parts: An Introduction*, *Int. J. Mod. Phys. A* **26** (2011) 2807 [1104.3993].

[69] S. Weinzierl, *Feynman Integrals. A Comprehensive Treatment for Students and Researchers*, UNITEXT for Physics, Springer (2022), 10.1007/978-3-030-99558-4, [2201.03593].

[70] E. Byckling and K. Kajantie, *Particle Kinematics*, A Wiley-Interscience publication, Wiley (1973).

[71] J.D. Bjorken, *Experimental tests of Quantum electrodynamics and spectral representations of Green's functions in perturbation theory*, Ph.D. thesis, Stanford U., 1959.

[72] L.D. Landau, *On the Analytic Properties of Vertex Parts in Quantum Field Theory*, *Zh. Eksp. Teor. Fiz.* **37** (1960) 62.

[73] N. Nakanishi, *Ordinary and Anomalous Thresholds in Perturbation Theory*, *Prog. Theor. Phys.* **22** (1959) 128.

[74] R.J. Eden, P.V. Landshoff, D.I. Olive and J.C. Polkinghorne, *The analytic S-matrix*, Cambridge Univ. Press, Cambridge (1966).

[75] C. Bogner and S. Weinzierl, *Feynman graph polynomials*, *Int. J. Mod. Phys. A* **25** (2010) 2585 [1002.3458].

[76] J.C. Polkinghorne and G.R. Screaton, *The analytic properties of perturbation theory — I*, *Nuovo Cim.* **15** (1960) 289.

[77] J.C. Polkinghorne and G.R. Screaton, *The analytic properties of perturbation theory — II*, *Nuovo Cim.* **15** (1960) 925.

[78] H.S. Hannesdottir, A.J. McLeod, M.D. Schwartz and C. Vergu, *Implications of the Landau equations for iterated integrals*, *Phys. Rev. D* **105** (2022) L061701 [2109.09744].

[79] A.V. Smirnov and A.V. Petukhov, *The Number of Master Integrals is Finite*, *Lett. Math. Phys.* **97** (2011) 37 [1004.4199].

[80] A.V. Smirnov, *Algorithm FIRE – Feynman Integral REduction*, *JHEP* **10** (2008) 107 [0807.3243].

[81] A.V. Smirnov and F.S. Chukharev, *FIRE6: Feynman Integral REduction with modular arithmetic*, *Comput. Phys. Commun.* **247** (2020) 106877 [1901.07808].

[82] C. Studerus, *Reduze – Feynman integral reduction in C++*, *Comput. Phys. Commun.* **181** (2010) 1293 [0912.2546].

[83] A. von Manteuffel and C. Studerus, *Reduze 2 - Distributed Feynman Integral Reduction*, 1201.4330.

[84] R.N. Lee, *Presenting LiteRed: a tool for the Loop InTEgrals REDuction*, 1212.2685.

[85] R.N. Lee, *LiteRed 1.4: a powerful tool for reduction of multiloop integrals*, *J. Phys. Conf. Ser.* **523** (2014) 012059 [1310.1145].

[86] F. Lange, J. Usovitsch and Z. Wu, *Kira 3: integral reduction with efficient seeding and optimized equation selection*, 2505.20197.

[87] R.N. Lee, *Group structure of the integration-by-part identities and its application to the reduction of multiloop integrals*, *JHEP* **07** (2008) 031 [0804.3008].

[88] P. Maierhöfer, J. Usovitsch and P. Uwer, *Kira—A Feynman integral reduction program*, *Comput. Phys. Commun.* **230** (2018) 99 [1705.05610].

[89] J.M. Henn, *Multiloop integrals in dimensional regularization made simple*, *Phys. Rev. Lett.* **110** (2013) 251601 [1304.1806].

[90] U. Aglietti, R. Bonciani, L. Grassi and E. Remiddi, *The Two loop crossed ladder vertex diagram with two massive exchanges*, *Nucl. Phys. B* **789** (2008) 45 [0705.2616].

[91] R. Bonciani, V. Del Duca, H. Frellesvig, J.M. Henn, F. Moriello and V.A. Smirnov, *Two-loop planar master integrals for Higgs→ 3 partons with full heavy-quark mass dependence*, *JHEP* **12** (2016) 096 [1609.06685].

[92] A. Primo and L. Tancredi, *On the maximal cut of Feynman integrals and the solution of their differential equations*, *Nucl. Phys. B* **916** (2017) 94 [1610.08397].

[93] A. Primo and L. Tancredi, *Maximal cuts and differential equations for Feynman integrals. An application to the three-loop massive banana graph*, *Nucl. Phys. B* **921** (2017) 316 [1704.05465].

[94] R. Tarjan, *Depth-first search and linear graph algorithms*, *SIAM Journal on Computing* **1** (1972) 146.

[95] M. Sharir, *A strong-connectivity algorithm and its applications in data flow analysis*, *Computers & Mathematics with Applications* **7** (1981) 67.

[96] H.N. Gabow, *Path-based depth-first search for strong and biconnected components*, *Information Processing Letters* **74** (2000) 107.

[97] J. Moser, *The order of a singularity in Fuchs' theory*, *Math. Z.* **72** (1959) 379.

[98] J. Horn, *Zur Theorie der Systeme linearer Differentialgleichungen mit einer unabhängigen Veränderlichen. II*, *Mathematische Annalen* **40** (1892) 527.

[99] M.A. Barkatou and E. Pflügel, *Computing super-irreducible forms of systems of linear differential equations via moser-reduction: A new approach*, in *Proceedings of the 2007 International Symposium on Symbolic and Algebraic Computation*, ISSAC '07, (New York, NY, USA), pp. 1–8, Association for Computing Machinery, July, 2007, DOI.

[100] M.A. Barkatou and E. Pflügel, *On the Moser- and super-reduction algorithms of systems of linear differential equations and their complexity*, *Journal of Symbolic Computation* **44** (2009) 1017.

[101] R.N. Lee, *Reducing differential equations for multiloop master integrals*, *JHEP* **04** (2015) 108 [1411.0911].

[102] W. Wasow, *Asymptotic expansions for ordinary differential equations*, Pure and Applied Mathematics, Vol. XIV, Interscience Publishers John Wiley & Sons, Inc., New York-London-Sydney (1965).

[103] D.J. Broadhurst, *Massive three - loop Feynman diagrams reducible to SC* primitives of algebras of the sixth root of unity*, *Eur. Phys. J. C* **8** (1999) 311 [hep-th/9803091].

[104] B.A. Kniehl, A.F. Pikelner and O.L. Veretin, *Three-loop massive tadpoles and polylogarithms through weight six*, *JHEP* **08** (2017) 024 [1705.05136].

[105] Y. Schroder and A. Vuorinen, *High-precision epsilon expansions of single-mass-scale four-loop vacuum bubbles*, *JHEP* **06** (2005) 051 [hep-ph/0503209].

[106] T. Luthe, A. Maier, P. Marquard and Y. Schroder, *Complete renormalization of QCD at five loops*, *JHEP* **03** (2017) 020 [1701.07068].

[107] X. Liu, Y.-Q. Ma, W. Tao and P. Zhang, *Calculation of Feynman loop integration and phase-space integration via auxiliary mass flow*, *Chin. Phys. C* **45** (2021) 013115 [2009.07987].

[108] Z.-F. Liu and Y.-Q. Ma, *Automatic computation of Feynman integrals containing linear propagators via auxiliary mass flow*, *Phys. Rev. D* **105** (2022) 074003 [2201.11636].

[109] M. Beneke and V.A. Smirnov, *Asymptotic expansion of Feynman integrals near threshold*, *Nucl. Phys. B* **522** (1998) 321 [hep-ph/9711391].

[110] V.A. Smirnov and E.R. Rakhmetov, *The Strategy of regions for asymptotic expansion of two loop vertex Feynman diagrams*, *Theor. Math. Phys.* **120** (1999) 870 [hep-ph/9812529].

[111] B. Jantzen, *Foundation and generalization of the expansion by regions*, *JHEP* **12** (2011) 076 [1111.2589].

[112] V.A. Smirnov, *Problems of the strategy of regions*, *Phys. Lett. B* **465** (1999) 226 [hep-ph/9907471].

[113] A. Pak and A. Smirnov, *Geometric approach to asymptotic expansion of Feynman integrals*, *Eur. Phys. J. C* **71** (2011) 1626 [1011.4863].

[114] B. Ananthanarayan, A. Pal, S. Ramanan and R. Sarkar, *Unveiling Regions in multi-scale Feynman Integrals using Singularities and Power Geometry*, *Eur. Phys. J. C* **79** (2019) 57 [1810.06270].

[115] B. Ananthanarayan, A.B. Das and R. Sarkar, *Asymptotic analysis of Feynman diagrams and their maximal cuts*, *Eur. Phys. J. C* **80** (2020) 1131 [2003.02451].

[116] B. Jantzen, A.V. Smirnov and V.A. Smirnov, *Expansion by regions: revealing potential and Glauber regions automatically*, *Eur. Phys. J. C* **72** (2012) 2139 [1206.0546].

[117] A.V. Smirnov, N.D. Shapurov and L.I. Vysotsky, *FIESTA5: Numerical high-performance Feynman integral evaluation*, *Comput. Phys. Commun.* **277** (2022) 108386 [2110.11660].

[118] G. Heinrich, S. Jahn, S.P. Jones, M. Kerner, F. Langer, V. Magerya et al., *Expansion by regions with pySecDec*, *Comput. Phys. Commun.* **273** (2022) 108267 [2108.10807].

[119] S.A. Teukolsky, B.P. Flannery, W. Press and W. Vetterling, *Numerical recipes in c*, *SMR* **693** (1992) 59.

[120] R.E. Cutkosky, *Singularities and discontinuities of Feynman amplitudes*, *J. Math. Phys.* **1** (1960) 429.